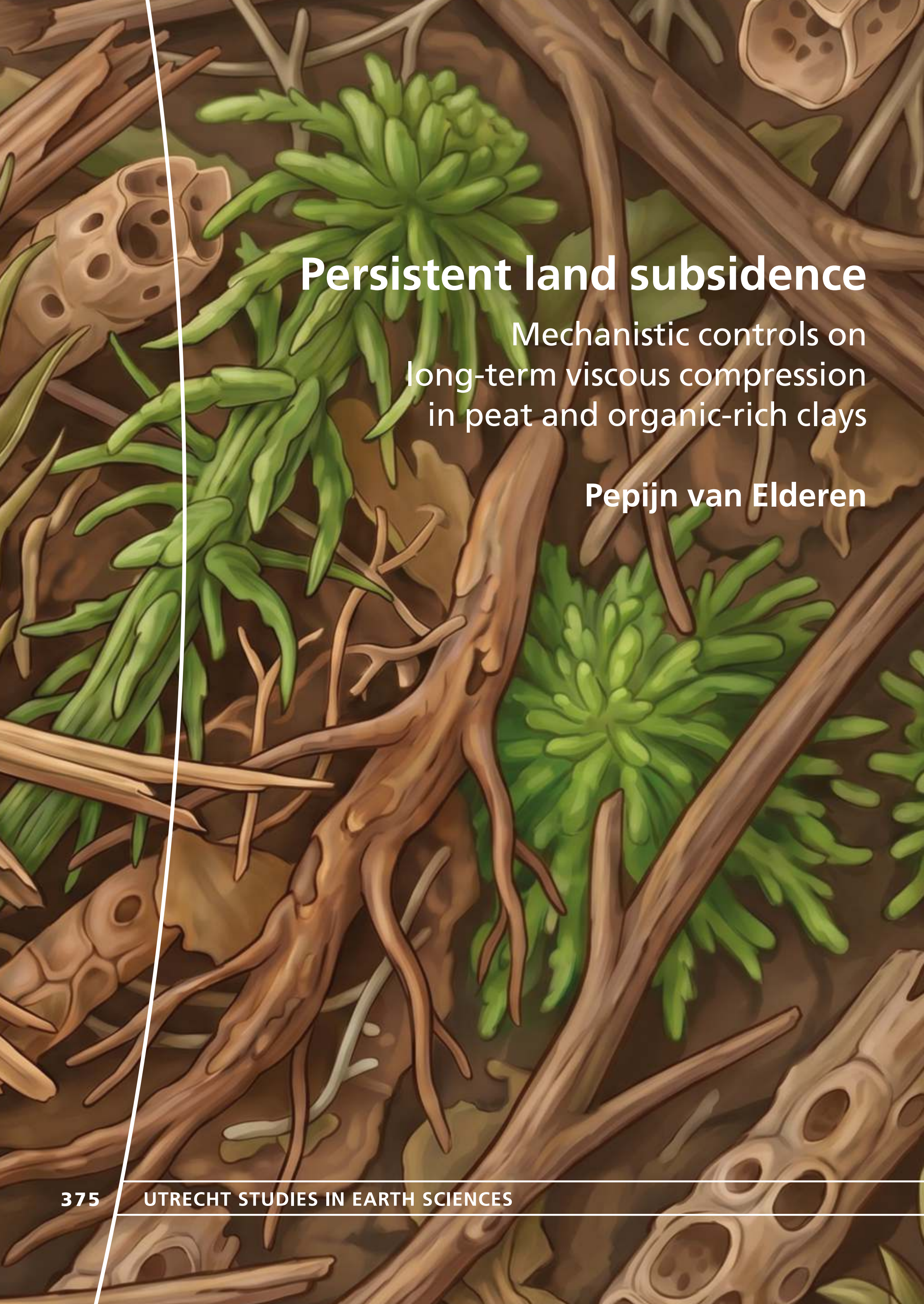

Persistent land subsidence

Mechanistic controls on long-term viscous compression in peat and organic-rich clays

Pepijn van Elderen

375 UTRECHT STUDIES IN EARTH SCIENCES

Persistent land subsidence:
Mechanistic controls on long-term viscous compression in peat and organic-rich clays

Pepijn van Elderen

ISBN/EAN: 978-90-6266-749-9
Published by: Faculty of Geosciences, Universiteit Utrecht, The Netherlands, in:
Utrecht Studies in Earth Sciences (USES), ISSN 2211–4335
Cover image: Artistic representation of plant remains in a peat matrix, produced by Pepijn van Elderen with the use of Illustrae
Cover design: Margot Stoete
Chapter covers:
Chapter 1 – Reed (Phragmites australis)
Chapter 2 – Round-leaved sundew (Drosera rotundifolia)
Chapter 3 – Marsh fern (Thelypteris palustris)
Chapter 4 - Cross-leaved heath (Erica tetralix)
Chapter 5 – Bog rosemary (Andromeda polifolia)
Chapter 6 – Bulrush (Typha latifolia)
References – Peat moss (Sphagnum palustre)
Layout and Printed by: Optima Grafische Communicatie (www.ogc.nl)
Correspondence to: pepijn.van.elderen@gmail.com

Persistent land subsidence:
Mechanistic controls on long-term viscous compression in peat and organic-rich clays

Aanhoudende bodemdaling:
Aanhoudende bodemdaling: mechanismen en processen achter viskeuze compressie in veen en organische klei
(met een samenvatting in het Nederlands)

Proefschrift

ter verkrijging van de graad van doctor aan de
Universiteit Utrecht
op gezag van de
rector magnificus, prof. dr. ir. W. Hazeleger,
ingevolge het besluit van het College voor Promoties
in het openbaar te verdedigen op

donderdag 9 juli 2026 des middags te 4.15 uur

door

Pepijn van Elderen

geboren op 27 januari 1997
te Breda

Promotoren:
Prof. dr. E. Stouthamer
Prof. dr. H. Middelkoop

Copromotor:
Dr. G. Erkens

Beoordelingscommissie:
Dr. R.M.A. Govers
Prof. dr. J. Griffioen
Prof. dr. ir. C. Jommi
Dr. H. Kooi
Prof. dr. C. Meisina

The research in this thesis is part of research project Living on Soft Soils – Subsidence and Society (Grant NWA.1160.18.259). This project is funded through the Dutch Research Council (NWO-NWA-ORC),Utrecht University, Wageningen University, Delft University of Technology, Ministry of Infrastructure and Water Management, Ministry of the Interior and Kingdom Relations, Deltares, Wageningen Environmental Research, TNO - Geological Survey of The Netherlands, STOWA, Water Authority: Hoogheemraadschap de Stichtse Rijnlanden, Water Authority: Drents Overijsselse Delta, Province of Utrecht, Province of Zuid-Holland, Municipality of Gouda, Platform Soft Soil, Sweco, Tauw BV, NAM.

Utrecht Studies in Earth Sciences 375

Persistent land subsidence
Mechanistic controls on long-term viscous compression in peat and organic-rich clays

Pepijn van Elderen

Utrecht 2026

Faculty of Geosciences, Utrecht University

Blad.
Nervatuur binnen een begrenzing,
Van natuurlijk evenwicht.

Icoon voor een begrip.
Blad met vele woorden.

Letters staan bijeen.
Ik werp ze in de lucht.

Ze zweven hoog.
Gaan en als ze komen.

Nieuw beeld in mijn hoofd.
In structuur met nieuwe woorden.

Verschijnt het, op
Blad

'Blad' from 'Poëzie in Woord en Beeld van Her en Komst', by Cees Dubbeldam.

Table of Contents

Summary

Low-lying coastal and deltaic regions worldwide are confronted with compaction of shallow, compressible subsurface layers, which results in land subsidence, the lowering of the surface. Land subsidence poses a significant problem since it increases flood risk, can damage buildings and infrastructure, enhances saltwater intrusion and coastal erosion. In many of these regions, including large parts of the Netherlands, subsidence rates exceed absolute sea-level rise and therefore directly impact the effectiveness of flood protection systems, water management strategies, and urban development policies. Subsidence in such environments is strongly controlled by the build-up of the shallow subsurface and the material properties of its layers. Areas dominated by sequences of peat and organic-rich clays often show the highest subsidence rates due to their high compressibility. These soft materials can compact strongly due to drainage, loading, and porewater pressure decrease. Compaction can be divided into various components, including consolidation, shrinkage and viscous compression. A part of compaction is elastic, which means that the deformation is reversible and the surface can rise again after subsiding. However, most problematic is inelastic compaction, which results in a permanent lowering of the surface. The various components of compaction each act at different time scales. Compaction acting over relatively short time periods up to several years, dominated by consolidation, is relatively well understood and incorporated into engineering practice. On the other hand, compaction over years to decades is more challenging to understand and makes long-term predictions uncertain.

Long-term compaction is largely caused by viscous compression: a time-dependent compaction process of subsurface material compression that persists under constant stress, the vertical pressure acting on the subsurface material. In other words, viscous compression continues even when boundary conditions remain unchanged, and therefore, it can continue for decades after initial loading or drainage. Especially peat and clay, as the most compressible subsurface materials, are susceptible to viscous compression. While viscous compression of clay has been studied substantially before, viscous compression of peat has received little scientific attention. Peat is also prone to decomposition, the breakdown of organic matter by microbes. This can weaken the peat structure, change material characteristics and increase its compaction rate. To further complicate the matter, peat and organic-rich clay exhibit strong spatial variability in composition, structure, and degree of decomposition. This variability extends both laterally and vertically, and material characteristics differ even within individual subsurface layers. These complexities are poorly represented in commonly used methods to quantify past, present and future subsidence, which rely largely on conceptual models and parameterisations that assume homogeneous material properties. Because of the limited understanding of viscous compression of peat, model predictions often underestimate long-term subsidence of peat and organic-rich clay, especially under low stress conditions, leading to discrepancies of orders of magnitude between predicted and observed compaction. The main objective

of the research is to advance the mechanistic understanding of viscous compression and its role in long-term compaction behaviour in order to help improving the predictive capacity of land subsidence models, particularly for peat and organic clays.

To reach this objective, three research steps were taken: 1) identify the mechanisms and processes that cause viscous compression in organic-rich subsurface layers, 2) determine and quantify the influence of organic matter decomposition on viscous compression, and 3) translate the improved mechanistic understanding into improved predictive capacity of subsidence models through more representative parameterisation of viscous compression.

A useful starting point to identify the mechanisms and processes of viscous compression of peat is to review the mechanisms and processes identified for viscous compression of clay. Although peat and clay are both very compressible, they have different material characteristics which are important for their compressibility. For example, clay has small, dense, often stacked particles with electrically charged surfaces, leading to a small adsorbed water layer, and strong attractive and repulsive forces between particles. Peat, on the other hand, has larger particles that physically grip onto one another, generally holds more water inside the particles, and originate from plant remnants. Both clay and peat show a mix of different sized pores, with peat having larger pores on average. Viscous compression of clay is governed primarily by micropore water expulsion, changes in the adsorbed water layer, and changing interactions of particles. These mechanisms also exist in peat, but the organic matrix, composed of fibres of variable integrity, size, and botanical origin, introduces additional complexity. Fibres can interlock more than clay particles, the plant cells contain water that cannot be expelled like water in clay micropores, and large particle contact areas generate resistance against movement. Furthermore, a lower or absent surface charge of fibres and decomposed organic matter diminishes the role of adsorbed water and can lead to more resistance between particles. Six key controls of viscous compression in peat were identified: degree of decomposition, progressive decomposition, clay fraction, temperature, pH, and ion concentration. The degree of decomposition and progressive decomposition are unique to peat compared to clay and therefore highly important in explaining the differences between the two materials. The six controls underscore that viscous compression of peat cannot be explained solely as a physical or biochemical process. Instead, it occurs as the result of a dynamic interaction between fibre-scale structure, porewater diffusion, and biochemical transformation.

Because the degree of decomposition and its temporal progression were found to play a central role in viscous compression, a more detailed investigation was needed to properly understand and quantify the interaction between viscous compression and decomposition. This considered both the effect of compaction on decomposition rates and the feedback of decomposition-induced changes on material compressibility. Decomposition was quantified through respiration tests, which measure the CO_2 produced during decomposition. Combined with compression tests it was possible to experimentally show that porosity acts as a critical control: reductions in pore space caused by compaction suppress microbial respiration in fibrous peat, which is relatively undecomposed. In already decomposed material, with lower porosity, compaction causes a smaller reduction in decomposition. Consequently, less decomposed peat experiences stronger compaction under equal loading conditions because its high porosity and flexible fibre structure permit substantial particle reorientation and compression. At the same time, the induced reduction in porosity constrains future decomposition by limiting oxygen and substrate transport. This interdependence implies that the degree of decomposition governs the initial compressibility, while progressive decomposition reduces the rate of future compaction. These findings challenge the assumption of most subsidence models that progressive decomposition is too slow to influence mechanical behaviour within engineering timescales of residual compaction of buildings, which is in the order of 10 years. Instead, the results show that decomposition and viscous compression limit each other and jointly control long-term subsidence.

To translate these mechanistic insights into improved predictive capacity, a large dataset consisting of results from oedometer and CRS compression tests, and supplementary characteristics tests was analysed. Materials listed either as "Peat" or "Clay" were grouped into lithological classes based on their material characteristics. The differences in the viscous compression parameter, indicating the amount of viscous compression per logarithmic unit of time, between the lithological classes were determined. Samples were grouped into four classes, i.e., Clay, Clayey Peat, Fibrous Peat, and Decomposed Peat, revealing that viscous compressibility generally increased with organic content, with fibrous peat showing the highest susceptibility to long-term compaction. However, decomposed peat displayed lower viscous compression susceptibility despite being organic-rich, reflecting its more compacted, interlocked structure and smaller residual pore space. For clastic materials, the viscous compression parameter could be predicted reasonably well using water content and dry bulk density. However, within the peat classes variability remained large, which made predictions uncertain. This variability of viscous compression intensity of peat highlights that specific organic structural characteristics such as fibre size, tensile strength, and botanical origin of the organic matter influence compressibility in ways not captured by the simpler bulk density and water content. Complementary to the identified interaction between viscous compression and decomposition, these results demonstrate that decomposition induces a systematic and progressive decrease in the compressibility of organic soils, which are directly relevant for improving the parameterization of viscous compression in predictive subsidence models.

Another improvement of predictive models lies in the way overconsolidated conditions are handled. Material is overconsolidated when its current effective stress is lower than its preconsolidation stress, which may result from past higher loadings, or when time-dependent processes such as viscous compression or aging have increased its apparent stiffness. This is expressed by the overconsolidation ratio, i.e., the preconsolidation stress divided by the current stress. Viscous compression under overconsolidated conditions can be assessed by analysing the viscous compression parameter for moments when the samples are overconsolidated in compression tests. The viscous compression parameter at overconsolidated conditions needs to be determined through an iterative method. This determination is usually done using a logarithmic method at normally consolidated conditions, when the applied or current stress is the maximum stress material has experienced. The analysis demonstrated that the viscous compression parameter can be several times higher (i.e., viscous compression occurs faster with a higher parameter value) when determined for overconsolidated conditions compared to normally consolidated conditions. Validation shows that viscous compression calculations with the new overconsolidated parameter values match measurements better than viscous compression calculations with the normally consolidated parameter values. For very high overconsolidation ratios (> 5) the viscous compression parameter values seem to decrease slightly. These ratios correspond to a high intrinsic time; the time material would need to reach its current compaction state with the currently applied load. High ratios indicate a high maximum stress previously, accompanied by fast compaction rates. As a result, intrinsic time at low stresses during later time periods after loading will drastically increase. Viscous compression thus first shows a logarithmically decreasing rate; then, at long intrinsic times, the rate stabilises or even increases, and eventually the rate will start decreasing again. Consequentially, the isotachs, timelines indicating the intrinsic time of material with stress and compaction state, are not equidistant, but can be non-equidistant or even bending or diverging. Further testing and modelling are needed to fully understand and integrate this varying viscous compression parameter into models.

Combining the insights from the individual chapters, the thesis discusses how viscous compression is currently understood and modelled. Rather than treating viscous compression and decomposition as independent mechanisms of volume loss, the results show that they limit each other as they both alter porosity, particle strength, water mobility, and microstructural integrity. Decomposition weakens fibres and organic particles, facilitating reorientation and collapse, while compaction (and thus viscous compression) restricts further decomposition by constraining microbial access to pore space. Effectively, decomposition enables more viscous compression in total, but spreads this additional compression over an extended period of time. This sequence of events explains long-term subsidence trends that conventional models cannot reproduce, i.e., the persistent compaction of peat layers despite decades of stable loading and groundwater levels, can be interpreted as the combined effect of evolving microstructure, stress history, and slow, ongoing decomposition.

A key implication of this mechanistic understanding is the need for a variable viscous compression parameter in predictive models. In current models, the viscous compression parameter is treated as a fixed material constant, but the findings of this thesis show that it evolves with decomposition state, effective stress, overconsolidation ratio, and intrinsic time. This not only allows models to capture the dynamic nature of viscous compression more realistically, but also might help to connect the laboratory scale, in order of centimeters, to field scales, in order of square meters to hectares.

Samenvatting

Laaggelegen kust- en deltagebieden worden wereldwijd geconfronteerd met compactie van ondiepe, samendrukbare ondergrondse lagen, wat resulteert in bodemdaling: het verlagen van het aardoppervlak. Bodemdaling vormt een aanzienlijk probleem, omdat dit proces het overstromingsrisico vergroot, schade kan toebrengen aan gebouwen en infrastructuur, en zoutwaterintrusie en kusterosie versterkt. In veel van deze gebieden, waaronder grote delen van Nederland, is gaat de bodemdaling sneller dan absolute zeespiegelstijging. Daardoor heeft bodemdaling een grote invloed op de effectiviteit van waterkeringen, watermanagement en stedelijke ontwikkeling. In laag gelegen kust- en deltagebieden wordt bodemdaling sterk bepaald door de opbouw van de ondiepe ondergrond en de materiaaleigenschappen van de verschillende lagen. Gebieden die worden gedomineerd door opeenvolgingen van veen, lagen van dode plantenresten, en organisch-rijke kleien vertonen doorgaans de hoogste bodemdalingssnelheden vanwege hun hoge samendrukbaarheid. Deze 'zachte' materialen kunnen sterk compacteren als gevolg van drainage, belasting en verlaging van de poriewaterdruk. Compactie kan worden onderverdeeld in verschillende componenten, waaronder consolidatie, krimp en viskeuze compressie. Een deel van de compactie is elastisch, wat betekent dat de vervorming omkeerbaar is en de bodem weer kan terugveren zodra bijvoorbeeld de belasting verwijderd wordt. Het meest problematisch is echter de inelastische compactie, die leidt tot een blijvende verlaging van het landoppervlak. De verschillende componenten van compactie werken ieder op andere tijdschalen. Compactie die plaatsvindt over relatief korte tijdsperioden, tot enkele jaren, en die wordt gedomineerd door consolidatie, is relatief goed begrepen en geïntegreerd in de praktijk. Compactie over perioden van jaren tot decennia is daarentegen moeilijker te doorgronden en maakt voorspellingen op lange termijn onzeker.

De compactie op lange termijn wordt grotendeels veroorzaakt door viskeuze compressie: een tijdsafhankelijk compactieproces waarbij ondergrondmateriaal blijft samendrukken onder constante stress, dat wil zeggen de verticale belasting die op het materiaal wordt uitgeoefend. Met andere woorden: viskeuze compressie gaat door, zelfs wanneer de randvoorwaarden onveranderd blijven, en kan daarom nog tientallen jaren aanhouden na een initiële belasting of drainage. Met name veen en klei, als de meest samendrukbare ondergrondmaterialen, zijn gevoelig voor viskeuze compressie. Hoewel viskeuze compressie in klei uitgebreid is bestudeerd, heeft viskeuze compressie van veen minder wetenschappelijke aandacht gekregen. Daarnaast is veen gevoelig voor afbraak (decompositie): het door micro-organismen afbreken van organisch materiaal. Dit kan de veenstructuur verzwakken, materiaaleigenschappen veranderen en de compactiesnelheid verhogen. De complexiteit neemt verder toe doordat veen en organisch-rijke kleien een sterke ruimtelijke variabiliteit vertonen in samenstelling, structuur en mate van decompositie. Deze variatie is zowel lateraal als verticaal aanwezig, en materiaaleigenschappen verschillen zelfs binnen individuele ondergrondlagen. Deze complexiteit wordt onvoldoende weergegeven in veelgebruikte methoden om bodemdaling in het verleden, heden en de toekomst te kwantificeren. Dergelijke methoden zijn grotendeels

gebaseerd op conceptuele modellen en parameters die uitgaan van homogene materiaaleigenschappen. Door het beperkte begrip van viskeuze compressie van veen onderschatten modelvoorspellingen vaak de bodemdaling op de lange termijn van veen en organisch-rijke kleien, vooral onder lage belastingen. Dit leidt tot verschillen van meerdere ordegroottes tussen de voorspelde en gemeten compactie.

Het hoofddoel van dit onderzoek is het vergroten van het mechanistische begrip van viskeuze compressie en haar rol in het lange termijngedrag van compactie, met als doel de voorspellende capaciteit van bodemdalingsmodellen te verbeteren, in het bijzonder voor veen en organisch-rijke kleien. Om dit doel te bereiken zijn drie onderzoeksstappen gezet: 1) het identificeren van de mechanismen en processen die viskeuze compressie van organisch-rijke ondergrondlagen veroorzaken; 2) het bepalen en kwantificeren van de invloed van decompositie van organisch materiaal op viskeuze compressie; en 3) het vertalen van het verbeterde mechanistische inzicht naar een verhoogde voorspellende capaciteit van bodemdalingsmodellen door middel van betere parameterisatie voor viskeuze compressie.

Een geschikt uitgangspunt voor het identificeren van de mechanismen en processen die verantwoordelijk zijn voor viskeuze compressie van veen is een analyse van de mechanismen die zijn vastgesteld voor viskeuze compressie van klei. Hoewel veen en klei beide zeer samendrukbaar zijn, verschillen zij wezenlijk in materiaaleigenschappen die bepalend zijn voor hun samendrukbaarheid. Klei bestaat uit kleine, dichte, vaak gestapelde deeltjes met elektrisch geladen oppervlakken, wat leidt tot dunne geadsorbeerde waterlagen en sterke aantrekkende en afstotende krachten tussen de deeltjes. Veen daarentegen bestaat uit grotere deeltjes die zich mechanisch in elkaar kunnen grijpen, doorgaans meer water vasthouden binnenin de deeltjes zelf, en afkomstig zijn van plantenresten. Zowel klei als veen worden gekenmerkt door poriën met verschillende afmetingen, maar waarbij veen gemiddeld grotere poriën heeft. Viskeuze compressie van klei wordt voornamelijk gestuurd door het uitpersen van water uit microporiën, veranderingen in de geadsorbeerde waterlaag en veranderende interacties tussen kleideeltjes. Deze mechanismen zijn ook in veen aanwezig, maar de organische matrix, bestaande uit vezels met wisselende decompositiegraad, grootte en botanische oorsprong, introduceert aanvullende complexiteit. Vezels kunnen sterker in elkaar grijpen dan kleideeltjes, plantencellen bevatten water dat niet op dezelfde manier kan worden uitgedrukt als water in de microporiën van klei, en grote contactvlakken tussen deeltjes genereren meer weerstand tegen verplaatsing. Bovendien vermindert een lage of afwezige oppervlaktelading van vezels en ontbonden organisch materiaal de rol van geadsorbeerd water en kan dit leiden tot grotere wrijving tussen deeltjes. Er zijn zes belangrijke factoren geïdentificeerd die viskeuze compressie van veen sturen: decompositiegraad, actieve decompositie, kleigehalte, temperatuur, pH en ionenconcentratie. De decompositiegraad en actieve decompositie zijn uniek voor veen ten opzichte van klei en spelen daarom een sleutelrol bij het verklaren van de verschillen tussen beide materialen. Deze zes factoren benadrukken dat viskeuze compressie van veen niet uitsluitend kan worden verklaard als een puur fysisch of biochemisch proces, maar voortkomt uit een dynamische interactie tussen veranderingen van de vezelstructuur, poriewaterdiffusie en biochemische transformatie.

Omdat zowel de decompositiegraad als de actieve decompositie een centrale rol blijken te spelen bij viskeuze compressie, was een gedetailleerdere analyse nodig om de wisselwerking tussen viskeuze compressie en decompositie goed te begrijpen en te kwantificeren. Hierbij is zowel gekeken naar de invloed van compactie op ontbindingsnelheden als naar de terugkoppeling van door ontbinding veroorzaakte veranderingen in materiaaleigenschappen op de samendrukbaarheid. Decompositie werd gekwantificeerd met behulp van respiratietesten, waarbij de CO_2-productie tijdens ontbinding wordt gemeten. In combinatie met compressietesten kon experimenteel worden aangetoond dat porositeit een cruciale rol speelt: afname van de porieruimte door compactie vermindert de microbiële respiratie in vezelrijk, weinig ontbonden veen. In reeds ontbonden materiaal, met een lagere porositeit, leidt compactie tot een geringere afname van decompositie. Minder ontbonden veen ondergaat sterkere compactie onder gelijke belasting, omdat de hoge porositeit en flexibele vezelstructuur aanzienlijke heroriëntatie en samendrukking van de deeltjes mogelijk maken. Tegelijkertijd beperkt de door compactie veroorzaakte porositeitsafname toekomstige decompositie door transport van zuurstof en substraat te reduceren. Deze wederzijdse afhankelijkheid impliceert dat de decompositiegraad de initiële samendrukbaarheid bepaalt, terwijl actieve decompositie de snelheid van toekomstige compactie reduceert. Deze bevindingen weerspreken de aanname die in veel bodemdalingmodellen wordt gehanteerd, namelijk dat voortschrijdende ontbinding te traag is om mechanisch gedrag te beïnvloeden binnen de restzettingsperiodes van gebouwen die ingenieurs hanteren, die ingenieurs hanteren, vaak in de orde van tien jaar liggen. In plaats daarvan laten de resultaten zien dat decompositie en viskeuze compressie elkaar beperken en gezamenlijk de lange-termijn bodemdaling sturen.

Om deze mechanistische inzichten te vertalen naar een verbeterde voorspellende capaciteit is een grote dataset geanalyseerd, bestaande uit resultaten van oedometer- en CRS-compressietesten, aangevuld met de materiaaleigenschappen van de monsters. Materialen die als “veen” of “klei” waren geclassificeerd, zijn gegroepeerd in lithologische klassen op basis van hun materiaaleigenschappen. De verschillen in de viskeuze compressieparameter, die de hoeveelheid viskeuze compressie per logaritmische tijdseenheid weergeeft, tussen deze klassen zijn bepaald. De monsters zijn onderverdeeld in vier klassen: klei, kleiig veen, vezelig veen en ontbonden veen. Hieruit blijkt dat de gevoeligheid voor viskeuze compressie in het algemeen toeneemt met het organische stofgehalte, waarbij vezelig veen het meest gevoelig is voor lange-termijn compactie. Ontbonden veen vertoonde echter een lagere gevoeligheid voor viskeuze compressie, ondanks het hoge organische gehalte, wat wijst op een dichtere, sterker in elkaar grijpende vezelstructuur met een lagere porositeit. Voor klastische materialen kon de viskeuze compressieparameter redelijk goed worden voorspeld op basis van watergehalte en droge bulkdichtheid. Binnen de veenklassen bleef de variabiliteit echter groot, wat de voorspelbaarheid beperkte. Deze variatie benadrukt dat specifieke organische structurele kenmerken, zoals vezelafmetingen, treksterkte en botanische oorsprong, de samendrukbaarheid beïnvloeden op manieren die niet worden vastgelegd met eenvoudige parameters zoals dichtheid en watergehalte. In combinatie met de vastgestelde interactie tussen viskeuze compressie en decompositie tonen deze resultaten aan dat decompositie leidt tot een systematische en geleidelijke afname van de samendrukbaarheid van organische bodems, wat direct relevant is voor het verbeteren van de parameterisatie van viskeuze compressie in voorspellende bodemdalingsmodellen.

Een verdere verbetering van voorspellende modellen ligt in de manier waarop overgeconsolideerde omstandigheden worden behandeld. Materiaal is overgeconsolideerd wanneer de huidige effectieve stress lager is dan de preconsolidatie stress, bijvoorbeeld als gevolg van vroegere hogere belastingen, of wanneer tijdsafhankelijke processen zoals viskeuze compressie of veroudering de ogenschijnlijke stijfheid hebben vergroot. Dit wordt uitgedrukt met de overconsolidatie ratio, gedefinieerd als de verhouding tussen de preconsolidatie stress en de huidige stress. Viskeuze compressie onder overgeconsolideerde omstandigheden is op een nieuwe manier geanalyseerd door de viskeuze compressieparameter te bepalen op momenten waarop monsters in compressietests overgeconsolideerd zijn. Deze parameter moet daarbij iteratief worden bepaald. Gewoonlijk wordt de viskeuze compressieparameter afgeleid met een logaritmische methode onder normaal geconsolideerde omstandigheden, wanneer de aangelegde spanning de hoogste spanning is die het materiaal heeft ondergaan. De analyse liet zien dat de viskeuze compressieparameter onder overgeconsolideerde omstandigheden meerdere malen groter kan zijn (dat wil zeggen: viskeuze compressie verloopt sneller als de parameterwaarde hoger is) dan onder normaal geconsolideerde omstandigheden. Validatie toont aan dat berekeningen met de nieuwe parameters voor overgeconsolideerde situaties beter overeenkomen met metingen dan berekeningen waarbij normaal geconsolideerde parameters worden toegepast. Bij zeer hoge overconsolidatie ratio's (>5) lijkt de viskeuze compressieparameter licht af te nemen. Deze hoge ratio's corresponderen met een hoge intrinsieke tijd: de tijd die het materiaal nodig zou hebben om onder de huidige belasting zijn huidige compactiegraad te bereiken. Hoge ratio's duiden erop dat het materiaal een hoge ogenschijnlijke maximale spanning en snelle compactiesnelheden heeft ervaren. Hierdoor neemt de intrinsieke tijd die bij lage spanningen in latere perioden hoort sterk toe. De snelheid van viskeuze compressie neemt daardoor eerst logaritmisch af, stabiliseert of neemt zelfs licht toe bij een hoge intrinsieke tijd, en kan uiteindelijk opnieuw afnemen naarmate tijd voortschrijdt. Als gevolg hiervan liggen isotachen, tijdlijnen die de intrinsieke tijd van materiaal weergeven als functie van spanning en compactietoestand, niet noodzakelijkerwijs op dezelfde afstand van elkaar, maar kan deze afstand ongelijkmatig zijn, maar ook kunnen de isotachen gekromd zijn of divergeren. Verdere experimenten en modellering zijn nodig om deze variabiliteit in viskeuze compressie bij overgeconsolideerde omstandigheden volledig te doorgronden en in modellen te integreren.

Door de inzichten uit de afzonderlijke hoofdstukken te combineren, bespreekt dit proefschrift hoe viskeuze compressie momenteel wordt begrepen en gemodelleerd. In plaats van viskeuze compressie en decompositie te beschouwen als onafhankelijke mechanismen van volumeverlies, laten de thesis resultaten zien dat zij elkaar controleren doordat beide processen porositeit, deeltjessterkte, watermobiliteit en microstructurele integriteit beïnvloeden. Decompositie verzwakt vezels en organische deeltjes, en vergemakkelijkt heroriëntatie en ineenstorting, terwijl compactie, en daarmee viskeuze compressie, verdere decompositie beperkt de porieruimte waarin microbacteriële afbraak kan plaatsvinden. Decompositie maakt dus per saldo meer viskeuze compressie mogelijk, maar spreidt deze extra compactie uit over een langere tijdsperiode. Deze opeenvolging verklaart lange termijn bodemdalingstrends die met conventionele modellen momenteel niet kunnen worden gereproduceerd: de aanhoudende compactie van veenlagen ondanks decennia van stabiele belasting en grondwaterstanden kan worden geïnterpreteerd als het gecombineerde effect van een evoluerende microstructuur, belastingsgeschiedenis en langzame, actieve decompositie.

Een belangrijke implicatie van dit mechanistische inzicht is de noodzaak van een variabele viskeuze compressieparameter in voorspellende modellen. In huidige modellen wordt deze parameter behandeld als een vaste materiaalconstante, terwijl de bevindingen van dit proefschrift aantonen dat deze verandert met de decompositiegraad, effectieve stress, overconsolidatie ratio en intrinsieke tijd. Dit maakt het niet alleen mogelijk om de dynamiek van viskeuze compressie realistischer te modelleren, maar kan ook helpen om de kloof te overbruggen tussen laboratoriumschaal (orde van centimeters) en veldschaal (orde van vierkante meters tot hectares).

Chapter 1:

General introduction

Land subsidence is a global phenomenon, occurring on every continent and in settings ranging from remote tectonic basins to densely populated urban areas. Its most severe and widespread impacts, however, are often found in wetland, coastal, and deltaic regions, where high population density coincides with highly compressible subsurface layers (e.g., Yuill et al., 2009; Erkens et al., 2015). Many of the world's major deltas, such as the Mekong, Mississippi, Yangtze, and Rhine-Meuse deltas, experience subsidence rates that exceed the rate of sea-level rise. This subsidence relative to sea level rise leads to an amplification of flood risk, threatens water management, and puts stress on current land use, while differential land subsidence causes damages to buildings and infrastructure (e.g., Teatini et al., 2005; Shi et al., 2008; Törnqvist et al., 2008; Sneed et al., 2013; Ye et al., 2016; Minderhoud et al., 2017; Van Asselen et al., 2018). Within these coastal and deltaic regions, the most susceptible areas to subside are locations with soft subsurface materials, particularly peat and (organic-rich) clays. Yet, the population of such low-lying and subsiding locations is often still increasing. As sea levels rise and human activity intensifies in many low-lying regions, the risks associated with land subsidence are becoming more pressing. Depending on the location, land subsidence is caused by either deep drivers, e.g., tectonics or hydrocarbon extraction, or shallow drivers, e.g., loading, drainage or groundwater extraction. Despite the widespread potential impacts, it remains challenging to understand the underlying mechanisms of especially long-term subsidence due to the heterogeneity in material composition and connected mechanistic behaviour of subsurface layers.

1.1 Drivers, mechanisms and processes of land subsidence

Given its widespread and growing impact, understanding the underlying mechanisms, processes and drivers of land subsidence in peat and organic-rich clay layers is essential to develop effective management strategies to mitigate subsidence and its negative impacts. Drivers are external influences that induce or modify subsidence. Examples of these drivers include hydrocarbon and groundwater extraction, loading of the subsurface by buildings and infrastructure, or drainage of waterlogged areas (Fig. 1.1). The surface lowering observed in affected areas results from a combination of physical and biochemical processes, e.g., consolidation or decomposition, leading to changes in the subsurface material, and mechanisms, which represent how processes lead to subsidence. For example, when a house is built, this generates loading onto the subsurface layer on which the foundation of the house is constructed. This loading is the *driver* in this example. As a result, porewater pressure in the loaded subsurface layers rises and causes the *process* of pore water flow towards lower pressure zones in the subsurface, which can be for example in the subsurface around the house. Because of this water outflow, pores in the subsurface below the house close, which is called consolidation and is the *mechanism* leading to subsidence.

Both processes and mechanisms of land subsidence act at different depths and over varying timescales (e.g., van Asselen et al., 2009). The processes and mechanisms are initiated by both natural and anthropogenic drivers (Fig. 1.1). At greater depths (hundreds of meters to kilometers), tectonic movements and isostatic adjustment act naturally over long timescales of decades to millennia, while hydrocarbon extraction and deep mining represent deep anthropogenic drivers and act over years to decades. At shallow (centimeters to meters) to intermediate depths (tens to hundreds of meters), drivers and processes act over shorter time spans of days to decades. Subsidence often shows a large spatial variability, along with spatial differences in drivers and subsurface heterogeneity, which in turn drive different mechanisms and processes of subsidence.

Loading and drainage lead to compaction of peat and organic-rich clay layers, while drainage also drives biochemical decomposition of organic material, facilitating elevation loss. The compaction is caused by the mechanisms shrinkage, consolidation and viscous compression. All these mechanisms lead to increased effective stress. Effective stress is defined as the total pressure, which is determined by loading, minus the porewater pressure, which carries a part of the total pressure (Terzaghi, 1925). Thus, the effective stress quantifies the pressure carried by the solid particles. Shrinkage is the volume reduction as a result of drying and a consequential increase in suction leading to a higher effective stress (e.g., Tempany, 1917; Lexmond et al., 2024), consolidation is the expulsion of overpressured porewater after a loading event leading to an effective stress decrease (e.g. Terzaghi, 1941), and viscous compression is the volume reduction as a result of reorientation of particles (e.g., Le et al., 2012) (Fig. 1.1). While consolidation and shrinkage are limited in time, depth or both, viscous compression continues under constant load even after porewater pressure has dissipated, and mathematically its rate never drops to absolute zero, making it a long-term and less predictable contributor to land subsidence. This process is especially relevant in peat and organic-rich clay, where high water content and organic matter facilitate prolonged deformation (Den Haan and Kruse, 2007). However, compared to other compaction mechanisms, viscous compression is less well understood and more difficult to quantify in predictive models of subsidence, particularly under low loadings. This challenge is evident from comparisons between laboratory-based compression tests and numerical model predictions for low-loading conditions, where measured compaction can exceed modelled values by factors of 10^4 to 10^6 (Deltares, 2024). A high-load field case at Kansai Airport near Osaka shows a similar discrepancy: the airport is projected to experience 3.9–6.2 m more subsidence than initial models at the start of construction predicted for 2100, attributed to inconsistencies between laboratory-based model outputs and field measurements (Hight and Leroueil, 2003; Mesri and Funk, 2015).

Compaction often simultaneously occurs with decomposition of organic material in the subsurface, which not only reduces the volume of organic solids, but also alters the material's microstructure and mechanical properties leading to a more tightly packed matrix (e.g., Brouns, et al., 2014). Both these changes are similar to what is believed to occur during viscous compression, but viscous compression and decomposition have mostly been addressed separately. Consequentially, the interaction between biochemical decomposition and mechanical viscous compression, and the resulting effect on subsidence remain poorly understood. This hampers our ability to mechanistically describe the unique long-term behaviour of organic-rich soils, especially in environments with fluctuating water levels and complex loading histories. In this thesis I examine the main contributor to long-term land subsidence in peat and organic clay layers, which is viscous compression, often referred to as creep (e.g., Den Haan, 1994).

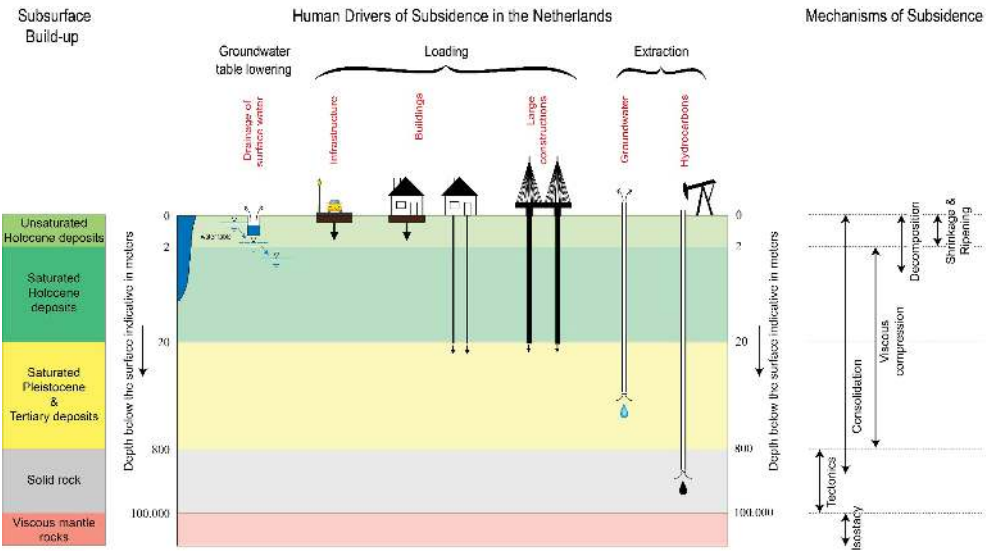

Figure 1.1: Schematic overview of drivers and mechanisms of land subsidence, with the associated subsurface constituents and indicative depth intervals of where these drivers and mechanisms occur. The shown depths are representative for the Netherlands. Modified after Minderhoud et al. (2015; 2025), Minderhoud (2019), van Asselen et al. (2019). Note the non-linear depth scale.

1.2 Characteristics of soft organic soils

To disentangle these coupled drivers, mechanisms, and processes of compaction in organic subsurface layers, it is essential to consider the fundamental material characteristics of organic soils The origin, composition, and microstructure of peat and clay directly control how it deforms and responds to prolonged loading. Peat forms under waterlogged conditions, which typically occur in protected environments behind coastal barriers or in areas of stagnant water distant from river channels. In these settings, limited or absent mineral sediment input during floods allows partially decomposed plant material to accumulate and be preserved in anoxic conditions. The hollow cellular tissue structure of the plant remains produces a substrate with very low density, extremely high water content, and a fibrous fabric. These characteristics make peat inherently soft and highly compressible, rendering it especially susceptible to subsidence once drained or subjected to loading (e.g., Landva, 2007; Mesri and Ajlouni, 2007). However, material properties such as internal structure and water-holding capacity vary strongly with plant type and clastic content, causing large spatial variability in subsidence behaviour even over short distances. Another important factor determining the variability of material characteristics is the state of the organic matter. Decomposition, the breakdown of organic matter, leads to a decrease in organic particle size, different pore size distribution, water content and susceptibility to compaction. Past decomposition, therefore, dictates the current material characteristics, while present and future decomposition can further change these characteristics, influencing long-term compaction. The material characteristics, decomposition history, and active decomposition can vary significantly in space. This spatial variability from multiple origins, together with its mechanical fragility, makes peat one of the most challenging and least understood subsurface materials to account for in engineering and land-use planning.

Organic-rich clay and clay-rich peat are transitional materials that typically form closer to river channels or marine environments than organic-rich peat. Here, water levels remain high enough for vegetation to develop and be preserved, yet flooding is more frequent and therefore sediment input is higher compared to areas where organic-rich peat is formed. Their composition, fine-grained mineral particles mixed with substantial organic matter, gives them properties that fall in between those of pure peat and mineral clays: less compressibility and more strength compared to organic-rich peat, but a higher subsidence potential compared to most clays (Al-Khafaji and Andersland, 1981; Zaffar and Luo, 2015). Organic-rich clay and clay-rich peat are often underrepresented in research and engineering practice, where they are commonly generalized as either ‘clay or ‘peat’, a simplification that overlooks their distinct and variable mechanical behaviour.

1.3 Land subsidence in the Netherlands

Understanding the behaviour of organic and transitional subsurface material is crucial in regions where they are abundantly present in the shallow subsurface, for example in the Netherlands, where they largely govern the magnitude and spatial variability of land subsidence. Especially the coastal-deltaic area of the country, covering c. 17.000 km^2 (Koster, 2017), faces subsidence caused by the drivers mentioned in section 1.1. Deep salt mining and especially gas extraction are the additional drivers of the subsidence in the northeastern part of the country. Most subsidence in the western and northern Netherlands, however, is driven by mechanisms occurring in the shallow subsurface, within the Holocene sequence, including groundwater table lowering, and loading from infrastructure and buildings (Erkens et al, 2016; Koster et al., 2018a; van Asselen et al., 2018). The subsurface in the coastal-deltaic area is characterized by predominantly highly organic and clay-rich layers, sporadically intercalated by sand bodies deposited by different generations of Rhine and Meuse river branches (e.g., Vos and van Heeringen, 1997; Berendsen and Stouthamer, 2000, 2001; Cohen et al., 2005; Stouthamer et al., 2011; Pierik et al., 2018; Vos et al., 2020). The sequence consisting of peat and clay layers can be >10 meters thick with the thickest Holocene sequence of more than 20 meters in the western part of the delta close to Rotterdam (Fig. 1.2) or in the northern former tidal inlets in the provinces of Friesland and Groningen (TNO-GDN, 2025). The development of the compressible layers in the western and northern part of the Netherlands is the result of 1) the long-standing presence of rivers which deposited clay in their flood basins, 2) the flooding of coastal areas by the sea with concurrent deposition of clay, and 3) the formation of the extensive peat fen and bog systems that developed in the western and northern Netherlands between the river branches (e.g., Vos et al., 2020). Since its formation, large volumes of peat have been mined for fuel purposes, and the remaining peat has faced considerable compaction and decomposition due to continuous groundwater level lowering for over 1000 years, which further decreased the remaining amount of peat in the Dutch subsurface (e.g., Erkens et al., 2016; Koster et al., 2018; van Asselen et al., 2018). As a result, the extent of peat occurrence in the current Dutch subsurface is still extensive (Fig. 1.3a and 1.3b), but 14.5 – 30.0 km^3 less than it used to be (Erkens et al., 2016).

The high compressibility of peat is well recognizable in maps of observed land subsidence rates in the western peat area, derived from GNSS and InSAR measurements (Fig. 1.3c). Subsidence rates are particularly high in areas where peat layers occur at shallow depth, in the order of multiple millimeters per year. Many of the largest Dutch cities, such as Amsterdam, Rotterdam and Utrecht, are situated within or at the rim of the peat area and thus face subsidence, causing damage to buildings and infrastructure. Striking is the historic city center of Gouda, which is situated in the middle of the western peat area with multiple meters of peat underlying the city centre, and experiences several millimeters of subsidence per year centuries after construction of the city and decades after the last surface raise (Kooi and Melman, 2024; NCG, 2025).

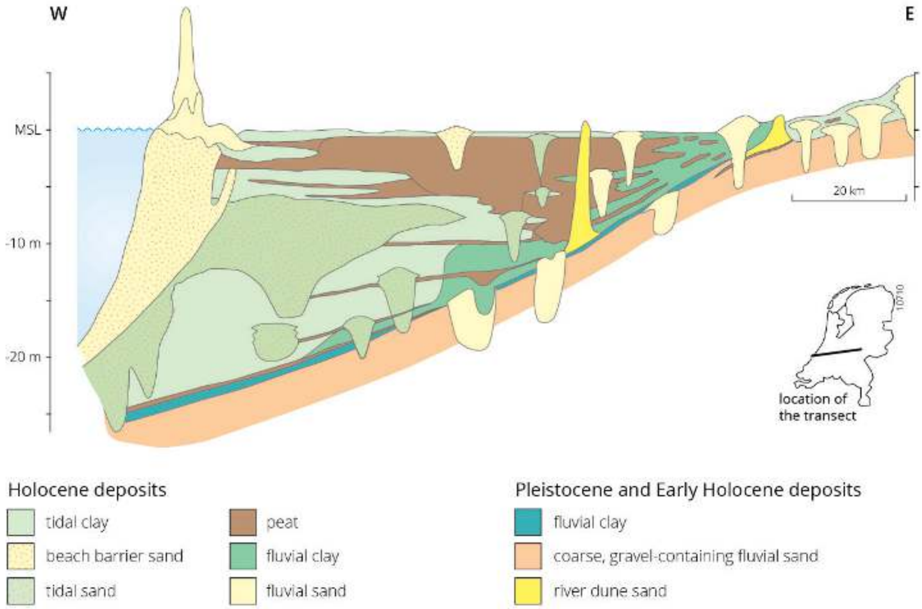

Figure 1.2: Schematic cross-section of the subsurface build-up of the Rhine-Meuse Delta in the Netherlands exemplifying the large depth of compressible layers that are present in the Netherlands (after Zagwijn, 1986; Stouthamer et al., 2023).

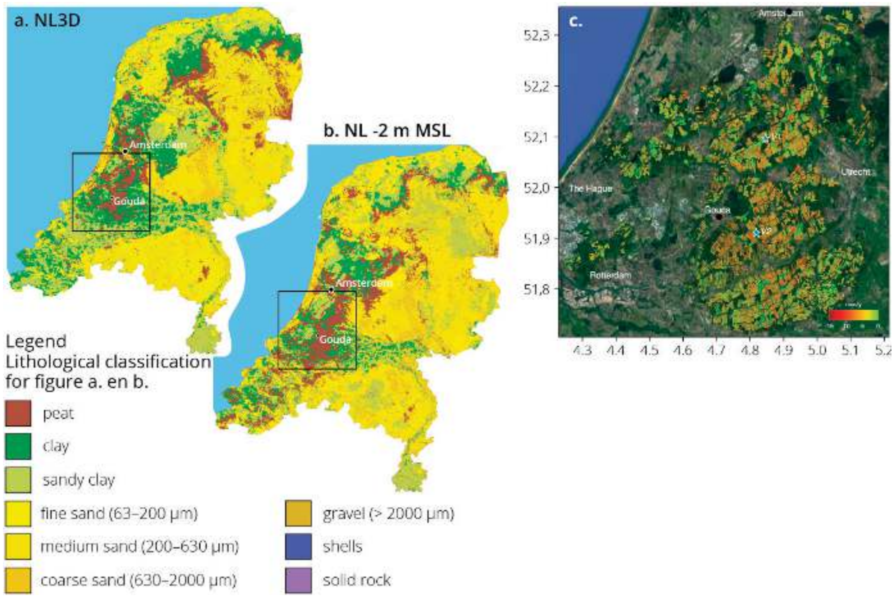

Figure 1.3: The spatial distribution of subsurface material in the Netherlands at a) the surface, and at b) 2 meters below the surface. These maps show the highest subsurface material probability at 250 x 250 x 1 meter resolution based on 540.000 borehole logs (TNO-GDN, 2025). c) Land subsidence rates in the peat meadow area of the western Netherlands derived from InSAR measurements (Conroy et al., 2024). On all three maps the cities of Amsterdam and Gouda are indicated. WGS84 coordinates are displayed in degrees north (y-axis) and east (x-axis).

The combination of land subsidence and sea level rise poses a growing challenge to water management in the low-lying coastal areas, where subsidence often outpaces sea level rise, effectively increasing flood (damage) risk, but also enhancing salinisation via ground- and surface water. In addition, greenhouse gas emission from decomposing peat layers contributes to global warming (Erkens et al., 2016; van der Net et al., 2025) and needs to be reduced according to the Paris Agreement and Dutch Climate Act (UNFCCC, 2015; EZK et al., 2019). These pressures drive Dutch ongoing research into land subsidence and underscore the need for a deeper understanding of the behaviour of peat and organic-rich clays, which dominate large parts of the Dutch subsurface. Mitigation strategies aiming at reducing subsidence and greenhouse gas emissions, e.g., rewetting or maintaining higher groundwater levels, however, can conflict with existing land-use practices and infrastructure demands. Together, these combined challenges highlight the urgency of improving mechanistic insight into the long-term deformation behaviour of organic soils, which is essential for developing sustainable and effective land-management strategies in the Netherlands.

1.4 Viscous compression

It is necessary to focus more closely on viscous compression as it plays a central role in the long-term behaviour, i.e., over years to decades, of peat and organic-rich clays. Viscous compression is a time-dependent deformation process that contributes substantially to long-term subsidence in peat and organic-rich clays. The occurrence of viscous compression is unrelated to overpressure of the porewater within subsurface layers and therefore continues even when boundary conditions like stress and temperature remain constant. As such, it is characterised by a gradual, continuous compression happening under constant effective stress, which enables long lasting deformation compared to for example consolidation. In oedometer tests the strain, i.e., relative height change of a sample, typically shows a logarithmic decrease with time. These two defining aspects are also at the core of how viscous compression is modelled. The equations to calculate viscous compression are based on a logarithmic relationship between deformation and time. This means that viscous compression develops uniquely for any combination of stress and compaction state, defining the deformation, and time. In geotechnical literature, viscous compression has traditionally been referred to as *creep*, *secondary consolidation*, or *secondary compression* (e.g., Den Haan, 1994; Mesri and Ajlouni, 2007; Zwanenburg et al., 2012; Kooi et al., 2018). However, these terms carry conceptual limitations that may not describe the actual characteristics of the process: 'creep' is used broadly across disciplines to describe slow progressive deformation of material and does not specify the nature of the deformation. For example, creep can also refer to shearing of soil materials related to horizontal stresses, which can be observed in slumps on mountains and failing dike slopes (e.g., Zwanenburg et al., 2012). The term 'secondary' suggests that the process occurs only after consolidation has ceased, but in peat and organic soils, pore pressure dissipation and time-dependent deformation often proceed simultaneously (Degago et al., 2011). Therefore, in this thesis, the term *viscous compression* is adopted, as it more accurately reflects the continuous, stress-controlled, viscous deformation behaviour observed in these highly organic, water-rich materials.

1.5 Problem definition

A central problem in subsidence prediction is the uncertainty surrounding the viscous compression of soft subsurface materials, especially peat and organic-rich clays. This uncertainty results in unreliable model estimates of viscous compression under low-stress field conditions which is further complicated by the high compressibility and strong spatial heterogeneity of these materials. To predict land subsidence and specifically viscous compression, various laboratory tests can be performed to understand and quantify the compaction behaviour. Although these tests, such as oedometer tests, provide valuable insights into time-dependent strain, their results can be difficult to translate to field conditions given the heterogeneity in composition and properties of organic-rich layers. This difficulty reflects a broader issue: the understanding of how viscous compression happens in these organic-rich layers remains incomplete, particularly when compared to the better-studied behaviour of mineral clays. In the field, extensometers and long-term surface displacement measurements (e.g., derived from InSAR measurements) can be used to validate laboratory compaction behaviour (van Asselen et al., 2020), but such comparisons are hampered by uncertainties about how much individual processes contribute to the measured deformation and how the processes interact under varying boundary conditions. An important part of this uncertainty lies in the yet poorly addressed interaction between viscous compression and biochemical decomposition.

Furthermore, subsidence models have been developed and applied in both academic research and engineering practice to support spatial planning, groundwater management, or infrastructure risk assessment (e.g., Bjerrum, 1967; Den Haan, 1994). These models often rely on empirical relationships or simplified conceptual models that primarily capture short-term, stress-dependent processes such as consolidation. Viscous compression at low stress conditions is typically underrepresented in these models (Deltares, 2024). Potential causes of the underrepresentation can be found in either the generic parameterization of viscous compression, which is based on high stress conditions, and rarely accounts for specific variations in material composition or decomposition state (e.g., O'Kelly and Pichan, 2013; Deltares, 2024), non-linearity over time of the logarithmic relationship between deformation and time (e.g., Den Haan and Edil, 1994; Feng et al., 2021), or in the effect of swelling on viscous compression (e.g., Vergote et al., 2022). These omissions limit the ability of models to accurately predict long-term surface lowering, particularly in organic soils at low stress conditions. As a result, subsidence predictions in these environments remain uncertain, especially beyond the timeframe of short-term monitoring or planning design horizons.

1.6 Objectives, approach and thesis outline

The main objective of the research described in this thesis is to advance the mechanistic understanding of viscous compression and its role in long-term compaction behaviour in order to help improving the predictive capacity of land subsidence models, particularly in peat and organic clays. To achieve this aim, I have defined three subobjectives:

1. Identify the mechanisms and processes that cause viscous compression in organic-rich subsurface layers with special attention to their large spatial variability in material characteristics.
2. Determine and quantify the influence of the organic matter decomposition state on viscous compression.
3. Translate the improved mechanistic understanding into improved predictive capacity of subsidence models through more representative parameterisation.

To address these objectives, I first carried out a comprehensive review of the mechanisms and processes driving viscous compression in peat and organic-rich clay (Chapter 2). Building on the established mechanisms for mineral clay, I explore how material properties and environmental conditions influence compression behaviour in both material types. This review provided further understanding of 1) why it is more difficult to predict viscous compression of peat than of clay, and 2) which unique mechanisms and processes of viscous compression in peat are currently not represented in predictive models.

To understand the interplay between mechanical processes (consolidation and creep) and decomposition rates in peat substrates with varying degrees of decomposition, laboratory tests were undertaken (Chapter 3). In these experiments I analysed for intact samples of fibric and decomposed peat, how porosity reduction under varying stress levels decreases decomposition rates. These findings contributed to construct a conceptual framework to describe the relationship between mechanical compression, porosity changes, and organic matter breakdown, crucial for understanding land subsidence in drained peatlands.

With a clearer understanding of viscous compression and its interrelation with decomposition, the next step was to incorporate this knowledge into improved model parameterisation. For this purpose, also material characteristics of peat were important as these can change as a result of progressive decomposition. The relationship between material characteristics and the viscous compression parameter was subsequently investigated using an existing extensive dataset containing geotechnical test results for various types of clay, organic clay and peat (Chapter 4). The results were used to predict the viscous compression parameter and to discuss whether adaptable viscous compression parameter values are required for accurate subsidence modelling in response to material changes over time, thus rendering the viscous compression parameter a variable rather than a fixed value.

Because this improved parameterization still did not fully explain the mentioned observed discrepancies between model predictions and measured long-term compaction at low stresses, I further evaluated how well current model parameterisations capture viscous compression across the full stress range. This was done by a validation analysis of the viscous compression parameter at various stresses, and for different compaction states of the material (Chapter 5). Through comparison of different ways of determining the viscous compression parameter value for both normally consolidated and overconsolidated conditions and subsequently assessing the impacts on predicted subsidence through simple 1D modelling, I evaluated whether the classic logarithmic function can be used to describe viscous compression behaviour for both normally consolidated and overconsolidated conditions.

Finally, in the Synthesis (Chapter 6), the results described in the preceding chapters are brought together to address the subobjectives and main objective. Furthermore Chapter 6 addresses the integration of viscous compression and decomposition, as well as the connection to the non-linearity of viscous compression discussed in Chapter 5. Lastly, remaining questions and recommendations relate to material characteristics, scaling from laboratory to field scale, and changing boundary conditions such as temperature and porewater salinity.

1.7 NWA-LOSS Research Program

The research presented in this thesis is part of the Living on Soft Soils (LOSS) - Subsidence and Society program (grantnr.: NWA.1160.18.259) (Stouthamer et al., 2020), within which multiple universities, research institutes, and societal partners in The Netherlands bundle expertise on land subsidence (Ministry of Infrastructure and Water Management, Ministry of the Interior and Kingdom relations, Rijkswaterstaat, Deltares Research Institute, TNO-Geological Survey of The Netherlands, Wageningen Environmental Research, Foundation for Applied Water Research STOWA, Hoogheemraadschap De Stichtse Rijnlanden, Water Authority Drents Overijsselse Delta, Province of Utrecht, Province of Zuid-Holland, Municipality of Gouda, Platform of Soft Soil Municipalities, Sweco, Tauw BV, and NAM).

The overall aim of this program is to develop an integrative approach to achieve feasible, legitimate and sustainable solutions for managing the negative societal effects of land subsidence, connecting fundamental research on subsidence processes to socio-economic impact of subsidence and to governance and legal framework design. The program is to contribute significantly to the ability to mitigate and adapt to subsidence in populated, governed deltas in the short and in the long term and via management of subsidence, lower GHG emissions and decrease risks and looming damage for low-lying delta plains under climate change. The program is comprised of five work packages covering all aspects of the 6M approach in dealing with subsidence, i.e., subsidence measuring and analysis of mechanisms, quantifying impacts, deliberating measures and evaluating performance (Erkens and Stouthamer, 2020):

1. Measuring and monitoring
2. Mechanisms and Green-House-Gas emissions
3. Impact analysis
4. Measures and governance approaches
5. Knowledge utilization and entrepreneurship

The research presented in this thesis is part of work package 2: Mechanisms and Greenhouse Gas Emissions. Work package 2 focuses on unravelling, understanding and quantifying the interacting processes leading to land subsidence. The (re)parameterization and increased understanding of processes are used in a new subsidence model which is validated and used by work packages 3 and 4 to calculate and determine the economical/societal consequences and implications of land subsidence. The results of this thesis furthermore contribute to improved prediction of long-term compaction, which is amongst others important to meet the residual settling requirements of newly constructed buildings. With the results from this thesis, land subsidence can be better predicted and these improved predictions contribute to the determination of mitigation options.

Chapter 2:

Viscous compression of clay and peat

Van Elderen, P., Erkens, G., Zwanenburg, C., Middelkoop, H., & Stouthamer, E. (2025). Viscous compression of clay and peat.

Earth-Science Reviews, 251, 104703. https://doi.org/10.1016/j.earscirev.2024.104703.

ABSTRACT

Viscous compression, the delayed slow compression of soils after loading, has emerged as a challenging process contributing to land subsidence in soft soil areas. Despite previous research on clay soils, there is still limited understanding of the processes and mechanisms of viscous compression of organic soils. As peat is more susceptible to viscous compression than clay, and the subsurface of subsiding deltas can contain substantial bodies of peat, understanding of processes, mechanisms and drivers is needed to predict the potential for and amount of viscous compression to occur and assess the effect of mitigation measures to delta subsidence. This study integrates findings from prior research on viscous compression behaviour of clay for a comprehensive comparison of the structural, geomechanical, chemical, and biological characteristics of clay and peat, to evaluate to what extent compression mechanisms in clay operate in a similar way in peat. The study focuses on mechanisms of viscous clay compression, which are: expulsion of micropore water, changes in the adsorbed water layer, and particle interactions. Our review establishes that these mechanisms also manifest in peat, albeit with varying contributions to the reorientation of peat fibres. Notably, the distinct pore structure and larger average pore diameters of peat result in water expulsion behaviour that is different from clay. Additionally, the negative electrical charge on clay mineral surfaces is stronger than that of peat fibre surfaces, influencing attraction or repulsion forces among particles and the adsorbed water. This study introduces decomposition of organic matter as an additional long-term control of subsidence. Decomposition weakens the peat structure and facilitates particle reorientation, which enhances the susceptibility to compression. On the other hand, when organic material is already decomposed, it shows lower compressibility compared to fibrous organic material.

2.1 Introduction

Clay, silt and peat naturally occur in fluvial and coastal depositional environments in deltas, which in many places host dense populations living in mega cities, intensive agriculture, industry and infrastructure. One of the most significant problems for areas with soft subsurface layers is local and regional land subsidence (e.g., Yuill et al., 2009; Erkens et al., 2015). As the surface lowers, problems arise or increase for the subsiding area, for example local damages to buildings and infrastructure, and increasing regional flooding frequency, duration and extent by rivers or the sea. The latter is of great significance for coastal deltas that, in addition to land subsidence, face absolute sea-level rise, resulting in even higher relative sea-level rise (e.g., Erkens et al., 2015, Figure 2; Fox-Kemper et al., 2021; Nicholls et al., 2021, NASA, 2023). One of the major processes causing land subsidence is compaction of normally and lightly overconsolidated subsurface material. This compaction is defined as the process following an increase in loading, which leads to a decrease in volume of deposits when individual particles – grains or fibres – are pressed together, and pore space is reduced. Subsurface layers consisting of clay and peat have a higher compaction potential than more sandy layers due to their high (initial) porosity (e.g., Revil et al., 2002; Dudoignon et al., 2007; Landva, 2007; Mesri and Ajlouni, 2007; Uyanık, 2019). Under natural conditions, compaction occurs under the burden of the weight of the soil material itself, which is called auto-compaction (e.g., Pizzuto and Schwendt, 1997; Allen, 2000; Massey et al., 2006; Zoccarato et al., 2022). Human activities cause additional compaction by loading of the subsurface by buildings and infrastructure (e.g., Wang et al., 2013; Erkens et al., 2015; Jones et al., 2016), hydrocarbon and groundwater extraction reducing pore pressure (e.g., Galloway et al., 1999; Wu et al., 2008; Thoang and Giao, 2015; Galloway et al., 2016; Minderhoud et al., 2017, van Asselen et al., 2024), and by artificial lowering of the shallow groundwater table through excessive drainage (e.g., Schothorst, 1977; Nieuwenhuis and Schokking, 1997; van den Born et al., 2016; Koster et al., 2018b; Page et al., 2020).

Compaction processes can be divided into three groups: micro-biological, physical and chemical processes (van Asselen et al., 2009). Micro-biological processes involve aerobic and anaerobic microbial decomposition of peat (e.g., Berglund et al., 2008; Dorrepaal et al., 2009; Brouns et al., 2014; Tolunay et al., 2024). Physical processes involve overpressured pore water expulsion, particle reorientation and compression of solids (e.g., Terzaghi, 1941; Berry and Poskitt, 1972; Navarro and Alonso, 2001; Mitchell and Soga, 2005). Chemical processes involve oxidation, water diffusion and changes in the composition of the adsorbed water layer (e.g., Bjerrum, 1967; Mitchell et al., 1968; Yin, 2002). From a mechanical perspective, the compaction process can also be divided into three different, time-related types of behaviour (Paul and Barras, 1998, Fig. 2.1). Type I comprises the *instantaneous compression*, which is the immediate rearrangement of the subsurface structure, and occurs within the order of seconds after the loading is applied. Type II is *consolidation*, which is the volume reduction that occurs following the expulsion of water due to overpressure in the pores. The hydrodynamic period, which is the duration of consolidation, can last from hours to days in the lab or weeks to years in in-situ conditions depending on hydraulic conductivity and the thickness of the subsurface layer that is compacted. The end of the hydrodynamic period is referred to as End-of-Primary (EOP), which is often reached within 24 hours in oedometer tests. Type III represents the *viscous compression* of subsurface material. Viscous compression was previously called 'delayed water expulsion' (Bjerrum, 1967) and is the result of the reorganisation of the structure when particles reorientate over time under constant pressure (Chai et al., 2012; Le et al., 2012; Zhao et al., 2020). This slow reorientation of particles without overpressure driven water expulsion is called the viscous behaviour of subsurface material.

This review focusses on the viscous compression behaviour of mainly peat, as well as clay, and therefore on both timescales at which Type II and III compaction occur. A term that is often used as a synonym for the viscous compression of subsurface layers is *creep*. The term creep is used to indicate both volume change or shear deformation (Tanaka et al., 2006), but only volume change is considered here as this contributes directly to land subsidence; shear viscous deformation of soft subsurface layers mainly impacts slope stability of steep cuttings or embankments (e.g., Rowe and Li, 2002; den Haan and Feddema, 2013; Zwanenburg and Jardine, 2015). Shear deformation of solid rock at typical depths of hundreds of meters to kilometres leading to land subsidence is a common topic in structural geology and reservoir engineering (e.g., Griggs, 1939; Singh, 1975; Wang et al., 2020). Due to these two reasons, viscous shear deformation is outside the scope of this paper.

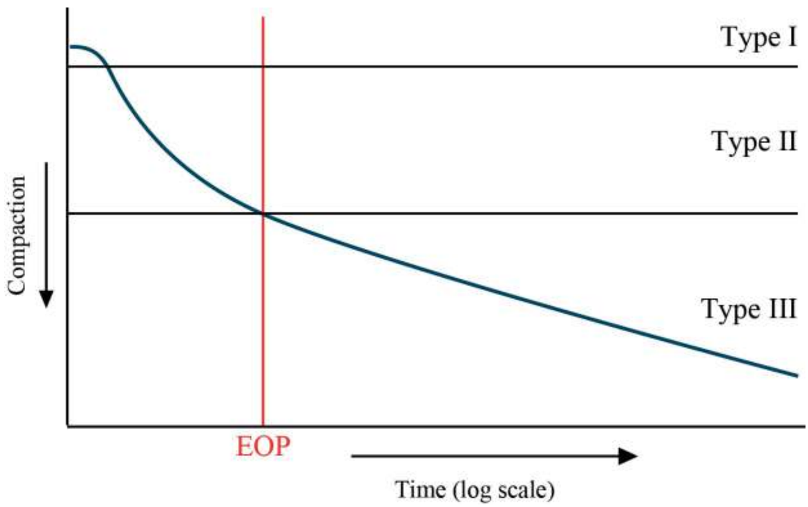

Figure 2.1: Schematic semi-log diagram of the compaction as a function of time after a single load increase. The diagram shows the three time-related types of behaviour of the 1D-compaction process from a physical or geotechnical perspective. The End-of-Primary (EOP) is indicated as the end of consolidation after a stress increase.

Several numerical models have been developed to quantify the amount of vertical displacement (strain) over time resulting from viscous compression (i.e., Bjerrum, 1967; Den Haan, 1996; van Asselen et al., 2009; Kooi and Erkens, 2020). These models are used to calculate the effect of load changes on viscous compression of subsurface layers as viscous compression of subsurface material can significantly contribute to the total land subsidence in the longer term. For example for peat, the San Joaquin Delta in California is facing long term subsidence of 2.5 to 7.5 cm/yr related to viscous compression of the reclaimed islands in the delta (e.g., Rojstaczer et al., 1991; Galloway et al., 1999; Drexler et al., 2009; Reinert, 2014). Peat areas in the Netherlands have subsided up to 8.5 meters since 1000 AD. In addition to consolidation, decomposition and excavation, viscous compression as a result of land surface drainage has substantially contributed to this long-term subsidence (e.g., van de Ven, 1993; Erkens et al., 2016; Koster et al., 2018a; van Asselen et al., 2018). Along the Louisiana coast, a typical subsidence rate of 2 – 7 mm/yr has been observed which is partially due to viscous compression following drainage of the Holocene clay and peat layers (Törnqvist et al., 2008; van Asselen et al., 2024; Voyiadjis et al., 2024). At the Kansai International Airport Islands near Osaka, Japan, viscous compression of subsurface clay layers may contribute 2 – 4.6 meters of the 20 meters of land subsidence that is expected to occur between the airports completion of construction in 1999 and 2100 (Puzrin et al., 2010; Mesri and Funk, 2015).

In geotechnical approaches, viscous compression is largely considered to be a physical-chemical phenomenon (Zain, 2019). The main mechanisms leading to viscous compression have been extensively studied for clay, and include micropore water expulsion, adsorbed water layer changes and particle interactions (Mitchell and Soga, 2005; Le et al., 2012). Yet, comparably little progress has been reported on understanding the mechanisms and processes leading to viscous compression of peat and the inherent reorientation of peat fibres. Also, the important environmental conditions to consider when calculating the amount of viscous compression in peat are currently unknown. Clearly, further insight in these processes and mechanisms is required to increase the predictive skill of subsidence models, enabling the development of measures to effectively mitigate viscous compression of peat to reduce total land subsidence.

One may hypothesize that the mechanisms and processes for peat are at least partly similar to those for clay. For example, both clay and peat do have adsorbed water around and within the particles that may be expelled and lead to viscous compression (i.e., Martin, 1962; Kay and Goit, 1977; Hobbs, 1987; Dolinar and Macuh, 2016). However, as clay has a sheet particle-structure, compared to the highly variable fibre structure of peat, the dynamics of particle reorientation in peat are likely not the same as in clay. Not only the contact between particles is different due to the structure, but also characteristics such as structural strength, porosity and permeability differ because of it. This will in turn impact the way and rate at which water is expelled from macro- and micropores. Moreover, understanding viscous compression of peat-clay mixtures, containing both mineral and organic fibrous material, will be further complicated by the interactions between the material types, for example when smaller clay particles occupy the larger pores in the fibre structure and consequentially reduce effective pore space.

Therefore, as starting point for this review towards understanding viscous compression of peat, we first address viscous compression, including the key mechanisms and processes, as well as the critical environmental conditions, as extensively reported in the literature for clay. Subsequently, through comparing the two materials and their characteristics, we evaluate how viscous compression would occur in peat. In this review we limit ourselves to comparing clay and peat as 'end-members', and leave implications for clay-peat mixtures for discussion.

To improve our understanding of viscous compression of peat, this review paper aims to 1) explore, identify and examine the different mechanisms and processes driving viscous compression as reported in literature for clay, and determine to what extent these mechanisms can explain viscous compression of peat, 2) identify relevant physical and chemical characteristics of peat controlling viscous peat compression, and 3) discuss implications of viscous compression of peat for land subsidence within this framework.

Based on boundary and initial conditions, and characteristics of peat, we expect that the major mechanisms of viscous compression of peat are micropore water expulsion, changes in the adsorbed water layer and inter-particle forces. An additional control of viscous compression is organic matter decomposition, which is inherent to peat and has a strong impact on the structure of peat. Using these hypotheses, the paper first focuses on the three mechanisms of viscous compression known for clay, and subsequently discuss these for peat, thereby considering possible relations between different mechanisms and the role of microbial decomposition.

2.2 Mechanisms, processes, environmental conditions and characteristics

This section presents an overview of the mechanisms described by Le et al. (2012) causing viscous compression of clay, together with the underlying processes, environmental conditions and material characteristics. The different terms used in this paper are presented in Fig. 2.2. Environmental conditions and material characteristics are placed at the base of the figure as these influence the rate and intensity of processes. For processes we consider the physical, (bio-)chemical and biological flow of material or energy in the system. Processes describe what is happening at the particle level without a direct link to viscous compression, while mechanisms relate the processes to what is happing in the soil that leads to particle reorientation.

It must be noted that most of the consulted sources for representative values for characteristics of peat and clay had a different focus than analysing their role in land subsidence processes. Therefore, it is sometimes unknown whether values correspond to uncompacted or compacted clay and peat. Lastly, decomposition of organic material plays a two-fold role, both through the initial state of decomposition as well as progressive decomposition occurring during viscous compression.

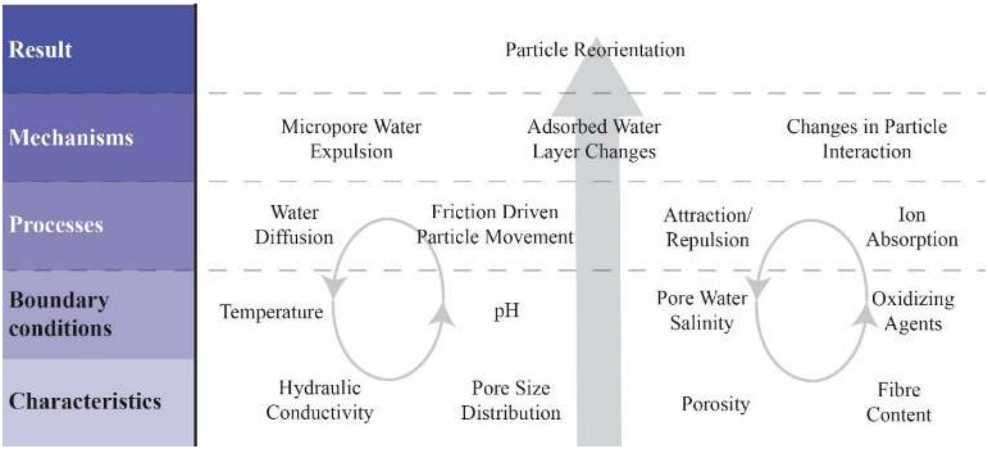

Figure 2.2: Overview of the various terms (right) used in this paper to explain viscous compression. Left: terms referred to when mentioned as a group. The arrow indicates the reading direction for the groups and terms. Characteristics and environmental conditions function at the lowest level affecting viscous compression, forming the initial setting for the processes. Processes direct the mechanisms which lead to particle reorientation. The latter causes the volume loss we observe as viscous compression.

2.2.1 Micropore water expulsion

Micropore water expulsion is one of the primary mechanisms of viscous compression of soft subsurface layers (e.g., Mitchell, 1993; Akagi, 1994; Navarro and Alonso, 2001; Mitchell and Soga, 2005). Micropore water expulsion under specific stress conditions is likely different in peat than in clay. As the internal structures of clay and peat are very different, it is very likely that the distribution of various pore sizes is not comparable. For example, pristine peat has typically a higher porosity than clay, which is respectively ~90% and 30-60% (e.g., Landva, 2007; Quinton et al., 2009; Rhezanezhad et al., 2012; Osipov et al., 2015), and a higher permeability. In this section pore size characteristics, the pore network and the expulsion dynamics of micropore water are discussed to get a clear view of the differences which may lead to differences in viscous compression.

2.2.2 Pore sizes

Clay pores can be divided into three classes. Macropores are defined as the spaces between larger particles or between aggregates of smaller particles (Fig. 2.3). The general range of the diameter of macropores is >10 μm (Matsuo and Kamon, 1977). Mesopores can be situated between larger particles or aggregates as well as situated within particle clusters or aggregates. The typical diameter of mesopores is 1-10 μm. Micropores are situated within clusters of clay particles or in between clay sheets. The typical diameter is <1 μm. As clay is considered to have individual particles of <2 μm, the boundary size between micropores and mesopores is at the scale of individual clay particles, whereas the boundary size between meso- and macropores is more comparable to stacks of clay particles.

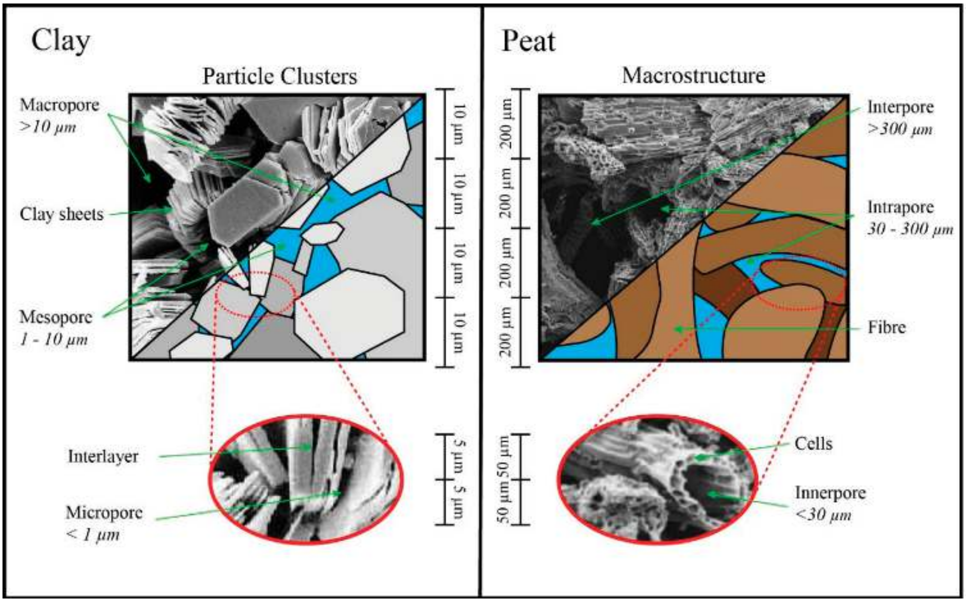

Figure 2.3: Combined SEM image and schematic particle structure with pore classes and dimensions. Left: Kaolinite clay; Right: Peat. SEM images on the left and right are reproduced from respectively Lanson et al. (2002) and Mesri and Ajlouni (2007).

For peat, an alternative to the macro-, meso- and micropores is a division based on size between inter-plant, intra-plant and inner-plant pores (Weber et al., 2017). Inter-plant pores in peat are the spaces between individual plant remains (Fig. 2.3), and are larger than macropores in clay. The smallest diameter of inter-plant pores is reported to be between 100 and 300 μm for various types of normally and lightly overconsolidated peat, among which Sphagnum peat is tested the most (Holden, 2009; Weber et al., 2017; Gharedaghloo et al., 2018; McCarter et al., 2020). Intra-plant pores are defined as the spaces between the smaller parts of plant remains, such as roots or leaves. Intra-plant pores share the lower diameter range of clay macropores as their typical diameter is between 30 and 100 μm. The spaces within plant structures are considered inner-plant pores, which have a diameter between 10 and 30 μm (Weber et al., 2017; McCarter et al., 2020).

Pore water can also be retained within the cells of plant material (Weber et al., 2017). Cell water is commonly situated in the apoplast, which is the space between the outer cell wall and the plasma membrane, and in the symplast, which is the space inside the plasma membrane excluding the cell nucleus (Barberon and Geldner, 2014). These cells make up most of the 'pores' with diameters smaller than inner-plant pores (<10 μm). Since water in cells does not flow as capillary flow or diffusion, cells are not considered as inner-plant pores. It is important to note the presence of this type of water, as breakdown of cell walls could enable cell water to flow out of the cell, resulting in further compaction. However, because of its non-capillary character, cell water is usually not taken into consideration.

The reported typical diameter of pore types varies per study, due to the variation in the studied subsurface material. Furthermore, indicated boundary diameters for pore size classes can also vary with the applied experimental technique (Beven and Germann, 1982) (Table 1). Since the upper boundary of inner-plant pores diameter varies up to 30 μm, it makes sense to combine mesopores and micropores into one class based on their diameter to compare the pore size distribution of clay and peat.

2.2.3 Pore network

The porosity can be divided into an active and an inactive part of the pore network. The active porosity, also called the effective, open or mobile porosity, consists of open, interconnected macropores and sometimes mesopores. The inactive porosity consists of partially or fully closed pores and dead-end pores, usually belonging to the meso- or micropore classes. Due to their shape and position, for example within clay particle clusters or within plant structures, water in these pores cannot flow out easily or not at all, excluding the pores from active contribution to the throughflow. In some cases, also macropores can be part of the inactive porosity when pores are clogged by, for example, gas bubbles or small particles. Porosity may rapidly change within a soil profile. For example, in Canadian Sphagnum and fen peat active porosity in the top centimetres of the soil is 50-60% of the total porosity (Quinton et al., 2009; Rezanezhad et al., 2012) but decreases rapidly with increasing depth. Gharedaghloo et al. (2018) showed that in fen peat, active porosity decreased to 27% at only 11 cm below the surface. Macropores are easily squeezed, such that relatively more meso- and micropores remain to make up the pore space. Since pore throats, the connections between pores, also get smaller, a larger portion of the total pore space becomes inactive due to the capillary suction in unsaturated conditions preventing the pore water to flow through the smaller pore throat and lower water diffusion rates in saturated conditions.

Macropores or inter-plant pores usually make up less than half of the total amount of pores, but often account for more than 70% of the water flux in both clay and peat, because of preferential flow, bypassing connected mesopores (Moret and Arrúe, 2007). The abundance of macropores in the subsurface decreases with depth due to compaction. Decomposition of peat can also lead to a decrease in the volume of macropores (McCarter et al., 2020).

Table 1: Pore dimension ranges for macro-, meso- and micropore classes for both clay and peat according to different authors. The type of material and the method used to determine the pore classes are also listed.

Author	Clay/ Peat	Type of Clay/ Peat	Method	Pore dimensions (μm)		
				Macro/ Inter	Meso/ Intra	Micro/ Inner
Matsuo & Kamon (1977)	Clay	Undefined	Microscopy	>10	1-10	0.01-1
Bruand et al. (1996)	Clay	Silty Clay Loam soil	Backscatter Electron Microscopy	>800	100-800	10-200
Filimonova et al. (2006)	Mixed	Montmorillonite + Soil Organic Content	Nitrogen Adsorption	>50	2-50	<2
Zaffar & Lu (2015)	Mixed	Vertisols + Soil Organic Content	Nitrogen Adsorption	>75	30-75	5-30
Mendes et al. (2020)	Clay	Sandy-Clayey soil	Soil Water Retention Curve	>30	0.3-30	0.05-0.3
Holden (2009)	Peat	Sphagnum/ Eriophorum	Infiltrometer Test	>250	-	<250
Weber et al. (2017)	Peat	Sphagnum	Falling Head + Modelling	>300	30-300	10-30

Another important characteristic associated to the pore network is the hydraulic conductivity, that generally decreases with lower active porosity. The hydraulic conductivity of both clay and peat is generally low, in the order of 10^{-6} to 10^{0} m/d (Mesri and Ajlouni, 2007; Tanaka et al., 2019; Hayashi and Hatakeyama, 2021). In contrast, hydraulic conductivity values of sandy deposits are in the order of 10^{0} to 10^{3} m/d. For the Dutch Pleistocene and Holocene deposits comparable values have been found for clay, peat and sand in aquitards (van Leer et al., 2023). Peat generally has a higher hydraulic conductivity than clay, but reported values vary with the testing conditions, the compaction state of the peat and clay and the decomposition state of peat. Hayashi and Hatakeyama (2021) showed that hydraulic conductivities for peat measured in-situ are approximately between 10 and 100 times higher than measured in a laboratory. Their explanation focusses on the strong anisotropy of hydraulic conductivity in peat and the limited vertical water flow in laboratory set-ups compared to the omni-directional flow in-situ. Furthermore, the larger in-situ layer thickness leading to differences in hydraulic gradients and drainage lengths between laboratory and field set-ups. Lastly, the heterogeneity of peat means a larger test in-situ levels out structural differences to at least some extent, whereas a laboratory sample might be representative for a maximum or minimum value, an explanation that also reflects the larger differences with increasing organic content that is mentioned. This upscaling feature is important to consider when discussing the implications of laboratory results for field settings. Also, a typical characteristic of peat is the larger decrease in hydraulic conductivity with decreasing void ratio, which is the ratio between the volume of pores and solids, due to its high compressibility. Therefore, highly compressed peat can have a lower hydraulic conductivity than clay. The decrease in hydraulic conductivity under increasing compression can be calculated using the altered relationship from Tavenas et al. (1983):

$$C_k = \Delta e \,/\, \log \frac{k}{k_0} \tag{2.1}$$

where C_k is the (dimensionless) index of change in hydraulic conductivity, Δe is the decrease in void ratio e and $log\frac{k}{k_0}$ is the relative change in the logarithm of the hydraulic conductivity. Based on various fibrous peat samples and kaolinite, illite and montmorillonite clay samples, it was shown that C_k of peat is twice that of clay (Tavenas et al., 1983; Mesri et al., 1997) for equal changes in void ratio. The hydraulic conductivity of uncompressed fibrous peat types can be between 100 and 10,000 times that of soft clay (Mesri et al., 1994). Lastly, clay and peat show a considerable hydraulic anisotropy. Both have small-scale internal structures with a predominantly horizontal orientation, such as clay mineral plates, individual fibres and stems of plant remains, favouring horizontal pore water flow over vertical flow. The anisotropy of conductivity in clay is more pronounced than that of peat, k_h/k_v being respectively ~10 and ~4 (Mesri et al., 1997).

2.2.4 Effect on viscous compression

Porewater expulsion occurs after a pressure or stress increase. During the consolidation phase (Type II in Fig. 2.1) over-pressured water is expelled mainly from the macropores. Once the excess pore pressure has dissipated the consolidation phase ends at EOP. During the subsequent viscous compression phase (Type III in Fig. 2.1) micropore water is expelled. This does not occur as a result of overpressure, but is assumed to be a delayed water expulsion that occurs from micropores to the macropores through diffusion.

Two hypotheses exist about micropore water expulsion during the consolidation phase (Degago et al., 2011). Hypothesis A assumes that the void ratio reached at the EOP only depends on the effective stress and not on the duration of consolidation. Assuming that viscous compression, partially due to micropore expulsion, is time dependent, it only occurs after the EOP (Type III in Fig. 2.1) and not during the consolidation phase (Type II in Fig. 2.1). Hypothesis B assumes that along with consolidation (macropore water expulsion) also viscous compression (micropore water expulsion) already occurs. Under this assumption field samples experience more strain at EOP for equal stress conditions than a laboratory sample because of the larger thickness of field samples and accompanying maximum drainage length. A larger thickness means that water has to travel longer to be expelled to complete consolidation and reach EOP, while laboratory samples need less time to reach EOP after loading (Fig. 2.4). After the EOP, further strain only occurs through viscous compression: micropore water continues to be expelled, while macropore water expulsion has ceased. Degago et al. (2011) conclude that measured compression of subsurface layers supports hypothesis B and reject hypothesis A. In agreement with the reasoning supporting this conclusion, hypothesis B is further considered in this paper. In some compression tests, a steepening of the logarithmic time-strain slope during the viscous compression phase (Type III in Fig. 2.1) is observed, which is referred to as tertiary compression (Den Haan and Edil, 1994; Augustesen et al., 2004). The release of particle-bound water in the pores is then hypothesised as the process leading to this steepening of the curve.

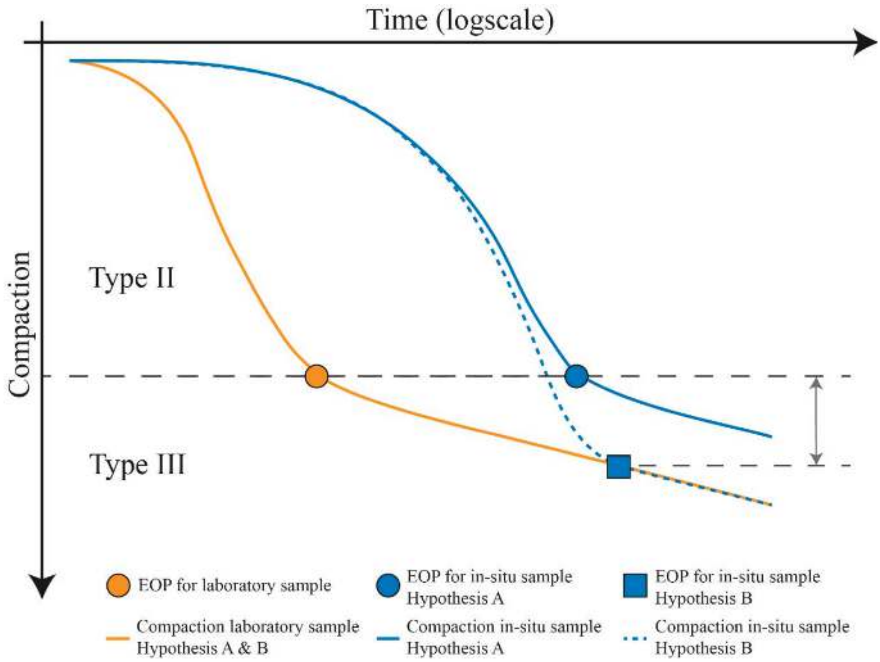

Figure 2.4: Compaction curves for laboratory samples (red line) and in-situ samples (blue lines) as a result of equal loading (equal $\Delta\sigma'/\sigma'_{v0}$). Because of the larger thickness of the in-situ sample, the End-of-Primary (EOP, indicated by the circles) is reached after more time than in laboratory conditions. Hypothesis A reasons that no viscous compression happens in Type II, which results in a EOP compaction valid for both laboratory and in-situ conditions. Hypothesis B reasons viscous compression does happen in Type II, which leads to more compaction at EOP. This is the case as viscous compression is time-related and for a thick sample that takes more time to reach EOP, also more viscous compression will take place (after Ladd et al., 1977 and Degago et al., 2011).

The different times required to drain macropores on the one hand versus meso- and micropores on the other is attributed to and referred to as 'double porosity'. Before the EOP, water from the macrostructure of macropores is expelled, while water from the meso- and micropores in the microstructures drains to the macrostructure they are connected to. After the EOP, only water from the microstructures drains to the macrostructure, and then further drains via the larger pores. In peat, the same sequential process may occur, where macrostructures are made up of inter-plant and intra-plant pores, whereas the microstructures comprise the inner-plant pores.

Subsurface microstructures are thus important characteristics, in which changes can lead to viscous compression of clay (i.e., Berry and Poskitt, 1972; Navarro and Alonso, 2001; Le et al., 2012), and likewise also for peat. The fast decrease in hydraulic conductivity of peat related to compaction (Mesri and Ajlouni, 2007; O'Kelly and Pichan, 2013; Tanaka et al., 2019) can be due to 1) increased tortuosity of the flow channels and/or, 2) the decreased diameter of the flow channel. However, in which of the pore types in peat these changes mostly or more extensively occur, cannot be determined from the available information on hydraulic conductivity.

2.3 Adsorbed water layer changes

The second mechanism of viscous behaviour in clay is adsorbed water layer changes (Mitchell and Soga, 2005; Le et al., 2012). The adsorbed water content of clay and peat will likely differ. Clay has a much stronger negative surface valency than peat, which is an important characteristic governing the adsorbed water layer, whereas hydrophilic and hydrophobic properties of peat are determined by the plant material. As the adsorbed water layer determines the flow resistance of the free pore water and the structural resistance of particles to move relative to each other, both influencing the viscous compression, it is necessary to understand the impact of the adsorbed water layer on the viscous compression. This section gives an overview of the characteristics of the adsorbed water layer and which characteristics of the free pore water and pore structure it controls.

2.3.1 Characteristics of the adsorbed water layer in clay

The water layer is adsorbed to the outside of clay particles due to the negative charge of the surfaces (Langmuir, 1938). In between clay sheets of 2:1 layered clay minerals, adsorbed water, often called interlayer water, can be found as well (Hoekstra and Doyle, 1971; Helmy, 1998; Mitchell and Soga, 2005; Brigatti et al., 2013; Lagaly and Dékány, 2013). The surface of most clay minerals is negatively charged as a result of isomorphous substitution, which is the substitution of one type of atom in a crystal by another with a similar size, but with a different valency and/or electronegativity (Prost et al., 1998; Brigatti et al., 2013; Lagaly and Dékány, 2013; Schoonheydt and Johnston, 2013). The edges of the clay mineral are positively charged at pH 7 to retain the net neutral charge of the mineral. Water molecules can be bonded to a clay mineral in three different ways (Martin, 1962; Mitchell and Soga, 2005; Schoonheydt and Johnston, 2013; Johnston, 2018): with dipole attraction, cation attraction and hydrogen bonding (Fig. 2.5). Water molecules and hydroxyl groups can act as a dipole, a molecule with a positive and a negative charged side, to directly attach to the negatively charged clay surface (Delville, 1993; Johnston, 2018). Another option is that a cation, such as K^+, functions as the connection between the water molecule and the clay surface (Martin, 1962; Low, 1962; Delville, 1993; Schoonheydt and Johnston, 2013). In this case, multiple water molecules can bind to the cation depending on the charge of the cation. Non-movable cations, such as Al^{3+}, Mg^{2+} or Na^{+}, in the adsorbed water layer also provide stable connections with the water molecules. Hydrogen bonding is the relatively strong attraction between a hydrogen atom and a strongly negative charged atom (Delville, 1993; Schoonheydt and Johnston, 2013; Johnston, 2018). Hydrogen bonding can lead to dipole-dipole bindings or covalent bindings. Water in the absorbed water layer further away from the clay surface can be bound through Van der Waals forces (Schoonheydt and Johnston, 2013; Johnston, 2018; Fig. 2.6).

The adsorbed water layer is organised into mono- and multilayers of water (H_2O) molecules or hydroxyl (OH-) groups that are fully or partially in contact with the adsorbent surface (Asay and Kim, 2005; Osipov, 2012). The adsorbed water layer can be divided into three types of bonded water layers: ice-like layers, transitional layer(s) and liquid water layers. The closest to the particle surface are the ice-like layers (Hoekstra and Doyle, 1971; Asay and Kim, 2005), which are commonly referred to as the Stern layer of the immobile layer (i.e., Gonçalves et al., 2010; Tang et al., 2016). The internal structural rigidity of these layers is caused by the strong bonding network of hydrogen that bonds to a very electronegative oxygen atom, creating a strong dipole and dipole connections (Fig. 2.5). This bonding network also results in a stronger bonding energy between the particle surface and the water molecules than with molecules further from the surface (Tang et al., 2016). These layers are followed by the transitional or diffuse double layer(s), after which further outward layers behave similarly to free bulk pore water as they are increasingly governed by thermal motion (Fig. 2.6; Asay and Kim, 2005, Tang et al., 2016). The formation of the different monolayers around clay particles is directly linked to water filled pore space, following an S-shaped sorption isotherm (Fig. 2.6; Osipov, 2012). The ice-like layers form between 0% and 30% water filled pore space (Fig. 2.6; Asay and Kim, 2005). The formation of the transitional layer happens between water filled pore space of 30% up to 60%. Above 60% water filled pore space, adsorption occurs in the form of liquid water multilayers (Tang et al., 2016). Generally, the total adsorbed water layer thickness is in the order of 10 Angström (10 Å = 1 nm) (Tokunaga, 2009; Tang et al., 2016). Individual monolayers are < 5 Å thick.

The thickness of the adsorbed water layer is determined by several factors. The most important are considered to be the temperature, total water content and the external specific surface area, which is the external particle surface area per unit mass of solid material (i.e., Langmuir, 1938; Mitchell, 1993; Fukue et al., 1999; Dolinar and Macuh, 2016). The amount of water adsorbed to clay particles, w_{ae}, (g/g) is calculated as follows (Mitchell, 1993):

$$w_{ae} = A_{Se}\, h\ \rho_w \tag{2.2}$$

Where A_{Se} is the external specific area of the material particles (m^2/g), h is thickness of the adsorbed water layer (m) and ρ_w the density of the pore water (~10^6 g/m^3).

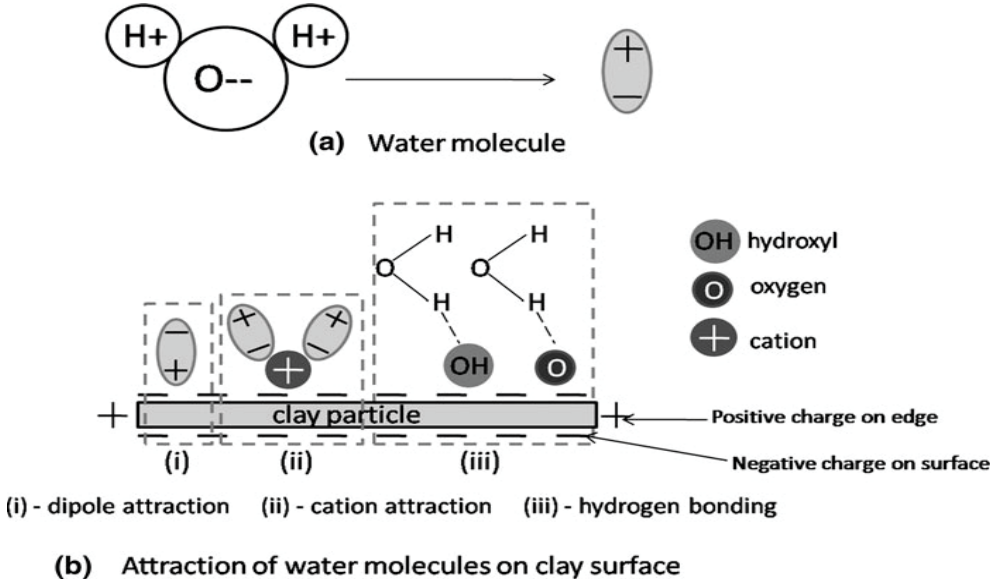

Figure 2.5: a) Water molecule shown as a dipole and b) attraction of water molecules directly to the surface of a clay particle via (i) dipole attraction, (ii) cation attraction and (iii) hydrogen bonding (Le et al., 2012, modified after Ranjan and Rao, 2011).

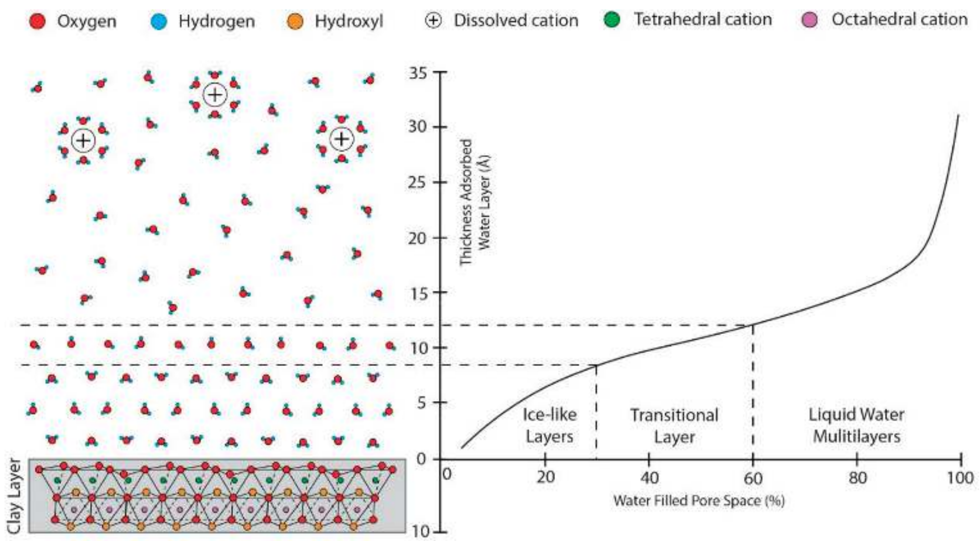

Figure 2.6: Molecular structure, and thickness of adsorbed water layers and types as a function of water filled pore space. Left: schematic illustration of the adsorption development of water molecules when the adsorbed water layer thickness increases with water filled pore space. Bottom left: a 1:1 structured clay particle (e.g.,e.g kaolinite), is shown as the surface to which the water is adsorbed. Top left: impression of organisation of adsorbed water molecules in the three adsorption layers. Right: evolution of the adsorbed water layer thickness and development of the three adsorption layer types with increasing water filled pore space. A fully saturated soil corresponds to 100% water filled pore space. Based on Asay and Kim (2005), Osipov (2011) and Brigatti et al. (2013).

As the water content, which is the weight of water as a percentage of the weight of solids, at the liquid and plastic limit (LL and PL) linearly increases with external specific surface area of different clay types, the thickness of the adsorbed water layer can be derived from the slope (Fig. 2.7). The LL indicates the water content at which the subsurface material changes from a liquid state to a plastic state, whereas the PL indicates the water content at which the subsurface material changes from a plastic state to a semi-solid state. The thickness of the water layer in between the clay particles is determined by the internal specific surface area A_{Si}, which is 10-100 times as large as the A_{Se} (Mitchell, 1993), but more so by the available exchangeable cations dissolved in the interlayer water (Bergaya et al., 2006).

Although the first layers of the adsorbed water layer are considered to be immobile, the adsorbed water in the outer layers (Fig. 2.5) can be expelled with increasing pressure (Tang et al., 2016). When all free pore water has been expelled, normal water flow can no longer occur, but small-scale diffuse lateral molecular movement is still possible in the viscous outer layers (Wensink et al., 2000; Singh and Wallender, 2008, Tokunaga, 2009; Tang et al., 2016). The presence of adsorbed water layers to the material decreases the effective pore channel diameters and thus limits the diffusion of pore pressure, especially under higher loading conditions when more or all free water has been expelled already.

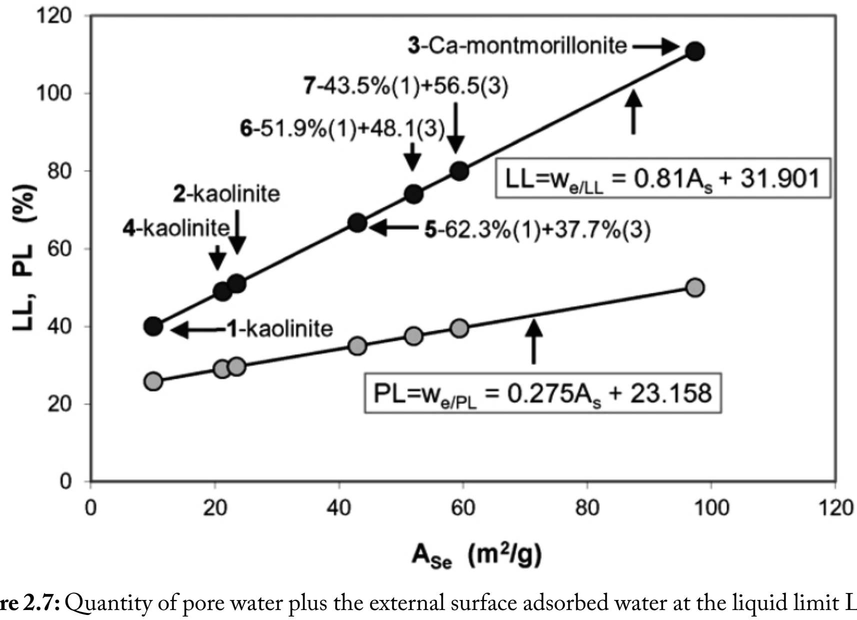

Figure 2.7: Quantity of pore water plus the external surface adsorbed water at the liquid limit LL water content (%) and plastic limit PL water content (%) as a function of the external specific surface area ASe (m2/g) (Dolinar and Macuh, 2016).

2.3.2 Water adsorption to peat

Water adsorption to peat fibres and decomposed organic matter can occur both on the surface of the particle as well as within the plant cells. The total capacity to adsorbed water is higher for peat than for clay owing to the high external surface area of peat of up to 100-280 m^2/g (Bunt, 1988; Naganuma et al., 1993). Peng et al. (2024) have shown for peat with varying organic content that adsorbed water can amount up to 60-80% of the total water content, although it might also comprise also water which other studies might classify as micropore water. Water adsorption to peat under unsaturated conditions follows similar dynamics as to clay as it is governed by the relative humidity and temperature in unsaturated conditions (Sehlstedt-Persson, 2008; Thybring and Fredriksson, 2021; Sweygers et al., 2022). However, the structural differences become apparent here as the plant cells play a vital role in the adsorption dynamics in peat. Within the plant structure water is bound in the cell walls via hydrogen bonding with free hydroxyl groups (Haygreen and Bowyer, 1982; Sehlstedt-Persson, 2008). Another option is bonding with carboxyl groups (-COOH) in the chemical structure of humic and fulvic acids which are more prominent in the latter (Delicato, 1996). Of the three main constituents of fibre cell walls, cellulose, hemicellulose and lignin, hemicellulose is the most hydrophilic substance due to its open structure and free hydroxyl groups, followed by cellulose which has three accessible hydroxyl groups when the polymers are not stacked to form crystalline microfibrils (Rowell, 2005; Stevens, 2010; Sweygers et al., 2022). Lignin has a hydrophobic nature and is of little importance to the water retention capability of fibres, though still attracts water better than crystalline cellulose which shows no adsorption at all (Kay and Goit, 1977; Baillie and Jayasinghe, 2004; Stokke et al., 2013; Sweygers et al., 2022). Water adsorption is highly dependent on the plant type as ratios between hemicellulose, non-crystalline cellulose, crystalline cellulose and lignin differ per species (Sweygers et al., 2022).

The adsorption of water to peat fibres is likely more complex than is the case for clay. Moreover, some plant parts, such as leaves, and plant species show natural hydrophobicity, whereas other parts are generally hydrophilic with carboxyl and hydroxyl groups on the surface (Delicato, 1996), resulting in a different behaviour towards water adsorption depending on the plant material in the peat (Doerr et al., 2000). Furthermore, the presence of the important decomposed compounds, namely humic and fulvic acids, and lignin create a complex sorption process in peat due to their complex and unique structure (Aho, 1986). Hydrophilic organic materials can become hydrophobic when they get covered by hydrophobic organic coatings, leading to a lower adsorbed water content (Kay and Goit, 1977). These coatings are highly hydrophobic and originate from a variety of sources: wax from plant leaves, root exudates, organic matter decomposition and microbial activity (Doerr et al., 2000; Atanassova and Doerr, 2010; Benito Rueda et al., 2016; Wu et al., 2020).

Organic matter decomposition can have a counterintuitive effect on the adsorbed water content: as the organic matter decomposes, the particles and fibres become smaller, resulting in a larger external specific surface area. This can be correlated to the cation exchange capacity (CEC) of peat as the CEC is found to be increasing with decreasing particle size (Levesque and Dinel, 1977), though this effect varies with the botanical origin of the peat. Increasing CEC with prolonged decomposition is also supported by Sparks (1986) who found the acids that are produced during decomposition to account for ~80% of the exchange capacity. One would expect then the adsorbed water content to increase after decomposition. However, hydrophobic coatings produced during decomposition have a repelling effect to water, decreasing adsorption (Doerr et al., 2000; Atanassova and Doerr, 2010; de Blas et al., 2010; Benito Rueda et al., 2016; Jiménez-Morillo et al., 2017). Furthermore, during decomposition mostly cellulose and hemicellulose levels decrease. As a result, the adsorbed water content would then also decrease. This aligns with the results of Volarovitch and Churaev (1966) and Romanov (1968) who report adsorbed water partitions of 30% and 11% for medium and highly decomposed peat respectively. Expulsion of adsorbed water in peat is hypothesized to be easier than in clay on surfaces due to the lower surface charge of peat fibres compared to clay particles resulting in more loosely adsorbed water in peat. However, the adsorbed water within the plant structure is harder to remove relatively.

2.3.3 Controls of changes in the adsorbed water layer

Laboratory tests show that multiple factors influence the adsorbed water layer. Some of these can be considered as constant conditions, such as surface charge density, or affect the adsorbed water layer in unsaturated conditions, such as the water vapor pressure, whereas three of these are important time-varying environmental conditions for variations in adsorbed water layer, and discussed here: pH, temperature and pore water salinity.

A change in pH affects the positive charge of the edges of clay minerals. The strength of the positive charge increases with decreasing pH, since the growing excess of H^+ ions in the pore water causes the protonation of the edge surface (Wanner et al., 1994; Lagaly and Dékány, 2013). An increase in pH will decrease the positive charge until the point of zero charge (PZC) is reached, after which the charge will change sign and become negative. The PZC of mineral soils can be different depending on composition and various experimental methods, and ranges between pH 2.0 to 9.1 (Wanner et al., 1994; Delicato, 1996; Lagaly and Dékány, 2013). Organic soils have their PZC between pH 3.4 to 6.2 and is lower with increasing organic content (van Raij and Peech, 1972; Morais et al., 1976). The adsorbed water layer around the clay mineral edges will change subsequentially with the changing charge. This will reverse the electric orientation of the dipole water molecule in hydrogen bonds and enable bonding via cations. In peat, pH slightly affects the solubility of the humic acids that can be produced by the decay of organic matter. Large quantities of humic acids cannot dissolve in water when the pH is below 6.5 (Delicato, 1996; Doerr et al., 2000) and will aggregate when in solution or remain attached to the solid surface, resulting in more repulsion between the particles (Delicato, 1996).

Temperature also affects the adsorbed water layer. Adsorption isotherms show that for the same vapour pressure less water remains adsorbed at higher temperatures (Martin, 1962; Kay and Goit, 1977; Renard and Ortoleva, 1997; Fig. 2.8). This temperature effect is smaller for low fibre contents, most likely as less water is adsorbed due to the production of hydrophobic lignin with decomposition, despite the higher surface area.

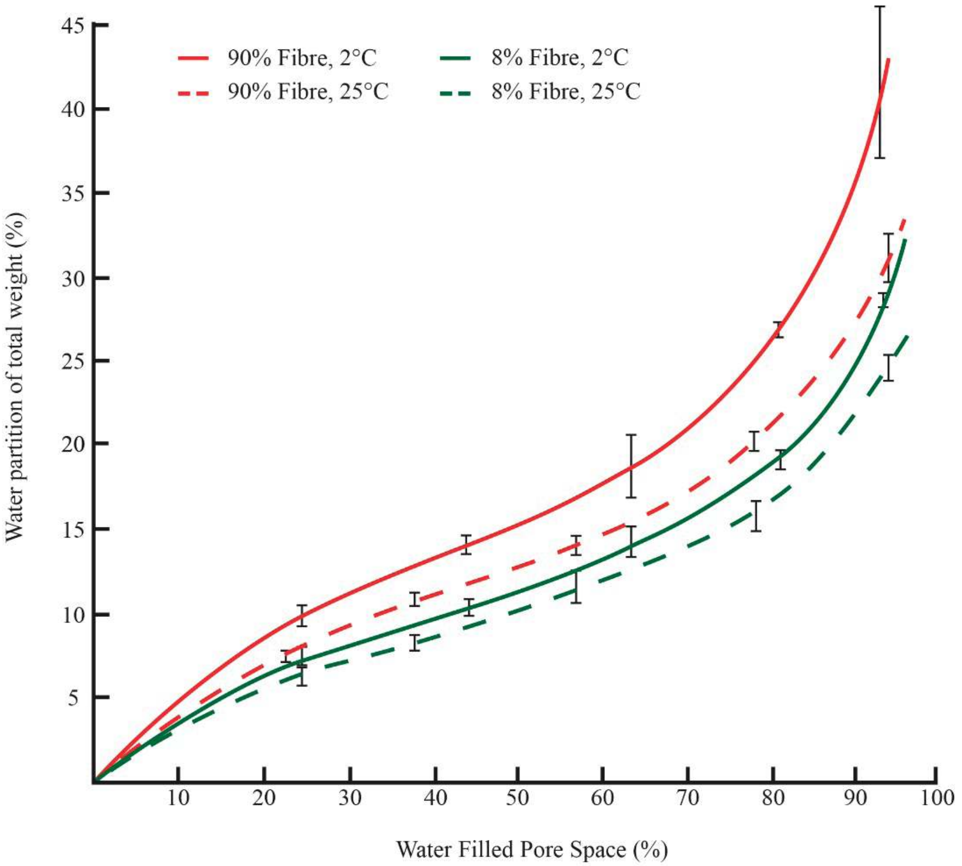

Figure 2.8: The water partition of the total weight of two Sphagnum peat samples from peat bogs near Sudbury, Ontario, as a function of the water filled pore space at 2° C (solid lines) and 25° C (dashed lines). Shown error bars are reproduced from the original figure. Samples consisted for 96-97% of organic matter and were first freeze-dried and desorbed before the water-holding properties were determined. The water partition of the total weight of the 8% fibre sample is lower for both temperatures, indicating adsorption of water onto peat is lower at low fibre contents (after Kay and Goit, 1977).

Salinity and sodicity have an effect on the adsorbed water layer because they influence ion charge in the pore water or at the surface of minerals. With increasing salinity, more charged ions are present in the pore water. To maintain an equilibrium charge at the boundary between the adsorbed water and the free water, the adsorbed water layer will become thinner to limit the contact area and therefore the required surface charge (Renard and Ortoleva, 1997;

Singh and Wallender, 2011). Sodium can adsorb easily to surfaces, especially of clay, reducing the surface charge (Gangwar et al., 2020). High sodicity will thus lead to smaller attraction forces between mineral surfaces and water, resulting in thinner adsorbed water layers. This would then result in easier pore water diffusion from the micropores to the macropores and enhance viscous compression.

2.3.4 Effect on viscous compression

The changes in the adsorbed water layer affect viscous compression of both clay and peat. The water flow of the liquid water multilayers (Fig. 2.6) may initiate slow reorientation of particles which in turn leads to viscous behaviour. Oppositely, pore flow resistance imposed by the adsorbed water layer is suggested to hinder the reorientation of the particles (Terzaghi, 1941). The adsorbed water layer furthermore delays pore pressure diffusion (Tang et al., 2016; Bjerrum, 1967). With less free water available in the pores, pressure diffusion durations in 8-cm thick clay samples increased from ~100 minutes for a stress increase of 50 kPa to 60-80 kPa, to 4,000-10,000 minutes for a stress increase of 100 kPa to 1200 kPa. This level of retardation of pressure diffusion is not expected to occur in peat, since the adsorbed water layer is less rigid due to the higher water content and generally larger pores in peat. Viscous compression in clay and peat samples occur over much longer periods than 10,000 minutes, yet this retardation of pressure throughout samples leads to larger effective stress before pore pressure is at the equilibrium level, resulting in potentially more consolidation and viscous compression. Adsorbed water can also become available for water expulsion when the environmental conditions change, for example when the pore water becomes more saline, the thickness of the adsorbed water layer will decrease, releasing adsorbed water. It has also been shown that smaller pore diameters induce thinner adsorbed water layers (Li et al., 2014).

2.4 Changing particle interaction

The third mechanism of viscous compression is through changing particle interactions. The way particles or fibres interact with each other is controlled by the structure of clay and peat and the types of (chemical) connection that can be established between the particles/fibres. Distances between particles can both increase or decrease, making it easier or harder respectively to reorientate particles (Mitchell and Soga, 2005; Le et al., 2012). Furthermore, the structural strength of clay is strongly related to the chemical composition of the clay minerals and the pore water, whereas the structural strength of peat relies on the original plant material and its preservation. Both peat and clay have their own response to changes in the structure and how reorientation could follow thereafter. This section explores the clay particle structure and the peat fibre structure together with the (bio)chemical interactions between clay particles or peat fibres themselves, before linking the structure and interactions to viscous compression.

2.4.1 Mineral and particle structure of clay

Clay mineral particles consist of two types of layers. The first layer type is the tetrahedral layer which is formed by tetrahedral cations, such as Si^{4+}, Al^{3+}, or Fe^{2+} and four oxygen atoms (Brigatti et al., 2013). The second layer type is the octahedral layer which is formed by an octahedral cation, such as Al^{3+}, Fe^{2+} or Mg^{+} and six oxygen atoms. Clay minerals can be divided into three groups based on how the tetrahedral and octahedral sheets are organized (Fig. 2.9): 1:1 clay minerals, 2:1 clay minerals and 2:1:1 clay minerals. The most common polytypes of these groups are kaolinite (1:1), illite and smectite (2:1), and chlorite (2:1:1).

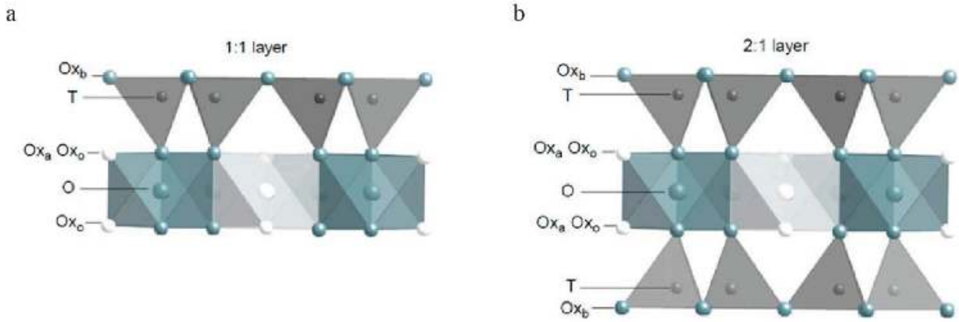

Figure 2.9: Models of a) 1:1 and b) 2:1 layer structures. Oxb, basal oxygen atoms; T, tetrahedral cations; O, octahedral cations; Ox_a, apical oxygen atoms; Ox_o, octahedral anions (OH, F, Cl) (Brigatti et al., 2013).

Kaolinite generally has the composition of $Al_2Si_2O_5(OH)_4$ (Brigatti et al., 2013). The isomorphic substitution potential of kaolinite is low, but negative surface charges still arise because of substitution of Si^{4+} by Al^{3+} (Ma and Eggleton, 1999; Mitchell and Soga, 2005). The charge at the edges of the mineral is positive for low pH values and negative for high pH values. Individual kaolinite minerals do not have an interlayer and are held together by hydrogen bonds, dipole and Van der Waals interactions (Miranda-Trevino and Coles, 2003; Brigatti et al., 2013). This produces a relatively strong clay structure that is hard to break down. If kaolinite plates are well-crystallized, they have a hexagonal form with a diameter of 0.1 – 4 µm (Fig. 2.10a) and a thickness of 0.05 – 2 µm (Mitchell and Soga, 2005).

Illite represents a group of clay minerals with a range of compositions: $^{IV}(Si_{4-x}\,Al_x)^{VI}\,(Al_{2-y}\,Mg_y)^{VI}\,O_{10}\,(OH)_2,\,(x+y)K^+$ (Brigatti et al., 2013). The potential for isomorphous substitution in illite is higher than in kaolinite. Illite has an interlayer composed of unexchangeable K^+ and H_3O^+ cations, but the K^+ concentration of illite is lower than for other mica minerals (Nieto et al., 2010). The particles of illite are small hexagonal flakes when it is well crystallized, with lateral and vertical dimensions below 0.1 µm and down to 3 nm respectively (Mitchell and Soga, 2005). Other shapes are also possible (Fig. 2.10b).

Smectites are clay minerals with a 2:1 structure defined by a hydrated ion interlayer. Montmorillonite, with composition formula $(M^{+}_{y}\cdot nH_2O)(Al^{3+}_{2-y}Mg_{2+y})Si^{4+}_{4}O_{10}(OH)_2$ in which M is the generic monovalent interlayer cation, is the most common type. Although smectites have a negative layer charge, the high potential for isomorphic substitution of divalent by trivalent cations leads to a more negative charge and substitution of trivalent cations leads to a positive charge. Because of the hydrated interlayer and large specific surface area, smectites are known for their swelling capacities, as the potential to adsorb water on both external and internal surfaces is considered unlimited (Brigatti et al., 2013). Dimensions of montmorillonite mineral particles, which can occur in film or needle like appearances depending on the type of substitution (Fig. 2.10c), are less than 2 μm for the length and 1 – 20 nm for the thickness (Mitchell and Soga, 2005).

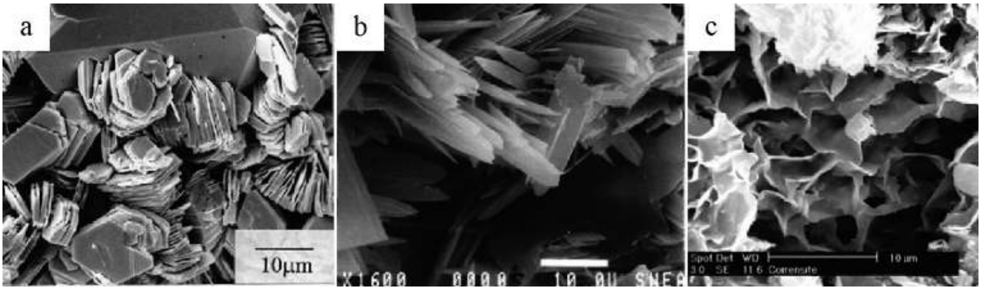

Figure 2.10: a) Kaolinite minerals, showing layering (Lanson et al., 2002), b) lath-shaped illite minerals (Lanson et al., 2002), c) corrensite (smectite) minerals (after M. Roe, Macaulay Institute, Aberdeen. 'Images of Clay Archive' of the Mineralogical Society of Great Britain and Ireland and The Clay Minerals Society. Source: https://www.minersoc.org/images-of-clay.html).

2.4.2 Macro and fibre structure of peat

The main structure of peat is composed of larger plant remains, e.g., twigs, leaves, roots, and smaller, decomposed organic material (Fig. 2.11). The structure of peat is heterogeneous on both large and small scales; it changes spatially within meters, because different types of peat are formed in various conditions from various vegetation types, and structural differences can occur as a result of different loading histories and clastic admixture. On a centimetre scale the structure differs depending on the part of the plant that is preserved at the location. Peat can be categorized in multiple ways, for example the organic content, the type of plant remains, the environment the peat has been formed in, the trophic class or the decomposition state of the peat (Lourenco et al., 2023). In the Netherlands eight botanical peat types are distinguished in geological descriptions (Bosch, 2005): reed peat, wood peat, sedge peat, Sphagnum peat, moss peat, Ericaceae peat, Eriophorum peat and Scheuchzeria peat. Classifications in England and Germany are similar (Gorham, 1957; Schulz et al., 2019). The botanical origin can indicate some characteristics of the peat structure and its strength, such as the presence of hyaline cells in Sphagnum that have reinforced cell walls. De Bruijn et al. (2014) found no relation between the botanical origin and viscous compression in oedometer tests, due to the large variations in other characteristics even within single botanical peat types, such as amorphity and organic matter content. Den Haan (1992) and Koster et al. (2018b) on the other hand, did find reed peat to be more compressible than wood peat.

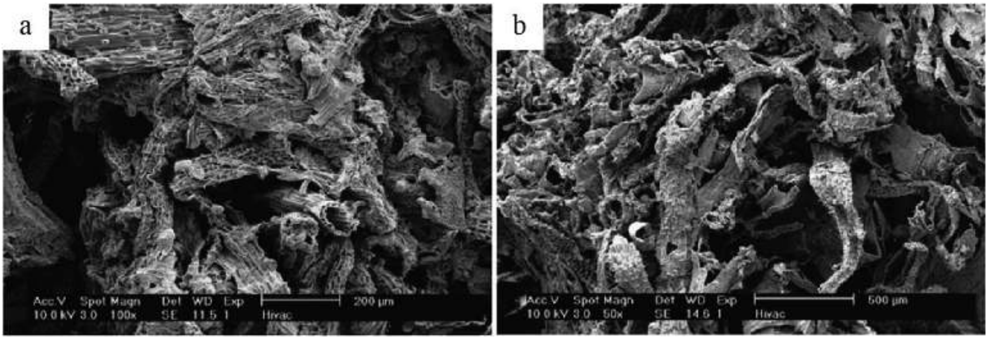

Figure 2.11: Scanning electron microphotograph of a) vertical section and b) horizontal section of fibrous Sphagnum peat (James Bay peatbog, Canada; Mesri and Ajlouni, 2007). Note that the scales of the two images are not equal.

From a geotechnical perspective on the role of peat structure in viscous compression and land subsidence, the fibre characteristics are more important than the botanical origin of the material; the state of the solids, with end-members fully intact fibres and fully decomposed organic matter, relates strongly to the strength of the peat and its resistance to deformation leading to volume loss. The botanical origin is only important when there is a clear with the geotechnical bulk parameters. Plant fibres are inherently bendable, since they consist of cells that are flexible (Mesri and Ajlouni, 2007). The amount, size and orientation of fibres can have a significant effect on the structural strength of the peat. Individual larger fibres still preserve a larger part of the structural strength of the original plants, when compared to the smaller fibres and decomposed organic matter (Edil and Wang, 2000; Mesri and Ajlouni, 2007). However, the large number of large inter-plant pores provides space for fibres to move, which is why pristine peat in general is known to have low shear strength (Landva, 2007; Mesri and Ajlouni, 2007). Although all peat types start fibrous and can become amorphous over time, the environmental conditions of the original vegetation may determine the susceptibility of the plant remains to become amorphous. For example, clay-poor reed peat is often amorphous, whereas clay-rich reed peat is more fibrous (Erkens et al., 2013) as the clay fills up pores in the peat, reducing the contact area for biological degradation by enzymes and bacteria.

Larger plant remains often dominate the structural strength of peat, especially in small samples used in laboratory set ups. In in-situ conditions, on a scale of tens of centimetres to a meter, entire logs of wood can be present in the peat, which are considerably more resistant to structural changes than individual fibres or clusters of fibres, which are very compressible and bendable (Mesri and Ajlouni, 2007; O’Kelly and Pichan, 2013). On a smaller scale of several centimetres, vertically orientated twigs, stems or large roots lead to higher strength as they can bear a major part of the effective stress, relieving the surrounding plant remains.

A final characteristic of peat that determines its structural strength is the tensile strength of the peat. In geotechnical laboratory tests, tensile strength represents the resistance of a sample against being pulled apart by opposing forces. High tensile strength originates from large fibres that interlock; peat with smaller fibres tends to have lower tensile strength (Erkens et al., 2013). The effect of reinforcement of the structure as a result of tensile resistance has been found in shear strength tests of Dutch and Canadian peat (Den Haan and Kruse, 2007; Sarkar and Sadrekarimi, 2020). These tests determined the tensile strength of horizontally orientated fibres. Effects in a vertical direction have not been reported, but tensible strength can be hypothesised to be an additional control on vertical deformation of peat substrate. Using vertically cut peat in shear strength tests with identical methods to determine tensile resistance can map the effects within the vertical direction.

2.4.3 Effect on viscous compression

The bonds acting between the particles play an important role in the potential reorientation or internal relative movement of particles under increasing stress. Stacks of clay minerals can become separated from each other, which is a process called dispersion. Dispersion can occur due to increasing contacts between the clay minerals and water, which weakens the hydrogen and dipole bonds between the minerals. When the water contains Li^+ or Na^+ exchangeable cations, dispersion occurs when the positively charged ions are adsorbed to the clay surface (Brigatti et al., 2013, Region III in Fig. 2.5). The layers become positively charged and can move so far apart that interaction ceases, with the clay structure losing strength. The opposite process of dispersion is coagulation, which is the process when clay minerals are bonded together. The main agent to induce coagulation in clay is salt. When the concentration of salt ions in the pore water increases, the adsorbed ions will move closer to the clay surface to reach the same concentration. As a result, the cation layer in between minerals will become thinner and minerals move closer together. Well-dispersed clay, like kaolinite and montmorillonite only need a minimal salt concentration to start the coagulation process (Brigatti et al., 2013). Organic cations, from for example the ammonium group, and acids, such as HCl, can function as a substitute for salt in triggering the coagulation of clay. The more strongly bound minerals then increase the strength of the clay. Through the changing distances between particles, dispersion and coagulation affect potential reorientation of particles, and thus viscous compression potential. Attractive forces active between the particles will initially restrict movement of particles, but if the external stress becomes sufficiently high, internal bonds will break and relative movement will speed up or further reorientation may occur (e.g., Taylor and Merchant, 1940; Terzaghi, 1941; Mesri and Godlewski, 1977).

The breakdown of interparticle bonds can also occur without the increase of effective stress. When metal ions are adsorbed to clay particles, the valency of the surface changes, usually leading to more space between the clay minerals and weakening the inter-particle bonding (Miranda-Treviso and Coles, 2003). This directly increases compressibility, and may further induce particle reorientation as well as opening-up of previously closed pores. In a similar way internal relative movement ('jumping') of suspended ions and molecules that are bonded to the clay surface may decrease interparticle bonding. This displacement requires that their bonding to the clay particles must be broken, which requires that a certain activation energy is reached; this can occur through a subsurface temperature increase (Low, 1960; Mitchell et al., 1968), which explains to some extent the temperature dependency of viscous compression. Dispersed individual clay minerals may come into suspension in the pore water and may end up stuck in the smaller pore throats. Furthermore, the larger clay coagulants are, arguably, relatively strongly bound within a structure compared to individual clay particles. Their larger and irregular size makes it more difficult to reorientate, and reorientation would require movement of numerous other particles as well. The result is that viscous compression is more difficult and slower as well. It is likely that these chemical bonding mechanisms more prominently occur in clay than in peat, due to the larger valency of the clay particle surfaces compared to peat particle surfaces. In contrast, interparticle bonding in peat is more determined by the physical interlocking of the irregularly-shaped particles.

2.5 Discussion: Viscous compression: clay versus peat

The review of the different mechanisms that lead to viscous compression revealed that the same mechanisms are causing the viscous compression of clay and peat, but the relative importance of mechanisms and underlying processes differs. Furthermore, peat characteristics and environmental conditions are affected by decomposition, which sets decomposition as a distinctive control of viscous compression of peat. Here, we highlight similarities and differences between the material characteristics, environmental conditions, and processes between clay and peat. We then explain how changes in each of them plays a role in the mechanisms and controls of viscous compression. We also indicate the relative importance of the various conditions and characteristics (Fig. 2.12). Subsequently, we discuss the role of organic matter decomposition as control of viscous compression of peat. This approach enables us to validate the comparison between the available knowledge on clay and its transferability to peat, and highlight unique conditions and characteristics to peat.

2.5.1 Material characteristics, environmental conditions, and processes

Material characteristics, environmental conditions and processes that affect viscous compression of peat or clay and their relative importance are shown in Fig. 2.12. In this section the effect of material characteristics and environmental conditions on processes affecting viscous compression is discussed, starting with the characteristics. As viscous compression is continuously happening, both the consolidation phase (Type II in Fig. 2.1) and the viscous compression phase (Type III in Fig. 2.1) need to be considered. A decrease in *hydraulic* *conductivity* limits the flow velocity of the pore water in the consolidation and viscous compression phases. This will not only increase the duration of the consolidation period, but potentially slow down fibre reorientation and hence viscous compression as micropore water expulsion depends on the macropores. It is likely that the effect is larger in peat as it generally has a higher hydraulic conductivity and changes therein are significant more easily. The larger average *pore size* of peat causes micropore water expulsion and water diffusion to contribute less to viscous compression compared to clay as more pores in peat expel water following pore pressure differences. The high initial *porosity* of peat has a relatively larger impact on particle interaction due to the larger size of fibres compared to clay particles. Higher porosity provides more spaces and less contact points between fibres for the friction-driven particle movement and therefore viscous compression to happen. Apart from the size of the fibres, the *fibre content* itself dictates the friction-driven particle movement in a similar way as fibres move with greater difficulty than decomposed organic matter.

Furthermore, the review shows that the differences in structural characteristics of clay particles and peat fibres lead to distinct responses to physical (temperature) and chemical (pH, pore water salinity, oxidizing agents) environmental conditions that determine the mechanisms of viscous compression (Fig. 2.12). Higher *temperatures* lead to acceleration of water diffusion and higher activation energy for jumping bonds involved in attraction/repulsion and ion adsorption. Temperature is also one of the environmental conditions that determines the equilibrium void ratio of organic soils (Al-Khafaji and Andersland, 1981) and with that determine the compressibility. Furthermore, a higher temperature increases both aerobic and anaerobic decomposition of peat, which impacts the fibre content and porosity and increases viscous compression. For an increase in temperature of 10 °C, peat decomposition rates can triple (Berglund et al., 2008; Dorrepaal et al., 2009), though a temperature increase of 2 °C would result in 25% faster decomposition in Dutch peatlands (Hendriks, 1992; Querner et al., 2012). A higher response with temperature increase is seen for aerobic decomposition (Szafranet-Nakonieczna and Stepniewska, 2014), while a higher temperature sensitivity of decomposition in general is seen at temperatures near the freezing point compared to temperate soil temperatures between 13 and 25 °C (Berglund et al., 2008; Dorrepaal et al., 2009). Through accelerating decomposition and associated decreasing porosity of peat, a temperature rise reduces its compaction potential. Changes in *pH* have a larger effect on chemical processes attraction/repulsion and ion adsorption in clay than in peat due to dependency of surface valence of clay particles. However, decomposition rate is also dependent on the pH, which is why pH changes are considered to be of equal importance for peat and clay. *Pore water salinity* is particularly important for viscous compression of clay, since higher salt content can slow down water diffusion and cause flocculation of clay particles, which decreases viscous compression rates. In peat, salt leads to more organic compound production (Strehse et al., 2018), potentially affecting the attraction/repulsion between fibres when the compounds are adsorbed. Laboratory tests show that aerobic decomposition slows down by 50% with a salt concentration increase of 4‰ of the groundwater, while anaerobic decomposition remains virtually unchanged (Brouns et al., 2014). The availability of *oxidizing agents* does not affect clay or its viscous behaviour, but is very important for changing the fibre content through decomposition with a subsequent change in viscous compression as described above.

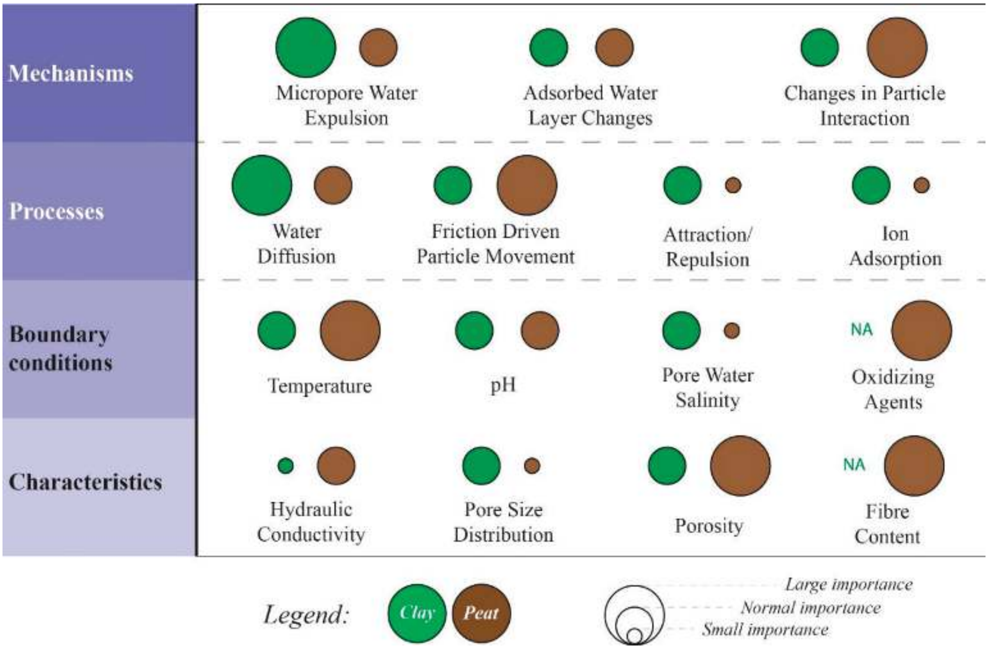

Figure 2.12: Proportional area diagram showing the relative importance of mechanisms, processes, environmental conditions and material characteristics of clay and peat for viscous compression. Relative importance is categorized in three classes: large, normal and small. Green and brown circles represent the relative importance of clay and peat respectively. When a term does not apply to either clay or peat and relative importance is zero, NA (not applicable) is shown.

Mineral-poor peat occurs in mires such as peat bogs and fens, whereas in the subsurface of deltas peat-clay mixtures such as organic clays and clayey peats are more commonly found. The location with respect to the nearby rivers and growth rate of peat on the one hand as well as the flooding frequency and intensity, and suspended sediment concentration of the nearby rivers on the other will determine the ratio of peat and clay in the material (Berendsen and Stouthamer, 2000; Gouw and Erkens, 2007; Davies-Vollum and Smith, 2008). Slightly to strongly humic clays contain up to 15-30% organic matter depending on the amount of silt and sand included, whereas organic clay can contain up to 22.5-55% organic matter, and clayey peat up to 35-70% (NNI (2019a); NNI (2019b). Peat-clay mixtures may have typical and interacting physical and chemical characteristics that render prediction of the effect on viscous compression mechanisms not straight-forward. Still, viscous compression of peat-clay mixtures has so far not been addressed specifically in previous studies, but was only considered alongside other subjects; from these studies we derived how mixing of the two materials affects viscous compression. For example, Al-Khafaji and Andersland (1981) indicated that the change of equilibrium void ratio after 24 hours of compression in an oedometer, incorporating both consolidation and viscous compression, is significantly stronger with increasing organic content, but that this dependency disappears almost mostly when effective stress exceeds 200 kN/m^2. Pore size distribution and connectivity of peat clay mixtures deviate from clays and mineral-poor peat as the smaller clay particles can fill larger pores in the peat, reducing the pore volume. Oppositely, reduction of organic matter in clayey soils is positively related to the amount of macro- and mesopores, and negatively related to the amount of micropores (Zaffar and Luo, 2015). This effect is more pronounced in the larger clay aggregates studied, between 2 – 5 mm. Beaudet and Charpentier (1998) found that fitting a mixing model to predict void ratios of silty clay loam-peat mixtures after loading works best when, mathematically, clay is allowed to occupy pores in the peat as well as vice versa. Also, clogging of pore throats by clay particles may occur, reducing hydraulic conductivity. The organic compounds and organic cations produced by decomposition can attach to clay particles and become hydrophobic (Güven, 1992; Brigatti et al., 2013), decreasing adsorbed water layer thickness and releasing interparticle forces leading to coagulation (Lagaly and Dékány, 2013). In contrast, experiments by Ivakhnova and Nevzorov (2020) using dry clay powder indicated that adding clay to peat, especially highly wettable smectites, can remove adsorbed water from peat fibre structures inciting accelerated viscous compression on a short time scale. Forces at peat fibre – clay mineral contacts are likely different than between mineral - mineral or fibre - fibre contact. Organic matter density has been reported to become independent of organic matter content when it exceeds ~20% by weight of the solids (Erkens et al., 2016), thus indicating that increasing clastic content does not directly compress the organic content present. This highlights the importance of organic material for the structural strength. The effect of increasing sand content has not been studied. It has been shown that increasing sand content up to 40% leads to decreasing virgin compression coefficients CR, while the effect on recompression is negligible (Celik and Canakci, 2014). Additionally, the internal surface angle increases, especially between 0% and 10% sand. This could be an indication of stabilization of the structure and less potential for particle reorientation.

2.5.2 Peat decomposition as control of viscous compression

The effect of the degree and rate of decomposition of the organic matter on viscous compression of peat is poorly understood (Price et al., 2005; Matthiesen, 2004; O'Kelly and Pichan, 2013). Nevertheless, it is generally agreed that an increase in the degree of decomposition of peat leads to a lower compressibility (Hobbs, 1986; Amaryan, 1993; Price et al., 2005; Huat et al., 2011), suggesting an negative feedback with viscous compression is possible as well (Berry, 1983; Landva and La Rochelle, 1983). Therefore, it is important to understand how the degree and rate of decomposition affects viscous compression and the underlying mechanisms.

Decomposition of organic matter directly leads to a volume loss because organic matter is consumed by microbes (Schothorst, 1977; van den Akker et al., 2007; Berglund et al., 2008; Dorrepaal et al., 2009; Brouns et al., 2014). The material characteristics and environmental conditions determining viscous compression behaviour are depending on the degree of decomposition, setting the state and situation in which decomposition and viscous compression is currently happening. Since formation in anoxic conditions, the peat might have been above the groundwater level, exposing it to oxygen. Under oxic conditions, decomposition occurs due to oxidation. Decomposition rates in these conditions are the highest within the aerated subsurface and oxygen exposure can accelerate decomposition and emission of anoxic peat manifold (Tolunay et al., 2024). Anoxic decomposition through microbial activity is much slower than oxic decomposition and depends on temperature, pH and oxidizing agents (Wardwell et al., 1983; Hobbs, 1987). In the past, the rate of decomposition has been considered to be too slow under anoxic conditions to actively play a significant role in changing the physical and chemical environmental conditions for viscous compression of peat (Hobbs, 1987). However, this has been contested by Pichan and O'Kelly (2012), O'Kelly and Pichan (2013) and Zain (2019) as they show a noticeable decrease in water content and secondary compression coefficient (C_α), the amount of viscous compression per log unit of time in Type III, within active decomposition experiments lasting up to 2 months.

Rather than a new mechanism, decomposition is found to be a control of viscous compression. Active decomposition changes porosity, fibre content, and size of those fibres. In combination with organic compounds produced during decomposition, these changes in material characteristics influence viscous behaviour resulting from the three main mechanisms of viscous compression; micropore water expulsion, adsorbed water layer changes, changes in particle interaction (Fig. 2.12). Moreover, the strength of the peat and the effective stress can be affected in the following ways:

First, decomposition influences the micropore water expulsion. The effect of active decomposition on the micropore water expulsion lies mainly in the availability of water to expel, specifically the cell water. In fibrous peat, between one third and two thirds of the water content is contained inside the fibres (O'Kelly and Zhang, 2013). The walls of these cells can break down as a result of active decomposition, which would enable the previously immobile cell water to be expelled and increase the direct compressibility of the peat. This is easier for plant tissue without lignin, which is harder to break down (Landva and Pheeney, 1980; Hobbs, 1986; Farell, 2012). Additionally, decomposition complicates pore water flow. Typical pore diameters decrease as peat decomposes (O'Kelly and Pichan, 2013), leading to lower hydraulic conductivity. Breakdown of fibres by bacteria associated to active decomposition can cause clogging, which prohibits water flow. The same holds for the gasses produced during active decomposition that further decrease the hydraulic conductivity.

Second, the state of decomposition also influences the adsorbed water layer (Hobbs, 1987; O'Kelly and Pichan, 2013). The breakdown of fibres can release adsorbed ions that affect the adsorbed water layer elsewhere in the peat. Gasses produced by active decomposition can replace the pore water in some pores and can also adsorb to particle surfaces of both clay and peat. Furthermore, as the fibres are broken down, their specific surface area increases, which can potentially increase the amount of absorbed water. Additionally, the decomposed peat particles are smaller than the fibres. As a result, the pore volume drops as particles fit more tightly together, also decreasing the interparticle distance, which may lead to stronger interparticle forces and limit particle reorientation even more (Hobbs, 1987; Price et al., 2005).

Third, the chemical interparticle forces decrease when the organic compounds adhere to the fibre surfaces as they have a hydrophobic character. Distance between the fibres could increase slightly due to this character, weaking forces and decreasing friction at the contact points between fibres.

Fourth, the breakdown of the cell structure leads to lower strength of the original plant structure, which may enhance the probability of particle reorientation. On the other hand, smaller decomposed particles are less susceptible to particle deformation (Farrell, 2012). Not every organic structure is decomposed in a similar way. Eutrophic peat shows higher decomposition rates when oxygenated then oligotrophic peat as phenolic compound concentrations are higher in oligotrophic peat, limiting decomposition (Brouns et al., 2014). Also, leaves are thinner than stems and major roots, and thus may more easily break apart. However, reinforced cell walls of hyaline cells in leaves (to store water and maintain cell shape in dry periods; Landva, 2007) give extra strength to the peat fibre structure.

Last, decomposition also produces gas bubbles, which can have a buoyancy effect on particles, lowering the effective stress and changing the hydraulic conductivity by obstructing pore throats (Kellner et al., 2004, Kellner et al., 2005). The lower effective stress leads to a decrease of the viscous compression rate.

2.5.3 Implications for land subsidence assessments

The new insights that have been acquired by this research based on literature review envelop an overview of the mechanisms that instigate viscous compression of peat and the role of decomposition. Though the results presented here are on a fundamental level, we believe that it will help addressing and dealing with land subsidence problems. It is expected that these insights will help the land subsidence community in the long run with better modelling and mitigation. With more information about the underlying mechanisms and controls, new additions and/or changes in the modelling methods can be triggered. For example, involvement of decomposition in geomechanical compaction calculations through direct coupling is in most methods absent, but new additions or changes can be made to directly couple loss of organic matter to volume changes of peat and peat-clay mixtures in the future using this review as a starting point. Furthermore, the list and discussion of controlling environmental conditions and material characteristics can help assessing the likelihood of viscous compression given current conditions as well as improving the investigation of the effectiveness of mitigation options. This is especially important for urban areas that continue to subside despite a long term status quo in the water management and loading conditions. An example of this is the city of Gouda in the Netherlands of which the city centre continues to sink several decades after the last anthropogenic loading has occurred. One of the main hypotheses is that ongoing compaction of the subsurface related to viscous compression is responsible for the subsidence rate seen at the surface. Similarly, rural areas facing problems resulting from ongoing compaction can benefit from the improved knowledge on viscous compression presented in this review.

2.5.4 Future research

This review creates an overview of the mechanisms of viscous compression of peat. Ideally, we would also like to discuss the quantification of the mechanisms of viscous compression and the influence of decomposition for peat, clay and mixtures of the two. However, since peat/organic matter is very heterogeneous in its characteristics and how it behaves with changes in the environmental conditions, it is very hard to provide ranges to be used for calculations at this point. This issue is further complicated by the fact that this review only looks at existing literature without incorporating own data. Likely, presented ranges would be very large and usage of the values becomes unjustified. Therefore, more information, especially based on experimental data, on the relation between decomposition, viscous compression and the individual mechanisms still needs to be acquired to validate ongoing theories (O'Kelly and Pichan, 2013). Zain (2019) explored the relation between active decomposition and viscous compression by comparing non-oxidised, partially oxidised and fully oxidised samples, showing that when samples are oxidized artificially with hydrogen peroxide an increase of viscous compression in the loading step after oxidation is visible. For in-situ conditions, the relation with viscous compression should also be investigated using oxidizing agents that are naturally present in the saturated zone, such as dissolved oxygen, phenols, and humic acids, or looking at micro-organism activity, as these have been found to be main contributors to anoxic decomposition (Keller et al., 2009; Walpen et al., 2018a; Walpen et al., 2018b; McGivern et al., 2021). Also, questions are still left unanswered on other characteristics and environmental conditions of the viscous compression of peat. For example, Hanson et al. (2001) already showed the temperature dependency of viscous compression of peat in laboratory and field tests. However, both the laboratory and experiments involved temperatures that do not often or not at all occur naturally in the subsurface. It was hypothesized that the temperature dependency is due to accelerated biodegradation, but it was not verified. An explanation for the settlement rate pattern under natural temperatures, which was less prominent and not following the temperature over the entire test duration, is not given.

Special attention for peat-clay mixtures can advance our understanding of the viscous compression behaviour of peat-clay mixtures significantly. As peat-clay mixtures widely occur in deltas, understanding their joint characteristics and interactions between both materials is essential for land subsidence studies. Also, this will help predicting the effect on compression behaviour when the composition of the subsurface changes over time. Specific studies, for example on the chemical influence of the pore water and the products of decomposition, can help better map the relative contribution of the mechanisms in peat. In the isotach method modelling, the most common modelling method for calculating compaction of subsurface layers by using lines of equal rate of strain and intrinsic time (Den Haan, 2003), decomposition might be introduced, either as an input parameter or as independent variable for the geotechnical compression indices, potentially changing these parameters from static to time-dependent. To take this step, correlations between geotechnical compression indices a (recompression index, related to RR), b (compression index, related to CR) and c (secondary compression index, related to C_α), and decomposition need to be analysed. Since the scale at which the individual mechanisms act is in the order of nanometers to centimeters, peat heterogeneity is going to be an issue when it comes to modelling, as is already the case with the current predictive models. Therefore, it is suggested that new information is tested in small, plot-scale models or even 1-D models to calibrate with measurements, before scaling up stepwise to models that can be used to predict regional to national scale areas.

2.6 Conclusion

Viscous compression of peat is a significant contributor of land subsidence, potentially affecting large areas and acting over long time periods. From this literature review, we identified a hierarchy of controls, processes and mechanisms that eventually result in viscous compression of clay under an applied loading, and compared how these operate in peat. Three key mechanisms have been reported to result in viscous compression of clay: micropore water expulsion, changes in the thickness and composition of the adsorbed water layer and changing particle interactions. Considering the porous structure of peat, the occurrence of adsorption water on organic material, and the fibrous material structure, it is likely that these three mechanisms contribute to viscous compression of peat as well. However, there are essential differences between peat and clay relevant to viscous compression as is to be expected given the two are completely different substances: peat is made up of fibres; these contain water in their cells which is hard to release, they can interlock physically, and lack the strong negative surface charge that clay minerals have. As a result, the underlying processes and contribution of the three mechanisms to viscous compression are different for peat: the smallest pores in peat are larger than in clay, which means they are more likely to drain normally instead of via diffusion. Furthermore, less adsorbed water and the physical interlocking lead to a distinct friction effect on reorientation.

A further important difference between clay and peat is that the latter can decompose, which strongly affects physical and chemical characteristics of peat over time. Furthermore, decomposition affects the three mechanisms, which is why decomposition of organic matter is proposed as another possible control of viscous compression of peat. When the organic matter is lost, it is likely that the structural strength of peat decreases as fibres break down, losing their inherent strength. Nonetheless, the effect on both the peat structure as a whole, as well as the investigated mechanisms identified in clay present decomposition as a control that cannot be ignored in the explanation of viscous compression of peat.

This review has shown that the viscous compression mechanisms, susceptibility to compression, and decomposition of peat are strongly controlled by physical, chemical and biological characteristics, and environmental conditions. The susceptibility to viscous compression of peat is determined by: 1) the fibre content, 2) the active decomposition, 3) the clay mineral content, 4) the subsurface temperature, 5) the pore water pH and 6) ion concentration of the pore water. The ratio between fibre and clay mineral content and the fibre size depends on the environment and changes therein between the moment the peat was formed and now. The other mentioned characteristics and environmental conditions are dependent on the current environment and depth of the peat. The most important of these characteristics and conditions is difficult to determine and also will vary for different types of peat. Future research on this topic should focus on quantifying the contribution of the driving processes to be able to better understand and mitigate viscous compression. Furthermore, lab tests revealing the dependency of viscous compression rate on changes of the important parameters can improve predictive calculation of viscous compression.

Acknowledgements

We are grateful for the input of Henk Kooi (Deltares Research Institute) and Bente Lexmond (Utrecht University) during the internal revision process, as the discussion of the physical and chemical aspects of clay, organic matter and pore water and their interaction improved the quality of the review.

The research presented is part of the project Living on soft soils: subsidence and society (grantnr. NWA.1160.18.259). This project is funded by the Dutch Research Council (NWO-NWA-ORC), Utrecht University, Wageningen University, Delft University of Technology, Ministry of Infrastructure and Water Management, Ministry of the Interior and Kingdom Relations, Deltares, Wageningen Environmental Research, TNO Geological Survey of The Netherlands, STOWA, Water Authority: Hoogheemraadschap de Stichtse Rijnlanden, Water Authority Drents Overijsselse Delta, Province of Utrecht, Province of Zuid-Holland, Municipality of Gouda, Platform Soft Soil, Sweco, Tauw BV, NAM.

Author contributions: CRediT

Pepijn van Elderen: Conceptualization, Investigation, Formal analysis, Visualisation, Writing – original draft, **Gilles Erkens**: Conceptualization, Supervision, Writing – review and editing, **Cor Zwanenburg**: Writing – review and editing, **Hans Middelkoop**: Writing – review and editing, **Esther Stouthamer**: Conceptualization, Supervision, Writing – review and editing.

Chapter 3:

The effect of compaction on short-term decomposition rates in peat samples with different degradation status

Tolunay, D., van Elderen, P., Hefting, M.M., Kowalchuk, G.A., Stouthamer, E., Erkens, G. (2025). The Effect of Compaction on Short-Term Decomposition Rates in Peat Samples with Different Degradation Status.

Submitted to: Terrestrial, Atmospheric and Oceanic Sciences, special issue; Ground Deformation in a Changing World: Land Subsidence, Climate, and Resilience

ABSTRACT

Porosity is a key characteristic determining land subsidence rates in drained peatlands by regulating subsidence mechanisms (consolidation, viscous compression, and decomposition) which, in turn, also influence peat porosity. This study aimed to investigate how consolidation and viscous compression change porosity and how porosity changes affect decomposition rates in peat substrates differing in degradation status. Intact peat samples, representing less decomposed fibric peat (FP) from saturated depths and more decomposed peat (DP) from vadose zone were collected from a drained peat meadow in the Netherlands. Samples were subjected to stress levels of 10 kPa and 40 kPa for three days in the laboratory, total porosity and void ratio were calculated before and after compaction. CO2 emission rates and β-D-Glucosidase potential activities were then measured to assess decomposition rates of compacted peat. Under the applied 10 kPa and 40 kPa stresses, void ratio decreased in the FP samples compared to uncompacted control samples by approximately 8.8% and 40.6%, and in the DP samples by 6.3% and 21.6%, respectively. In FP samples, consolidation likely accounted for over 50% of porosity reduction with viscous compression (creep) playing a minor role, while, in DP samples, viscous compression relatively had a greater contribution. Average decomposition rates declined by 33.1% and 48.1% for FP, and by 11.2% and 14.4% for DP compared to controls, upon compaction at 10 kPa and 40 kPa, respectively. Our findings demonstrate that subsidence mechanisms are interconnected through changes in porosity, affecting land subsidence rates. Future studies should focus on the interactions of mechanisms rather than disentangling them.

3.1 Introduction

Peatlands comprise 8% of the surface area in the Netherlands, covering approximately 270.000 ha (Aben et al., 2024; Arets et al., 2023). Extensive drainage for agriculture and loading because of urban development have resulted in current land subsidence rates up to 10 mm/yr in these vulnerable areas (Fokker et al., 2018; Koster et al., 2018; Timmerman et al., 2021; Van Asselen, 2011). These high rates of subsidence lead to socio-economic and environmental challenges, such as increased flood risk, higher CO_2 emissions, and damage of buildings and infrastructure (Dinar et al., 2021; Prosperi et al., 2023; Vermeersen et al., 2018).

Human-induced land subsidence in agriculturally used drained peatlands is driven by both physical and biochemical mechanisms. Several studies have estimated their relative contributions to subsidence rates in the unsaturated zone to be approximately 28% and 72%, respectively (Erkens et al., 2016; Leifeld et al., 2011; van Asselen et al., 2018) Physical mechanisms of subsidence in peat include irreversible shrinkage, consolidation and viscous compression (Galloway et al., 2016; van Asselen et al., 2009). Shrinkage is the decrease in peat volume as a result of drying, leading to reduced moisture content and increased suction pressure in the unsaturated zone (Cornelis et al., 2006; Seidel et al., 2023). Consolidation refers to volume changes due to the expulsion of over-pressured pore water (den Haan, 1994; Oleszczuk et al., 2022; Terzaghi, 1941). Viscous compression (creep) is the result of micropore water expulsion, adsorbed water layer deformation and changing particle interactions leading to viscous structural rearrangement under constant stress (Le et al., 2012; van Elderen et al., 2024). In drained peatlands, drainage dynamics have caused large impacts and heterogeneity in the level of compaction, which differs with depth and lateral space, as well as over time.

Land subsidence in peatlands also results from the biochemical mechanisms of aerobic and anaerobic decomposition of organic matter (OM), including both peat and fresh organic compounds (Schothorst, 1977; Tolunay et al., 2024). Once peat is drained and exposed to oxygen, there is a shift from anaerobic to aerobic decomposition, which can continue over centuries, depending on environmental conditions and material characteristics. Microorganisms and chemical oxidation convert OM into inorganic forms like CO_2, CH_4, N_2 or N_2O, weakening the peat structure and causing volume loss (Brouns et al., 2016; Galloway et al., 2016; Harpenslager et al., 2024). Over time, high decomposition rates change the characteristics of peat by increasing its level of degradation. As peat becomes more decomposed, shifting from fibric to degraded forms, the physical mechanisms of subsidence and the future decomposition rates are also affected (O'Kelly and Pichan 2013). Currently, studies on land subsidence often examine processes of physical and biochemical mechanisms separately, however the rate of these processes were determined by the same controls such as material characteristics (e.g., porosity and degradation degree) and environmental conditions (e.g., temperature and moisture content) (van Elderen et al., 2024), stressing interaction between the two processes (O'Kelly and Pichan, 2013).

Porosity, a key material characteristic of peat, interlinks mechanisms by defining void space and affecting deformation, shrinkage, consolidation, and decomposition. In turn, these mechanisms feedback to alter peat porosity (Huat et al., 1988; Pichan and O'Kelly, 2013). Natural peat in saturated conditions has high porosity and a large void ratio, which make it highly compressible. Thus, increasing the effective stress leads to the collapse of these large pores, resulting in compacted peat (Rezanezhad et al., 2016; van Asselen et al., 2009). Porosity also influences OM decomposition rates by regulating water availability, nutrient distribution, and oxygen diffusion (Fig. 3.1a) (Du et al., 2023; Toosi et al., 2017a; Wang and Zhang, 2024). Larger pores (>30 µm) enhance oxygen availability and nutrient mobility, thereby accelerating decomposition (Ruamps et al., 2013). Ruamps et al. (2011) and Strong et al. (2004) found that 15-60 µm pores support the fastest decomposition rates, while Kravchenko and Guber (2017) observed that 30-90 µm pores contribute most to overall decomposition. However, most of such research has been conducted in mineral soil, not in peat, with a primary focus on the decomposition of fresh organic compounds.

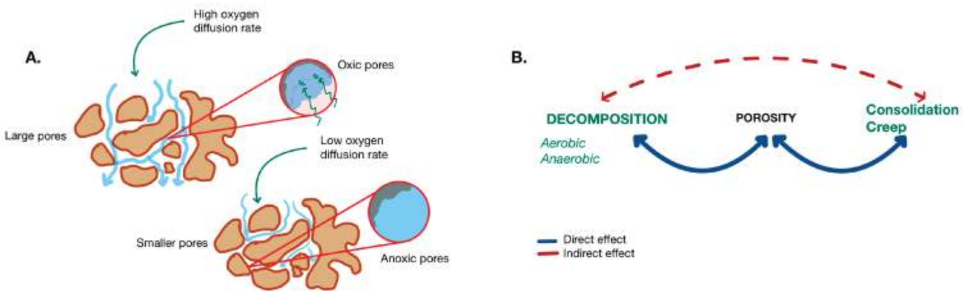

Figure 3.1: a) The impact of porosity changes on the environmental factors of peat. b) Relationship between decomposition, consolidation and creep (viscous compression) and the porosity as a material characteristic for this interaction

Physical mechanisms generally decrease porosity, although some, including the poroelastic component of consolidation and swelling, can increase it (Biot, 1941; Philip, 1969; Schäffer et al., 2010). OM decomposition also has dual effects (Pichan and O'Kelly, 2013). While it ultimately leads to reduced particle size and pore size (Kleimeier et al., 2017), it can also enlarge pore space via particle size reduction, and through gas accumulation (De Gryze et al., 2006). Since decomposition alters porosity in different ways, it can indirectly influence the physical land subsidence mechanisms (Fig. 3.1b). Feng et al. (2021) showed from unidirectional consolidation and permeability tests that temporarily accelerated viscous compression in peat, called tertiary consolidation, is at least partially the result of organic matter decomposition. This potential interaction between land subsidence mechanisms is often overlooked, even though it can provide insights into which environmental conditions and peat material characteristics in different time frames might be associated with faster subsidence rates. Therefore, incorporating porosity-driven interactions into process-based models may improve predictions of land subsidence and CO_2 fluxes from drained peatlands. This perspective allows one to account for site-specific factors, ultimately leading to more effective management strategies such as drainage adjustments or rewetting to mitigate subsidence and GHG emissions in drained peatlands (Stouthamer et al., 2020).

Given the significance of the interaction of physical and biochemical mechanisms affecting subsidence, our study focuses on 1) how consolidation and viscous compression control the magnitude and rate of porosity change in peat with varying degradation status, and 2) how porosity change affects decomposition rates in peat with varying degradation status over a period of several days. In addition, based on the literature and experimental results, this study aims to propose a new conceptual framework for subsidence mechanisms under saturated and unsaturated conditions, providing a new perspective for land subsidence research.

We hypothesized that consolidation would be the main driver of porosity reduction in both fibric peat (FP) and decomposed peat (DP) given the limited period of compaction, with viscous compression playing a more important role in decomposed peat. This is because DP generally has smaller and less pores, and is therefore less compressible, both limit consolidation. In addition, increasing stress would reduce decomposition rates by decreasing porosity, with less impact on DP samples versus less decomposed FP samples, due to initial lower porosity of decomposed peat. We tested our hypotheses by altering porosity with a standard oedometer loading test and subsequently measuring CO_2 emission rates and b-D-Glucosidase potential activities in the compacted samples as a proxy for decomposition rates.

3.2 Materials and methods

3.2.1 Field sampling

Peat samples were collected from a Dutch peat meadow area close to the village of Assendelft (52° 28' 33.6"N 4° 44' 24.1"E). Peat formation occurred between 5000 and 1000 yr BP in back-barrier marsh conditions with the peat surface reaching a maximum height of 2 m above average mean sea level (a.M.S.L.) (Van de Ven, 1993). Currently, the elevation of the peat surface is 2 m below a.M.S.L. due to, firstly, drainage since 1000 yr BP resulting in land subsidence of over two meters and, secondly, extensive peat excavation in the 19^{th} century when more than 1 m of peat was removed (Van de Ven, 1993; Vos et al., 2020). The sampling site, used for dairy farming, has a surface elevation of -1.5 to -1.8 m a.M.S.L. The groundwater table fluctuates between 0.1 and 0.8 m below the surface (Erkens et al., 2021). The top 0.3 m of the peat layer is clay-rich (loss on ignition - LOI < 40%), while the peat layers deeper than 0.3 m showing LOI values of 50–80%. Degradation below the clay-rich layer is generally H5-H6 on the Van Post scale, except for the intervals 0.3 - 0.4 m and 2.0 – 2.5 m (H7-H10 and H1-H4 respectively). Fibrousness maxima occur between 1.7–2.0 m. Sedge dominates the peat matrix, with reed becoming more prevalent in the deeper peat layers (Fig. 3.2). (Erkens et al., 2013). Further site details are given in Boonman (2024) and in Supplementary A.1 (Fig. A1 – A4, Table A1).

The sampling depths were determined based on long-term monitoring data of the groundwater table, the clay content from soil profile data and the level of decomposition as classified with the adapted humification scale since the Van Post Scale is not very representative for drained Dutch peatlands (Erkens et al., 2021, 2013). In addition, another soil profiling was conducted prior to sampling (Table A1). Four field replicates for the vadose and saturated zones were collected with the peat sampler 50 cm from a central point in the field where the gauge for soil profiling was taken. From each hole, full casings of three rings per depth were collected using the sampler designed by van Asselen and Roosendaal (2009). A 104 mm wide and 320 mm long stainless-steel tube with a sharp cutting edge were used to cut peat to allow smaller diameter subsampling in the laboratory without the disturbances created by the field sampling. The tube holds three 85 mm long PVC liners. After collection, the PVC liners were pushed out, cut at the interfaces, and capped to prevent water drainage and air intrusion. The sample in the upper casing was taken from a depth of 30 to 60 cm and contains decomposed peat (DP) that is unsaturated during part of the year, with an average dry bulk density of 0.20 g/cm^3. The sample in the lower casing was taken from a depth of 100 to 130 cm and contains less decomposed, fibric peat (FP), which remains permanently below the groundwater table, with an average dry bulk density of 0.09 g/cm^3. The collected samples were transferred in a cooling box to the laboratory fridge at 10°C with 80% humidity.

3.2.2 Experimental design

The laboratory experiments consisted of 1-D oedometer compression tests and respirometer measurements under saturated conditions. Only ring 3, representing the deepest 10 cm of each zone (50-60 cm for DP and 120-130 cm for FP), was used for the experiment because of the clastic content seen in the soil profile log represented by the upper rings of the DP samples (Fig. 3.2).

Standard procedure was followed to prepare samples for the oedometer (ASTM D2435-04, 2011). The inside of a metal confining ring with a diameter of 63 mm and a thickness of 20 mm was oiled to decrease wall surface friction during compression, after which the empty ring was weighed. Samples were then carefully trimmed to fit the ring tightly avoiding any space between the sample and the ring wall. The filled ring was weighed again before being built into the oedometer and the basin within which the sample ring is placed is filled with water to mimic saturated conditions. Two stress levels for the single load tests were selected, respectively 10 and 40 kPa, with 10 kPa recognized to be below or at the preconsolidation

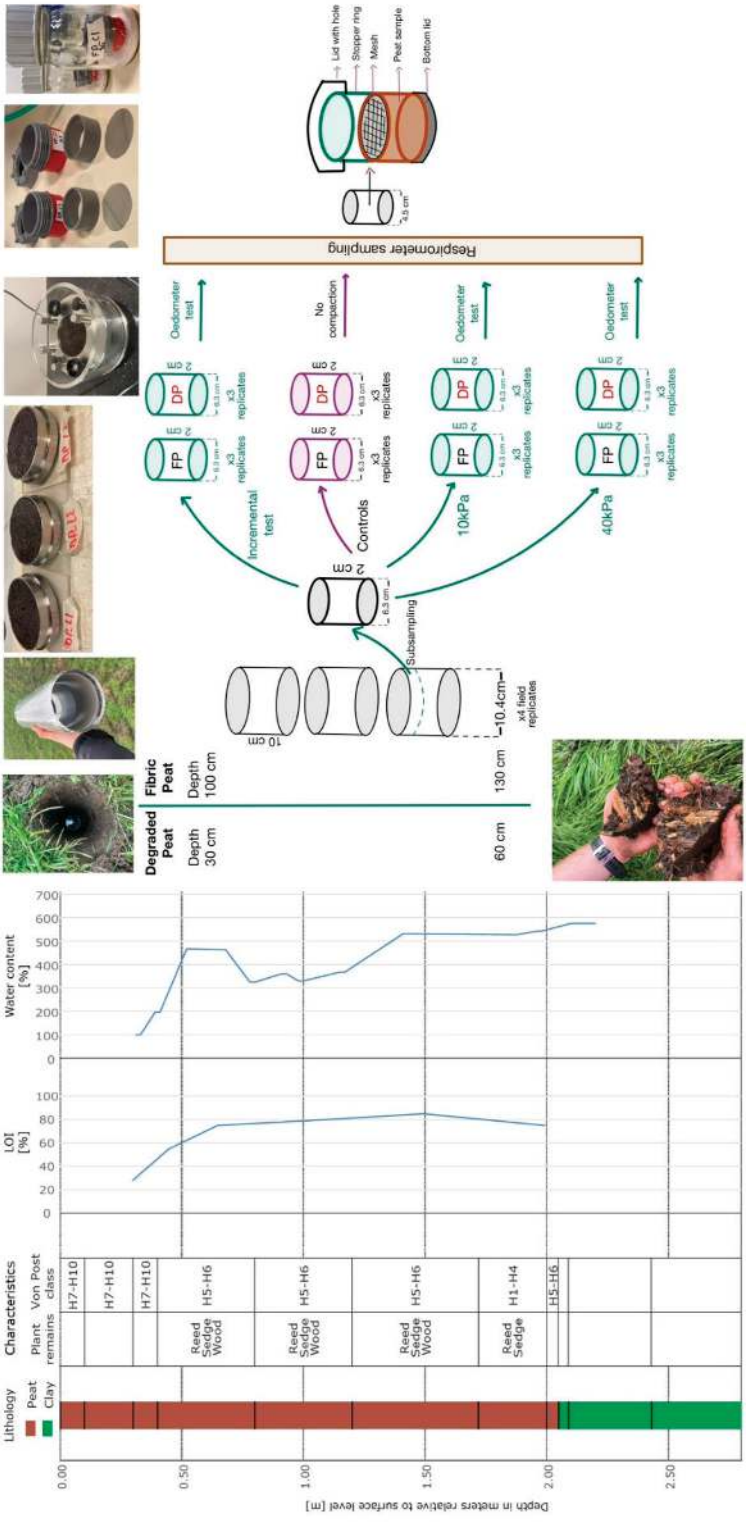

Figure 3.2: Soil profile of the study site and experiment flow of fibric peat (FP) and decomposed peat (DP) samples

stress for both DP and FP, causing only elastic compression and viscous compression. On the other hand, 40 kPa also causes virgin compression, which means more deformation will happen.

Three compression replicates (*n* = 3) were prepared for both treatment and control samples. Control samples bypassed the oedometer test and were directly placed in the respirometer. For respirometer measurements, 2 cm thick peat samples were taken from the cores using a sampler ring with a 4.5 cm diameter. The size of the sampling ring was determined based on the diameter of the respirometer bottles. The 2 cm thickness was chosen to ensure consistency across all samples, as it matches the standard size for oedometer tests. A stainless-steel mesh was placed on top of each sample to allow gas exchange. Then, a stopper ring was installed inside the sampler ring with height adjustment via an adjustable lid to avoid any elastic rebound (Fig. 3.2). Hence, this measure prevents shrinkage-swelling and in treatment samples, porosity change is solely due to compaction. The prepared control samples were placed in 500 mL glass bottles with perlite to maintain stable moisture content during measurement. The height of the samples was monitored before and after respirometer measurements using a digital calliper to ensure that shrinkage-swelling behaviour was avoided. The samples were connected to the respirometer, and accumulated CO_2 concentrations in the headspace were recorded for 5 to 6 days. Initial measurements of dry bulk density, β-D-Glucosidase exoenzyme potential activity (PA), carbon content, and pH were taken using the remaining sample material after sampling for the respirometer. Initial bulk density measurements were used to calculate the initial total porosity and void ratio.

Treatment samples were subjected to a single load for 67 hours, either at 10 kPa or 40 kPa. Shock effects can lead to rapid compaction, blocking pores and hindering water dissipation, which is not representative of peat meadow conditions. Therefore, to avoid any shock effects, the 40 kPa was not applied at once, but via two 1-hour build-up loading steps of 10 and 20 kPa. After the oedometer tests, samples were weighed to determine their wet bulk density. Samples were then subsampled for oxic respirometer measurements using a sampler ring (4.5 cm diameter), and the remainder of the sample after sampling for the respirometer was used to measure dry bulk density. This dry bulk density data was used to calculate the carbon content, total porosity and void ratio after compaction. A mesh, a stopper ring and an adjustable lid were placed on the sub-samples as in the control samples. The height of the peat was measured before and after respirometer measurements to ensure that height differences did not exceed 1 mm. By maintaining a stable temperature in a climate-controlled room (T = 8 °C), consistent moisture content, and controlled sample height, the aim is to prevent shrinkage and swelling in the samples. Upon completion of the respirometer measurements, the samples were analysed for pH, and β-D-Glucosidase exoenzyme PA.

3.2.3 Measured and estimated parameters

Height measurements and geotechnical parameters

Precise settlement measurements of the sample surface, as well as applied (effective) stress, were recorded over time during both the incremental and single loading oedometer tests. The settlement measurements were transformed automatically to linear strain (ε_C). Linear strain defines normalized height decrease and its range is between 0 and 1 and is calculated as follows (Terzaghi, 1937):

$$\varepsilon_C = \frac{h_0 - h}{h_0} \tag{3.1}$$

where h_0 is the initial height and h is the measured height at a given time during the test. Three Bjerrum-isotach parameters are needed to define both the consolidation and the viscous compression of the sample: the recompression ratio (RR) indicating the stress-related poroelastic behaviour, the virgin compression ratio (CR) indicating the full stress-related behaviour when loads exceed the preconsolidation stress, and the viscous compression coefficient (C_α) indicating viscous compression behaviour (NEN 6744, 2007). Preconsolidation stress (σ'_{pc}) is the apparent maximum effective stress a sample has experienced, either in the field or throughout a laboratory test. Values for RR, CR, C_α and σ'_{pc} were taken from Erkens et al. (2021) (Table 3.1) who performed incremental oedometer tests on samples taken at the same location and at similar depths (0.52 – 0.54 m and 1.41 – 1.43 m below the surface representing DP and FP respectively).Using a simplified isotach model, the total strain comprised of the elastoplastic strain (ε_{epl}) and viscous compression strain (ε_{vcr}) can normally be calculated for each of the single load oedometer tests following equations 3.2 and 3.3, respectively (Deltares, 2014; Kooi et al., 2018; Visschedijk, 2010):

$$\varepsilon_{epl} = RR \log_{10}\frac{\sigma'_{pc}}{\sigma'_0} + CR \log_{10}\frac{\sigma'}{\sigma'_{pc}} \tag{3.2}$$

$$\varepsilon_{vcr} = C_\alpha \log_{10}\frac{t + \tau}{\tau_{ref}} \tag{3.3}$$

in which σ'_0 is the initial in-situ stress of the sample (kPa), σ' is the applied effective stress (kPa), t is the time (days), τ is the intrinsic time (days), and τ_{ref} is the reference time (days). Intrinsic time τ was calculated using:

$$\tau = \tau_{ref}\left(\frac{\sigma'_{pc}}{\sigma'_v}\right)^{\frac{CR - RR}{C_\alpha}} \tag{3.4}$$

For τ_{ref}, it is common to take 1 day. In the case of 40 kPa, σ'_v exceeds the initial preconsolidation stress for both DP and FP, updating the preconsolidation stress to σ'_v, and hence intrinsic time after one day of testing is 1 day. Further explanation about the reference time and related intrinsic time can be found in Visschedijk (2010) and den Haan (2003).

Only one value for ε_{epl} and ε_{vcr} can be calculated for each DP and FP using the parameter values from Erkens et al. (2021). To allow the replicates to show relative differences in consolidation and viscous compression linked to their differences in total compaction during the oedometer test, we only calculate the ε_{vcr} and subtract this from the total strain to get ε_{epl}.

Table 3.1: Geotechnical compaction parameters for peat at depths corresponding to Degraded and Fibrous Peat (Erkens et al., 2021).

Parameter [unit]	*Degraded Peat*	*Fibrous Peat*
Depth [m]	0.52 – 0.54	1.41 – 1.43
Recompression coefficient RR [-]	0.066	0.062
Virgin compression coefficient CR [-]	0.51	0.58
Viscous compression parameter C_α *[-]*	0.048	0.028
Preconsolidation stress σ'_{pc} *[kPa]*	17.5	9.6

Physical-chemical properties

Dry bulk density and gravimetric water content were measured by sampling a known volume of a given peat sample before and after the oedometer test. The wet weight of these samples was measured, after which the samples were placed in a 70°C oven for 72 hours. The difference between the wet and dry weight is used for determining water content. To calculate the dry bulk density of the samples (g/cm^3), we divided dry weight by the volume. Dry bulk density data was later used to calculate for carbon content per volume (gC/cm^3). To avoid clay-rich samples and to isolate the dynamics in organic material as much as possible, we excluded DP samples with a dry bulk density higher than 0.25 g/cm^3 (Rezanezhad et al., 2016). Instead, we collected additional samples within the same ring with lower clastic content. Dried samples were further used to measure organic matter content by using loss on ignition (LOI) methodology. Organic content was burnt at 550 °C for 5.5 hours prior to measuring the weight of the resulting ash.

The measured dry bulk density was utilized to calculate the porosity in combination with the particle density:

$$n = 1 - \left(\frac{\rho_{dry}}{\rho_{particle}}\right) \tag{3.5}$$

With n being the porosity (-), ρ_{dry} is the dry bulk density (g/cm^3) and $\rho_{particle}$ is the particle density (g/cm^3). The particle density can be determined experimentally via sample submersion and water volume displacement. For this study, the particle density is reverse calculated using typical specific densities for the organic and clastic constituents, relatively 1.40 g/cm^3 and 2.65 g/cm^3 (Skempton and Petley, 1970; Redding and Devito, 2006; Schjønning et al., 2017), and the measured LOI values (-) following the formula (modified from Poelman, 1975)

$$\rho_{particle} = (1.40\, LOI) + (2.65\,(1 - LOI)) \tag{3.6}$$

The void ratio e (-) is calculated from porosity data which reflects the relative volume of voids to the volume of solids in a sample. It is directly related to the porosity n via:

$$e = \frac{n}{1 - n} \tag{3.7}$$

Controls samples were calculated for porosity and void ratio one time while compressed samples were calculated for porosity and void ratio before and after the compression.

The pH of the samples was measured by adding 30 mL of Milli-Q water to five grams of fresh peat, and the mixture was shaken for two hours at 22°C. The samples were then centrifuged at 4000 rpm for 10 minutes, and the supernatant was used to measure pH using a Sentix 41 pH electrode (WTW GmbH, Weilheim, Germany).

Three milligrams of oven-dried peat samples were placed into aluminium cups, rolled to form small balls, and used to determine the carbon content (gC/gDW) using an elemental analyser (FlashSmart™ Elemental Analyzer, Thermo Fisher Scientific Inc., USA).

Basal respiration rates

Both control and compacted samples were measured for basal respiration rates (BRR) with oxic head space using a respirometer to determine the CO_2 emissions (Biometric Systems, Germany, and Biont Research, The Netherlands). Samples were placed in 500 mL glass bottles, and the accumulation of CO_2 in the oxic headspace of these bottles was monitored at intervals of 120 minutes. The system automatically flushes the headspace with air when CO_2 levels reach 0.4 ppm. After the measurements, the dry weight of the samples was determined by placing them in a drying oven for 72 hours at 70°C. Observed basal respiration rates were corrected for shifts in pH using CO_2 and pH relations derived from Henry's law (Henry, 1803) and expressed as rates '$\mu g\ CO_2\ gC^{-1}\ h^{-1}$' using the dry weight and carbon (C) content.

β-D-Glucosidase potential activity

A substrate addition assay with fluorogenic 4-methylumbelliferone (MUF) was used to determine β-D-Glucosidase potential activity (PA) under oxic conditions (adapted from Dunn et al., 2014). One gram of fresh peat was placed in stirring Turrax tubes (IKA®-Werke GmbH & Co. KG, Germany) with 7 mL of 1 mM substrate (4-MUF β-D-glucopyranoside, Sigma-Aldrich®, USA). Samples were blended well and incubated for one hour in the dark. Controls were treated the same way, using 7 mL of Milli-Q water instead of the substrate. The slurry was then transferred to 2 mL Eppendorf tubes and centrifuged at 14,000 rpm for five minutes. The supernatant was measured using black bottom 96-well plates (Thermo Fisher Scientific Inc®, USA) with fluorescence spectroscopy (Excitation: 360/40, Emission: 460/40). Standard curves for each technical replicate were prepared using 4-methylumbelliferone sodium salt (98%, M1508; Sigma-Aldrich®, USA).

3.2.4 Data analysis

All statistical analyses were conducted using the computing environment R (R Core Team, 2025). Tailored codes for basal respiration were developed by Biont Research, The Netherlands. Basal respiration rates (BRR), β-D-Glucosidase PA, bulk density, porosity and pH were compared between control and treated groups. Void ratio comparison was made only between the initial and post-compression values of the treated samples. Normality within each group was assessed using Shapiro-Wilk tests, with variances equality evaluated via Levene's test. Two-sample t-tests were then performed to compare group means. For 10 kPa samples, the test was conducted without assuming equal variances due to observed significant differences (Levene test, $p < 0.05$). Conversely, for 40 kPa samples, equal variances were assumed (Levene test, $p > 0.05$). The samples were grouped based on the degradation status (fibric and decomposed peat – FP and DP) and analysed separately.

Decomposition status (decomposed vs fibric peat), treatment (Control, 10 kPa and 40 kPa), pH, porosity, void ratio, carbon content, and bulk density were tested as explanatory (fixed) variables for predictor variables (BRR and β-D-Glucosidase PA) with a linear mixed model followed by ANOVA (Type II). Replicates were added to the model as random variable. Corrected akaike information criterion (AICc) was used to determine the best fitting model and the explanatory variables.

3.3 Results

3.3.1 Oedometer test derived geotechnical parameters

The porosity and void ratio changes over time for the single load tests are presented in Fig. 3.3. Porosity (-) changed by 0.0074 ± 0.0010 or 0.85% for DP-10kPa, 0.0067 ± 0.0017 or 0.72% for FP-10kPa, 0.0274 ± 0.0011 or 3.11% for DP-40kPa and 0.0562 ± 0.0017 or 6.23% for FP-40kPa (Fig. 3.3a). Fitted values of C_α for the single load tests were consistently lower than their incremental counterparts, with the exception of the 40 kPa-loaded decomposed peat samples. The variability within the groups was low, except for 10 kPa-loaded decomposed peat samples. For instance, sample DP2-10kPa showed a steepening curve towards the end of the oedometer test compared to the other two DP-10kPa samples, leading to higher C_α and therefore a higher variability. The void ratio changes show a similar pattern to porosity changes (Fig. 3.3b). Void ratio (-) changed by 0.44 ± 0.09 or 6.34% for DP-10kPa, 1.10 ± 0.11 or 8.82% for FP-10kPa, 1.65 ± 0.03 or 21.63% for DP-40kPa and 3.78 ± 0.12 or 40.62% for FP-40kPa Void ratio of FP at 10 kPa shows relatively more change compared to porosity since void ratio shifts rapidly at higher porosity.

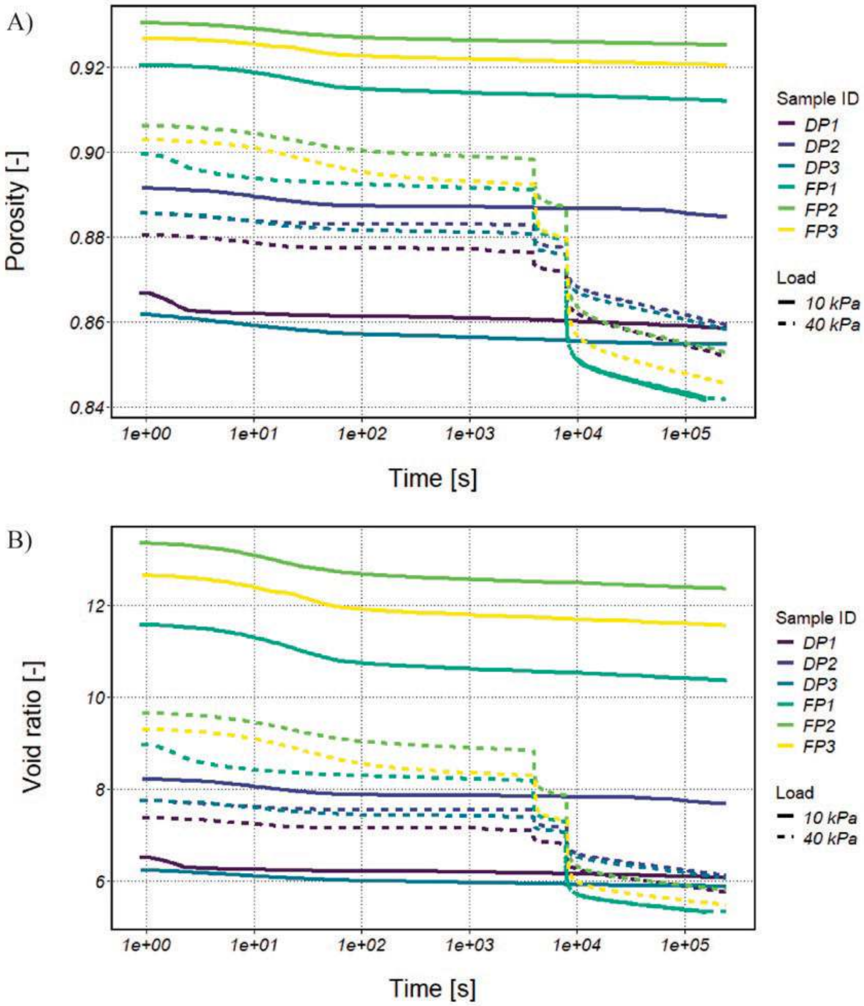

Figure 3.3: a) Porosity as a function of the logarithm of time derived from single load oedometer tests on Assendelft peat. b) Void ratio as a function of the logarithm of time derived from single load tests on Assendelft peat. Solid lines indicate loading with 10 kPa, dotted lines indicate loading with 40 kPa. Sample IDs are divided into decomposed and fibric peat (DP and FP) and replicate number.

Treatment samples with a 40 kPa load, from both FP and DP, exhibited the greatest height loss compared to those subjected to incremental testing and the 10 kPa load. (Fig. 3.4a). The physical mechanisms leading to major height loss differed between samples. The largest proportion of height loss in DP samples was due to viscous compression, except for the first and third replicate of DP-10kPa, while consolidation was the primary mechanism for height loss in FP samples, with proportions of consolidation contribution of 55.1 ± 24.9% for DP-10kPa, 40.0 ± 3.6% for DP-40kPa, 71.3 ± 1.1% for FP-10kPa, and 77.4 ± 2.7% for FP-40kPa (Fig. 3.4b).

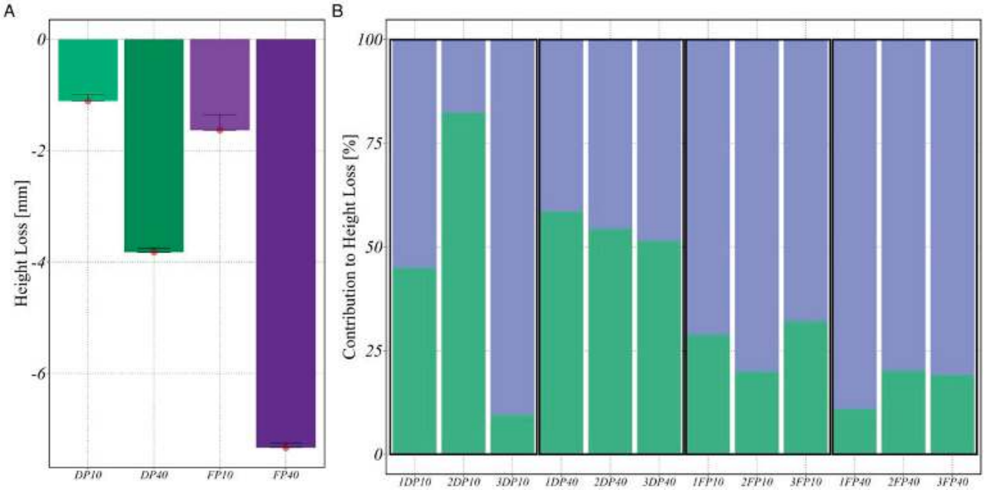

Figure 3.4: a). Height loss in mm from samples during loading treatments (*n*=3). b) The contribution of consolidation (blue-top bars) and viscous compression (green-bottom bars) to the height loss due to compaction (1,2,3= field replicates, DP = Decomposed peat samples, FP= Fibric peat samples, Inc = Incremental test, 10 = Applied loading 10 kPa, 40 = Applied loading 40 kPa).

3.3.2 Physical - chemical properties

The initial dry bulk density of FP samples was, on average, 0.09 g/cm^3, while that of DP samples was 0.14 g/cm^3. Compaction treatments resulted in higher dry bulk density values for both FP and DP samples, although the increase was statistically significant only for FP samples at the 40 kPa stress level (t-test, $p < 0.05$). For FP samples, mean dry bulk density increased by 30.3% under 10 kPa stress and by 87.1% under 40 kPa stress, while for DP samples, it increased by 40.2% under 10 kPa stress and by 32.5% under 40 kPa stress compared to controls. Overall, the mean dry bulk density of compacted DP samples (0.17 ± 0.03 g/cm^3) was higher than that of compacted FP samples (0.12 ± 0.04 g/cm^3).

Applying stress significantly reduced only the total porosity of FP samples with 40 kPa stress (t-test, $p < 0.05$). For FP samples, mean total porosity decreased by 2% under 10 kPa stress and by 5.4% under 40 kPa stress, compared to the control samples. For DP samples, mean total porosity decreased by 2.5% under 10 kPa stress and by 3.0% under 40 kPa stress, but these changes were not statistically significant (Fig. 3.5b). Changes in void ratio were compared only between the initial and post-compression values of the treated samples. It followed a similar pattern to those observed in total porosity, with notable differences between FP and DP samples. For FP samples, the void ratio decreased by 8.8% under 10 kPa stress and by 40.6% under 40 kPa stress. For DP samples, the void ratio decreased by 6.4%% under 10 kPa stress and by 21.6% under 40 kPa stress. The absolute decrease in void ratio was greater for FP samples than for DP samples under the 10 kPa treatment.

The average pH of DP samples remained unchanged with compaction (4.89 ± 0.31), while the controls of FP samples had slightly higher pH values than the compacted FP samples (6.94 ± 0.06, 6.59 ± 0.20, respectively). Total carbon (TC) content (gC/gDW) was not significantly affected by compaction in any of the treatments compared to the controls (t-test, $p > 0.05$). Mean TC decreased by 6.5% in compacted DP samples compared to the controls, whereas there was a slight decrease of 0.89% in FP samples. The carbon content per unit volume (gC/cm^3) decreased by 29.3% in DP samples with compaction, whereas FP samples showed an average increase of 62%. Bulk density (g/cm^3), pH, LOI (%) and C content (gC/gDW) values of control, 10 kPa and 40 kPa samples can be found at the Table A2.

3.3.3 Decomposition rates

Basal respiration rates (BRR) decreased with increasing stress in both FP, and DP samples compared to the control samples (Fig. 3.5b). This reduction was significant for FP samples (t-test, $p < 0.01$) but not for DP samples (t-test, $p > 0.1$). The most notable decrease was observed in FP samples with high load (40 kPa). Average decomposition rates declined by 33.1% and 48.1% for FP, and by 11.2% and 14.4% for DP, upon compaction at 10 kPa and 40 kPa, respectively compared to controls. However, increasing the stress level from 10 kPa to 40 kPa did not result in a significant change in BRR for either FP or DP samples. Average BRR rates from DP samples (7.98 ± 0.84 mgC gC^{-1} h^{-1}) were higher than those from FP samples (5.69 ± 1.82 mgC gC^{-1} h^{-1}), except for the control samples of fibric peat. Applying a 10 kPa load to decomposed peat samples resulted in BRR rates (7.78 ± 0.84 mgC gC^{-1} h^{-1}) similar to the control samples of fibric peat (7.80 ± 0.90 mgC gC^{-1} h^{-1}) (Fig. A6). b-D-Glucosidase exoenzyme potential activity (PA) also decreased with compaction, but a significant reduction was only observed in FP samples with low load (10 kPa) compared to the controls (t-test, $p < 0.05$). Interestingly, b-D-Glucosidase PA was relatively higher in 40 kPa samples than 10 kPa samples for both decomposed and fibric peat samples (Fig. 3.5c) (Fig. A6).

3.3.4 Relationship between decomposition and physical-chemical properties

Basal respiration rates (BRR) were best explained by porosity ($p < 0.01$) and degradation status ($p < 0.001$), with an interaction between these two parameters ($p < 0.01$) (linear mixed model, random intercept SD: σ_u=0.599076, residual SD: σ_ϵ=0.7079554). In DP samples, BRR could not be linearly estimated by the measured parameters, whereas there was a stronger linear relationship between BRR and other parameters in FP samples, particularly, bulk density, void ratio and pH (Fig. 3.6a, 3.6b, 3.6c). Although geotechnical parameters C_α and CR for viscous compression rate determination may have some relationship with BRR, they were not sufficient to estimate respiration rates alone. While BRR positively correlated with the contribution of viscous compression to total height loss, the contribution of consolidation showed a negative correlation with BRR (Fig. 3.6d). No significant relation was found between β-D-Glucosidase PA and the other parameters.

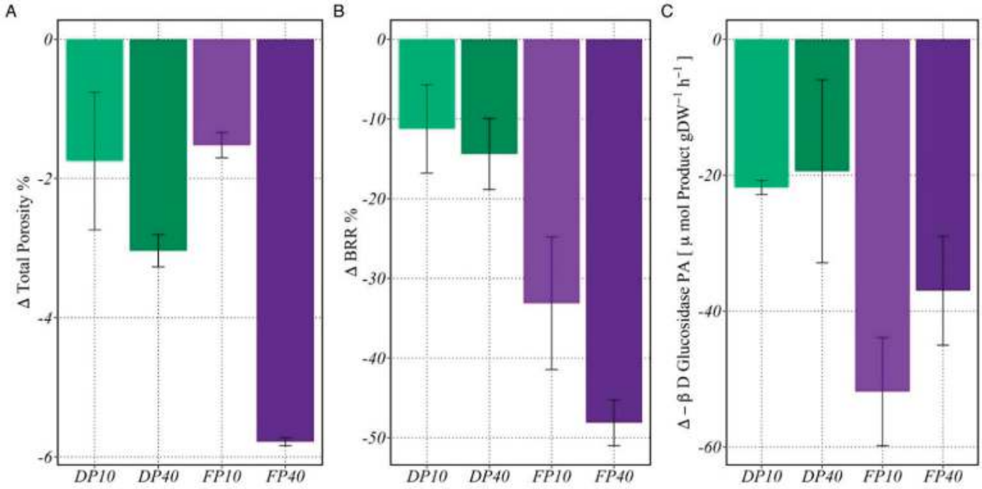

Figure 3.5: a) Total porosity changes from samples during loading treatments, b) Basal respiration rates, and c) β-D-Glucosidase PA changes from decomposed and fibric peat samples under different compaction levels (DP = Decomposed peat samples, FP= Fibric peat samples, 10 = Applied loading 10 kPa, 40 = Applied loading 40 kPa).

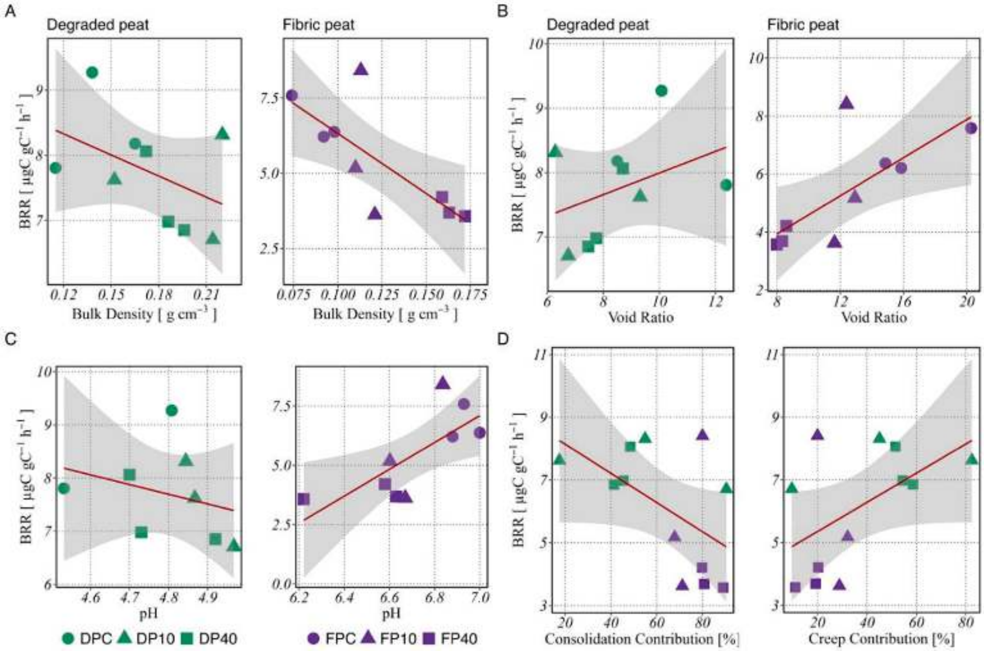

Figure 3.6: Relationship between basal respiration rates (BRR) and explanatory variables (Linear regression with 95% CI) a) dry bulk density, b). void ratio, c) pH of decomposed and fibric peat samples from controls and treatments d) Relationship between land subsidence mechanisms from treatment samples (DPC = Decomposed Peat – Controls, FPC = Fibric Peat – Controls, DP = Decomposed peat samples, FP= Fibric peat samples, 10 = Applied loading 10 kPa, 40 = Applied loading 40 kPa).

3.4 Discussion

This study investigated the mechanical processes consolidation and viscous compression that change porosity and how porosity change affects decomposition rates in peat substrates differing in degradation status. Our findings indicate that increased stress reduces porosity, which in turn lowers CO_2 emissions (basal respiration rates - BRR). This reduction in BRR was more pronounced in less decomposed peat samples (Fibric Peat – FP) compared to more decomposed peat samples (Decomposed Peat – DP).

3.4.1 Evaluation of the geotechnical measurements

The RR and CR values taken from Erkens et al. (2021) for DP were significantly lower than the reported range of values for Holocene peat samples taken at similar depth intervals in the Netherlands and align more with clayey samples from the same area (den Haan and Kruse, 2007). The two C_α values on the other hand align with the lower and upper boundary for peat, respectively. Compared to Middleton peat from Canada, which has parameter values for RR, CR and C_α of 0.115, 0.884 and 0.099 respectively (Edil and Den Haan, 1994), FP is significantly lower on accounts of RR and CR and has a similar C_α. All three parameter values for DP from Erkens et al. (2021) are lower than those for the Middleton peat, but at the same order of magnitude. An explanation for the observed differences with literature is the heterogeneity of the peat at the sampling location, which involves material characteristics initial porosity and accompanying water content, fibrousness, and LOI, and influences the mechanic behaviour of the samples in the oedometer. The division in compaction between consolidation and viscous compression corresponded to the higher values of RR and CR for FP compared to DP, indicating a strong response of elastic behaviour before the preconsolidation stress and significant virgin compression behaviour after the preconsolidation stress leading to consolidation. The high viscous compression parameter value for FP indicates that viscous compression happens relatively fast, yet, over a timespan in the order of days compaction still is dominated by consolidation, especially the elastic compression as consolidation dominates at 10 kPa without virgin compression occurring. Compaction of DP was expected to be originate less by recompression and more by viscous compression at low loading. However, our results showed large variations, with only the second replicate out of three experiencing more than 50% viscous compression, which coincides with the observed steeping of the viscous compression curve of DP2-10kPa. No errors in the set-up or outliers in characteristics have been identified that can explain this steepening.

3.4.2 Evaluation of physical - chemical properties

The compaction of peat in our study clearly depended on its degree of decomposition. Less decomposed fibric peat—with its loosely arranged, intact fibres and larger pore networks—is inherently lower in dry bulk density initially. However, under the mechanical stress we applied, its open structure is far more susceptible to compaction. This leads to an increase in dry bulk density, as the large, interconnected pores are rapidly reduced eliminated (Frene et al., 2024). In contrast, decomposed peat, which has already undergone substantial consolidation and loss of fibrous structure, starts out with a higher dry bulk density and shows only a modest further increase in bulk density when stress is applied. Similarly, decreases in total porosity and void ratio reveal that fibric peat loses its pore space more readily during compaction due to the closure of its relatively larger pores, reflecting a fundamental alteration in its microstructure.

These relational differences concur with a broadly carried understanding that the physical structure of less decomposed fibric peat makes it more vulnerable to mechanical compaction under stress (e.g., Berry and Poskitt, 1972; Dhowian and Edil, 1980; Gunaratne et al., 1998; Van Asselen and Roosendaal, 2009; Wong et al., 2009; O'Kelly and Pichan, 2013). Erkens et al. (2021) also showed that increased decomposition results in a higher dry bulk density and a less compressible matrix. In addition, studies by Boelter (1968) and Laiho et al. (2006) indicated that, as peat undergoes further decomposition, its dry bulk density increases while porosity decreases, fundamentally altering its consolidation behaviour.

pH and C content (gC/gDW) were not significantly influenced by compaction, which was also reported in another study (Bellabarba et al., 2024). Even though the pH change was not significant for FP samples, a slight relation exists with compaction, showing higher pH and higher respiration rates, with no clear trend for DP samples. Both parameters can be valuable for understanding long-term dynamics; therefore, their changes should be monitored in the context of long-term response.

3.4.3 Decomposition rates

Basal respiration rates

Our results demonstrate that compaction of peat samples leads to a reduction in basal respiration rates (BRR) in terms of CO_2 emissions consistent with findings from other studies (Beylich et al., 2010; Deurer et al., 2012; Frene et al., 2024; Ruser et al., 2006). The reduction of averaged BRR ranged between 19.4 and 51.9% depending on the compaction level and the degradation status of the peat. Samuel and Evers (2024) reported a 33.9% reduction in average CO_2 emissions due to compaction from tropical peatlands, which aligns with our findings. The reduction in BRR across all samples can be attributed to the observed decrease in total porosity and increase in bulk density, as also similar results reported in other studies (Chamindu et al., 2019; Ricardo et al., 2011; Strong et al., 2004). Jayarathne et al. (2021) and Kuncoro et al. (2014) found that compaction leads to isolated pores where oxygen diffusion is limited. This hinders aerobic microbial activity, thereby reducing short-term CO_2 emissions. Horgan and Ball (2005) and Kiuru, et al. (2022a, 2022b) further demonstrated that reduced pore connectivity in compacted soils shifts microbial processes toward anaerobic pathways, often increasing CH_4 and N_2O emissions, as confirmed by Carlesso et al. (2019) and Samuel and Evers (2024). Our study focused on links to land subsidence and peat degradation, rather than total GHG forcing. However, future studies should consider these gases to project total GHG emissions from drained and compacted peat, especially when evaluating restoration practices for these lands.

The reduction in BRR was significant only for the FP samples compacted at both 10 and 40 kPa. The minimal change observed in the BRR in the DP samples can be attributed to the peat's degradation status and the initial total porosity. The material characteristics of the decomposed peat samples are already characterized by high bulk density, a lower void ratio, smaller pores and higher tortuosity (Gong et al., 2022; Pichan and O'Kelly, 2013; van Asselen et al., 2009). Therefore, compacting DP samples did not significantly affect physical properties which in turn led to minimal changes in BRR. In addition, the substrate (available organic material) might be more limited or altered its form compared to the less decomposed FP samples (Gebert and Zander. 2024; Kleimeier et al., 2017; Klingenfuß et al., 2014). There was a decrease in BRR, but no significant change, from the 10 kPa compacted samples to the 40 kPa compacted samples. This might be due to the sample size and the heterogeneity of the peat samples, a limitation that could be overcome by increasing the number of replicates in the future. Another potential explanation is that after reaching a certain stress level, the major drivers of decomposition rates may shift from physical factors to other factors such as temperature, available carbon, or moisture content (Bell et al., 2018; Ruser et al., 2006; Xu et al., 2016).

There is a clear relationship between BRR, total porosity, and degradation status, with lower BRR rates observed in samples with lower void ratios and higher degradation status. Other studies have also explained decomposition rates with the same factors, which supports our results that show a robust link between physical material characteristics and microbial processes (Ryan and Law, 2005; Yan et al., 2016; Mohseni and Bol, 2021; Frene et al., 2024). However, additional technical replicates are needed to increase the statistical power of the results. Several previous studies on porosity and BRR have highlighted the importance of intermediate pore sizes (15-60 μm) for faster decomposition, primarily due to optimal conditions for microbial and fungal activity at these pore sizes (Chamindu et al., 2019; Quigley et al., 2018). Kravchenko et al. (2021), Strong et al. (2004) and Toosi et al. (2017a, 2017b) all found that decomposition rates are highest in these intermediate pores, likely due to enhanced enzyme activity and sufficient oxygen supply. Larger pores (>60 μm) impede decomposition, likely due to reduced microbial contact with substrates and increased predator activities, while smaller pores (<4 μm) restrict oxygen diffusion, resulting in slower decomposition rates. Since consolidation mainly affects macropores and viscous compression affects micropores, macroporosity was expected to decrease more significantly in FP samples than in DP samples (Bruand et al., 1996; Holden, 2009; Weber et al., 2017; Zaffar and Lu, 2015). In our experimental set-up, we did not measure the pore-size distribution. Instead, we theoretically estimated pore-size distribution (Fig. A7-A9; following e.g., Jayakody et al., 2014; Luo et al., 2019) based on soil water retention curve measurements derived within the Netherlands Research Programme on Greenhouse Gas Dynamics in Peatlands and organic soils (NOBV) at the same site. Our theoretical approach indicates that compaction might increase the proportion of pores in the size range of 15 to 60 μm in FP samples. Over the long term, we anticipate that the decomposition of FP samples will accelerate due to increased oxygen exposure and optimal pore-size distribution. For DP samples, on the other hand, an increase in microporosity (<10 μm) may lead to relatively lower decomposition rates due to the restriction in oxygen diffusion of these pores (Li et al., 2023). However, most research on pore size distribution and decomposition has been conducted in mineral soil rather than peat, limiting our ability to compare with previous research. Therefore, our theoretical approach requires future testing to validate its applicability in drained peatlands.

β-D-Glucosidase potential activity

In our data, the reduction in b-D-Glucosidase potential activity (PA) with compaction averaged approximately 30%, whereas a study conducted by Dick et al. (1988) reported reductions from silty clay loam samples ranging from 41% to 75%. Another study on exoenzyme activity alteration with compaction found that moderately compacted samples exhibited similar b-D-Glucosidase PA to uncompacted samples, while highly compacted samples showed a clear 1.5-fold reduction in activity (Siczek and Frac, 2012). These results are different from our findings, which might be due to the contrasting availability of peat substrate as compared to soil samples with lower organic matter. Our data indicated that 10 kPa compaction led to a greater reduction in enzyme activity than 40 kPa samples for FP samples. This discrepancy may be due to higher activity of anaerobic microbial community in 40 kPa samples, since pores were more isolated, leading to limitations in to access nutrients or easily degradable substrates (Nayak et al., 2022). Additional studies focusing on enzyme dynamics under varying compaction stresses could provide more insight into this phenomenon.

3.4.4 Conceptual model for land subsidence mechanisms

Our study aimed to integrate different disciplines to enhance understanding of land subsidence by examining the interaction between physical and biochemical mechanisms from drained peatlands. Porosity emerged as a critical factor linking both physical and biochemical processes, highlighting the need to understand its role in subsidence. This research represents a first step toward integrating these perspectives and developing a more holistic understanding of land subsidence mechanisms. We propose a conceptual model that accounts for the dynamic contributions and interactions between these mechanisms in land subsidence from drained peatlands over short timescales based on our experiment and over longer timescales based on literature and a theoretical approach for saturated conditions (Fig. 3.7).

In the short term from hours to weeks, our conceptual model suggests that consolidation might be the primary contributor to subsidence in drained peatlands, which is supported by data presented here and previously reported (van Asselen et al., 2018). Under saturated conditions, consolidation occurs rapidly as the peat loses water and volume, potentially leading to a significant reduction in void ratio and total porosity, which contributes to initial subsidence. However, as time progresses, the rate of decomposition of organic material may become a more dominant factor, especially when intermittent oxic conditions are considered, facilitating both consolidation and viscous compression (creep). During this mid-term period, decomposition can accelerate volume loss, especially in the drained peat layers, which can become unsaturated and support aerobic microbial activities. This process might interact with consolidation through a feedback loop. Decomposition may weaken the peat structure by altering porosity and changes the strength of peat fibres, thereby facilitating further consolidation. This suggests that there may be possible positive feedback where decomposition enhances consolidation by increasing the porosity. Conversely, as consolidation reduces pore size and decreases total porosity, it could create more isolated anoxic pores, which may negatively impact decomposition rates, indicating a potential negative feedback effect of consolidation on decomposition. However, compaction can also enhance the exposed amount of carbon per volumetric unit, which could lead to more decomposition and as a result higher GHG emissions (Aben et al., 2024). In the vadose layer, shrinkage and swelling mechanisms play a critical role in the seasonal movement of the peat profile. These processes can also influence the interaction between decomposition and consolidation mechanisms. In addition, irreversible shrinkage in this zone can contribute up to about 15% of total land subsidence, highlighting the importance of further investigating its interaction with other mechanisms (Erkens et al., 2016; van Asselen et al., 2018). However, in our study, we did not focus on these processes in order to keep the framework concise and aligned with the parameters monitored in our compaction experiment. The way these mechanisms influence each other, either positively or negatively, likely depends on initial peat characteristics such as porosity, pore connectivity, and peat botanical origin, as well as environmental conditions like nutrient availability, moisture content and temperature. This highlights the importance of site-specific research to identify the factors that determine current and future subsidence rates.

In the long term, from years to centuries, viscous compression (creep) is the predominant driver of subsidence, particularly in saturated deeper peat layers in lightly overconsolidated, where decomposition rates are low due to lower temperatures and full saturation (van Elderen et al., 2025). Viscous compression might be influenced by anaerobic decomposition, with one possible scenario being that decomposition might modify the fibre alignment, thereby facilitating viscous compression (Landva and Pheeney, 1980). Alternatively, viscous compression could affect the availability of electron donors (i.e., organic matter) and acceptors (i.e., NO_3^-, Fe^{3+} and SO_4^{2-}) necessary for decomposition by altering the pore connectivity, potentially creating both positive and negative feedback loops between the two processes. These interactions, particularly the effect of decomposition on viscous compression and vice versa, remain uncertain and require further investigation.

Unlike the commonly used approach that directly translates decomposition rates into subsidence rates, the proposed perspective highlights physical mechanisms as the primary drivers of land subsidence, consolidation, viscous compression and shrinkage-swelling. Decomposition processes interact with these mechanisms by altering porosity and weakening the physical structure of peat, thereby contributing to subsidence. Physical mechanisms and decomposition remain active over time, although their driving potential evolves with changes in porosity.

In our experiment, we explored the broader impact of porosity on decomposition rates and its potential interactions with viscous compression and compaction over short periods of time under saturated conditions, providing just one piece of the puzzle. Future research should focus on detailed examination of porosity levels, utilizing pore-scale analysis to understand how decomposition evolves over months to years, how it modifies pore structures, and how these changes influence physical mechanisms under both saturated and unsaturated conditions. Additionally, while our model does not explicitly incorporate the shrinkage-swelling behaviour of peat in the unsaturated zone, we recognize that this behaviour is likely intertwined with both decomposition and other physical mechanisms, especially since moisture and temperature regulate all these mechanisms in a changing climate and with changing land use.

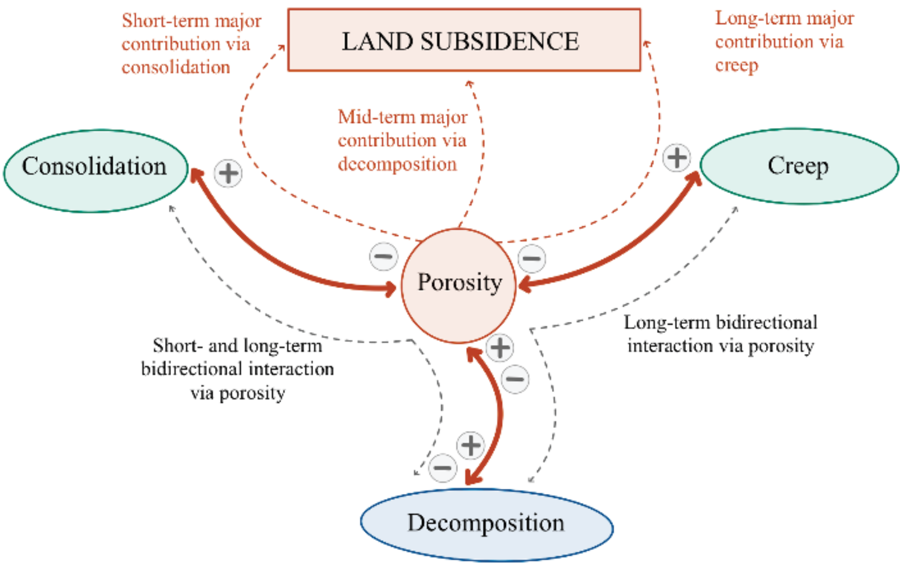

Figure 3.7: Conceptual framework illustrating the contributions of consolidation, creep (viscous compression), and decomposition to land subsidence rates in drained peatlands, highlighting porosity as a central factor influencing and mediating interactions among these mechanisms. (+) and (-) represent positive or negative impacts of one element on another depending on the position of the symbol. For instance, the (+) symbol close to the consolidation mechanism indicates that higher porosity increases consolidation rates and the (-) symbol close to porosity shows that consolidation reduces porosity.

3.5 Conclusions

Our study examined how mechanical processes, including consolidation and viscous compression, influence changes in porosity and how porosity changes impact decomposition rates over short time periods ranging from days to a week. We found that compaction decreases porosity, which reduces basal respiration rates (BRR) in terms of CO_2 emissions in the short term. In less decomposed fibric peat, compaction significantly decreased porosity, leading to a pronounced reduction in BRR. In contrast, more decomposed peat exhibited smaller changes in porosity, resulting in a less substantial decrease in BRR. Furthermore, in both decomposed and fibric peat samples, consolidation was the main driver of measured compaction, while viscous compression plays a more significant role in fibric peat as compared to decomposed peat.

These findings highlight how changes in porosity due to compaction influence microbial activity and affecting carbon cycling, revealing potential interactions between physical and biogeochemical subsidence mechanisms. The proposed conceptual framework also offers a new perspective and encourages interdisciplinary studies on human induced land subsidence rates in peatlands. Future research should investigate the links between pore-size distribution, decomposition rates and long-term effects of compaction on peatland carbon dynamics under saturated and unsaturated conditions, as well optimize mitigation strategies for subsidence and associated greenhouse gas emissions in peatlands.

Acknowledgements

We thank Sander Houdt and Ewan Zwart for conducting the pilot experiment upon which this research is based, and Bas van Dam for facilitating Ewan's experiments in the laboratory. Additionally, our sincere gratitude goes to Mark de Hart for his invaluable assistance and support during our experiments at Deltares, Delft Laboratories. We also appreciate Peter Veenhuizen's invaluable design of the respirometer sampling. The long-term Dutch peatland monitoring program "Nationaal Onderzoeksprogramma Broeikasgassen Veenweiden" (NOBV) shared their data to help us to overview our results (https://www.nobveenweiden.nl/).

Funding

The research presented in this paper is part of the project living on soft soils: subsidence and society (grantnr.: NWA.1160.18.259). This project is funded by the Dutch Research Council (NWO-NWA-ORC), Utrecht University, Wageningen University, Delft University of Technology, Ministry of Infrastructure and Water Management, Ministry of the Interior and Kingdom Relations, Deltares Research Institute, Wageningen Environmental Research, TNO-Geological Survey of The Netherlands, STOWA, Water Authority: Hoogheemraadschap de Stichtse Rijnlanden, Water Authority: Drents Overijsselse Delta, Province of Utrecht, Province of Zuid-Holland, Municipality of Gouda, Platform Soft Soil, Sweco, Tauw BV, NAM. For more information: https://nwa-loss.nl/.

Author contributions: CRediT

Duygu Tolunay: Conceptualization, Methodology, Investigation, Formal analysis, Visualisation, Writing – original draft, **Pepijn van Elderen**: Conceptualization, Methodology, Investigation, Formal analysis, Visualisation, Writing – original draft, **Mariet M. Hefting:** Conceptualization, Supervision, Writing – review and editing, **George A. Kowalchuk**: Supervision, Writing – review and editing, **Esther Stouthamer**: Supervision, Writing – review and editing, **Gilles Erkens**: Conceptualization, Resources, Supervision, Writing – review and editing.

Chapter 4:

Assessing the viscous compression parameter for land subsidence modelling from material characteristics

van Elderen, P., Erkens, G., Zwanenburg, C., van Essen, H., Stouthamer (2025). Assessing the viscous compression parameter for land subsidence modelling from material characteristics.

Submitted to: Netherlands Journal of Geosciences, special issue: Land Subsidence

ABSTRACT

Compaction of soft subsurface layers occurs through different mechanisms, namely consolidation, viscous compression, autocompaction, and shrinkage. Viscous compression is a key long-term process often the most significant component of compaction over long time periods. The rate of viscous compression over time is defined by the viscous compression parameter (C_α), which describes the amount of strain per logarithmic unit of time with constant effective stress. Overall compressibility of different material can often be linked to their material characteristics, yet for viscous compression this is still problematic. Understanding the relationship between material characteristics and C_α is essential for improving compaction predictions in soft subsurface layers such as clay and peat. This study investigates how C_α varies with subsurface material characteristics and explores its predictability based on specific material characteristic values. An extensive dataset of one-dimensional compression tests on Holocene peat and clay samples from the Rhine-Meuse delta and coastal zone in the Netherlands was analysed. Using principal component and clustering analyses, four distinct lithological classes were identified and labelled based on organic fraction: Clay, Clayey peat, fibrous Peat and decomposed Peat. All four lithological classes show increasing median sample C_α values with decreasing bulk densities and increasing water content and void ratio, with C_α values ranging from 0.0074 in the 'Clay' material type to 0.0293–0.0384 in the two 'Peat' material classes. Compared to currently applied traditional lithological classifications and default model values in the Netherlands, the material type-specific C_α values provide a more accurate and data-driven alternative. Regression analysis using the full dataset, with water content and dry bulk density as the predictors, yielded a better prediction of C_α (R^2 = 0.70) than for regressions per material type. Due to large variability within the peaty material types, upper and lower C_α bounds (0.02–0.06) are recommended in practical applications for 'Clayey Peat' and 'Peat' subsurface layers, as these values are consistently observed across the full range of water content and dry bulk density within these clusters. While the C_α values for 'Clay' are similar to standard values (0.0035 – 0.0123), C_α values for 'Clayey Peat' and 'Peat' are up to three times higher than the standard values, which would result in twice or thrice the amount of viscous compression over the same time period. Finally, we emphasize the need for adaptable C_α values in models to reflect evolving material characteristics over time, driven by decomposition.

4.1 Introduction

Land subsidence is often caused by the compaction of subsurface material after fluid extraction, excessive water drainage, loading from constructions, or natural processes and occurs through physical, chemical and biological processes (e.g., van Asselen et al., 2009; Minderhoud et al., 2017; van Elderen et al., 2025). The compaction of subsurface material involves three primary mechanisms: stress-dependent elastic deformation, stress-dependent plastic deformation and time-dependent deformation (e.g., Terzaghi, 1941; Mesri, 1973; Mitchell and Soga, 2005; van Asselen et al., 2009). Time-dependent deformation, referred to as viscous compression, creep or secondary compression, unfolds under sustained loading conditions (e.g., Bjerrum, 1967; Den Haan and Edil, 1994; Chai et al., 2012, Le et al., 2012, Zhao et al., 2020). This slow, continuous compaction, called viscous compression from here onwards, has a particularly large contribution to compaction in clay-rich and organic subsurface layers, which have a high initial compressibility and porosity (e.g., Edil and Dhowian, 1979, Den Haan and Edil, 1994; Mesri and Ajlouni, 2007; Le et al., 2012). Viscous deformation originates from structural adjustments within the matrix of the material that occur over timescales from hours up to decades because of water diffusion from micropores, changes in the adsorbed water layer, and shifting particle interactions (Le et al., 2012; van Elderen et al., 2025). The relative contribution of these driving mechanisms of viscous compression depends on material characteristics and environmental conditions, as well as on decomposition of organic matter, the latter being an important control on the viscous compression mechanisms and structural integrity of peat (Augustesen et al., 2004; Le et al., 2012; O'Kelly and Pichan, 2013; van Elderen et al., 2025).

Numerical modelling plays a pivotal role in quantifying and predicting land subsidence resulting from compaction of unsolidified subsurface material. Existing conceptual models are based on different representations of compaction mechanisms in such materials, such as the nucleus of strain model (Geertsma, 1973; Fokker and Orlic, 2006), the NATSUB3D model (Xotta et al., 2022) and the isotach model (Bjerrum, 1967; Den Haan, 1994). The latter is based on the isotach rheological principle, which states that the strain rate of the subsurface is uniquely determined by the applied stress. According to this principle, the strain state, defined by the amount of previous compaction and the in-situ stress, corresponds to a specific compaction rate that progressively decreases with time. Lines of identical compaction rates can be represented by so-called 'isotachs'. The model uses three main compaction parameters: the recompression ratio (RR), virgin compression ratio (CR), and viscous compression parameter (C_α), the latter to describe viscous compression (Fig. 4.1). CR characterizes elastoplastic deformation under first-time ('virgin') loading and is determined in a semi-logarithmic plot from the slope of effective stress versus linear strain, while RR characterizes fully elastic deformation and is described by the slope of the unloading curve (Visschedijk, 2010). The C_α parameter describes the rate of compression over time that continues when the loading remains constant, representing the viscous compression behaviour of the subsurface layers. An equal amount of strain happens every log unit of time between two isotachs (Fig. 4.1). The isotach model has been applied successfully in large-scale regional studies, predicting land subsidence in deltaic areas where extensive groundwater extraction leads to significant subsurface compaction (e.g., Bakr, 2015; Minderhoud et al., 2017; Keogh et al., 2021) or where extensive surface drainage leads to compaction of clay and peat in the subsurface (van Asselen, 2010; Koster et al., 2018; Fokker et al., 2019). On a local scale, it has proven valuable in construction projects, such as the design of foundations for water retaining structures and infrastructure, where long-term settlement is a design quality requirement and must be accurately predicted to minimize structural damage by residual settlement (e.g., Kurihara et al., 1993; Nishimoto and Hayashi, 2008; Yamazoe et al., 2025).

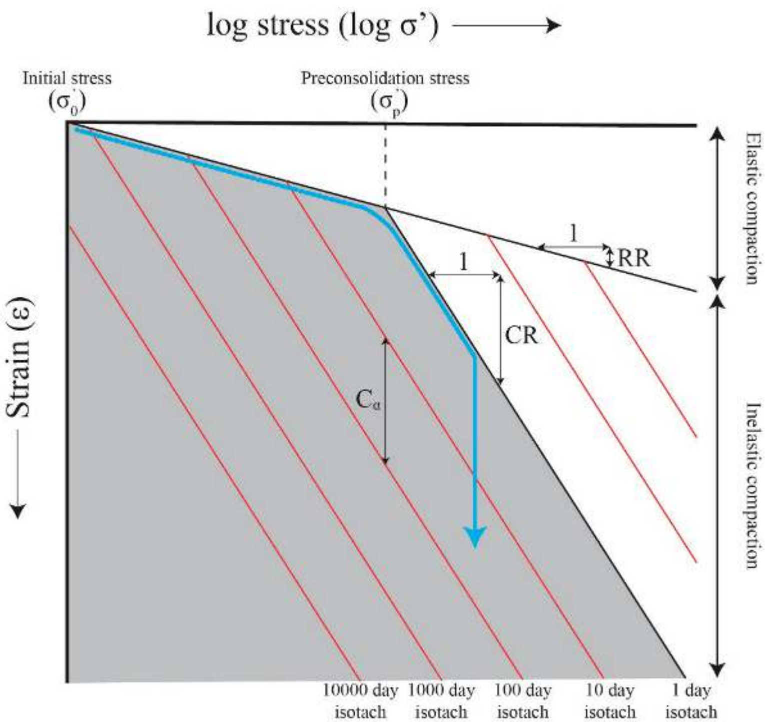

Figure 4.1: Stress-Strain diagram displaying standard compaction behaviour, indicated with the blue line. Elastic compaction occurs along the RR line up to the preconsolidation stress. Beyond the preconsolidation stress compaction occurs along the 1 day isotach. When the final stress has been reached, compaction follows a vertical path in the diagram crossing mutliple isotachs. The rate can be determined with the isotachs, indicated by the red lines. Between every isotach is a factor 10 in time. Isotachs in this diagram are linear, parallel and equidistant.

Despite its usefulness in application, the isotach model still faces challenges in calibration and validation, particularly in determining C_α. The C_α value of organic subsurface layers shows large variability in laboratory measurements (Fox and Edil, 1996; Den Haan and Kruse, 2007; Mesri and Ajlouni, 2007). When using the isotach model to predict viscous compression, standard values and ranges for C_α are applied that are based on major lithology classes, like peat and clay, and on compactness (Mesri and Godlewski, 1977). However, uncertainties in the chosen value for the C_α parameter lead to considerable uncertain or incorrect estimates of long-term subsidence. In addition, this approach disregards the heterogeneity of the material observed within these major lithological types, which could be key to understand the large variability seen in organic layers.

Therefore, this study aimed to determine: (1) how viscous compression parameter values vary with material characteristics of peat and clay, and 2) to what extent knowledge of these material characteristics improves the estimation of the viscous compression parameter for different subsurface materials in compaction models.

To achieve these aims, we analysed an extensive dataset comprising material characteristics and geotechnical parameters, including the viscous compression parameter, from peat, clay and peaty clay/clayey peat samples from the Holocene subsurface of the Rhine-Meuse delta and coastal zone of the Netherlands. The extensive dataset enabled a robust analytical approach, capturing a wide range of lithologies and depositional settings of the material. The full dataset was used to identify lithological classes based on material characteristics, i.e., water content, void ratio, saturated density, dry density and particle density, followed by regression analysis to develop predictive models for C_α based on material characteristics, and to determine to what extent C_α varies within and between lithology type clusters. Together, these steps enabled a detailed evaluation of how variation in material composition influences viscous compression behaviour, supported by the statistical strength and representativeness of the underlying dataset.

4.2 Materials and Methods

4.2.1 Dataset description and filtering

For this study we used a dataset composed by Deltares Research Institute (an applied research institute that works on innovative solutions in the field of water and subsurface) that contains the results of geotechnical laboratory tests of 603 undisturbed peat and clay samples. The samples were collected for research and local advisory projects over multiple years at various locations in the Rhine-Meuse delta, the coastal peatlands of the western Netherlands and in the marine clay area in the Northern Netherlands (Fig. 4.2). Different sampling methods were used, including manual, piston and mechanical coring (pulse drilling, continuous drilling) of which the latter involved also heavy machinery to collect samples with a large diameter of 40 cm and thickness of 80 cm (DLDS; Zwanenburg, 2017). The dataset entries comprise geotechnical compression test and material characterization test results. The main texture class of 232 samples in the dataset was labelled as clay and of 349 samples as peat, based on visual description in the field or laboratory during the projects using the NEN5104 lithological texture classification (NNI, 1989). Of 22 samples the main texture class was not labelled. In the dataset coordinates and absolute or relative depth of the samples were unfortunately predominantly given as averages grouped by sampling project, without giving information on relative positions of the samples, rendering them unusable for further spatial analyses.

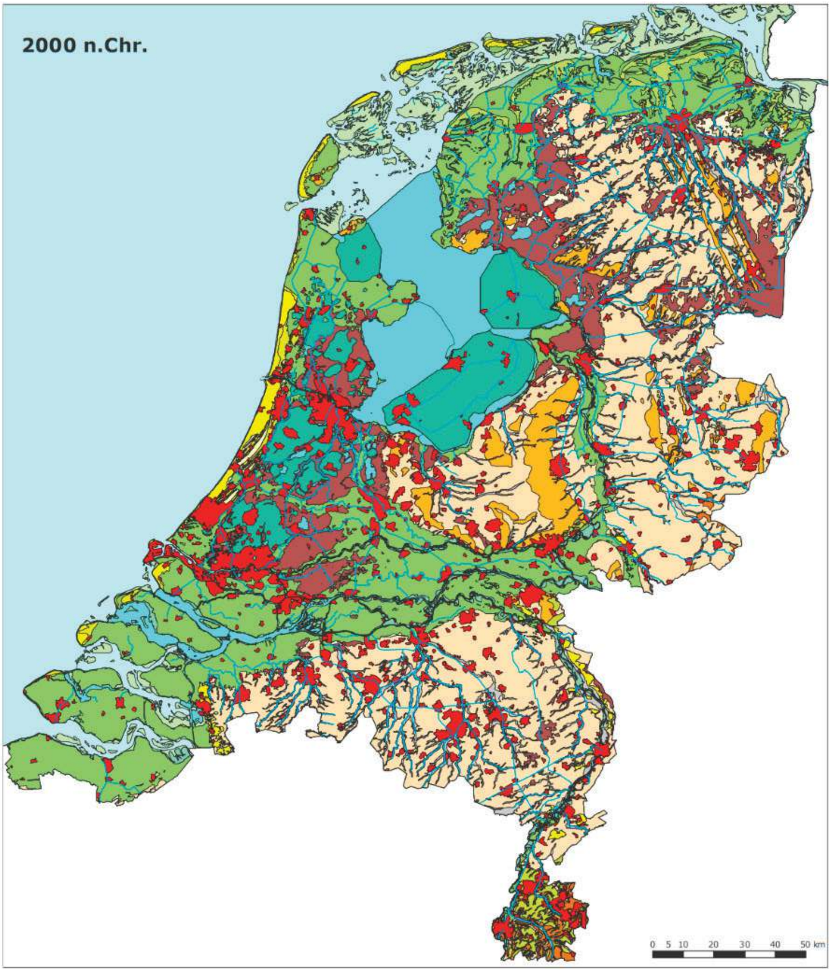

Figure 4.2: Paleogeographic map of the Netherlands for 2000 CE (after Vos et al., 2018). The Pleistocene deposits are depicted in (light) orange colours. Light green areas indicate the diked Holocene floodplains and saltmarshes, dark green areas reclaimed land, and brown areas peatlands. Urban areas are shown in red.

The dataset provides for each sample the results of both incremental loading oedometer tests and constant rate of strain (CRS) tests. Oedometer tests measure the height of a sample over time when subjected to stepwise loading, whereas in CRS tests a constant strain rate is enforced while measuring the load needed to accomplish that as well as the height of the sample over time. Testing procedures for both the oedometer and CRS tests followed from the standard test method for one-dimensional consolidation properties of saturated cohesive soils as described in ASTM D4186-06 and NEN-EN-ISO 17892-5 (ASTM, 2006; ISO, 2017). No noticeable differences were observed between the parameter values of similar samples of the two types of tests. Analysis of the applied stresses, elapsed time, and raw and normalized sample height data produces various compression parameters used in modelling, which were also recorded in the dataset. This includes C_α as the main parameter used in the relation between material characteristics and viscous compression in this research.

Next to measured data, five material characteristics from the database were considered in this study: 1) water content by mass (*WC*), 2) wet bulk density (ρ_{wet}), 3) dry bulk density (ρ_{dry}), 4) particle density (ρ_{solids}), and 5) void ratio (*e*). These material characteristics were chosen as they describe the solid and fluid components of the subsurface material. Prior to analysis, the dataset was filtered to remove missing or extreme values based on the criteria outlined in Table 4.1, to ensure the robustness of the clustering results. The cut off value of C_α was set at the maximum value deemed realistic for this parameter; samples with higher C_α values were rejected for analysis. As upper acceptable limit for the particle density reported in the database we determined the maximum particle density reported for clay of 2860 kg/m^3 (Schjønning et al., 2017). After filtering, a total of 553 samples was used.

Table 4.1: Selection criteria for the dataset to exclude zero, negative and missing values, and extreme values that may affect the clustering.

Parameter [unit]	*Criteria*
Viscous compression parameter [-]	$0 < C_a < 0.1$
Water content [%]	**WC** > 0
Wet bulk density [kg/m^3]	$\rho_{wet} > 0$
Dry bulk density [kg/m^3]	$\rho_{dry} > 0$
Particle density [kg/m^3]	$0 < \rho_{solids} < 2860$
Void ratio [-]	$e > 0$

First, the value range of each material characteristic per main texture class indicated in the dataset was determined. The material characteristics were then checked for collinearity using Pearson's correlation before applying Principal Component Analysis (PCA) to enable low-dimension clustering and regression. Clustering of the samples based on the PCA results was done using a Gaussian Mixture Model. The following clusters, or lithological classes as they are called henceforth, show the effectiveness of using these cluster to determine the viscous compression compared to exisiting parameter ranges. Subsequently, multi-dimensional regression of C_α on a minimal set of material characteristics was applied to both the full dataset as well as to the identified clusters individually. An overview of these steps is presented in Fig. 4.3.

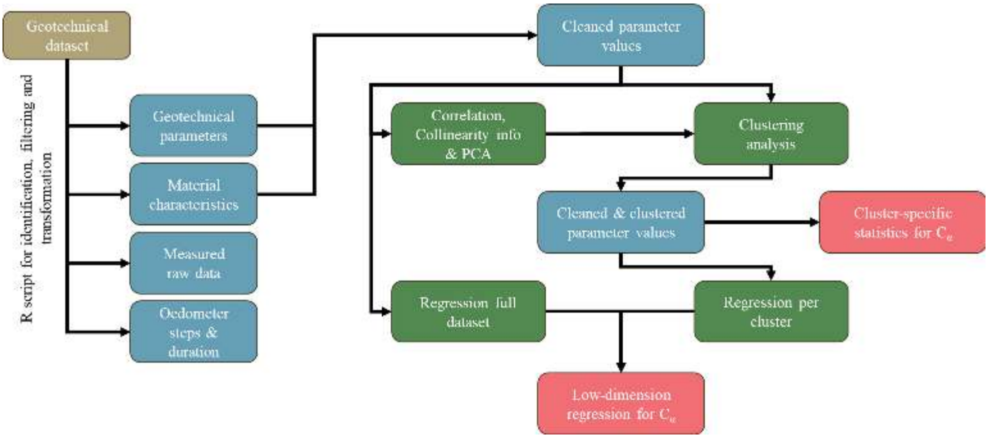

Figure 4.3: Data processing system diagram showing the various steps taken and the associated data types. Data output from compression tests was split into geotechnical parameters, material characteristics, main texture class and measured data, after which geotechnical parameters and material characteristics were filtered for NA, zero and unrealistic values. The characteristics were checked for correlation and collinearity, and clustering used the output of the PCA. Regression analysis was performed on both the full dataset as well as the clusters with the appropriate regression model.

4.2.2 Correlation analysis

Since several material characteristics given in the dataset are mutually related or can be derived from each other (e.g., sample water content from dry and wet bulk densities), and to reduce the number of mutually correlated and redundant variables in the clustering and regressions, a Pearson correlation matrix was constructed first to determine the internal linear relationships among the material characteristics. The viscous compression index C_α was only included to assess its correlation with the material characteristics, but not to take into consideration for clustering. Following this, Principal Component Analysis (PCA) was applied to the material characteristics to capture the greatest variability in the dataset (explanation provided in Supplementary B.1). Using the principal components instead of the original material characteristics benefited the clustering by separating groups of data points as much as possible. Furthermore, any collinearity between the material characteristics was eliminated with the method.

4.2.3 Organic fraction determination

Naturally, mixtures of clastic and organic material occur in low-lying coastal and delta systems, represented by a lower organic fraction than peat. However, the data cannot directly be separated on organic fraction based on the available material characteristics. To determine the lithological class of the clusters a quantification of the organic and clastic fractions was needed. Since sample-specific sand, silt and clay fractions are unknown, a general clastic fraction was used for the clastic mass density ($\rho_{clastic}$). Clay, silt and sand generally have particle mass densities of 2700 kg/m^3, 2700 kg/m^3 and 2650 kg/m^3 respectively, while organic mass density (ρ_{org}) is 1470 kg/m^3 (Poelman, 1975; TAW, 1996; Erkens, 2009). Organic fraction f_{org} was then calculated using (adjusted from Poelman, 1975, TAW, 1996 and Erkens, 2009):

$$f_{org} = \frac{\frac{1}{\rho_s} - \frac{1}{\rho_{clastic}}}{\frac{1}{\rho_{org}} - \frac{1}{\rho_{clastic}}} \quad (4.1)$$

Particle densities (ρ_s) reported in the dataset range between 400 and 3000 kg/m^3, of which the extremes are thus lower and higher than the clastic and organic mass densities that make up these samples. Therefore, sample particle densities have been recalculated using the indicated final water content, as full saturation can then be assumed, and final dry bulk density, resulting in a range between 1000 and 2500 kg/m^3, apart from a small number of outliers (Supplementary B.2). These recalculated lower and upper particle density limits were adopted as effective values for ρ_{org} and $\rho_{clastic}$ in the organic fraction calculation. This approach assumes that the dataset contains samples approaching end-member compositions, i.e., nearly 'pure' peat at the low-density end and nearly 'pure' clay at the high-density end. Organic fraction values exceeding 100% were capped at 100%, while negative values were set to 0% to account for all outliers. The organic fraction classification was then defined using the calculated organic fraction and the threshold indicated by the red line in Fig. 4, which represents silty clay in terms of clay/silt/sand mixture as the clastic end member. Silty clay was selected as a representative clastic material because samples with higher organic content are predominantly clay-rich, whereas samples with lower organic content exhibit a wider range of clastic compositions.

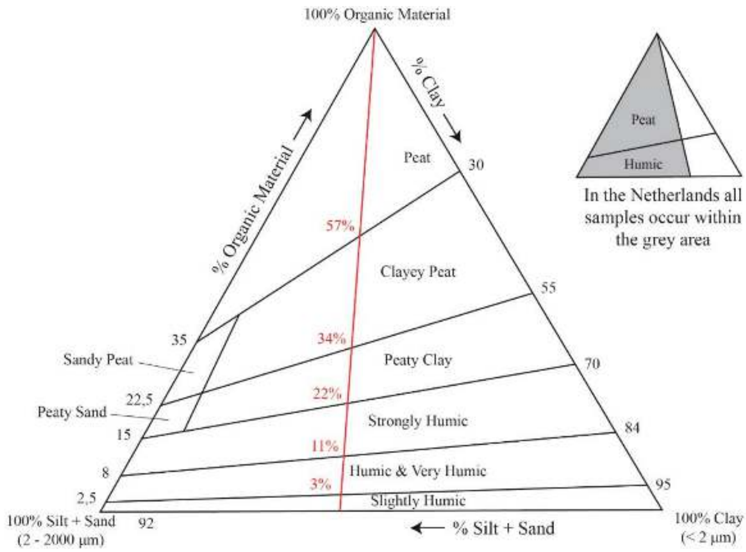

Figure 4.4: Classification of samples by their weight percentage of organic material (after De Bakker and Schelling, 1966; NNI, 1989). The red line indicates samples with a clastic component consisting of 42,5% clay, 42,5% silt and 15% sand, which is the composion of silty clay in the USDA classification system (Schoeneberger et al., 2012). The percentages in red denote the organic fraction at the lithological type boundaries.

4.2.4 Cluster analysis

To investigate which groups of samples could be defined by their material characteristics, how these groups link to lithological types, and how viscous compression behaviour varies between different lithological types, a multi-step clustering approach was applied (Supplementary B.3). First, K-means clustering was applied to the PCA-transformed data, using 25 random initializations to ensure robustness of the clustering results (Hartigan and Wong, 1979; Supplementary B.3). The output of K-Means served as initialization for a Gaussian Mixture Model (GMM), enabling the identification of probabilistic cluster memberships (Dempster et al.,1977; Supplementary B.3). As an alternative method, Density-Based Spatial Clustering of Applications with Noise (DBSCAN) was considered (Ester et al., 1996, Supplementary B.3). However, when using the commonly recommended elbow point method and the dimensionality rule to determine parameters, DBSCAN produced numerous small clusters and classified a significant portion of the data as outliers. To integrate the strength of outlier detection observed in DBSCAN, a threshold of 0.99 for cluster probability was applied within the GMM. This threshold excluded datapoints with a lower probability of cluster assignment and instead labelled them as unclassified. Both K-Means and GMM were applied across a range of two to ten unique clusters. To choose the optimal number of clusters three statistical metrics were obtained to assess the quality of the clustering: the silhouette score, the BIC score and the Jensen-Shannon Divergence (JSD) score (Supplementary B.4).

4.2.5 Regression analysis

To predict C_α, (multiple) linear regression of C_α was applied on the material characteristics using the entire dataset. In addition, separate regressions were performed for each cluster defined by the earlier clustering analysis. For the full dataset regression, linear, quadratic, logarithmic and non-linear models were tested for the independent variables. Model performance was evaluated based on mean squared error (MSE) and the statistical significance of the regression terms (p-values), while models with a significant amount of negative predicted C_α values, which go against the nature of viscous deformation, were rejected. The regression model was left unchanged for the cluster-specific regression to evaluate the usefulness of the full dataset regression per cluster. This approach allowed for assessing how well the full dataset regression generalized to individual clusters, ensuring model consistency while avoiding unnecessary complexity.

4.3 Results

Boxplots of the key material characteristics and viscous compression parameter (C_α) values for clay and peat as indicated in the dataset reveal distinct characteristic differences between the clay and peat types indicated in the dataset (Fig. 4.5). Differences between clay and peat are evident especially in terms of water content and void ratio, where peat exhibits significantly higher values and wider interquartile ranges than clay. Wet bulk densities and dry bulk densities are generally lower for peat with low variability, consistent with its high organic matter content which has a lower specific density. Finally, particle density is substantially lower in peat, with a skewed distribution and both high-end and low-end statistical outliers, whereas clay shows mainly low-end statistical outliers. Considerable differences between clay and peat are found in the viscous compression behaviour. Clay has a median viscous compression parameter value of 0.0088, with first and third quartiles at 0.0039 and 0.0149, and a maximum value of 0.0682. Peat shows significantly higher values than clay for C_α , with a median of 0.0313 and first and third quartiles of 0.0261 and 0.0373 respectively. Maximum and minimum C_α values for peat are 0.0588 and 0.0043 respectively. The lithological distributions of C_α underline the fundamental differences in physical composition and characteristics between clay and peat. These differences in material characteristics also explain the differences in the viscous compression parameter values. The higher values of C_α seen for peat can be related to the high water content and void ratios, representing the large pore volume which can be partially, yet more rapidly compressed through viscous compression. Furthermore, low bulk and particle densities reflect the hollow fibres, which in turn can be compressed, unlike clay particles.

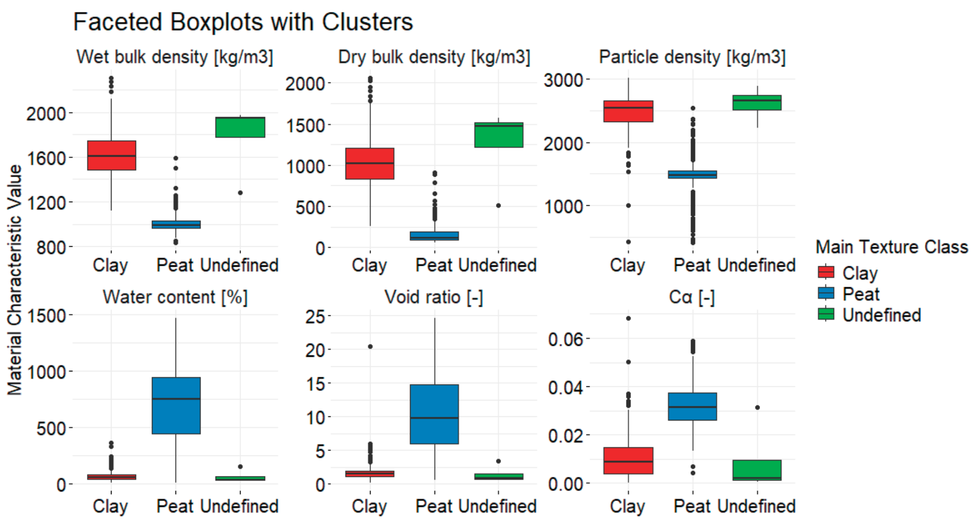

Figure 4.5: Boxplots showing the range of viscous compression parameter C_α and five material characteristics per main lithological class indicated in the dataset. Dots indicate statistical outliers within the shown class.

4.3.1 Material characteristics correlation

Strong – and obvious – positive correlations were found between water content and void ratio (ρ = .93) (Fig. 4.6a), wet and dry bulk density (ρ = .99), and bulk density and particle density (ρ > .8). The two groups of characteristics (water content/void ratio versus bulk/

particle density) showed strong negative correlations with each other ($\rho < -.7$), apart from void ratio and particle density, confirming the expected collinearity between material characteristics. The viscous compression parameter (C_α) positively correlates with water content and void ratio, and strongly negatively to all density characteristics.

The PCA results further reflect these dependencies. The PC1 axis clearly reflects the contrast between the two characteristics groups: high PC1 values are associated with high water content and void ratio, while negative PC1 values were dominated by the high density values. PC1 alone explains 85% of the dataset's variance, with the first two PCs explaining 95% of total variance (Fig. 4.6b; Supplementary B.1). All variables have small negative values on PC2, indicating limited orthogonal variance. PC3 explains an additional 4.3% of the variance, accumulating to 99.3% in total.

Given this high degree of collinearity of material characteristics dimensionality reduction was necessary to avoid redundancy and overfitting in clustering. Since principal components eliminate collinearity while retaining nearly all variance, the first three principal components (PC1–PC3) were used for clustering. The rotation matrix used to derive the PC values is included in Supplementary B.1. Water content and dry bulk density were subsequently selected as representative predictive variables for the regression models, as they (1) capture the core contrast between the two correlated variable groups, (2) are commonly measured in geotechnical investigations in a single, easy to execute test, and (3) showed clear and opposite relationships with C_α.

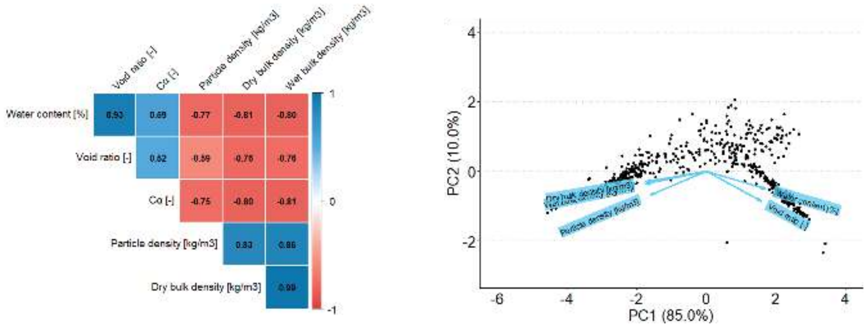

Figure 4.6: a: Correlogram of five material characteristics and the viscous compression parameter C_α showing internal correlation. The correlation coefficients are ordered using the First Principal Component (FPC) method. Blue colours indicate a positive correlation, while red colours indicate a negative correlation. b: Principal component analysis result of material characteristics of peat and clay samples. The first two principal components are shown on the x- and y-axes, together explaining 95% of the total variance of the dataset.

4.3.2 Sample clusters by material characteristics

After determining 9 different configurations of clusters with GMM, the statistical assessments were not unanimous on an optimal number of clusters (Supplementary B.4). Nonetheless, based on these assessments, four clusters were chosen as most optimal to use for further analysis. In total, 50 samples were not assigned to a cluster as a result of the classification confidence threshold of .99. The four clusters show distinct differences in their material characteristics, organic fractions and viscous compression parameter (C_α), (Table 4.2, Fig. 4.7, expanded ranges in Supplementary B.5).

- **Cluster 1** is characterized by relatively high bulk and particle densities, along with low water contents and void ratios. It exhibits the lowest organic fractions and the smallest C_α values of all clusters. The distribution of C_α has a particularly narrow interquartile range and minimal spread between extremes, indicating a consistently low viscous compressibility within this group.
- **Cluster 2** has lower bulk and particle densities than Cluster 1, with moderate water contents and void ratios. The organic fraction is higher, and the median C_α is more than four times greater than that of Cluster 1, suggesting a clear increase in viscous compression susceptibility. While the interquartile range of C_α remains moderate, the overall spread is wider, indicating greater internal variation than in Cluster 1.
- **Cluster 3** is marked by the lowest particle densities and contains the highest organic fractions. Water content and void ratio values are also high. This cluster exhibits the highest median C_α, with values more tightly distributed than in Cluster 2, though the values are overall higher. These features suggest a strong association between high organic content and increased viscous compressibility.
- **Cluster 4** has slightly higher water content and similar wet bulk density as Cluster 3, but has substantially higher void ratios and less variation in particle densities. Although the organic fraction is similarly high, the median C_α is notably lower than in Cluster 3, with least variation of all clusters. This suggests a relatively uniform material behaviour with moderate viscous compression.

The calculated organic fraction values, in combination with Fig. 4.4, were used to infer the dominant lithological composition of each cluster. As the full range (minimum to maximum) of organic fractions across each cluster spans nearly the entire spectrum of materials shown in Fig. 4.2, the interquartile range (IQR) was used as a more representative basis for classification. Based on the IQR, Cluster 1 corresponds to materials classified as clay, slightly to strongly humic clays or peaty clays in Fig. 4.2. Cluster 2 aligns with clayey peat, and peats containing a relatively high proportion of clastic material. Clusters 3 and 4 both represent the highly organic peat class. Compared to Cluster 3, Cluster 4 is characterized by higher particle density, a doubled void ratio, and a modest increase in water content.

Table 4.2: Statistical summary (median, IQR, and range) of the material characteristics and corresponding lithological classes for each cluster.

		Wet bulk density (kg/m^3)	*Dry bulk density (kg/m^3)*	*Particle density (kg/m^3)*	*Water content (%)*	*Void ratio (-)*	*Organic fraction (%)*	*Viscous compression parameter (-)*	*Lithological class*
	Median	1627	1056	2568	54	1.347	24.1	0.0074	
Cluster 1	IQR	1523 – 1769	916 – 1272	2376 – 2651	39 – 68	0.995 – 1.660	16.7 – 32.2	0.0035 – 0.0123	Slightly Humic Clay – Peaty Clay
	Min - Max	1291 – 2308	563 – 2062	1000 – 2854	9 – 140	0.185 – 2.705	1.6 – 100.0	0.0002 – 0.0296	
	Median	1163	388	1972	202	3.915	56.0	0.0296	
Cluster 2	IQR	1114 – 1243	313 – 460	1612 – 2197	165 – 251	3.186 – 4.789	49.3 – 65.6	0.0224 – 0.0374	Clayey Peat - Peat
	Min – Max	998 – 1364	232 – 910	1075 – 2677	10 – 361	0.647 – 7.044	25.3 – 100.0	0.0108 – 0.0682	
	Median	990	121	937	727	6.510	85.2	0.0384	
Cluster 3	IQR	964 – 1010	96 – 150	743 – 1079	577 – 898	5.609 – 7.280	74.2 – 92.1	0.0338 – 0.0439	Fibrous Peat
	Min – Max	878 – 1214	69 – 260	414 – 2631	366 – 1236	3.808 – 20.463	1.7 – 100.0	0.0231 – 0.0588	
	Median	968	97	1482	902	14.338	76.7	0.0293	
Cluster 4	IQR	950 – 987	85 – 115	1453 – 1512	754 – 1015	12.075 – 16.117	68.1 – 82.0	0.0253 – 0.0337	Decomposed Peat
	Min – Max	837 – 1111	61 – 187	1413 – 1828	426 – 1470	7.586 – 24.620	24.6 – 100.0	0.0178 – 0.0584	

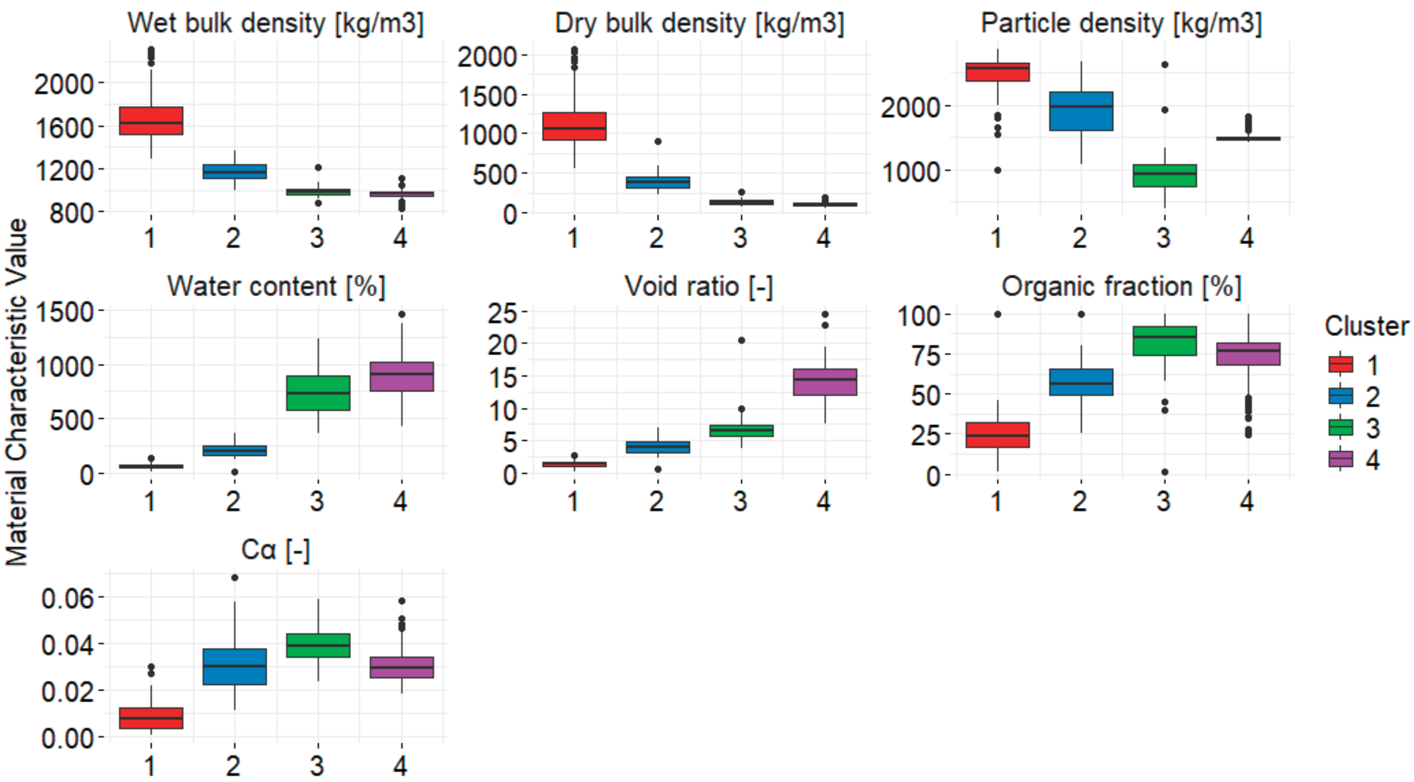

Figure 4.7: Boxplots showing the ranges of five material characteristics, organic fraction and the viscous compression parameter for four clusters assigned with a Gaussian Mixture Model (GMM). The material characteristics serve as input variables for this GMM through their principal components. Outliers outside of any cluster are categorized as NA and not included these plots. Organic fraction is added to determine the lithological class of the clusters. Clusters: 1 = C*lay*, 2 = *Clayey Peat*, 3 = *Fibrous Peat* , 4 = *Decomposed Peat*.

The slightly higher water content in Cluster 4 is consistent with its higher particle density: if we take hypothetical fibrous and decomposed peat samples with equal dry bulk densities of 100 kg/m^3 and particle densities of 950 and 1500 kg/m^3, their resulting porosities would be 0.895 and 0.933, respectively. Assuming a water density of 1000 kg/m^3, this corresponds to water masses of 895 kg/m^3 and 933 kg/m^3 per cubic meter of wet soil, giving similar water contents of approximately 895% and 933% (water mass / solid mass). The void ratio, however, shows a much larger difference of 8.52 versus 14.00, reflecting the greater total pore volume in decomposed peat with similar bulk densities. These characteristics are consistent with more humified material, which is typically associated with higher bulk densities and reduced compressibility (Mesri and Ajlouni, 2007; Huat et al., 2009; Berry, 1983; O'Kelly and Pichan, 2013). The differences in median C_α values between Clusters 3 and 4 align with this interpretation as decomposed organic matter is less prone to reorientation and viscous compression due to smaller size of the particles and lower amount of water inside the structure. Given the overall characteristics of the clusters, we interpret and refer to them as the following lithological classes: Cluster 1 will be referred to as 'Clay', Cluster 2 as 'Clayey Peat', Clusters 3 as 'Fibrous Peat' and Cluster 4 as 'Decomposed Peat'.

4.3.3 Regression models

The dataset shows a large variation of the viscous compression parameter, and also shows a considerable range within each lithological class. This introduces uncertainty in determining accurate 'default' parameter values for practical modelling cases where no laboratory tests are available. To address this, multiple regression models were developed to predict C_α from material characteristics, both for the full dataset and for the individual lithological clusters identified earlier. Among the material characteristics, water content (WC) and dry bulk density (ρ_d) showed the strongest correlations with C_α under logarithmic transformation, and thus for the full dataset the best-performing regression model was:

$$C_\alpha = 0.0396 \log WC + 0.0255 \log \rho_d - 0.1333 \quad (4.2)$$

The model achieved an $R^2 = .61$ ($p < .001$), indicating a moderately strong fit. As expected, C_α increases with increasing water content and decreases with increasing dry bulk density (Fig. 4.8a and b). The residual standard error (RSS) was 0.0088 (Fig. 4.9a). Larger residuals were observed for high original C_α values, especially at high water contents and low bulk densities, where predicted values tend to flatten around 0.040. In contrast, original values show larger variability between approximately 0.020 and 0.060. The model tends to overpredict low C_α values. These patterns highlight the difficulty of accurately capturing the viscous compression behaviour with a single regression model, especially of highly organic, water-rich peat layers.

Regression models were also applied to the individual lithological clusters to assess whether predictions could be improved relative to the full dataset model and to better understand the applicability of the global regression across different material types. All cluster-specific regressions used a logarithmic transformation of both water content and dry bulk density, consistent with the approach for the full dataset. Negative predicted C_α values were set to zero as negative values are physically impossible. While these models did not necessarily outperform the full regression in terms of predictive accuracy, they provided insight into the dominant controls on viscous compression within each cluster (Fig. 4.8c and d). The resulting regression equations are:

$$C_{\alpha,Clay} = -0.0060 \log WC - 0.0491 \log \rho_d + 0.1675 \quad (4.3)$$

$$C_{\alpha,Clayey\ Peat} = 0.0108 \log WC - 0.0206 \log \rho_d + 0.0581 \quad (4.4)$$

$$C_{\alpha,Peat-fibrous} = 0.0566 \log WC + 0.0622 \log \rho_d - 0.2529 \quad (4.5)$$

$$C_{\alpha,Peat-decomposed} = 0.0263 \log WC + 0.0400 \log \rho_d - 0.1268 \quad (4.6)$$

Differences between clusters primarily concerned the relative contribution of each predictor. In Clay and Clayey Peat, dry bulk density was the dominant factor influencing C_α, while water content had limited explanatory power especially in Clay. In the Fibrous Peat and Decomposed Peat clusters, both predictors contributed to the model, with dry bulk density generally having a stronger influence.

However, the predictive performance of the cluster-specific models was generally lower than that of the full dataset model. Only the Clay regression showed a moderately good fit, with $R^2 = 0.52$ ($p < .001$) and an RSS of 0.0041 (Fig. 4.9b), outperforming the full model within that class—though it occasionally predicted negative C_α values, which are physically unrealistic. The Clayey Peat model performed worse than the full dataset model, with $R^2 = .14$ ($p = .004$) and RSS of 0.0103. Both Fibrous Peat and Decomposed Peat regressions had very low predictive power ($R^2 = 0.02$, $p = .50$ and $R^2 = 0.05$, $p = .01$, respectively), and predicted C_α values clustered around 0.040 and 0.030, despite large variation in measured values. These results further support the use of the full dataset regression for general prediction purposes, especially when cluster identity is unknown or when local calibration is impractical.

Alternative regression approaches were tested for the clusters to improve fit for the Clayey Peat and Peat clusters, but none substantially increased predictive performance ($R^2 \leq .20$). In summary, the full dataset regression provides a more robust and practical tool for predicting the viscous compression parameter across all lithologies. For Fibrous and Decomposed Peat, average values and ranges may be more reliable than regression-based predictions for use in modelling and validation.

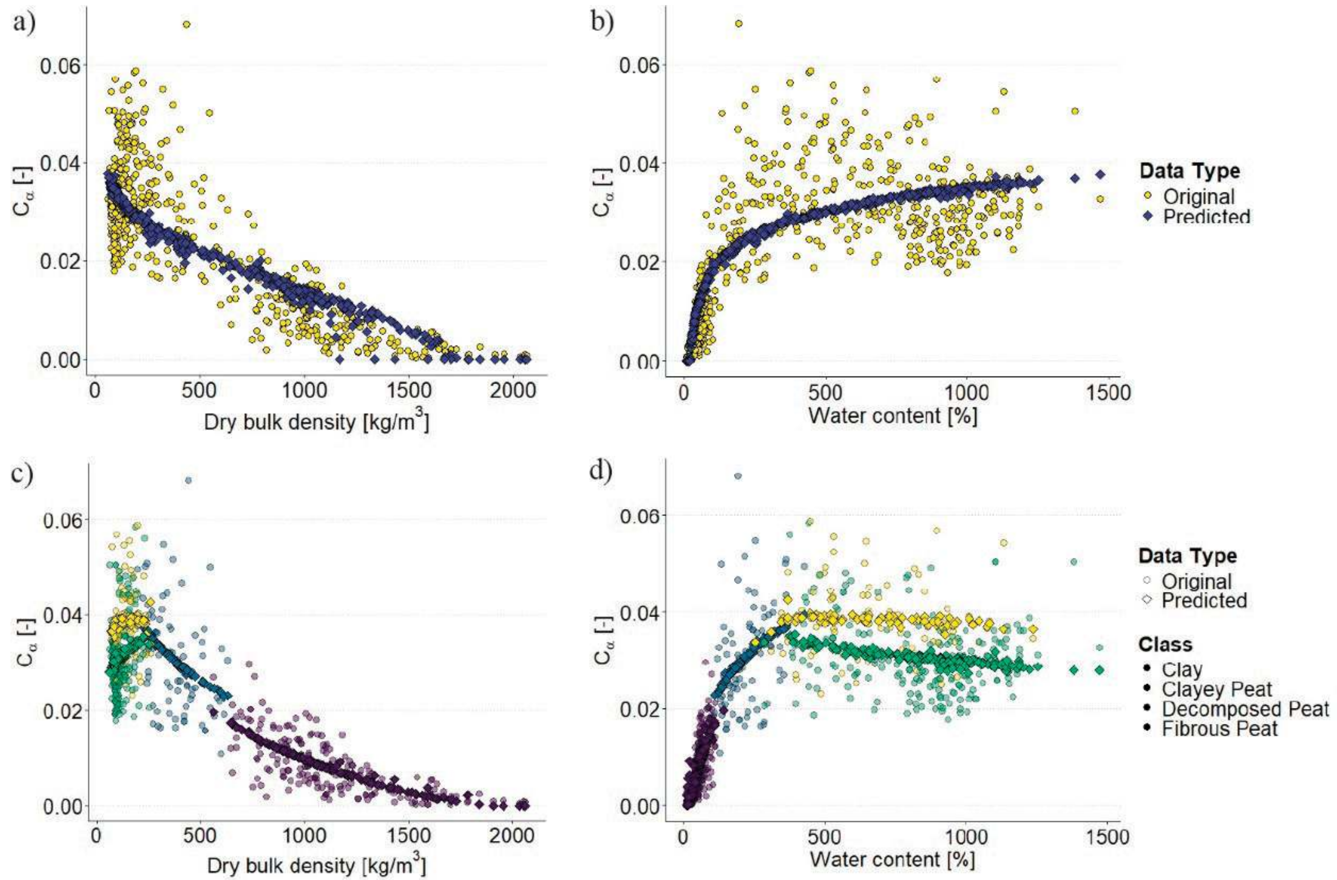

Figure 4.8: Scatter plots of viscous compression parameter against a) dry bulk density, entire dataset, b) water content, entire dataset, c) dry bulk density per cluster, d) water content per cluster. The colours for a) and b) indicate original and predicted values. The colours for c) and d) indicate which cluster a data point belongs to. Circles and diamonds represent the original and predicted values respectively.

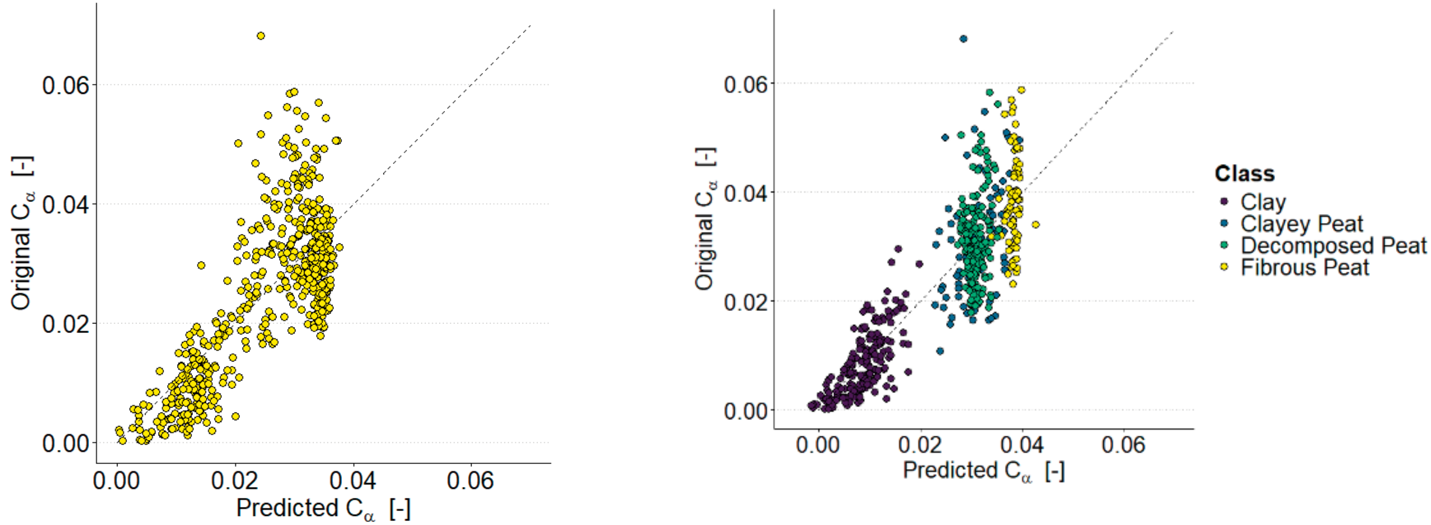

Figure 4.9: Original C_α values vs fitted C_α values. a) Fitted values based on multiple linear regression using all original data points (R2 = .61), b) fitted values based on multiple linear regression per cluster (R^2 = .51, R^2 = .14, R^2 = .05, R^2 = .02 in order of the legend).

4.4 Discussion

4.4.1 Material characteristics versus C_α

A key point of discussion is whether material classes resulting from this dataset can be used to improve predictions of viscous compression through straightforward preliminary parameterisation, compared to the traditional soil texture classes. Our results separate the dataset samples into more classes than the broad clay–peat division commonly assigned in the field or laboratory, but fewer than the detailed organic soil classes presented in Fig. 4.4. This indicates that organic content alone does not explain the observed variation in material characteristics as effectively as our clustering approach, which instead groups four classes of humic or peaty clay with largely similar properties. Within peat, however, the clustering provides a particularly meaningful distinction by separating fibrous and decomposed peat. This shows that the state of the organic matter, when it dominates the material, is a critical determinant of viscous compression behaviour.

The distinction between fibrous and decomposed peat is noteworthy because it reveals contrasting compressibility behaviour. While fibrous peat shows higher C_α values, decomposed peat exhibits lower C_α values despite its higher void ratios. This contradicts the common assumption that greater void space leads to greater potential for compaction and viscous compression. Interestingly, C_α values for decomposed peat are more comparable to those of Clayey Peat, even though the two classes differ in most material characteristics. The main consistencies are found in particle density, and to a lesser extent in organic fraction, both of which show patterns aligned with C_α. One plausible explanation is that particle density reflects the mobility of soil particles: denser organic particles, which retain less water within their microstructure, are less prone to rearrangement and therefore less susceptible to viscous compression (Le et al., 2012; van Elderen et al., 2025). This may be because denser particles require a greater initial force to overcome inter-particle friction.

To evaluate the practical relevance of the observed C_α values in our dataset, it is essential to place them in the context of existing reference values used in land subsidence assessments. A comparison with values from Dutch geomechanical practice, listed in NEN-EN 1997-1 (NNI, 2016), and from delta-scale land subsidence modelling in the Mississippi Delta (Keogh et al., 2021, derived from NNI, 2006) provides insight into how our C_α values influence subsidence calculations (Table 4.3). Although the NEN-standard values were designed to provide lower and upper bounds for settlement calculations rather than to reflect natural variability, they still offer a useful benchmark against which to situate our results. In contrast, our dataset is intended to capture the statistical distribution of C_α values and to explore explanatory trends, thereby offering a broader and more representative frame of reference. Bulk density values correspond relatively well between the NEN-standard and our classes, but the agreement in C_α values is far less consistent. The NEN-standard C_α values for clay, sandy clay, and organic clay classes fall within the range of our Clay class, while the Mississippi Delta C_α values for clay and silty clay loam textures are slightly lower, which might reflect a higher silt percentage compared to the Dutch samples. In contrast, the C_α ranges of Clayey Peat, fibrous peat, and decomposed peat extend well beyond the NEN-standard C_α values, in some cases by a factor three. These differences suggest that our classes provide a more refined framework for identifying compressibility variations within peat layers than is possible using current standard categories alone. They also imply that current assessments may underestimate viscous compression in organic-rich subsurface layers, potentially leading to substantial underestimation of long-term land subsidence.

Table 4.3: Characteristic values of the viscous compression parameter and wet bulk densities from clustering, and the standard used for geotechnical risk assessments in industry (NNI, 2016) and Mississippi Delta subsidence modelling (Keogh et al., 2021). Values for the clustering represent the inter quartile range of the lithological class. Values for both the standard and the Mississippi Delta represent the low and high averages. The NNI standard provides an indication of consistency (loose, average, compact) per subsurface texture which has been merged in this table for the benefit of the comparison with the clustering results.

	Clustering		*Dutch Standard*		*Mississippi Delta*	
Subsurface Texture	ρ_{wet} *(kg/m³)*	C_α *(-)*	ρ_{wet} *(kg/m³) ± 5%*	C_α *(-) ± 25%*	ρ_{wet} *(kg/m³)*	C_α *(-)*
Clay	1523 – 1769	0.0035 – 0.0123	1400 – 2000	0.003 – 0.013	1800	0.0025 – 0.0046
Sandy Clay	-	-	1500 – 2100	0.0007 – 0.009	-	-
Silty Clay Loam	-	-	-	-	1900	0.0020 – 0.0037
Organic Clay	1523 – 1769	0.0035 – 0.0123	1300 – 1600	0.008 – 0.015	-	-
Clayey Peat	1114 – 1243	0.0224 – 0.0374	-	-	-	-
Peat (fibrous and decomposed	950 – 1010	0.0253 – 0.0439	1000 – 1300	0.012 – 0.023	1050	0.0153 – 0.0230

A key question left unanswered is how much of the observed compaction originates from viscous compression, as this determines the broader interpretation of the results. One way to assess the relative contribution of viscous versus virgin compression is by examining their ratio in the isotach model. Originally, Mesri and Godlewski (1977) defined this ratio as $C_c/C_{\alpha e}$, where C_c is the coefficient of compression and $C_{\alpha e}$ the coefficient of secondary compression, both based on the void ratio – logarithm of stress curve. These parameters correspond to CR and C_α, respectively, which are based on the strain – logarithm of stress curve, and the relationship remains valid (Den Haan and Kruse, 2007). A high CR/C_α ratio indicates that virgin compression accounts for a larger share of total compressibility, while lower ratios reflect a stronger influence of viscous compression. Importantly, the ratio represents relative susceptibility rather than absolute dominance of one process over the other.

To illustrate this, we take the mean values for Clay and Clayey Peat (Fig. B8): if C_α increases from 0.008 to 0.031 while CR increases from 0.18 to 0.40, the ratio falls from 23 to 17. Although viscous compression contributes relatively more in the second case, virgin compression still accounts for a substantial absolute share of total compaction. The contribution in decomposed and fibrous peat are derived in the same way and results in ratios of 17 and 13. Typical ratios reported by Mesri and Godlewski (1977) are ~50 for granular soils, ~25 for inorganic clays, ~20 for organic clays, and ~17 for peat. Den Haan and Kruse (2007) further proposed an S-shaped curve describing how CR/C_α evolves with increasing wet bulk density (Fig. 4.10). Applying this ratio to our dataset reveals two main observations (Fig. 4.10). First, samples within the Clay cluster tend to show significantly higher CR/C_α ratios than predicted by the reference curve, implying that these materials are less prone to viscous compression than according to Den Haan and Kruse (2007). Second, decomposed peat diverges from the expected pattern of decreasing ratios with decreasing wet bulk density. Moreover, while decomposed peat and clayey peat show similar C_α values, a comparable relationship is observed between fibrous peat and clayey peat for the CR/C_α ratio. The higher ratios of decomposed peat align with the lower mean C_α values for this class compared to fibrous peat at similar bulk densities. Two hypotheses may explain this behaviour. One is that decomposed peat particles, being denser and containing less internal water, are less prone to rearrangement, so more of the compaction occurs through virgin compression of macropores. An alternative explanation is that once a material is more susceptible to virgin compression, this limits the extent to which viscous compression can develop. Testing this hypothesis would require consolidation experiments under increasing stresses with intermittent phases of viscous compression.

4.4.2 Practical application

This study demonstrates that regression across the full range of material characteristics can provide meaningful estimates of the viscous compression parameter to use in modelling when laboratory determination is in process or unavailable. However, predictions at the material class level remain subject to uncertainty, particularly for peat. In highly organic samples with low dry bulk density and high water content, variability remains large, suggesting that simple empirical models should be applied cautiously. For practical purposes, class-based representative values are therefore recommended. For clayey peat, fibrous peat, and decomposed peat, upper and lower limits of 0.060 and 0.020 for C_α, respectively, can be used as best- and worst-case scenarios to guide design and assessment. Relative to the median C_α values of each material, taken as representing 100% viscous compression per logarithmic time unit, the upper limit corresponds to approximately 203%, 156%, and 205%, while the lower limit corresponds to 68%, 52%, and 68% for clayey peat, fibrous peat, and decomposed peat, respectively.

4.4.3 Future research

This study can serve as starting point for prediction of other geotechnical model parameters, for example the virgin compression ratio CR or the recompression ratio RR. With this dataset, one similar to it, or using the material characteristic ranges resulting from this study one can determine mean values for these parameters and look into regression estimation similar to the method presented here. Another improvement can be made by incorporating more data into the analysis, for example from other countries than the Netherlands, to validate the usage of the results in various conditions and potentially discover new relationships between material characteristics and viscous compression. Furthermore, our results spike the question which changes in viscous compression occur when organic subsurface layers undergo decomposition, as we indicate a clear distinction between the viscous compression of fibrous and decomposed peat. This might have a critical impact on the long-term settlement assessments for mitigation options. If C_α values for peat are higher than currently assumed, but decrease over timescales of decades due to decomposition, the viscous compression occuring over a 1 year period will be larger than previously predicted, up to twice the amount for normally consolidated peat using the values from Table 4.3. Contribution of viscous compression over a 10 or 100 year period might be equal or lower than presumed in current assessments because of the reduction of C_α with decomposition and, therefore, viscous compression rate over logarithmic time decreases rather than stays constant.

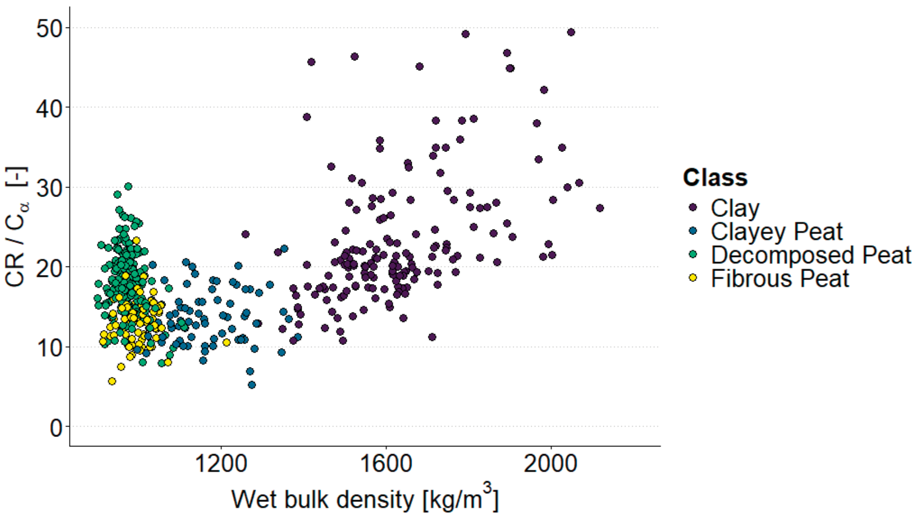

Figure 4.10: Ratio between virgin compression parameter CR and viscous compression parameter C_α as a function of dry bulk density. The black curved line indicates the relationship found by Den Haan and Kruse (2007) on samples from Sliedrecht, the Netherlands.

4.5 Conclusion

Our research aimed to determine lithology-based variation of viscous compression parameter C_α values used in compaction models for land subsidence assessments, and to evaluate whether simple material characteristics can help the determination of viscous compression parameter values for different soft substrate lithologies. An extensive dataset of compression tests on peat and clay enabled the identification of four distinct lithological classes based on water content, wet and dry bulk densities, particle density, and void ratio: Clay, Clayey Peat, Fibrous Peat, and Decomposed Peat. Median viscous compression parameter (C_α) values increase with increasing organic fraction from 0.0074 for Clay to 0.0296, 0.0384 and 0.0293 for Clayey Peat, Fibrous Peat and Decomposed Peat respectively. The lithological class-specific C_α median values and ranges are an improvement compared to existing standard values. Prediction of the viscous compression parameter can be done relatively well when using the entire dataset (R^2 = .61, $p < 0.001$) as opposed to fits per individual lithological class. Predictions for Clay are still significant (R^2 = .52, $p < .001$), whereas predictions for Clayey Peat and Fibrous Peat and Decomposed Peat show low significance ($R^2 < 0.15$, $p \geq .01$) with near horizontal fits. These fits provide an adequate average which should be used in combination with minimum and maximum C_α values of 0.020 and 0.060, corresponding to approximately halving and doubling of the amount of viscous compression over time. Lastly, we highlight that an adaptable viscous compression parameter for peat with shifting material characteristics over time, e.g., due to decomposition, can advance modelling precision.

Acknowledgements

We are grateful for the input of Hans Middelkoop (Utrecht University) during the internal revision process, as the discussion of material characteristics and their interaction improved the quality of the review. Furthermore, we want to thank Deltares research institute for giving access to their geotechnical parameter dataset, which serves as the spine of this paper. The research presented is part of the project Living on soft soils: subsidence and society (grantnr. NWA.1160.18.259). This project is funded by the Dutch Research Council (NWO-NWA-ORC), Utrecht University, Wageningen University, Delft University of Technology, Ministry of Infrastructure and Water Management, Ministry of the Interior and Kingdom Relations, Deltares, Wageningen Environmental Research, TNO Geological Survey of The Netherlands, STOWA, Water Authority: Hoogheemraadschap de Stichtse Rijnlanden, Water Authority Drents Overijsselse Delta, Province of Utrecht, Province of Zuid-Holland, Municipality of Gouda, Platform Soft Soil, Sweco, Tauw BV, NAM.

Author contributions: CRediT

Pepijn van Elderen: Conceptualization, Methodology, Investigation, Formal analysis, Visualisation, Writing – original draft, **Gilles Erkens**: Conceptualization, Supervision, Writing – review and editing, **Cor Zwanenburg**: Resources, Writing – review and editing, **Harry van Essen**: Resources, Writing – review and editing, **Esther Stouthamer**: Conceptualization, Supervision, Writing – review and editing.

Chapter 5:

Viscous compression rates in soft subsurface materials for overconsolidated conditions

5.1 Introduction

Viscous compression is an important yet not fully understood component of land subsidence due to compaction of shallow soft subsurface material. Viscous compression causes long-term irreversible compaction regardless of overpressure in pores after a stress increase, and thus it can also happen under constant effective stress. The process occurs through ongoing reorientation of soil particles (e.g., Le et al., 2012; van Elderen et al., 2025). Viscous compression is particularly significant in soft subsurface layers consisting of clay and peat as the elongated shape of their particles and water-holding internal structure could make reorientation impactful. Viscous compression is also referred to as 'creep' or 'secondary compression' (e.g., Den Haan, 1994).

One of the most important characteristics of viscous compression is its time-dependency. The viscous compression rate is generally observed to decrease logarithmically with time under constant stress conditions (e.g., Buisman, 1940; Terzaghi, 1943; Bjerrum, 1967; Den Haan, 1994). Compaction models therefore assume that the viscous compression strain develops linearly when put against logarithmic time. Isotach models present this constant strain development with logarithmic time as a set of intrinsic timelines, isotachs, which are considered as linear, parallel and equidistant (e.g., Den Haan, 1994). A single isotach represents a unique strain rate observed for a given sample- or layer-specific stress-strain combination. The intrinsic time linked to an isotach is a conceptual measure that expresses how long the current stress would have needed to act to produce the observed strain. Each isotach represents an amount of intrinsic time ten times larger than the isotach above it (Fig. 5.1b). Intrinsic time is a concept which represents the time a subsurface layer or sample would have needed to acquire the current compaction state if the current stress conditions were applied without ever changing since deposition or formation. So, when intrinsic time for a layer or sample for a specific stress condition is calculated to be 10000 days, it means that if the material would be deposited or formed today and subjected to this specific stress condition, it would take a layer or sample 10000 days to get the current compaction state.

A layer or sample is considered overconsolidated when its current effective stress is lower than its preconsolidation stress, which may result from past higher loadings, or when time-dependent processes such as viscous compression or aging have increased its apparent stiffness. The intrinsic time of this layer or sample will consequentially be high. The amount of overconsolidation is expressed by the overconsolidation ratio (OCR): the ratio between the preconsolidation stress (the apparent maximum stress the material has experienced so far) and the current stress. For overconsolidated stress conditions, the current stress is lower than the preconsolidation stress leading to an OCR > 1. In a stress-strain diagram (Fig 5.1b), overconsolidated conditions occur in the grey part where current stress is lower than preconsolidation stress. When loading increases and exceeds the preconsolidation stress the material becomes normally consolidated. Rapid deformation linked to the created overpressure of the porewater, called consolidation, occurs immediately after stress application. While a part of consolidation is elastic, most of the deformation is inelastic (Fig. 5.1b). For normally consolidated stress conditions the current stress equals the preconsolidation stress, and OCR is equal to 1. This situation is represented in the right part of Fig. 5.1b. OCR can also be less than 1, occurring when the stress increase is faster than consolidation, for example with fast sedimentation rates. Both normally consolidated conditions and overconsolidated conditions occur in the field. Normally consolidated conditions can be seen when soft layers are loaded by embankments or artificial fills. The drained peatlands and clay areas in the Netherlands, being drained for ~1000 years (Van der Ven, 1994/ Erkens et al., 2016) can be considered to be under overconsolidated conditions. Subsurface layers in drained peatlands and clay areas have been subjected to low loads over long timespans, which would mean that the viscous compression is far advanced along its logarithmic time path, i.e. the layer has a high intrinsic time. When intrinsic time is high, modelled rates will decrease significantly and mathematically approach zero for these overconsolidated conditions, (OCR > 1). Several laboratory experiments have shown that over time the behaviour of viscous compression can change, seen as a steepening of the logarithmic time – strain curve (Fig. 5.1a). If this happens, then more viscous compression occurs compared to the theoretically established logarithmic compaction over time.

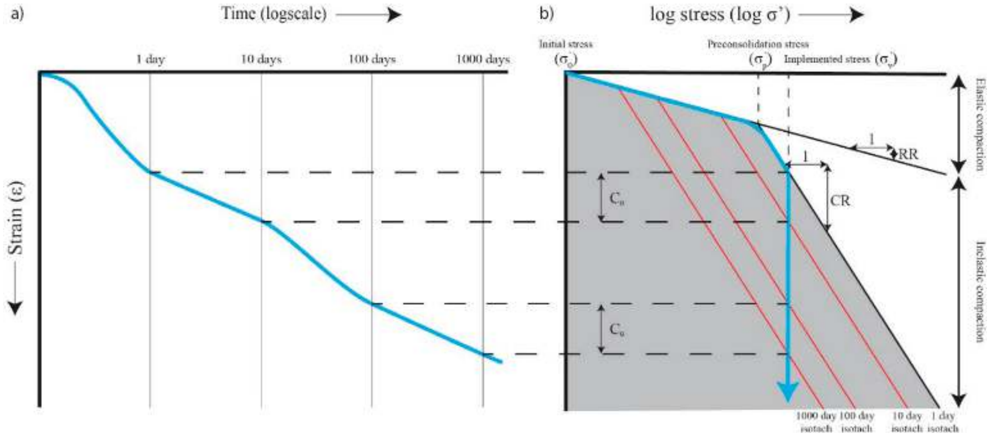

Figure 5.3: Time-strain (a) and stress-strain (b) diagrams showing the compaction of a peat sample (in blue) after a single stress increase from overconsolidated conditions to normally consolidated conditions, exceeding the preconsolidation stress. With developing viscous compression the sample becomes overconsolidated again. The viscous compression includes the temporary steepening strain development during tertiary compression in the time-strain diagram (between 10 and 100 days) and the corresponding greater distance between isotachs in the stress-strain diagram. The red lines indicate isotachs. Strain is the change in height relative to initial sample height [-].

The time-dependent character of viscous compression in this study is described according to the Bjerrum-isotach model (Bjerrum, 1967; Den Haan, 1994) as it is worldwide one of the most commonly used for subsidence calculations (e.g., Bakr, 2015; Mesri and Funk, 2015;

Keogh et al., 2021). The model calculates linear strain, i.e., the normalized height loss relative to the starting height that results from an applied stress to a body of material. The total linear strain is made up of both elastic strain and visco-plastic strain ε_{vp} (-), of which the latter is calculated as:

$$\varepsilon_{vp} = (CR - RR)\log\frac{\sigma'_v}{\sigma'_p} + C_\alpha \log\frac{\tau}{\tau_{ref}} \tag{5.1}$$

where *CR* is the virgin compression ratio (-) and *RR* is the recompression ratio (-), $\sigma_v^{'}$ is the vertical effective stress (kPa), $\sigma_p^{'}$ is the preconsolidation stress (-), τ is the intrinsic time (days), and τ_{ref} is the reference intrinsic time (days) commonly set to 1 day. *CR* and *RR* represent the amount of linear strain from consolidation, water expulsion resulting from porewater pressure differences, following an effective stress increase above and below the preconsolidation stress respectively (Fig. 5.1b). The first term in the equation therefore describes the plastic virgin compression occurring beyond the preconsolidation stress, while the second term describes viscous compression.

According to geotechnical standards, the viscous compression parameter C_α, i.e., the slope coefficient of viscous compression (Fig. 5.1a), is determined by fitting trendlines to the tail of log time-strain curves per loading step beyond the preconsolidation stress in incremental oedometer tests, i.e., under normally consolidated conditions (Fig. 5.2). To get a singular C_α value per sample the average of all C_α values fitted per loading step beyond the preconsolidation stress is taken. C_α denotes the relative strain (i.e., height change divided by the initial height) between two isotachs (Fig. 5.1b). The intrinsic time which these isotachs represent, for a given stress condition at loading step n, is calculated as follows:

$$\begin{aligned} \tau_1 &= \tau_{ref}\,\frac{\sigma'_{pc}}{\sigma'_{n=1}}^{\frac{CR-RR}{C_\alpha}} \\ \tau_* &= \tau_{n-1}\,\frac{\sigma'_{n-1}}{\sigma'_n}^{\frac{CR-RR}{C_\alpha}} \\ \tau_n &= \tau_* + \Delta t_n \end{aligned} \tag{5.2}$$

Where τ_1 is the initial intrinsic time for the end of the first load step based on the load of the first load step ($\sigma_{n=1}^{'}$) and the preconsolidation stress ($\sigma_{pc}^{'}$), τ_{ref} is the intrinsic time of the reference isotach and typically is 1 day, τ_{n-1} is the intrinsic time at the end of the previous load step, Δt_n is the duration of the current stress condition and $\sigma_n^{'}$ is the effective stress for loading step n (kPa). Intrinsic time for the first loading step in an oedometer test uses OCR instead of the current and previous effective stresses.

Oedometer test measurements of clay for overconsolidated stress conditions have shown modest, but noticeable viscous compression over time, while isotach models predict negligible to effectively zero viscous compression over time for the same overconsolidated conditions, and thus underestimate the compaction seen in measured laboratory data and field data (Deltares, 2024). Although only tested for clay, this discrepancy may also occur for peat.

As a result, it remains a challenge to accurately predict long-term compaction response of subsurface layers in overconsolidated conditions, for example in drained peatlands. Data from oedometer tests shows considerable viscous compression over time at low stresses, implying that the slope of logarithmic viscous compression is steeper than theoretically anticipated. The steepening of the logarithmic time – strain curve sometimes observed in laboratory experiments (Fig. 5.1a) could explain the elevated levels of viscous compression compared to the theoretically established logarithmic compaction over time under overconsolidated conditions. In modelling terms: the viscous compression parameter C_α has increased. This contradicts the fact that in models C_α is a static parameter applicable to all stress and intrinsic time conditions. Normally, C_α is determined from a single loading step at normally consolidated conditions (OCR = 1) in oedometer tests, but when C_α varies with stress level and intrinsic time, then values determined under normally consolidated conditions may not be applicable for overconsolidated conditions, and isotachs are either not linear, parallel, or equidistant.

Researchers have considered the observed steepening of viscous compression over logarithmic time as a new compaction phase, called 'tertiary compression', occurring superimposed on viscous compression (Edil and Dhowian, 1979; Den Haan and Edil, 1994; Augustesen et al., 2004; Feng et al., 2021; Fig. 5.1a). During tertiary compression, isotachs (red lines in Fig. 5.1b) may diverge, bend, or become non-equidistant, of which the latter is visualised in Figure 5.1b; the distance in strain between the 10- and 100-day isotachs is greater than between the 100- and 1000-day or the 1- and 10-day isotachs. These studies show by means of laboratory experiments on fibrous and amorphous peat samples as well as clay samples that isotach distortion may occur for any stress condition. Yet, in peat, under normally consolidated stress conditions and after relatively small loading increments, acceleration of viscous compression occurs more quickly but less intense compared to peat under normally consolidated stress conditions with large stress increments or overconsolidated stress conditions. This means that the rate of this tertiary compression depends on both the stress under which it occurs and the intensity of the stress increase which initiated it. In other words, viscous compression is determined not only by material characteristics as discussed in Chapter 4, and organic matter decomposition as mentioned by for example O'Kelly and Pichan (2013) and Feng et al. (2021), but also by the stress and OCR.

The relationship between viscous compression and stress has been investigated extensively. One of the first is the consolidation theory of Terzaghi (Terzaghi, 1943) that focuses on the relation between the viscous compression parameter C_α and coefficient of consolidation C_c, which is the amount of consolidation after a log increase in stress. This theory assumes that different subsurface material types each show a specific combined sensitivity to consolidation and viscous compression, referred to by Terzaghi as primary and secondary consolidation respectively. In other words, viscous compression can be estimated when only the consolidation behaviour is known. This assumption is represented by a constant ratio C_α/C_c , being respectively 0.02, 0.04, 0.05, and 0.06 for granular soils, inorganic clays, highly organic clays, and peat (Mesri, 1973, Mesri and Godlewski, 1977, Tavenas et al., 1978, Graham et al., 1983). Higher values indicate a relatively large contribution of viscous compression to total compaction. The implication here is that since C_c is stress-dependent, C_α must be so as well. Mesri and Godlewski (1977) found from compression experiments that the C_α/C_c ratio also shows no time-dependence, hence both C_c and C_α need to change in the same way with stress, time and strain. Important to state is that Mesri and Godlewski (1977) assume that consolidation and viscous compression happen in sequence, often referred to as hypothesis A in this context (Degago et al., 2011), whereas the work in this thesis assumes that viscous compression occurs simultaneous with consolidation and continues after consolidation is finished, in literature referred to as hypothesis B. The assumption of sequential consolidation and viscous compression (hypothesis A) inherently implies that viscous compression depends on the duration of consolidation, the overpressure of the porewater, and thus the applied stress.

Swelling in oedometer tests has been proven to distort the isotachs, which are suggested to become non-linear and curve towards the elastic compression line (the RR line in Fig. 5.1b) (Vergote et al., 2021, 2022; Deltares, 2024). This theory is important to consider for viscous compression under overconsolidated conditions as overconsolidated subsurface layers have often experienced swelling before sampling. Furthermore, during sampling stress is removed from the sample, leading to swelling and potential distortion of how compaction is measured in the laboratory compared to the behaviour in the field. Given the variety in isotach distortion possibilities, it is uncertain how distortions should be implemented in current isotach-based models.

To be able to analyse the variability of viscous compression for different stress conditions and assess if modelled viscous compression for low stress situations can be improved, this chapter aims to determine the viscous compression parameter C_α at overconsolidated conditions for soft subsurface materials: clay and organic clay, clayey peat, and peat. Alternatively, improved modelled viscous compression under overconsolidated conditions can potentially be acquired by using other C_α values determined under normally consolidated conditions than is currently done. To compare this to values determined under overconsolidated conditions, assessing variation of C_α under normally consolidated conditions is needed. Two research questions are defined to achieve the research aim: 1) what is the best estimated value of C_α for sample-specific stresses under overconsolidated conditions (i.e., OCR > 1), and 2) to what extent can the measured viscous compression under overconsolidated conditions be approximated better in isotach models using the maximum (and minimum) C_α values per sample which are determined from laboratory tests under normally consolidated conditions (i.e., OCR = 1)?

For the first research question, we hypothesized that all or a part of the tested samples show increasing C_α with increasing OCR and intrinsic time under overconsolidated conditions, exceeding the range of C_α values observed under normally consolidated conditions. Higher C_α values result in more modelled viscous compression which matches the measurements of viscous compression under overconsolidated conditions better than when using C_α values determined under normally consolidated conditions. For the second research question, we expect C_α to exhibit variability under normally consolidated conditions, with maximum C_α values that would have a significant effect on model results of viscous compression. Aside from the possibility that C_α differs with stress level at normally consolidated conditions (e.g., Mesri and Godlewski, 1997) variation is also expected because the regression window is determined via an algorithmically optimal breakpoint per loading step rather than a visually determined breakpoint leading to different C_α values. To test these hypotheses, we analysed a large dataset of geotechnical oedometer test data (stress, strain, and time) and their corresponding geotechnical subsidence modelling parameters (RR, CR, and C_α) for peat and clay from the Holocene subsurface of the Rhine-Meuse delta and back-barrier coastal zone of the Netherlands. As we focussed on the viscous compression, we disregarded elastic and virgin compression in this study and analysed only the tail of each oedometer loading step. For every loading step in each oedometer test, trendlines were fitted to the tail of compression over time, using a linear trendline for overconsolidated conditions and a logarithmic trendline for normally consolidated conditions. First for overconsolidated conditions, linear back casting is needed to determine C_α from the slope of compaction over time since intrinsic time is still unknown if C_α has not been determined yet. So, an iterative solution is needed in which C_α is adjusted until it consistently satisfies both the data trend and the intrinsic time calculation. Secondly, by applying a logarithmic trendline to all normally consolidated loading steps we were able to determine the variation of C_α under normally consolidated conditions (Fig 5.2) for the second research aim. Comparing C_α values between loading steps of the same oedometer test shows the way C_α changes between overconsolidated and normally consolidated conditions and with intrinsic time.

5.2 Materials and methods

In this section first the equations to determine strain under normally consolidated and overconsolidated conditions are presented, which are used to derive C_α. Subsequently, the dataset structure and the procedure for determining C_α from oedometer tests therein is described, including the comparison of C_α values across different loading steps of single samples. Finally, the method for validating the obtained C_α values using a simplified isotach model is presented.

5.2.1 Description of the dataset

The dataset used for this project consisted of data of 437 oedometer tests performed on peat and clay samples from the Rhine-Meuse delta and coastal plain of the Netherlands. Oedometer tests measure compaction in terms of sample height over time and record the applied stress (Fig. 5.2a). Typically, the oedometer test consists of eight loading steps, which increase in load apart from one mandatory unloading step and a sequential reloading step. The total amount of loading steps can differ. The height decrease (or increase) was transformed into linear strain by dividing the height change since the beginning of the oedometer test by the initial height. Furthermore, water content, wet and dry specific weight, particle weight, and void ratio were recorded in the database as well as the preconsolidation stress, and geotechnical compaction parameters *RR*, *CR* and C_α. This dataset-registered C_α is normally determined from the first occurring normally consolidated loading step and is from here on referred to as 'reference C_α'.

5.2.2 Determination of C_α

Since the derivation of C_α relies on a reformulation of Eq. 5.1, the equation is first rewritten such that it gives the strain difference $\Delta\varepsilon_{v,time}$ resulting only from viscous compression, as the first term is constant over time, over time period $\Delta t = t_2 - t_1$:

$$\Delta\varepsilon_{v,time} = C_\alpha \left(\log\frac{\tau_* + t_2}{\tau_{ref}} - \log\frac{\tau_* + t_1}{\tau_{ref}}\right) = C_\alpha \left(\log\frac{\frac{\tau_* + \Delta t}{\tau_{ref}}}{\frac{\tau_*}{\tau_{ref}}}\right)$$
$$\Delta\varepsilon_{v,time} = C_\alpha \left(\log\frac{\tau_* + \Delta t}{\tau_*}\right) = C_\alpha \log\left(1 + \frac{\Delta t}{\tau_*}\right) \quad (5.3)$$

First, the normally consolidated conditions are considered. This is defined as $\sigma_n' = \sigma_p'$ or OCR = 1 and intrinsic time τ = 1 day. With intrinsic time τ = 1 day, Eq. 5.3 can be expressed as:

$$\Delta\varepsilon_{v,time} = C_\alpha \log(1 + \Delta t) \quad (5.4)$$

and C_α is equal to the slope of the tail of a logarithmic time-strain curve. This is the part of the time-strain curve after stress has been increased, elastic strain has been completed, overpressure of porewater has dissipated, and further strain is only due to time-dependent viscous consolidation. When the sample is under normally consolidated conditions the intrinsic time is equal to the measurement time.

When overconsolidated conditions are considered, defined as $\sigma_n' < \sigma_p'$ or OCR > 1, intrinsic time is calculated according to Eq. 5.2, and $\tau_* \gg \Delta t$. As a result, $\frac{\Delta t}{\tau_*} \rightarrow 0$. For very small values of $\frac{\Delta t}{\tau_*}$, the logarithmic term can be approximated as $\log(1+\frac{\Delta t}{\tau_*}) \approx \frac{\Delta t}{2.3^* \tau_*}$, and Eq. 5.3 can be simplified to Eq. 5.5:

$$\Delta\varepsilon_{v,time} = C_\alpha \frac{\Delta t}{2.3\,\tau_*} = a\Delta t \quad (5.5)$$

with a being equal to $\frac{C_\alpha}{\tau}$. In this situation, viscous compression has progressed significantly over time, i.e., the intrinsic time is in the order of hundreds to thousands of days, while Δt

during a single loading step of the oedometer tests is typically 1 day. This results in measurements exhibiting linear behaviour, and with very small strains developing over time, represented by a. Since τ is calculated using Eq. 5.2, slope (a) of the linear tail of a time-strain curve is calculated with C_α following:

$$a = \frac{C_\alpha}{2.3\ \tau_{n-1}\ \frac{\sigma'_{n-1}}{\sigma'_n}^{\frac{CR-RR}{C_\alpha}}} \tag{5.6}$$

A numerical solution for C_α can then be found using a non-linear solver of Eq. 5.6 using time-strain step data for overconsolidated conditions.

5.2.3 Determination and comparison of C_α from the dataset

Linear regression was performed on the tail of the time-strain curves of each loading step per oedometer test to calculate the C_α, using eq. 5.5 & 5.6 for overconsolidated loading steps and eq. 5.4 for normally consolidated loading steps. A steeper slope of the viscous compression curve indicates a higher C_α value (Fig. 5.1a). In the ideal case that viscous compression is a perfect logarithmic process, both methods would have the same C_α value as a result. The RR and CR values per test, and OCR values per step per test are retrieved from the dataset.

Given the large number of samples and steps, correct determination of the starting point of the tail of the time-strain curve was automated. Automation was achieved using the 'segmented' function from the 'segmented' R package (Muggeo, 2003). This function fits a desired number of linear regression models to predict the data. The result is a so-called segmented or broken-line relationship providing a predefined 'npsi' number of breakpoints, which describe the most likely point in time where the linear relationship changes slope, which are indicated as red dots in Fig. 5.2b and c. The number of breakpoints 'npsi' was looped from 1 to 4. The most optimal npsi was determined by the lowest residual sum of squares (RSS) of the last segment and the corresponding last breakpoint was taken as starting point of the tail and regression could be performed (the blue lines in Fig. 5.2b and 5.2c). This optimal breakpoint time value had to be ≥10% of the total step duration to ensure a significant time period is taken over which slope a is determined or an NA value would be returned instead.

For samples under normally consolidated conditions, a transformation of time to the logarithm of time is needed, because the 'segmented' function can only apply linear fits while a logarithmic fit is needed to extract C_α according to Eq. 5.4. Next, the mean, maximum and minimum C_α value of all normally consolidated loading steps was calculated to use in the comparison with C_α value derived per overconsolidated loading step of the same oedometer test.

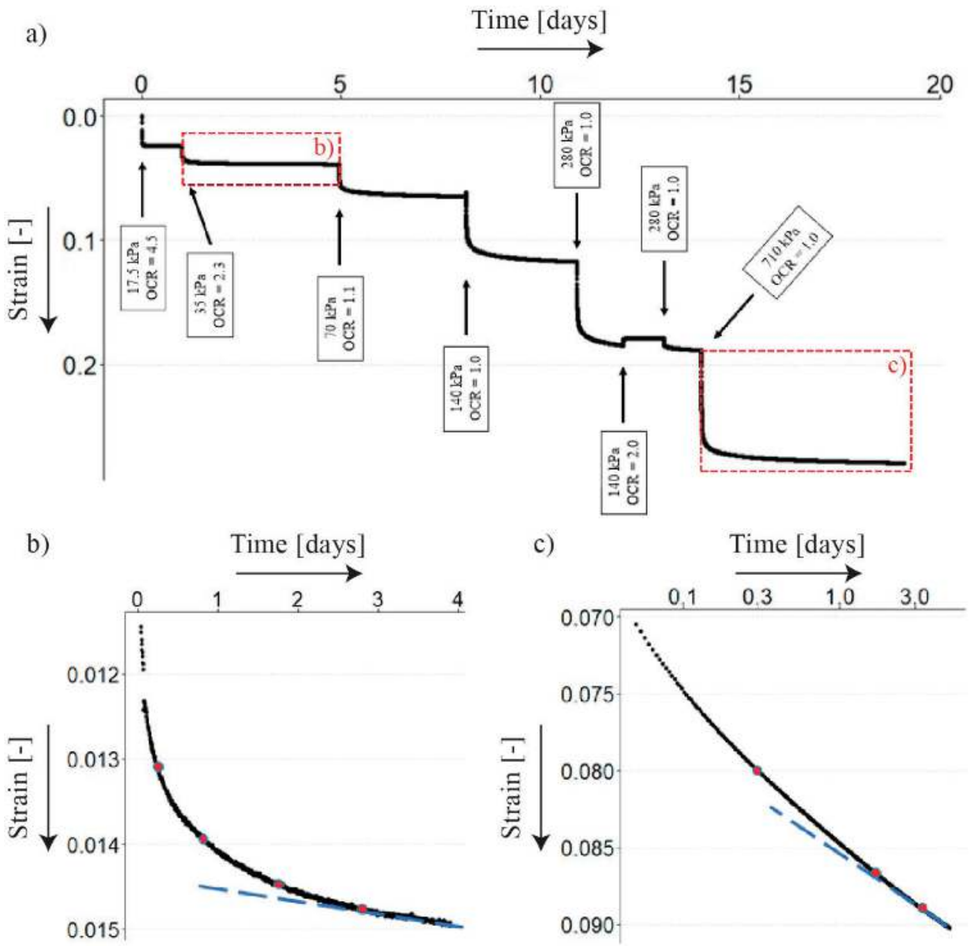

Figure 5.2: a) Time-Strain diagram showing the 7 loading steps and 1 unloading step after 12 days of an example oedometer test, including stress and OCR per step (initial preconsolidation stress = 78.4 kPa). The second and eighth step are indicated in red and detailed plots are shown in panel b and c. The first and last 1% of the total time of these steps has been removed to prevent disruption of segmentation by consolidation and adjustment errors. b) Time-Strain diagram for overconsolidated conditions (OCR > 1). The red dots indicate the breakpoints obtained with algorithmic segmentation of the data. The linear regression of the last segment is used to determine slope 'a' used in Eq. 5.6. c) Logarithmic time-strain diagram for normally consolidated conditions (OCR = 1). The red dots indicate the breakpoints obtained with algorithmic segmentation. C_α was determined through logarithmic regression of the time-strain curve, which is here presented as a linear line in the semi-log plot.

The measured (log) time-strain data from the oedometer tests was partitioned based on the loading step break indices, indicating points in time when a loading event occurred. The data from the first and last 1% of time per step was removed to eliminate any possible interference in the measurements right before or after the loading event which can dominate the segmentation. Assuming a standard length of 24 hours per step as prescribed in ASTM D4186-06, NEN 5118 and NEN-EN-ISO 17892-5 (ASTM, 2006; NNI,1991; ISO, 2017) the 1%

time removed from the load step duration equals approximately 15 minutes. The intervals between successive loading steps are in the order of 1-3 days, while the total oedometer test duration is often more than a week.

5.2.4 Isotach model validation

To evaluate the plausibility of the C_α values resulting from the overconsolidated loading step regressions, we used different C_α values to predict compaction rates using the isotach method for a case-study oedometer test and compared the predicted with the measured compaction. Four different C_α values for the specific oedometer test were used for the predictions:

- the reference C_α value listed in the dataset
- the maximum C_α value under normally consolidated conditions
- the minimum C_α value under normally consolidated conditions
- the C_α determined per individual loading step under overconsolidated conditions

For the RR, CR and OCR the values initially listed in the dataset were used.

5.3 Results

C_α values for overconsolidated conditions (OCR > 1) were generally higher than for normally consolidated conditions (OCR = 1) (Fig. 5.3). Note that C_α under overconsolidated conditions was determined from a linear trendline and under normally consolidated conditions from a logarithmic trendline. The individual C_α values per loading step within an oedometer test vary up to one order of magnitude higher between overconsolidated and normally consolidated conditions. The C_α values obtained under overconsolidated conditions tend to first increase with further increase in OCR (more overconsolidated), and decrease for OCR > 3, and often exceed typical laboratory C_α ranges reported for clay and peat in literature (determined under normally consolidated conditions). Median C_α values start to decrease for the highest OCR bins (OCR > 3). These trends emphasize the relevance of a separate estimation of C_α for different overconsolidated conditions across different OCR regimes.

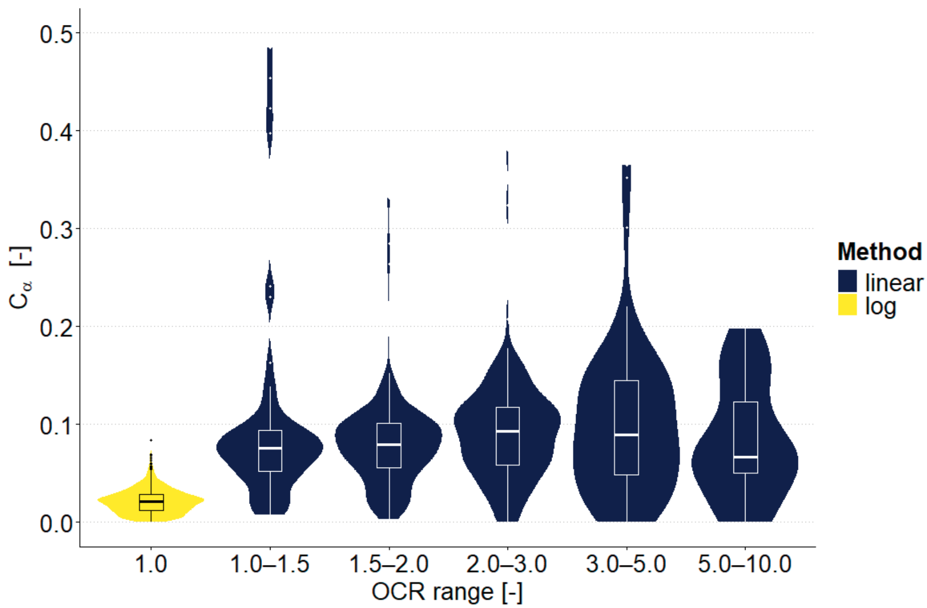

Figure 5.3: Combined violin and boxplot of C_α values determined per loading step in oedometer tests, grouped by the overconsolidation ratio (OCR) of each step. To show the bulk of the data, C_α values were clipped at 0.5. The violin shapes represent kernel density estimates, where wider regions indicate a higher frequency of C_α values within that OCR group. Boxplot elements (median, interquartile range) are overlain to highlight central tendency and dispersion. Increasing OCR is linked to an increase in C_α value, but decreases for high OCR values (> 3) which show a slightly decreasing C_α value.

5.3.1 Linear-derived C_α values per overconsolidated loading step

The values of C_α determined for overconsolidated conditions (OCR > 1) using the linear method show a general increase with rising step-specific OCR (Fig. 5.4a). However, the range of C_α also increases, without a clear trend across the full dataset. To further explore this variation, the results were grouped by lithological class similarly as used in Chapter 4; Clay, Clayey Peat, Fibrous Peat, and Decomposed Peat. This reveals that overconsolidated samples classified as Peat tend to exhibit higher C_α values with increasing OCR, whereas Clay samples show a more moderate trend (Fig. 5.4a).

C_α values under overconsolidated conditions will not necessarily be equal between samples consisting of the same material when subjected to the same OCR condition. Thus, to prevent misinterpretations it is better to normalize absolute C_α values under overconsolidated conditions with the reference C_α value of the dataset instead. This preserves the overall increasing trend with step-specific OCR, while reducing the apparent spread in the data (Fig. 5.4b). Near OCR = 1, i.e., very slightly overconsolidated conditions, the intrinsic time is short and C_α values are lower than the reference C_α values. All four lithological classes exhibit similar normalized patterns, with most values sitting at 100 – 10000% of the reference C_α value(Fig. 5.4b).

The intrinsic time offers additional insight into time-dependent compression: C_α values under overconsolidated conditions tend to peak around an intrinsic time of ~200 days (Fig. 5.4c). This trend is observed across all lithological classes. A similar trend is observed in the normalized C_α values (Fig. 5.4d), suggesting that the highest intrinsic times do not necessarily coincide with the largest OCRs.

While the patterns in Fig. 5.4c and 5.4d summarize all data, individual sample analysis is used to test whether C_α values under overconsolidated samples consistently show a parabolic pattern with increasing intrinsic time. This is illustrated in Fig. 5.5, which presents three representative samples with the most loading steps with overconsolidated conditions. For sample 203, C_α values under overconsolidated conditions first increase and then decrease with increasing intrinsic time. Not all samples in the dataset show the parabolic pattern of C_α with increasing intrinsic time as can be seen for samples 208 and 209 which show a decreasing C_α value with increasing intrinsic time. This is likely the case because of the iterative character of calculating intrinsic time and adjusting the C_α value.

5.3.2 C_α values per loading step under normally consolidated conditions

The mean C_α values determined for normally consolidated conditions per test closely match the reference C_α values originally listed in the dataset (Fig. 5.6a). Compared to lower reference C_α values (< 0.02), our method generally returns slightly higher values, while for higher reference C_α values, our method returns lower $C_\alpha$values. Differences between the two are likely due to variations in the fitting window of the regression and the high possibility that not all steps above the initial preconsolidation stress (PcS) steps were included in the dataset value's calculation.

To assess within-test variability, the minimum and maximum C_α values from individual normally consolidated loading steps (OCR = 1) were compared to the mean C_α value computed over all normally consolidated loading steps per individual oedometer test (Fig. 5.6b). The reference C_α values more closely resemble the maximum C_a values obtained per oedometer test. Figure 5.6b shows two clear envelopes: one above and one below the 1:1 ratio line, delineated by upper and lower bounds on the observed range estimated to be 1.875 and 0.28 times the mean value. The practical impact of this variation is considerable, given that in current practice C_α is also determined from a single loading step. For example, a 1-meter-thick subsurface layer is predicted to undergo 1 cm of viscous settlement in one year using the mean C_α value for the calculation. When the maximum value is used, the prediction of viscous compression could increase up to approximately 1.875 cm, while the minimum value would result in just 0.28 cm in the most extreme case. Over 10 years, the corresponding estimates would be 2 cm, 3.75 cm, and 0.56 cm, respectively. This highlights the importance of accurately constraining C_α variability as it directly affects long-term subsidence predictions.

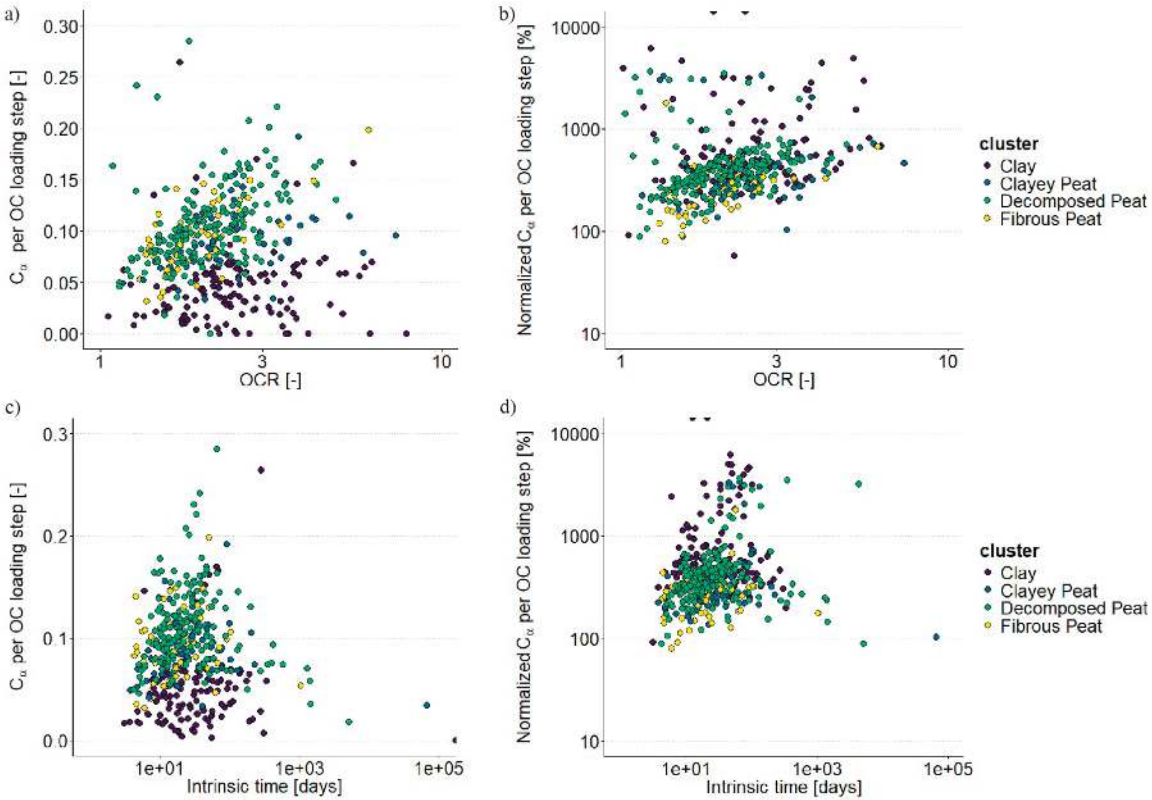

Figure 5.4: C_α values for samples under overconsolidated (OC) conditions (OCR >1) derived per loading step using the linear regression method per oedometer loading step and clustered by lithological class: (a) plotted against the OCR, (b) plotted normalized as percentage of the reference C_α value of the same oedometer test against the OCR, (c) plotted against the calculated intrinsic time, (d) plotted normalized as percentage of the reference C_α value of the same oedometer test against the calculated intrinsic time. Graphs portray the bulk of the data. Outliers are clipped at C_α > 0.3, and Normalized C_α < 10%. Full graphs are presented in the supplementary (Fig. C3)

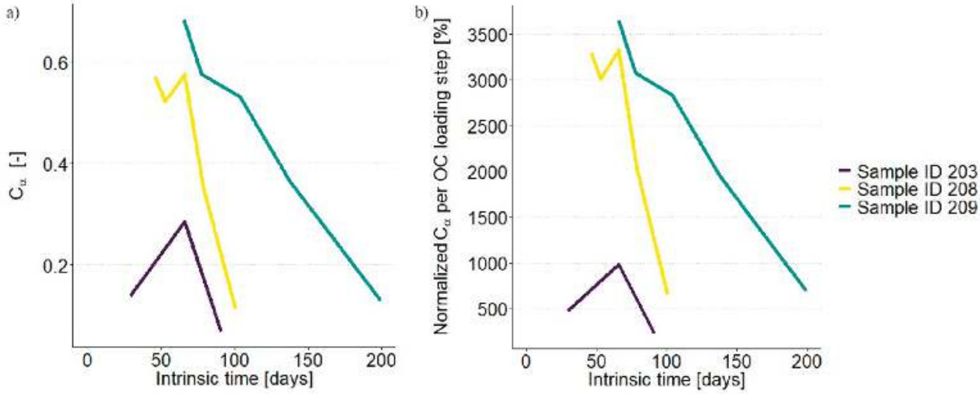

Figure 5.5: Evolution of C_α values for overconsolidated (OC) loading steps (OCR > 1) per oedometer test for three peat samples: (a) plotted against the calculated intrinsic time per step, (b) plotted as percentage of the reference C_α value of the same oedometer test against the calculated intrinsic time.

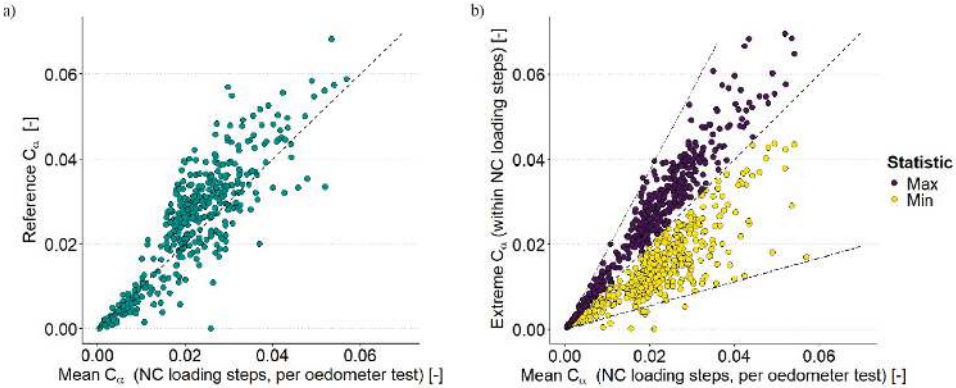

Figure 5.6: (a) The reference C_α values given in the database per oedometer test plotted against the mean of all C_α values for normally consolidated (NC) loading steps per oedometer test. The dashed 1:1 line indicates perfect agreement. (b) Maximum and minimum C_α values of normally consolidated loading steps per oedometer test plotted against the mean of all C_α values for normally consolidated steps determined with regression per oedometer test. Upper and lower dashed lines delineate maximum and minimum possible C_α values seen for individual, normally consolidated loading steps as a function of the mean C_α value of all normally consolidated loading steps.

5.3.3 Comparison of isotach model predictions using differently derived C_α values to measured compaction

The most critical implication of differentiating C_α values with intrinsic time lies in the impact on isotach-model-based subsidence predictions. To illustrate this, a representative sample from the dataset was selected for forward calculation of viscous strain. This sample, classified as Clay, had a water content of 54%, a dry bulk density of 1020 kg/m^3, particle density of 2285 kg/m^3 and a void ratio of 1.24. The recompression ratio (RR) and virgin compression ratio (CR) were 0.033 and 0.233, respectively, with a preconsolidation stress of 78.4 kPa.

The oedometer test consisted of eight steps in total, of which the first three steps using loads below the preconsolidation stress (overconsolidated conditions), and the fifth and sixth step comprising the unloading and reloading cycle.

The second loading step was analysed as this step had a longer duration and which allows intrinsic time computation based on the first loading step as a reference. The OCR was 2.25, which is representable for conditions where observations and model results differ (Deltares, 2024), with an effective stress of 34.8 kPa. Four different C_α values were used for model simulation of the viscous compression over time:

- Reference dataset C_α, based on normally consolidated conditions: 0.0110
- Step-specific C_α for overconsolidated conditions: 0.0351
- Maximum C_α for normally consolidated conditions: 0.0137
- Minimum C_α for normally consolidated conditions: 0.0080

Figure 5.7a shows the measured strain data and the calculated strain curves over time using the four C_α values. The lines of the reference (yellow) and max C_α value (blue) are not visible in this figure since they plot at virtually the same location as the min C_α line (green). A distinct offset is observed in total strain between the measurement data and the model results, caused by the differences between measured and calculated elastic strain. To isolate viscous behaviour, the tail of the loading step is highlighted (Fig. 5.7b). In this region, the choice of C_α value significantly affects the predicted strain.

All model runs underestimate the measured viscous strain. However, the model using the step-specific C_α value for overconsolidated conditions performs best, predicting approximately 56% of the observed viscous strain. In contrast, the model using the reference C_α value results in predicting just 0.000008%, of the observed viscous strain and results using the C_α values determined for normally consolidated conditions (both maximum and minimum) also severely underestimate viscous strain, effectively predicting negligible compression.

The cause of this discrepancy lies in the calculated intrinsic time. For the reference and C_α values for normally consolidated conditions, intrinsic times range from 137,000 days (~375 years) to over 651 million days (~2 million years), making the 2-day measurement window (= Δt) insignificant in the context of Eq. 5.3. These large intrinsic times originate from the combination of the RR, CR and C_α values leading to a high exponent of OCR in Eq. 5.2. The result is a drastic increase of intrinsic time using the reference, maximum and minimum C_α cases, while calculated viscous strains approach zero. In contrast, the intrinsic time associated with the step-specific C_α value is 101 days, making the 2-day measurement period relatively meaningful and allowing viscous strain to accumulate in the model result.

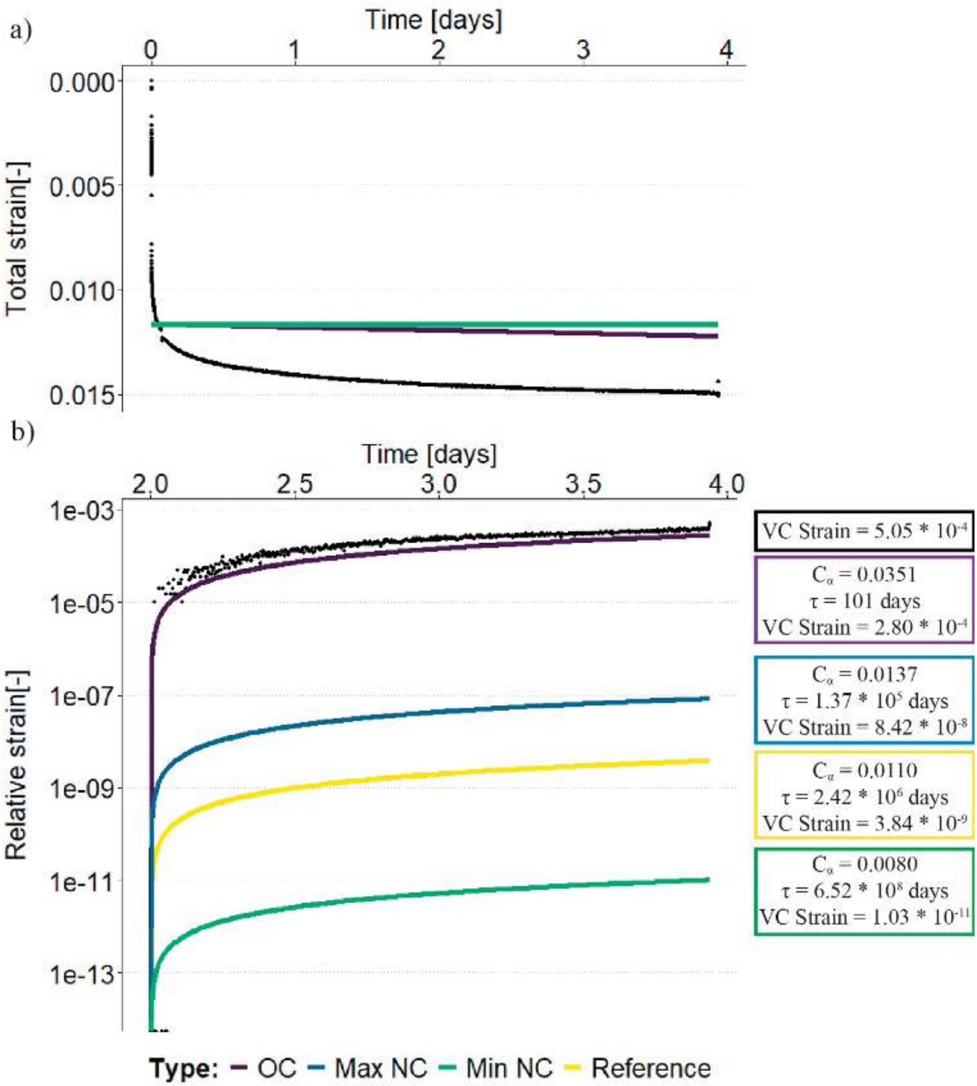

Figure 5.7: Measurements from an oedometer test (black dots) and isotach model outputs with different C_α values (coloured lines). OC refers to the overconsolidated conditions C_α, NC indicates normally consolidated conditions. (a) Time-strain plot where the green line overlies the yellow and blue lines with similar values on this scale, and the red dashed box indicates the zoom in to isolate viscous behaviour, (b) Time-logarithmic strain plot with strain normalized to the strain at two days after the loading event. The coloured boxes on the right correspond to the coloured curves. VC strain is the strain due to viscous compression measured in the oedometer test or calculated by the model over the shown time period.

5.4 Discussion

This study systematically evaluated C_α values derived for overconsolidated and normally consolidated conditions, respectively through linear and logarithmic regression methods, across 437 oedometer tests. The outcomes were compared with the reference C_α values listed in the dataset. For normally consolidated conditions (OCR=1), distinctive variation was observed between maximum and minimum C_α values per loading step per oedometer test. The relationship between C_α, OCR, and intrinsic time reveals limitations of the standard approach in overconsolidated regimes (OCR > 1), with implications for isotach-based settlement modelling.

5.4.1 Implementation into the traditional isotach model

The C_α values for overconsolidated loading steps vary significantly per step and often exceed the ranges established for normally consolidated conditions. This suggests that isotachs might not always be equidistant for overconsolidated conditions, which is a departure from the conceptual isotach model presented in Fig. 5.1, which assumes linear, parallel, and equidistant isotachs. Under these conditions, viscous compression may not show the expected linear behaviour over logarithmic time. Variable C_α values can be used within a C_α-isotach model if C_α is regarded as a time- and stress-dependent parameter. This would imply altering the spacing between isotachs from the traditional equidistant, linear form to a non-equidistant or curved pattern.

A critical assumption when using C_α derived either for normally consolidated or overconsolidated conditions in modelling is that the slope of the viscous compression–log(time) curve remains constant. Under normally consolidated conditions (OCR = 1), this assumption holds, because the intrinsic time is effectively reset when the load exceeds the preconsolidation stress. In this case, the oedometer test captures the full intrinsic time interval and the derived C_α is representative for the complete isotach behaviour at the load-step specific stress and time conditions (Fig. 5.8a).

In contrast, for overconsolidated conditions, oedometer tests only cover a small portion of the intrinsic time, as has been shown by for example Fig 5.7 with intrinsic times in the hundreds to millions of days. When C_α is estimated using the linear method, the slope of the viscous compression curve is captured only for the short time window observed and therefore corresponds to a short period on the intrinsic time scale (Fig. 5.8b). If the calculated linear-derived C_α is larger than for the C_α determined for normally consolidated conditions, the strain over logarithmic time curve will not be linear but show an increasing slope. For the calculation of intrinsic time a constant slope of the viscous compression curve is assumed, and hence the calculated intrinsic time using the overconsolidated C_α will underestimate the full intrinsic time if the rate of viscous compression changes along the intrinsic time axis, which is one of the possibilities causing the mismatch between measured and modelled compaction for overconsolidated conditions.

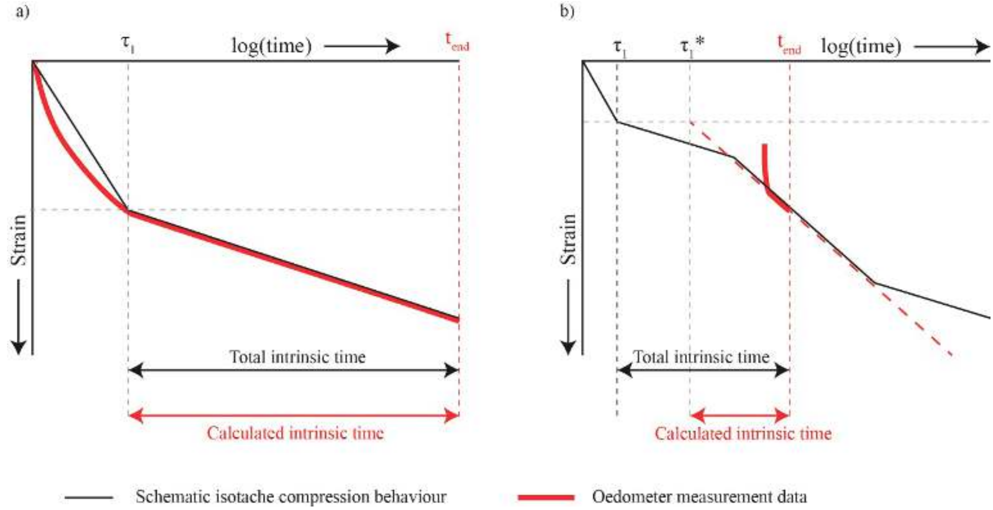

Figure 5.8: Conceptual strain-time diagram for two oedometer test scenarios: (a) normally consolidated conditions (OCR = 1), and (b) overconsolidated conditions (OCR > 1). The black lines represent the theoretical mechanistic compaction following the isotach concept, showing what the strain development of a sample would look like if the applied stress in the examples was applied uniformly since the original deposition or formation. The strain development includes elastic and virgin compression, and their extent is indicated by the horizontal dashed line. Thick red lines indicate the portion of the strain–time curve actually measured during the oedometer test. The dashed diagonal red line indicates the linear strain development with log time due to viscous compression as measured during the oedometer test, based on which C_α is determined. Vertical dashed lines denote key time points: τ_1 is the theoretical reference time (e.g., 1 day), the moment when consolidation should be completed and after which only viscous compression occurs; τ_1^* is the reference time calculated iteratively with the C_α value for overconsolidated conditions and shows that intrinsic time lowers with increasing C_α when RR and CR remain constant; and t_{end} is the final time point of the measurement interval, used to compute the intrinsic time. The end of the black strain curve on the right represents a temporary accelerated viscous compression case commonly indicated as tertiary compression. This is, however, only one of the possible continuations of the strain curve after the end of measuring.

This mismatch between total intrinsic time and calculated intrinsic time for overconsolidated conditions helps explain two notable findings:

1. Why the intrinsic time calculated using C_α for overconsolidated conditions is several orders of magnitude lower than when using the reference values as seen in Fig. 5.7b.
2. Why some C_α values for overconsolidated conditions tend to first increase and then decrease with increasing (calculated) intrinsic time as seen in Fig. 5.4.

Understanding how variable C_α values work, requires recognizing that an increase in C_α leads to a slower decrease in the viscous compression rate over time when the isotachs become more widely spaced. However, this does not necessarily imply a change in the actual viscous compression rate itself, which depends on the position of the stress–strain state relative to the isotachs (Fig. 5.1). Ideally, our results would enable a revised version of Fig. 5.1 in which the spacing between isotachs is governed by C_α values relative to the intrinsic time. However, due to the described discrepancy between the actual and estimated intrinsic times, it is currently with our data not possible to correctly space the isotachs in such a diagram.

Our findings may align with a model that incorporates curved isotachs after swelling rather than strictly parallel as described by (Vermote et al, 2022). As mentioned earlier, isotach distortions can be non-equidistant spacing, but also include bending of the isotachs. As bending is proposed to lead to a denser grouping of isotachs near the elastic compression line in Fig. 5.1, it could also lead to higher viscous compression rates for a specific stress-strain condition shortly after swelling. Isotachs can also becoming non-equidistant as a result of swelling: swelling reduces the effective stress, i.e., increases OCR and intrinsic time, but according to our results intrinsic time increases differently than predicted by the isotach model. Bending can lead to denser grouped, i.e., varyingly spaced, isotachs near the elastic compression line, and a stress reduction would lead potentially to a smaller increase of intrinsic time and a smaller reduction of viscous compression rate. Curved isotachs thus may provide an accurate explanation of viscous compression in overconsolidated layers, although a hybrid framework using both bent and non-equidistant isotachs could prove most effective as it serves both the effects of viscous compression rate changes over long time periods and of swelling. Furthermore, our findings share similarities with the elasto-viscoplastic model for clay compression (MIT-SR) designed by Yuan & Whittle (2018; 2021). The model incorporates a compression rate-sensitivity parameter, which allows the viscoplastic strain rate to be dependent on the internal state of the material which allows characterisation of isotach behaviour as well as temporary strain rate behaviour. In other words, the viscous compression over time is dependent on the strain rate history and thus the past compaction and stress conditions. This aspect of MIT-SR is similar to the dependence of C_α on OCR shown by our analysis.

5.4.2 Applicability of a variable C_α-isotach model in subsidence settings

A variable C_α-isotach model might be used to explain the persisting subsidence seen in agricultural drained peatlands where low stress-high OCR conditions prevail. An illustrative example is presented in Massop et al. (2024) where the deformation of multiple subsurface layers within the topmost 1.4 meters of a drained peatland has been monitored using subsidence platens over a period of more than fifty years. Their observations revealed consistent compaction over time of all layers, with annual compaction rates decreasing with depth from 4.8 mm/year at the surface to 1.0 mm/year at 1.4 meters below the surface.

Throughout the studied period, mean lowest groundwater levels per year fluctuated between 0.3 and 1.1 meters below the surface, depending on the season. It is remarkable that the anchors at depths of 1.2 and 1.4 meters showed sustained subsidence despite remaining fully saturated. These saturated layers also experienced periodic elastic compression and rebound as a result of the seasonal groundwater level fluctuations with a range of ~1 meter (Van Asselen et al., 2025). The sustained subsidence of the deeper anchors happened under conditions of relatively stable surface water management since 1970, and in absence of loading events. This implies a near-constant effective stress regime, conditions under which the standard isotach model with reference C_α values determined under normally consolidated conditions predicts extremely slow viscous compression of buried layers due to large intrinsic times. However, the observed continuous deformation of the saturated layers with about 1 mm/year challenges this expectation. If one assumes a variable C_α, subsidence rates can stabilize and subsidence continues for decades, even under near-static effective stress conditions, in this case aligning closely with the field data.

This same mechanism may also explain sustained subsidence in build-up peatland settings, such as the city centre of Gouda, the Netherlands, where most historic buildings are founded on deep sand layers, but public spaces such as streets and parks continue to subside (Kooi and Melman, 2024). These areas have an artificial fill layer that serves as a foundation (Van Asselen et al., 2018), which is commonly underlain by compressible subsurface layers. In these urban environments, groundwater levels are maintained close to the surface to prevent subsidence and foundation damage as much as possible. Under conditions of constant effect stress, i.e., long after the last loading event (e.g., road reconstruction), traditional models predict limited deformation. However, ongoing subsidence of roads and public spaces (Kooi and Melman, 2024) suggests that long-term modelled compaction due to time-dependent viscous processes is underestimated. The variable C_α-isotach model helps resolve this discrepancy by capturing a more dynamic evolution of compression rate as a function of both OCR and time since loading.

5.4.3 Future research

To advance our results into a variable C_α-isotach model and potentially later into a practical and more applicable method, future research should focus on pinpointing the temporal evolution of C_α, and how it varies with stress level and OCR. A central objective would be to determine when during a laboratory or field test C_α begins to change, and how this transition relates to the material's mechanical state. This research can function as an extension of the existing curved isotach concept by allowing for variable isotach spacing, for time periods long after the last alteration of effective stress. Incorporating curved, non-equidistant isotachs that reflect changes in viscous strain rate over time will require a fundamental modification of the isotach model. Long-duration oedometer tests of mostly peat, but also clay samples, will be critical to this effort, as they are needed to capture the gradual evolution of viscous compression over months to years. These oedometer tests would provide the empirical data necessary to describe and model time-dependent changes in C_α more accurately, possibly by combining C_α determination from individual loading steps, both above and below the preconsolidation stress, representing the viscous compression rate at different moments along the intrinsic timeline. This first needs to be tested and evaluated but could provide a starting point for further development.

To ensure the framework's validity and applicability, experimental results must be directly linked with field data. This includes subsidence measurements in drained peatlands, characterized by their high OCR and low stress, as well as in build-up settings where surface loading conditions are more variable. Such a coupling between in-situ monitoring and laboratory tests where boundary conditions are kept as similar as possible will be key to validating the revised isotach model and establishing reliable guidelines for geotechnical practice.

5.5 Conclusion

This study presents an alternative for determining the viscous compression parameter (C_α) under overconsolidated conditions, which is typically done under normally consolidated conditions to improve model predictions of viscous compression under overconsolidated conditions. For overconsolidated conditions (OCR > 1), there is a discrepancy between measurements and model results. By analysing a large dataset of oedometer tests, we show that when C_α is derived from overconsolidated loading steps in oedometer tests using an iterative method, the parameter values often deviate substantially from reference values determined at normally consolidated conditions (OCR = 1). Very overconsolidated cases (OCR > 5) can produce values 100 times as high. These deviations are related to increasing OCR and intrinsic time, revealing that C_α is not constant over time, but rather evolves with the stress history and duration of viscous compression. Using the mean, minimum and maximum C_α values obtained for normally consolidated loading steps instead of the reference C_α value cannot solve the discrepancy between measurements and model results seen for overconsolidated conditions.

Our findings deviate from the assumption of equidistant isotachs and suggest that the spacing of isotachs might vary over time, particularly for long-term viscous deformation. The applied linear back-casting method to determine C_α captures part of this evolution but underestimates the intrinsic time, which complicates correct implementation into the current isotach model. Variation in isotach spacing would have significant implications for predictive modelling cases, where low-stress and stable loading conditions prevail. Observed continuous subsidence in such settings, previously difficult to predict with constant-C_α isotach models, can be better understood through a variable C_α-isotach model.

Chapter 6:

Synthesis

Viscous compression of soft subsurface materials is an important and critical process contributing to the globally-relevant land subsidence, given the long time period over which it can continue under constant stress conditions in the subsurface. A defining characteristic of the process is that it does not cease when external conditions change: changes in load, adjustments in groundwater levels, or shifts in effective stress may alter its rate, but the underlying microstructural evolution continues. This persistence stems from time-dependent rearrangement of the solid matrix and, in organic soils, from gradual biochemical modification of the organic material, allowing deformation to accumulate long after consolidation has ended. Because of this, the process has been a topic of great interest since the formulation of the first consolidation theories in the first half of the 20th century (Terzaghi, 1923; Buisman, 1940; Taylor and Merchant, 1940; Terzaghi, 1941). Though theory and practice have come a long way since then, major issues are still left unsolved. One of those issues is viscous compression of soft subsurface layers, in particular of peat and organic clays, instigating incorrect viscous compression predictions by subsidence models under low stress conditions in the field in combination with the high compressibility and large heterogeneity of peat and organic clay (Mesri et al., 1997; O'Kelly and Pichan, 2013). Improving our understanding and prediction of viscous compression of these organic constituents is a considerable challenge given a lack of mechanistic knowledge on viscous compression with varying material characteristics and incomplete understanding of how material characteristics drive the variation of viscous compression in models.

In the light of these challenges, the aim of this research was:

to advance the mechanistic understanding of viscous compression and its role in long-term compaction behaviour in order to help improving the predictive capacity of land subsidence models in peat and organic clays.

In this chapter, the main conclusions of the thesis are summarised based on the research subobjectives (SO). By combining the key findings on mechanistic understanding of viscous compression and the relation with decomposition, a variable viscous compression parameter is introduced and discussed. This variable viscous compression parameter may also have implications for modelling and therefore the benefits and limitations of this adaptation are discussed. Lastly, remaining research questions and emerging scientific challenges from this project are considered for future research.

6.1 Main conclusions

Chapter 2 focuses on the mechanistic understanding of viscous compression, related to SO 1: Identify the mechanisms and processes that cause viscous compression in organic-rich subsurface layers with special attention to their large spatial variability in material characteristics. In clays, three main mechanisms leading to viscous compression are identified: micropore water expulsion, changes in the adsorbed water layer, and particle interactions. These processes also occur in peat, but the relative importance differs due to the fibrous organic structure of peat. Intracellular water and fibre interlocking introduce additional resistance to particle movement compared to resistance between clay particles, and water adsorption plays a smaller role than in clay because of the lower surface valency and hydrophobic organic components. Six key controls of viscous compression in peat were identified: fibre content (or decomposition state), progressive decomposition, clay fraction, temperature, pore water pH, and ion concentration. The variability in types of control (physical, biological or chemical) shows that viscous compression in peat is a multidisciplinary phenomenon.

Chapter 3 demonstrates how compaction alters the decomposition rate for peat with varying degrees of decomposition and devices a conceptual model to explain the bidirectional interaction between viscous compression and decomposition, answering SO 2: Determine and quantify the influence of the organic matter decomposition state on viscous compression. Laboratory experiments showed that compaction alters porosity, which in turn modulates microbial respiration and decomposition. In fibric peat, porosity reductions strongly suppress basal respiration rates, whereas in decomposed peat the effect of porosity reduction is smaller under equal loading conditions. As a result, initially the degree of decomposition controls the amount of compaction, with a lower degree of decomposition leading to a higher compaction, while at the same time the amount of progressive decomposition is affected by this compaction, limiting present and future decomposition as porosity decreases. The relative contribution of consolidation and viscous compression to the total compaction also shifts with the degree of decomposition: consolidation dominates in fibric peat, while viscous compression becomes more important in decomposed peat. This pattern reflects the oxic, drained conditions that decomposed peat is or has been subjected to, and under which both decomposition and irreversible consolidation have occurred.

Chapter 4 provides a classification of material characteristics and a prediction for the viscous compression parameter based on those material characteristics, linked to SO 3: Translate the improved mechanistic understanding into improved predictive capacity of subsidence models through more representative parameterisation. Samples used in oedometer tests were classified based on their material characteristics (i.e., Clay, Clayey Peat, Fibrous Peat, Decomposed Peat) and subsequently the classes were compared by their viscous compression parameter values. The results revealed that viscous compressibility generally increases with organic content, with fibrous peat showing the highest viscous compression parameter (C_α) value. Water content and dry bulk density predict C_α well for clastic material, but for peat (>25% OM), variation is larger and predictions of C_α less precise. Notably, decomposed peat shows a lower C_α than fibrous peat and thus is less susceptible to viscous compression. These results show that decomposition causes measurable changes in material properties directly linked to compression behaviour.

Chapter 5 examined the influence of stress state and history on viscous compression, covering SO 3: Translate the improved mechanistic understanding into improved predictive capacity of subsidence models through more representative parameterisation, and also contributes to SO 1. Conventional isotach models assume a constant C_α and parallel isotachs, but oedometer tests show that C_α varies substantially with overconsolidation ratio (OCR, the ratio between the preconsolidation stress and the current stress) and time, sometimes by orders of magnitude. This demonstrates that isotachs are not equidistant, particularly under low-stress or high-OCR conditions, and challenges the predictive reliability of standard models. The results indicate that viscous compression evolves with stress history and intrinsic time (total time needed at current stress to get to the current compaction state), often leading to underprediction when conventional assumptions are applied.

Together, these findings enhance our understanding of the mechanisms and processes underlying viscous compression, including the contribution of decomposition. The broader implications of this enhanced understanding are discussed in the next two sections.

6.2 Mechanisms and processes causing viscous compression

Fibres and decomposed organic particles form a large part of the solid structure of peat and within that structure each fibre or particle has numerous contact points with other fibres/particles. In this characteristic lies the essence of viscous compression of peat, which, similar to clay, originates from reorientation of fibres/particles to an approximately horizontal position when stress is applied and is the only active deformation mechanism when effective stress is stable. The surfaces at the contact points between fibres/particles generate friction, which is dependent on the type and state of the organic material, potential existing bonding forces, the presence and thickness of an adsorbed water layer, pH, and ion concentration (Chapter 2). The size of fibres is typically larger than that of decomposed organic matter (particles), resulting in more contact points for fibres and a higher total friction force working against movement. This is why fibre content and the degree of decomposition both control viscous compression. At the same time, porewater needs to move to allow particle reorientation. Because viscous compression happens irrespective of overpressure, it is argued that this moving porewater escapes mostly from micropores through water diffusion. As temperature controls the diffusion rate it is an important boundary condition for viscous compression.

The development of viscous compression is traditionally approximated over time by a simple logarithmic equation. It is observed that the slope of this logarithmic curve is not constant (Chapter 5), and this divergence of behaviour is seen more often and more pronounced in fibrous peat than in decomposed peat and clay (Augustesen et al., 2004; Mesri and Ajlouni, 2007). Instead of following a single logarithmic trend with continuously decreasing strain rates, some samples exhibit a clear steepening of the strain–intrinsic time curve. This temporarily accelerated viscous compression may be interpreted as the mechanical result of evolving microstructure: either loss of fibre stiffness and decreasing intra-particle strength through progressive decomposition, or localised pore collapse through shifts in thermal activity, or both. Possibly, progressive decomposition and thermal activity together can explain the occurrence of accelerated viscous compression in both peat and clay. Temperature, pH and ion concentration are important for thermal activity in both clay and peat as well as for progressive decomposition in peat. They also explain the difference in severity between peat and clay, given that progressive decomposition is unique to peat and facilitates further viscous compression.

This combination of mechanisms, processes and controls of viscous compression is not entirely consistent with the concept incorporated in current isotach models used to predict compaction. Their conceptualization is more static, which does not reflect material characteristic changes, but in that aspect also lies the workable simplicity of the isotach models: after the compaction parameters are determined in the lab, one would be able to model any stress-strain combination and know what the effect of stress changes or progressive time would be. Yet, compaction in low stress conditions proof to be difficult to predict (Chapter 5), because progressive decomposition can alter material characteristics and change the viscous behaviour of peat. Furthermore, the isotach models were originally developed for high stress case studies encountered in mainly construction, meaning they are not tailored to low stress conditions.

At the field scale, subsurface profiles often contain mixtures of clay and peat or spatially variable peat layers with variable fibre content, organic particle integrity, and degrees of decomposition. Besides, boundary conditions such as pH and ion concentration can differ between peat-clay mixtures and peat or clay. As a result, under the same stress conditions such mixtures likely experience less viscous compression than peat, but more than clay. The same is true for the occurrence and magnitude of temporarily accelerated viscous compression, which would potentially be in between peat and clay. The interaction between organic matter and clay particles on a structural level can cause a unique mechanistic behaviour of viscous compression. Decomposed organic matter can bind with clastic particles to form mineral associated organic matter (MAOM). This binding is strong, leading to a lower susceptibility to further decomposition and mechanically a MAOM particle reorientates as one entity. This differs from other forms of decomposed material, such as dissolved organic matter (DOC) or not/partially decomposed particulate organic matter (POC), which move largely independent of clastic particles. As a result, long-term subsidence patterns may become highly variable, even within a single mapped lithological unit, and even more difficult to approximate with the current models.

Combined, the insights of this thesis suggest that commonly used interpretations of viscous compression, which treat solids as mechanically stable and the compression rate as governed solely by fixed material properties, may not fully represent the dynamic nature of organic-rich soils. Incorporating evolving material properties and coupled decomposition-viscous compression in models may help explain compression behaviour observed in Chapters 2, 3 and 5, and ultimately may improve the skill of these models in predicting viscous compression.

6.3 Interaction between viscous compression and organic matter decomposition

Considering that viscous compression of peat and organic-rich clay is related to microstructural and bio-physical conditions, the question is whether decomposition may interact with viscous compression, something which is not assumed in current models. The results of this thesis show that viscous compression and decomposition are not strictly separate processes as they are both continuous and pore scale–driven mechanisms that are likely affected by each other over time. Both processes act under largely stable stress conditions, both depend critically on porosity, and both alter porosity in ways that can either reinforce or constrain the other. Consequently, this interaction between biochemical and mechanical processes may be more relevant for long-term subsidence than previously recognised.

Critical is the distinction between degree of decomposition, i.e., the material state resulting from past decay, and progressive decomposition, i.e., ongoing biochemical breakdown during the process of compaction. The degree of decomposition is well known to influence compressibility by altering fibre content, structure, and water retention (Landva and La Rochelle, 1983; Price et al., 2005; Huat et al., 2011; Farrell, 2012). In contrast, ongoing decomposition has long been considered too slow to affect compressibility within typical laboratory timescales (Hobbs, 1986), and therefore its influence on viscous compression has remained largely undetermined. Some earlier studies did suggest that decomposition may contribute to long-term subsidence (e.g., Wardwell et al., 1983), but without addressing possible implications for non-linear viscous behaviour or temporarily accelerated viscous compression.

The findings in this thesis indicate that progressive decomposition, although slow, can plausibly influence the microstructural conditions that govern viscous compression and hence decomposition needs to be taken into account in the context of compaction. Porosity emerges as the central mediator of this interaction as both processes are governed by the distribution of pore space and simultaneously act to alter it. Under constant effective stress, viscous compression gradually reduces microporosity. At the same time, decomposition removes material preferentially at pore–solid boundaries (Schlüter et al., 2022), slightly increasing local porosity or leaving it unchanged, but weakening particle surfaces by removing easily degradable constituents. This weakening can increase the susceptibility of particles to internal microstructural collapse, reorientation, or deformation; these are all processes that contribute to viscous compression and even, when sufficiently pronounced, to consolidation. Reduced pore connectivity at the local scale further decreases hydraulic conductivity and permeability.

Collectively, these mechanisms share reciprocal influences: decomposition may facilitate viscous compression by progressively reducing internal structural resistance (Fig. 6.1), while (viscous) compression limits decomposition by reducing accessible surface area, and restricting nutrient and oxidant supply. Other biochemical by-products, for example the formation of gas bubbles and microbial colonies that locally block pores (Beckwith and Baird, 2001; Kellner et al., 2005), may further modulate the hydraulic and mechanical response. The direction and magnitude of these interactions are likely site- and material-dependent, and their quantitative contribution remains uncertain; nevertheless, they provide a mechanistic basis for interpreting some of the non-linear and time-dependent behaviour observed in Chapters 4 and 5.

These interacting mechanisms can explain why decomposed peat is generally less susceptible to viscous compression than fibrous peat (Chapter 4; Hobbs, 1986; Price et al., 2005). More decomposed material contains a larger proportion of resistant organic structures and typically holds less water. The consolidation and shrinkage happening under the unsaturated conditions needed for rapid decomposition lead to a more compacted or interlocked structure that reduces the susceptibility for further compression (right panel of Fig. 6.1), as also suggested by Taccari and Zwanenburg (2019). These observations suggest steps in between decomposition and volume loss: decomposition modulates material characteristics, which in turn affect the physical processes that produce viscous compression and lead to volume loss.

The results on viscous compressibility in relation to the degree of decomposition therefore point toward a framework in which mechanical and biochemical processes co-evolve, rather than acting as independent and additive contributors to subsidence. Such a framework provides a possible explanation for observations of continued viscous compression over several decades in settings where stresses and groundwater levels have remained stable. For example, the multiple meters of peat beneath the historic city centre of Gouda mentioned in Chapter 1 have continued to compact for decades after the application of the last artificial land fill at rates that exceed those predicted by conventional isotach models. According to these models, viscous compression should decay to near-zero under constant load after several decades. However, the interaction between viscous compression and anaerobic decomposition, either through decomposition and changing viscous compression susceptibility or the steepening of the strain curve with intrinsic time identified in Chapter 5, may provide an explanation for the continuing subsidence over decades as observed in Gouda.

6.4 Enhanced viscous compression model predictions

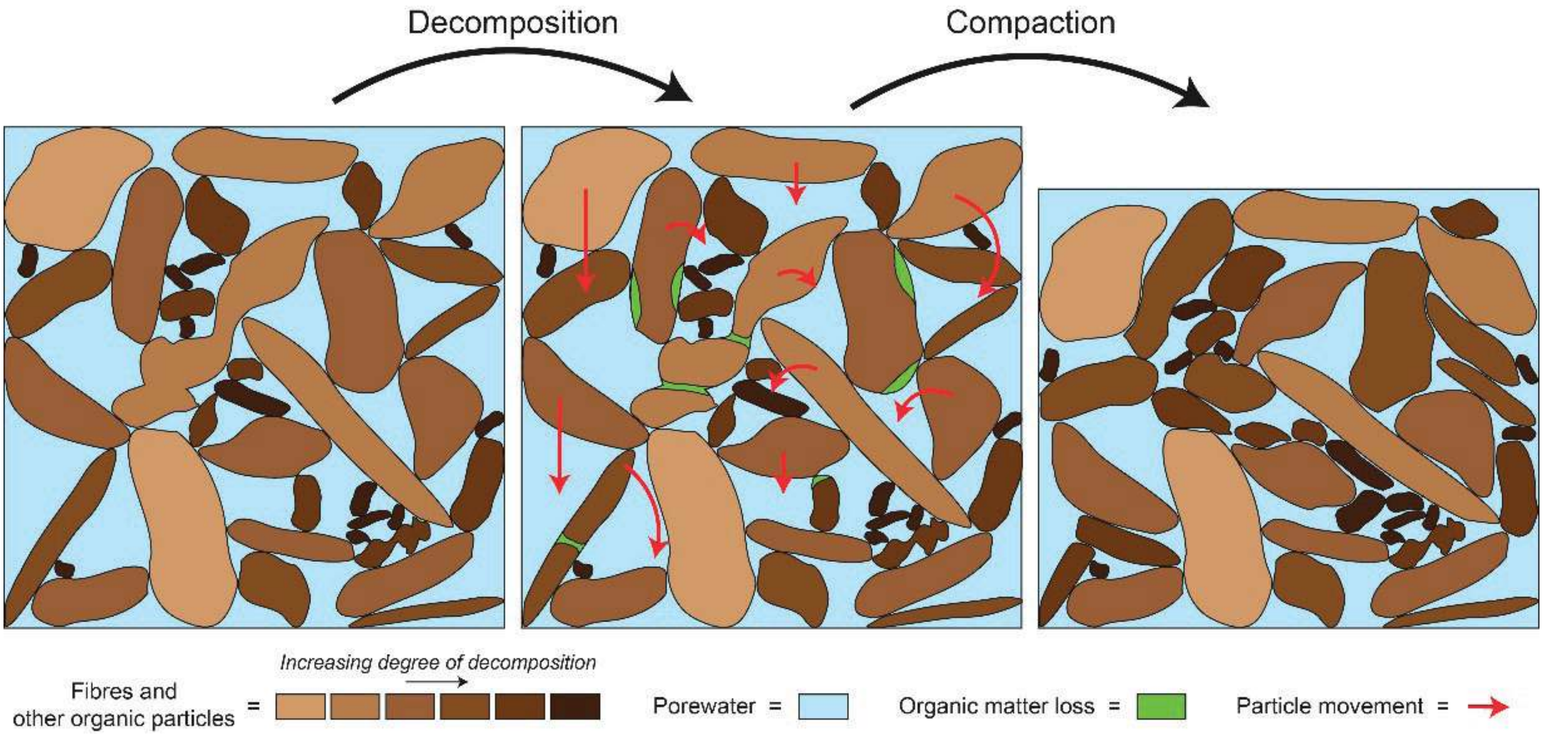

Figure 6.1: Schematic illustration of a decomposing and compacting peat matrix with both intact fibres and decomposed organic material. The matrix experiences constant vertical stress throughout the figure. In reality, the decomposition and compaction happen simultaneously. *Left:* The partially decomposed peat matrix before progressive decomposition and compaction. *Middle:* Progressive decomposition removes organic material from the larger fibres, in some cases breaking up the fibre. This, together with the present stress, initiates particle movement and reorientation. *Right:* The compacted peat matrix after decomposition, consolidation and viscous compression.

While most commonly used conventional isotach-based models rely on a single, constant viscous compression parameter (C_α) value to represent viscous compression, the findings of this thesis (Chapters 2–5) show that C_α is likely not a fixed material property but evolves with decomposition state, stress history, and intrinsic time. The latter is the concept that describes how material ages. In other words, the time a subsurface layer or sample would need to reach the current compaction state given the current stress condition, corresponding to the various isotachs and the distance from the 1-day isotach (Fig. 4.1). When C_α evolves with intrinsic time, viscous compression at a fixed stress does not always decrease along a simple logarithmic curve. Instead, the strain-rate curve can steepen again as intrinsic time increases, indicating renewed or accelerating viscous compression rather than continuously diminishing rates (e.g., Den Haan and Edil, 1994; Augustesen et al., 2004). A similar conclusion is drawn by Feng et al. (2021), who indicate from oedometer tests combined with LOI tests that slow, linear compression, referred to as 'tertiary consolidation', observed during a high stress (800 kPa) compression test is caused by a combination of pore drainage and progressive decomposition. The question is whether they observe the same temporarily accelerated viscous compression as is discussed in this thesis: the stresses applied in their tests were considerably higher than observed in field conditions and cover only normally consolidated conditions (OCR = 1), whereas the analysis in Chapter 5 shows increasing C_α with increasing intrinsic time for overconsolidated conditions (OCR > 1). Feng et al. (2021) divide the compaction phases based on deformation over time rather than strain over logarithmic time, where the former would show a logarithmic curve for viscous compression. This curve is more difficult to partition than strain over logarithmic time since this deformation over time curve will not show a linear part, thus knickpoints indicating accelerated rate are not as clear. An alternative to a variable C_α would be a change in the intrinsic time concept, where the progression of time would not be linear with changes in stress. However, this alternative could be overlapping with the variable C_α idea, since C_α is part of the calculation of intrinsic time.

Implementing a variable C_α under progressive decomposition (O'Kelly, 2017) would enable coupling the mechanical progression of compression to changes in physical and biochemical properties, for example, reductions in porosity and water content, or progressive decomposition of the organic matrix (Chapters 3 and 4). In practice, this would require linking the viscous compression parameter to one or more state variables that reflect material condition, rather than treating it as an external constant. This coupling would also need to account for stress-dependent behaviour identified in Chapter 5, so that C_α responds to changes in effective stress and overconsolidation ratio as well as to the internal evolution of peat and clay in the subsurface.

A central consideration in implementing such a variable parameter is the distinction between the two commonly used formulations of the isotach model: the linear strain approach, which uses C_α for the viscous compression parameter and is used in this thesis as it is globally the most commonly used parameter, and the natural strain approach, which uses c for the viscous compression parameter (Den Haan, 1994). In the linear strain formulation, C_α represents the slope of the linear strain–log(time) curve and is sensitive to the initial porosity and reference stress conditions, making it dependent on the chosen strain reference frame. In contrast, the natural strain formulation expresses viscous compression as a time-dependent strain rate (c) relative to the current strain state, which allows for a more direct description of material behaviour independent of initial geometry. A variable C_α proposed in this thesis aligns conceptually more closely with the natural strain framework. Incorporating a state-dependent c value over a static c value would allow viscous strain rates to respond directly to evolving material properties, rather than indirectly through changes in void ratio or strain. The approach could also improve transferability of parameters between laboratory tests and field-scale models, which has been a persistent limitation of conventional C_α-based approaches.

Ultimately, implementing a variable viscous compression parameter would not only align modelling practice with the mechanistic understanding developed in this thesis, but also enables models to describe the change of viscous compression rate over time because of shifting material characteristics or intrinsic time. While this requires probably difficult new calibration strategies and long-term experimental data to constrain parameter evolution, it offers a clear path towards improving the reliability of subsidence predictions in areas with an organic-rich subsurface. Adopting a variable C_α in modelling might also improve representation of field-scale heterogeneity in compaction models. Peat rarely consists of uniform layers, but instead shows considerable variation in fibre content, decomposition state, and clay fraction at the metre to decimetre scale (Chapters 2 and 4). Under the current constant-- $_\alpha$ approach, such heterogeneity is reduced to averaged layer properties, which masks local variations in viscous behaviour and produces overly smoothed subsidence predictions. A variable-C_α (or c) formulation, in contrast, would allow different parts of the subsurface to evolve at different rates depending on their composition (Chapter 4) and stress history (Chapter 5). Clearer differentiation of C_α would be particularly valuable for modelling areas with interbedded peat and clay, where current models tend to misrepresent the cumulative effect of small, locally concentrated zones of high viscous compressibility and clearer differentiation can enable more detailed layering in models. Besides, interbedded layers potentially show small-scale variation in OCR and thus variation in intrinsic time and viscous compression rates. However, taking both compaction and stress history into account would further complicate parameterisation of the model as more characteristics would need to be tested, while the main points of critique on the isotach model already are the complexity of its many parameters and the expensive testing needed to determine their values for each individual subsurface layer. The prediction of C_α based on water content and dry bulk density presented in Chapter 4 can on the other hand reduce the costs of determining isotach parameters since only a relatively cheap drying test of a sample is needed. Modellers can also minimize uncertainty by calculating the bandwidth of viscous compression over time using the suggested upper and lower end C_α values for highly organic subsurface materials. Decreasing this bandwidth can only be done by further analysis of predictive material characteristics for a better estimation of C_α or simply by measuring compaction with a oedometer test and determining C_α therefrom.

6.5 Future challenges and recommendations

The research presented in this thesis increased our understanding of viscous compression in peat and organic clays, in particular on how viscous compression functions in combination with decomposition and under various stress levels. Specifically, this work highlights that the degree of decomposition, often not fully taken into account in current practice, determines critical material characteristics, such as water content and structural strength, in turn affecting viscous compression. Moreover, ongoing decomposition must be considered when describing gradual changes in material composition and state over time. This is additional to the fact that the viscous compression rate depends on intrinsic time, and therefore on effective stress and preconsolidation stress. While the research has largely answered the initial questions, considerable challenges remain. The most important challenges and recommendations I envision to further improve the understanding and especially the quantitative assessment of viscous compression are the following:

1. *Integrated testing and modelling of physical and biochemical land subsidence processes.* The variable C_α proposed in this thesis requires further support from tests and quantitative measurements before it can be applied in practice. As a first step, the concept of variable C_α should be validated through simultaneous laboratory testing of compaction and decomposition, for example long-duration oedometer tests (e.g., in the order of months) which can also measure CO_2/CH_4 concentrations similar to incubation tests used in biological research. This will allow quantification of how viscous compression rates change with ongoing decomposition at different decomposition states (i.e., the experimental setup of Chapter 3 applied in reverse order). In case time is restrictive, an acceleration of decomposition through for example increasing oxygen or alternative electron acceptors. A model based on these test results would enable researchers and practitioners to address both land subsidence and decomposition simultaneously.

2. *Incorporating fibre characteristics into behaviour classification and prediction of peat compaction*. A better understanding of how fibre characteristics in peat and organic clay determine their structural strength is needed to explain the variability in compressibility of these subsurface materials. The lithological classification of samples based on material characteristics defined in Chapter 4 shows that the state of decomposition distinguishes the general viscous compression behaviour of peat. However, both fibrous and decomposed peat, as well as clayey peat, display considerable variability in viscous compression, which may originate from differences in fibre characteristics. Previous findings (Chapter 2) suggest that large tensile strength and fibre size can hinder viscous compression. These

properties vary with both the botanical origin of the organic material and its degree of decomposition, thus can explain the relationship between viscous compression and decomposition in more detail, and can potentially improve C_α estimation. Using a more sophisticated understanding and classification of fibre characteristics would allow for more accurate differentiation of viscous compression behaviour. Such a field description exists (Erkens et al., 2013), but is not used widely as it incorporates all material characteristics possible and thus exceeds what is strictly necessary. Tensile strength and fibre length could potentially serve as additional predictors for estimating the viscous compression parameter, although they are more difficult to measure than water content or dry bulk density. Building a dataset wherein both fibre content and size, tensile strength, and isotach parameters from oedometer tests are present is essential to take this next step.

3. *Scale down: measuring micropore and particle orientation over time.* Conceptual models of viscous compression focus on the reorientation of particles and the expulsion of micropore water (Chapter 2). However, the timing of these processes remains partially unclear and complicates the translation of understanding into practice. Locating and quantifying structural changes during compaction, for example through visualization using X-ray tomography, can help clarify when and where subsurface deformation occurs, and which processes are responsible. Such visualization is particularly important for tracking micropores and their size changes, but it can also capture structural changes caused by shrinkage and swell. This would improve the integration of shrinkage and swell and viscous compression in modelling. In addition, imaging data could support further pore network modelling, which is essential for understanding hydrological behaviour of peat and greenhouse gas emissions.

4. *Scale up: determining and translating differences between conventional (small-scale) laboratory testing, large-scale laboratory testing and in-situ measurements.* Upscaling compressibility parameters from laboratory experiments to field conditions has long been a challenge, particularly for peat, where spatial heterogeneity of material characteristics and compressibility complicates the prediction of long-term compaction over large areas. Larger-scale testing equipment, for example for samples of 80 centimeters high with a diameter of 40 centimeters (Taccari and Zwanenburg, 2019) and/or extended testing durations in the order of several months to years can better mimic field conditions, and their results can serve as a bridge between conventional laboratory tests and in-situ measurements. For example, the evolution of the viscous compression rate with intrinsic time (Chapter 5) can be quantified under such conditions and then compared directly with long-term field measurements of for example extensometers over multiple years.

5. *Exploring the seasonality of viscous compression under annual temperature fluctuations and long-term climate change.* Temperature dependency is a well-established aspect of viscous compression and compaction, as in Chapter 2 is shown that higher temperatures increase

the viscous compression rate. For this reason, strict temperature regulations are in place for laboratory testing. However, little is known about how strongly viscous compression responds to the relatively small soil temperature changes observed between seasons, typically between 5 and 15 degrees Celsius change over half a year in The Netherlands. This question is particularly important in the context of climate change, which is expected to raise mean annual temperatures and potentially amplify seasonal fluctuations. Because higher temperatures also strongly increase decomposition rates, compression tests conducted under higher temperature conditions (but similar stress conditions) could further clarify how strong the facilitation of decomposition for viscous compression is, especially for the range of current and predicted soil temperature changes.

6. *Quantifying the effect of increasing salt porewater content on viscous compression.* Continuous groundwater extraction and sea-level rise are driving subsurface (groundwater) salinization in many coastal regions, with largely unknown consequences for compressibility of formally freshwater peat layers. Building on the lab experiment analysis by Lexmond et al. (2024), which demonstrated the behaviour of shrinkage and swell under varying salt porewater concentrations, a similar approach could be used to investigate how viscous compression responds to increasing salinity in subsurface layers. Hypothetically, increased salinity could lead to more viscous compression of peat and organic clays because of reduced forces between particles, with an effect similar to dispersion. On the other hand, water diffusion of salt water is slower than that of freshwater, hampering viscous compression rates. Such insights would improve predictions of long-term elevation change in coastal areas affected by ground- and surface water salinization.

Supplements

Supplement A:

A.1 Background information on sampling location

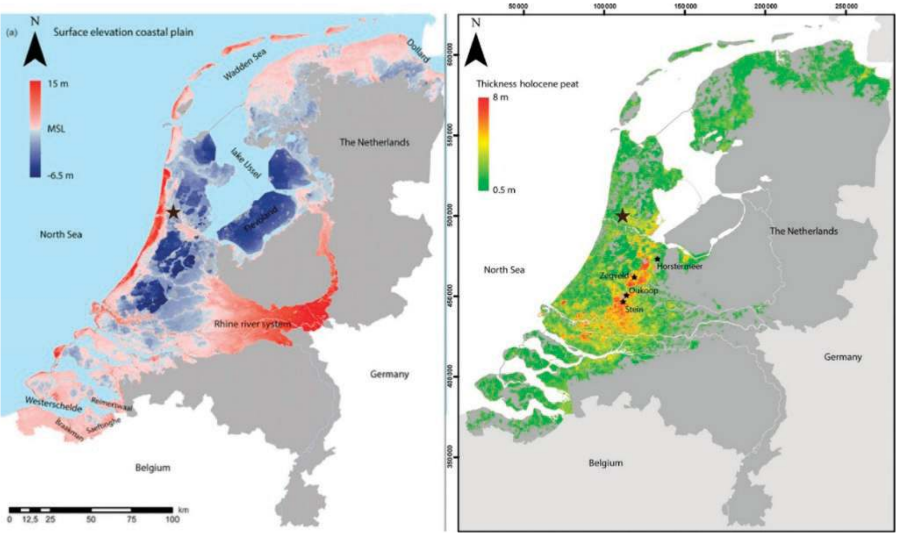

Figure A1: Elevation and peat thickness of The Netherlands with field site Assendelft marked by the black star (after: Koster et al., 2018).

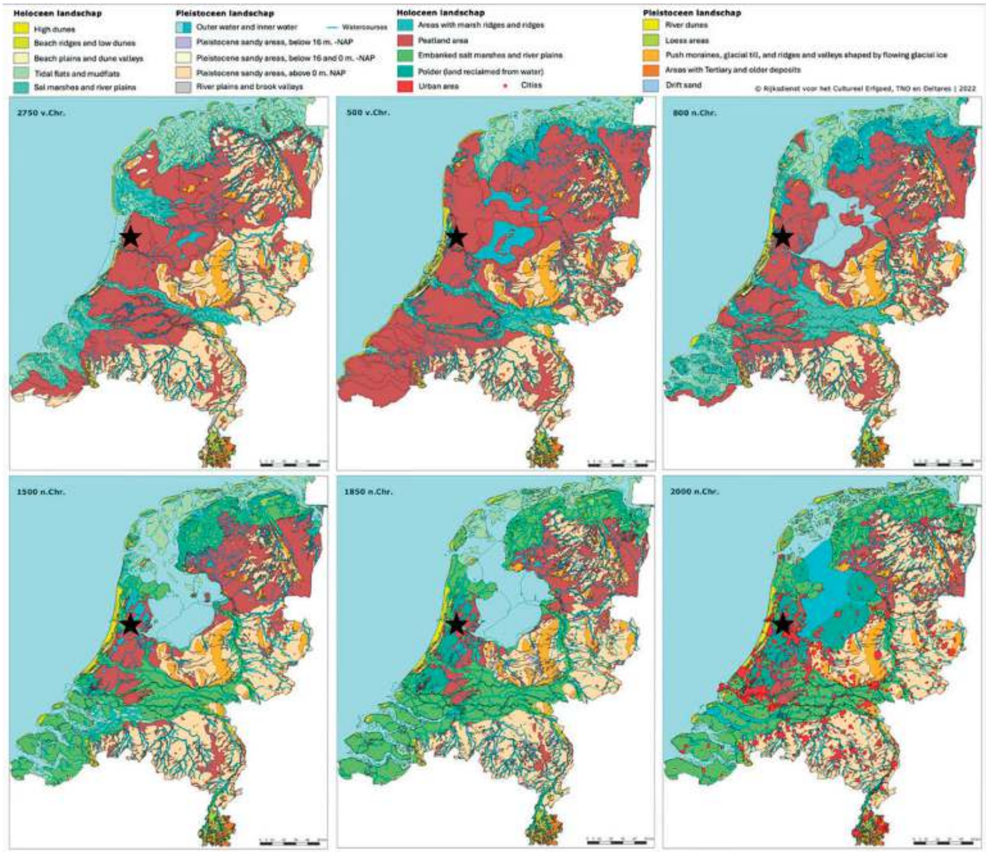

Figure A2: Paleogeographic reconstruction of the area with field site Assendelft marked by the black star (paleogeographic maps Vos et al., 2020).

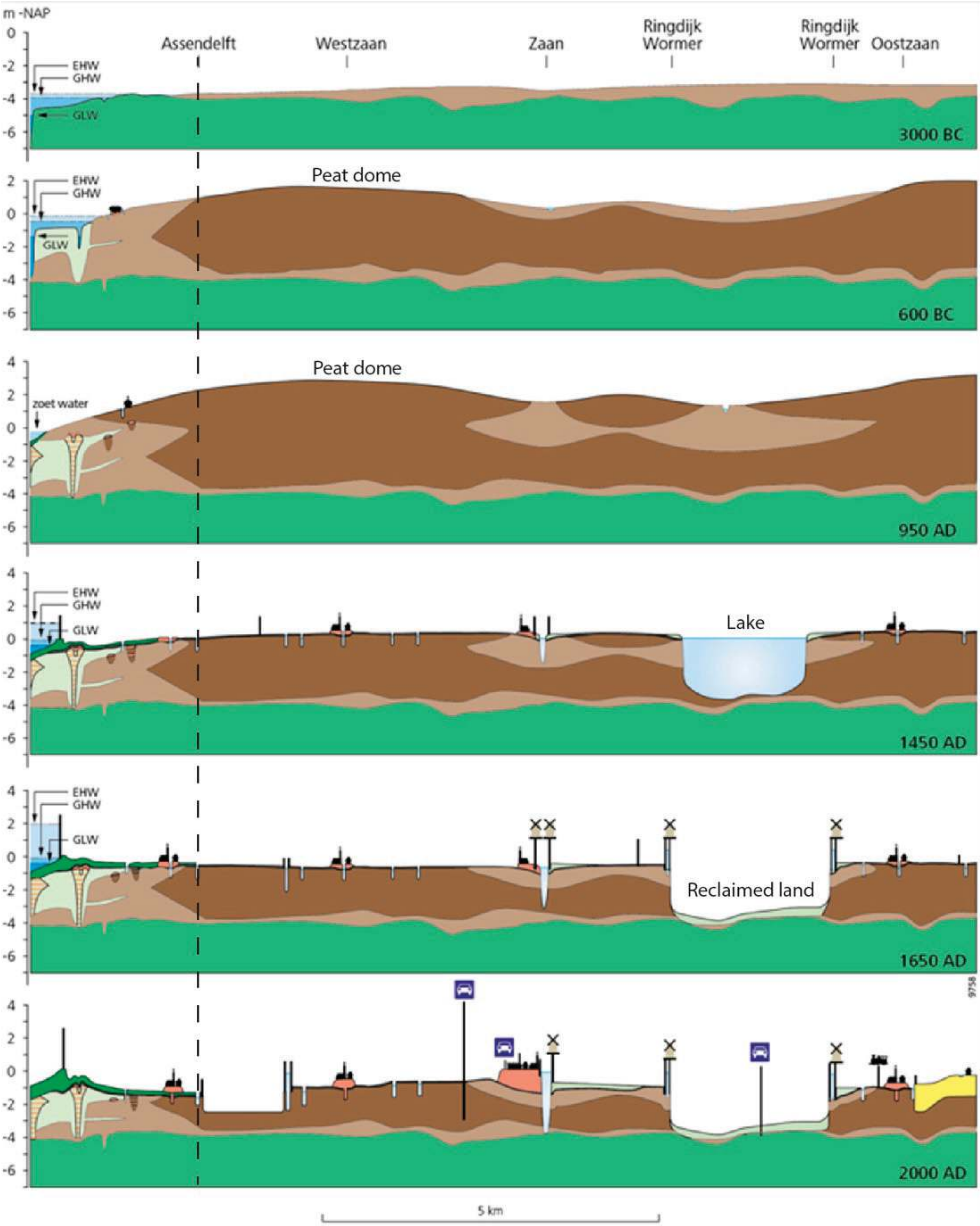

Figure A3: Subsurface build-up of the field site, Assendelft, The Netherlands, over time (after Van de Ven, 1993).

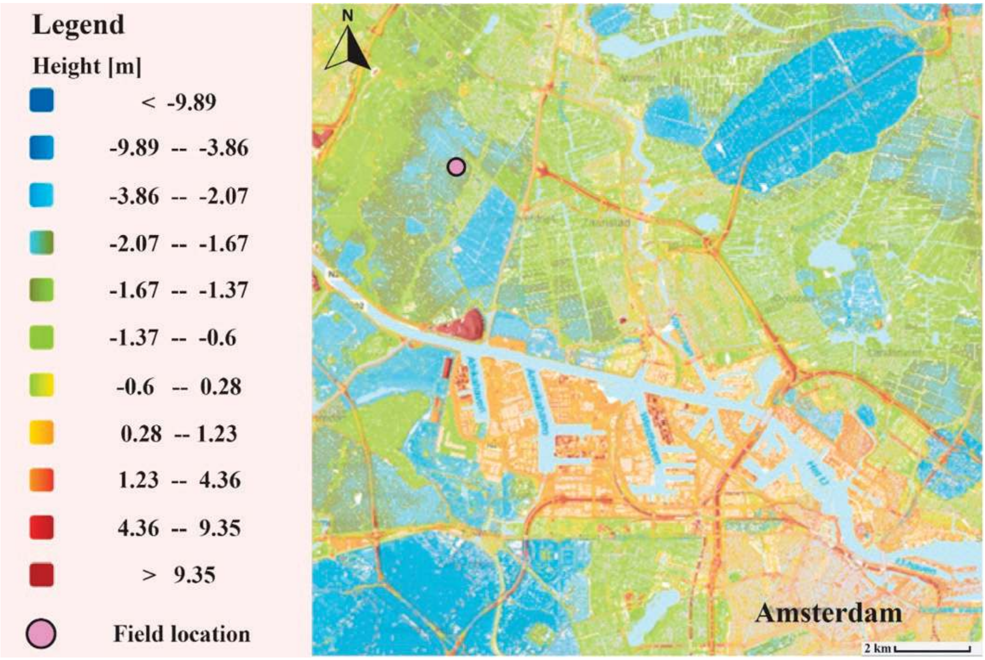

Figure A4: Topographic map of the field site in Assendelft (source: https://viewer.ahn.nl/AHN4/DTM/0/6.5465/52.26738/3). Note that the elevation of all green and blue coloured areas is below Dutch Ordanance Datum (~MSL).

Table A1: Soil profile description of the site (Date: 15/03/2024, GPS: N52°, 28.560, E4°44.401 (2 m accuracy), Relative to Dutch Ordanance Datum (~MSL): -4 m.

Depth [cm]	Colour	Texture	Notes
0-20	Grey brown	Clay -M2	Fresh roots, worm, old plant remains
20-30	Grey brown	Clay-M2	Visible roots, degraded root remains, not fibrous
30-40	Brown	Peat	Ground water, some roots, not many fibres
40-50	Brown	Peat	Sedge, reed, fibrous 20 %
50-60	Brown	Peat	Reed, sedge, fibrous 20 %
60-70	Brown	Peat	Reed, sedge, fibrous 60 %, horizontal reed
70-80	Brown	Peat	Reed, sedge, alder wood, fibrous 60 %
80-90	Brown	Peat	Sedge, reed, traces of wood, fibrous 30 %
90-100	Brown	Peat	Sedge, alder wood (2cm), reed, fibrous 30 %
100-110	Brown	Peat	Reed, alder wood (2cm), fibrous %20
110-120	Brown	Peat	Reed, fibrous 30 %
120-130	Brown	Peat	Reed, wood, fibrous 40%
130-140	Brown	Peat	Reed, fibrous 40%
140-150	Brown	Peat	Sedge, traces of reed, wood, fibrous 30 %
150-160	Brown	Peat	Sedge, traces of reed, wood (1cm), fibrous 30 %
160-170	Brown	Peat	Sedge, reed, degraded wood, fibrous 50 %
170-180	Brown	Peat	Reed, sedge, fibrous 60 %

Table A1: Soil profile description of the site (Date: 15/03/2024, GPS: N52°, 28.560, E4°44.401 (2 m accuracy), Relative to Dutch Ordanance Datum (~MSL): -4 m. (*continued*)

Depth [cm]	Colour	Texture	Notes
180-190	NO SAMPLE		
190-200	Brown	Peat	

Table A2: pH, bulk density (g/cm^3), LOI, C content (gC/gDW), porosity and void ratio values of control (C), 10kPa and 40 kPa samples from different degradation status (decomposed peat =DP, fibric peat = FP, *n*=3).

Code	PH [-]	Dry Bulk Density [g/cm3]	LOI [%]	C [gC/gDW]	Porosity [-]	Void ratio [-]
DPC	4.98 ± 0.59	0.139 ± 0.025	88.6 ± 1.63	0.472 ± 0.024	0.914 ± 0.011	10.86 ± 1.52
DP10	4.90 ± 0.10	0.195 ± 0.038	83.1 ± 3.64	0.437 ± 0.025	0.873 ± 0.002	6.99 ± 1.22
DP40	4.78 ± 0.12	0.185 ± 0.012	79.9 ± 1.65	0.445 ± 0.006	0.884 ± 0.018	7.61 ± 0.13
FPC	6.94 ± 0.06	0.088 ± 0.013	87.2 ± 0.68	0.482 ± 0.003	0.939 ± 0.014	15.52 ± 4.74
FP10	6.70 ± 0.10	0.115 ± 0.006	89.9 ± 0.80	0.481 ± 0.006	0.926 ± 0.005	12.52 ± 0.83
FP40	6.48 ± 0.22	0.165 ± 0.007	89.6 ± 1.00	0.475 ± 0.015	0.903 ± 0.003	9.31 ± 0.34

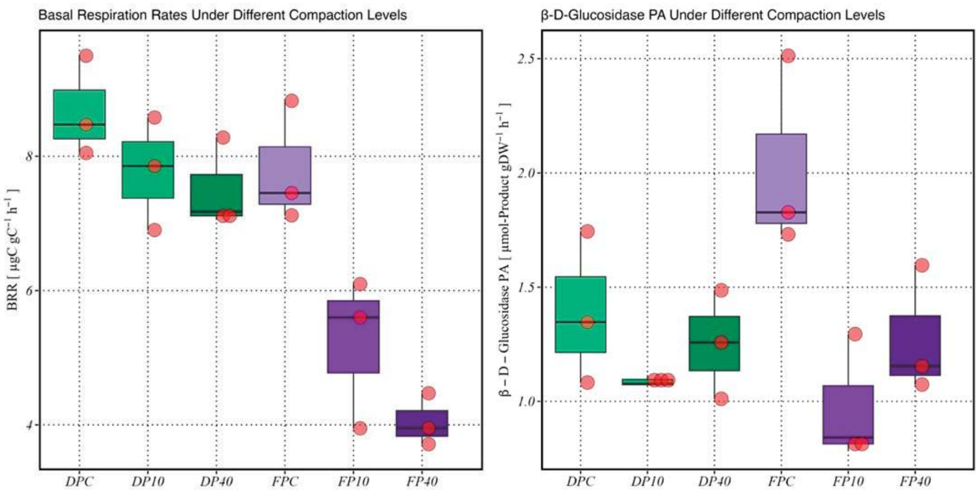

Figure A5: Absolute values of Basal Respiration Rates (BRR) and β-D-Glucosidase exoenzyme PA from control (C), 10kPa and 40 kPa samples with different degradation status (decomposed peat = DP and fibric peat = FP).

A.2 Theoretical calculation of pore size distribution

Calculation

Initial pore size distribution (PSD) of the subsurface material was determined by analysis of the soil water retention curves (SWRC) measured by the Netherlands research programme on greenhouse gas dynamics in peatlands (NOBV) at the same site for different depth intervals; 10 – 20 cm, 35 – 45 cm, 50 – 60 cm, and 85 – 95 cm. The SWRC's are measured following an adaptation of the Wind evaporation method by incorporating an automated, computer-controlled set-up for sample testing with height measurements of the sample surface (Halbertsma and Veerman, 1994; Wind, 1968). The drying SWRC resulting from this method was then converted to Van Genuchten-Mualem model parameters (van Genuchten, 1980).

The PSD was calculated based on the saturated moisture content, the drying SWRC and the theoretical suction heads needed to drain specific pore sizes. This suction head is related to a specific pore size through the effective pore diameter r of the largest water filled pore using the Young-Laplace equation from the capillary tube theory (Bear, 1972; Danielson and Sutherland, 1986; Goetz and Price, 2015):

$$r = \frac{2\gamma \cos\beta}{\rho g h} \tag{A.1}$$

where γ is the surface tension of water (N/m), β is the liquid-solid contact angle in degrees, ρ is the density of water (g/cm^3), g is the gravitational acceleration (m/s^2), and h is the suction head. Here, the surface tension of water at 15 °C of 73.50 · 10^{-3} N/m (Vargaftik et al., 1983) is taken for γ, and 0° is taken for β to represent a fully wettable soil (Valat et al., 1991; Weber et al., 2017). The effective diameter is an approximation of the actual as this method is designed for tubes, whereas the irregular shape of pores in peat will deviate from the theoretical drainage pattern based on the calculated effective diameter.

Results and Interpretation

The measured SWRC's indicated an increase in initial porosity from 0.711 at 10 – 20 cm depth to 0.926 at 85 – 95 cm depth (Fig. A6). Initial porosities from the SWRC's matched the values determined for the oedometer samples. Initial pore size determination showed a clear trend in micro- and macro-porosity relatively within this increase in initial porosity. With increasing depth, microporosity (< 10μm) decreased significantly with depth from 35.4% between 10 – 20 cm to 8.4% between 85 – 95 cm depth, especially the pore volume consisting of pores with a diameter smaller than 4μm (Fig. A6). Macroporosity (>300μm) on the other hand increased with depth significantly between the same depth intervals from 38.3% to 66.2%, while the mesopores (10 – 300μm) did not show particular large changes in contribution to the total porosity. These results correspond well to earlier findings showing a lower average pore diameter with increasing degree of decomposition in the top part of the soil (Gharedaghloo et al., 2018; McCarter and Price, 2014; Rezanezhad et al., 2010).

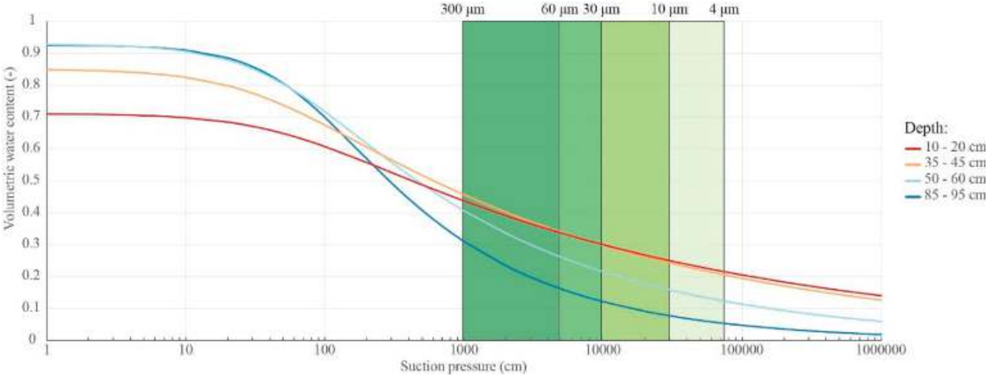

Figure A6: Soil water retention curves for the peat meadow in Assendelft at four different depths within the top meter of the subsurface. Four zones are indicated which represent pore size classes calculated based on the Young-Laplace equation. The pore size boundaries are related to suction pressure assuming full wettability and a water-solid contact angle of 0°.

It has been highlighted that decomposition is most effective in specific pore sizes (Mtambanengwe et al., 1956; Scott et al., 1996; Strong et al., 2004). Therefore, it is necessary to interpret the changes in the pore size distribution as a result of the compaction. The pore size distribution was expected to shift after compaction and porosity decrease during the oedometer test. Actual pore size measurements were not performed, which means that changes to specific pore classes followed from the division of compaction into consolidation and viscous compression. Since consolidation mainly affects macropores and viscous compression affects micropores (e.g., O'Kelly and Pichan, 2013; van Elderen et al., 2025), macroporosity was expected to decrease more significantly in FP samples than in DP samples. The opposite was true for the expected microporosity. Available literature is inconclusive concerning the specific range of diameters considered as micropores (Bruand et al., 1996; Holden, 2009; Weber et al., 2017; Zaffar and Lu, 2015). Hence, it remains unclear whether pores within the optimal pore size range for decomposition with diameters between 15 – 60 µm are compressed as a result of consolidation, viscous compression or a combination of the two. It is likely that the relative contribution of the optimal pore size for decomposition between 15 – 60 µm to porosity has increased after compaction because of the large initial proportion of >300 µm pores. These pores can be compressed partially, changing to an effective pore diameter between 15 – 60 µm, increasing the ideal pore size contribution to porosity and potentially boosting decomposition. Subsequentially, this principle is expected to be more prominent in the FP than in the DP, since the proportion of macropores in FP is larger.

Not only compaction, but also decomposition can alter the pore size distribution over time. Another documented result of decomposition besides GHGs emissions was the change of OM surfaces from hydrophilic to hydrophobic and the production of hydrophobic acids and its impact on mechanical compaction (Atanassova and Doerr, 2010; Kay and Goit, 1977; Wu et al., 2020). The DP samples, which are in a further state of decomposition and possibly more hydrophobic for that reason, show more compaction originating from viscous compression compared to the less decomposed FP samples. The hydrophobicity of a surface is represented in the contact angle β, which increases with increasing hydrophobicity. For the initial SWRC's, we assumed full wettability of the peat, taking 0° for contact angle β. However, literature stresses that the contact angle is heavily dependent on the decomposition degree and the type of plant remains (Goetz and Price, 2015; Waniek et al., 2005; Weber et al., 2017). The most extreme contact angles are seen for air-dried woody, herbaceous and sphagnum peat samples have been shown to be hydrophobic and assume contact angles >90° (Michel et al., 1999; Szajdak and Szatylowicz, 2010; Valat et al., 1991). Though such oblique contact angles are unlikely to occur in wet samples, decomposition and the resulting increased hydrophobicity of peat could lead to higher contact angles. Assuming a higher contact angle effectively means a decrease in the wettability of peat. Also, the drainage pattern will change as higher angles will result in lower suction pressures needed to drain a specific pore diameter during a drying experiment, and pore classes will shift to the left side of the SWRC (Fig. A7a-c). Hence, decomposed peats will deviate from the SWRC (Fig. A6), and contribution of pores between 15 – 60 μm diameter to total porosity will be different due to the hydrophobic character of the peat.

Adding to the importance of porosity and pore size distribution for decomposition is the key material characteristic hydraulic conductivity that is determined by porosity and pore size distribution and changed by compaction and decomposition itself. One of the limits of decomposition is the nutrient availability and is determined by hydraulic conductivity among others. Peat is known for a sharp decrease in hydraulic conductivity as the void ratio decreases with compaction (Hayashi and Hatakeyama, 2021; Mesri and Ajlouni, 2007; Tanaka et al., 2019). This occurs because tortuosity increases, which is the lengthening of the flow paths for pore water (Gharedaghloo et al., 2018; Rezanezhad et al., 2010). As hydraulic conductivity decreases, the supply of nutrients and oxygen needed for decomposition is also reduced (McCarter et al., 2020), which is similar to limitation of viscous compression rates following decreased hydraulic conductivity (van Elderen et al., 2024). Therefore, compaction has a two-sided limiting effect on decomposition by reducing both pore space and hydraulic conductivity. Decomposition also has a negative effect on hydraulic conductivity: gas bubbles produced during decomposition can hinder flow as they are entrapped in the pore structure. Furthermore, other byproducts of decomposition and bacterial colonies themselves can clog pores and reduces flow (O'Kelly and Pichan, 2013).

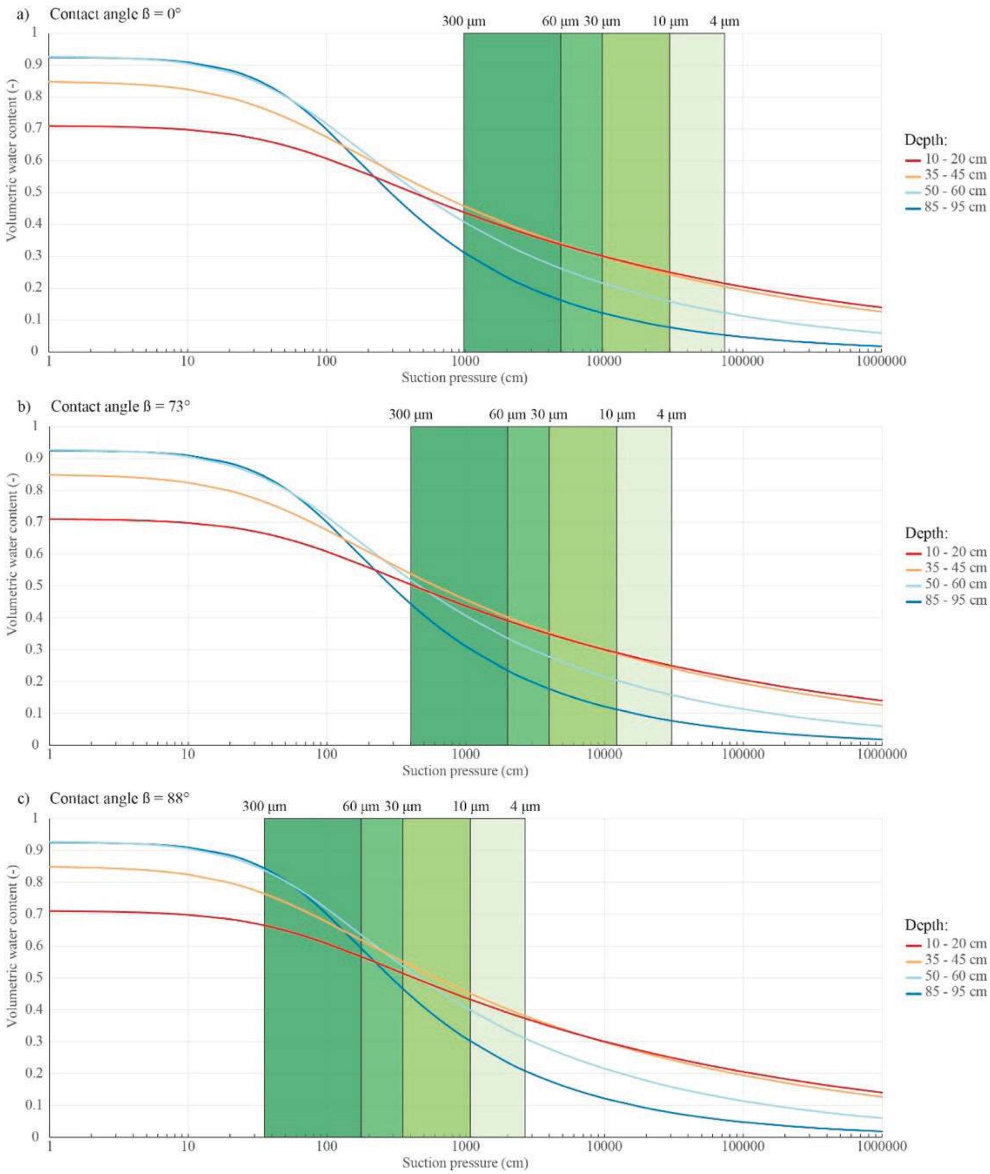

Figure A7: Soil water retention curves of Assendelft peat samples calculated following the van Genuchten - Mualem parameters after drying measurements using the adjusted Wind method. Samples from four different depths were dried and measured. Zones indicating different pore size classes are shown in shades of green. The graphs show changing suction needed to drain pores as result of increasing wetting contact angle β due to decomposition of organic matter: a) β = 0°, b) β = 73°, c) β = 88°.

Assuming the same SWRC as shown in Fig. A6, a shift in hydrophobicity and hence in contact angle will cause a decrease in macropores at all depth intervals and an increase in all other pore size classes (Fig. A8). Most prominent of these is the increase in the smallest class, <4 μm. Largest changes are seen in the case of the 85 – 95 cm depth interval, for which <4 μm pores quadruple and macropores drop from 66.2% to 8.5% when changing the contact angle from 0° to 88°. Consequentially, a larger part of the porosity is classified as, or behaves as, micropores, and viscous compression of pores should become the main process of compaction as water in these pores will not be expelled, following conventional capillary theory under the more hydrophobic conditions. This principle confirms the trend seen in our data.

Further investigation into pore size distribution after compaction and decomposition could provide valuable insights into how microbial communities respond to changing pore architectures, as well as the feedback mechanisms between consolidation, viscous compression, and decomposition. Future studies should also focus on pore-scale changes to better understand how physical changes influence decomposition and vice versa in drained peatlands.

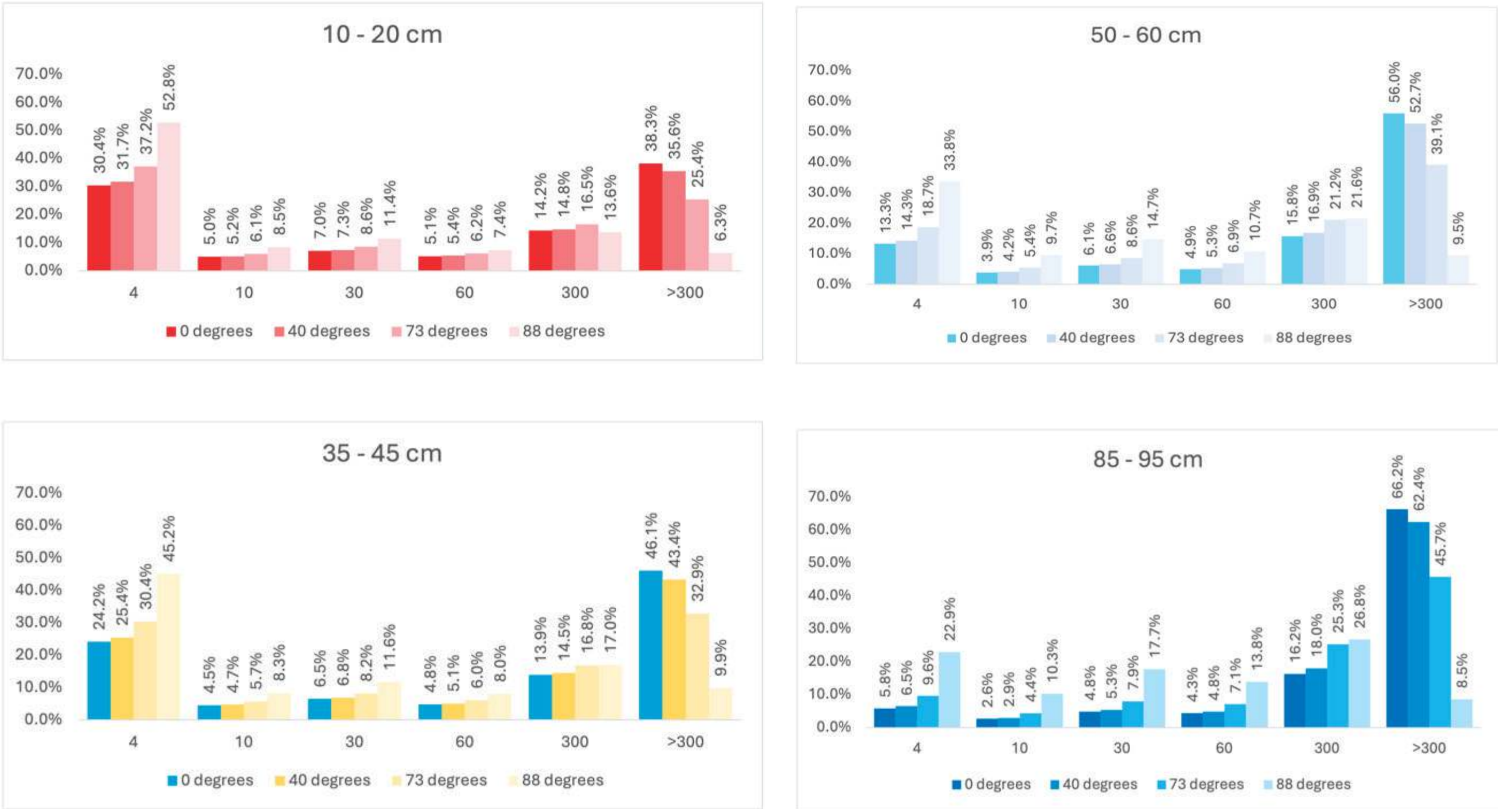

Figure A8: Contribution of pore size classes to total porosity with changing contact angle γ. Four different depths are shown: 10 – 20 cm, 35 – 45 cm, 50 – 60 cm and 85 – 95 cm.

Supplement B:

B.1 Principal Component Analysis (PCA)

This analysis was performed using the 'prcomp' function from the 'stats' package in R, which standardizes the data before performing the decomposition (Venables and Ripley, 2002; R Core Team, 2024). Its base requirement is a numeric or complex matrix with the values called 'x'. This data frame was scaled and centered by subtracting the mean and dividing by the standard deviation of each variable, ensuring all features contributed equally to the analysis. In the function this is handled by assigning 'scale' and 'center' to TRUE. The covariance matrix of the scaled data was then calculated to examine the relationships between the variables. This is different from the Pearson's correlation coefficient which is also used separately in this research. PCA was performed through the eigen decomposition of this covariance matrix, where the eigenvectors correspond to the directions of the principal components and the eigenvalues represent their respective contributions to the overall variance.

The data was projected onto the first two principal components (see Fig. 4.5). With three components chosen based on the cumulative variance criterion, it was ensured that at least 95% of the total variance was retained (Table B1). To interpret the PCA results, scatter plots of the first few principal components were used to visually explore potential clusters in the transformed data space. A scree plot was also generated to evaluate the proportion of variance explained by each component, while a biplot provided insight into how the original variables contributed to the first two principal components (see Fig. 4.5). The principal component values which are used for the clustering can be calculated using the eigenvectors shown in Table B2, combined with the scaled and normalized values of the material characteristics.

Table B1: Importance of the principal components, including their standard deviation.

	PC1	PC2	PC3	PC4	PC5
Standard Deviation	2.0628	0.7058	0.4638	0.1596	0.0780
Proportion of Variance	0.851	0.0996	0.0430	0.0051	0.0012
Cumulative Proportion	0.851	0.9507	0.9937	0.9988	1.0000

Table B2: Eigenvalues of the material characteristics per principal component.

	PC1	PC2	PC3	PC4	PC5
Water Content	0.45362	-0.38972	0.42183	0.62854	-0.26334
Wet Bulk Density	-0.46509	-0.28225	0.40884	0.18347	0.70938
Dry Bulk Density	-0.46366	-0.23135	0.49495	-0.38475	-0.58179
Particle Density	-0.42726	-0.51899	-0.63258	0.32478	-0.20605
Void Ratio	0.42472	-0.66752	-0.09887	-0.56370	0.21564

B.2 Organic fraction calculations

For the calculation of organic fraction the particle density was needed, but values listed in the dataset were deemed to show ranges exceeding common end-member particle densities for peat and clay. This might be the consequence of measuring partially unsaturated samples, a result of sample storage, while assuming full saturation in the measurement and following calculations. The particle density of the samples ρ_s was recalculated using:

$$\rho_s = \frac{\rho_d}{1 - \frac{WC}{WC + 100}} \tag{B.1}$$

With ρ_d being the dry bulk density and WC being the water content. Initial water content and dry bulk density values were present in the dataset for all samples. Only for the oedometer test data the water content and dry bulk density after the end of the test were also available. Both the initial and final values result in a mostly linear pattern for the calculated particle density as a function of the dry bulk density, apart from samples with very low final dry bulk densities (Fig. B1). Particle densities calculated with the final dry bulk densities are consistently higher than their initial counterparts (Fig. B2). As samples are kept in saturated conditions during a test, the final particle density values are used for determination of the organic fraction.

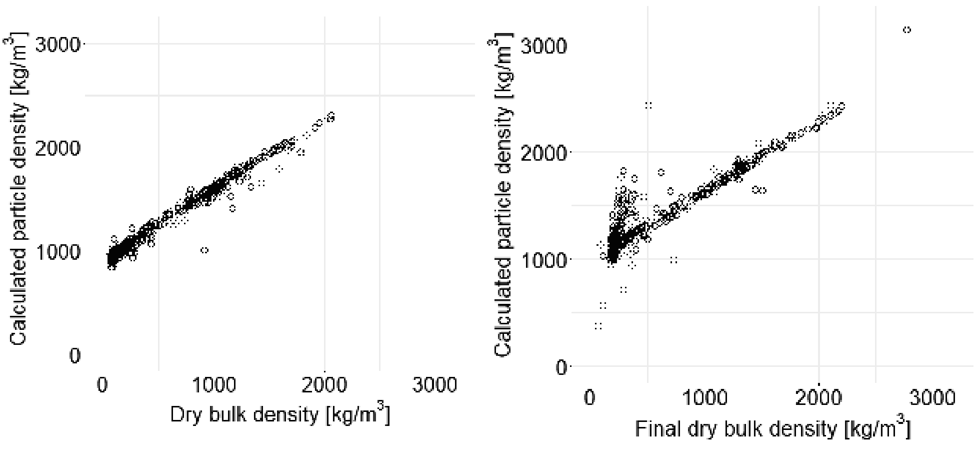

Figure B1: a) Calculated particle density as a function of the initial dry sample density reported for the entire dataset. b) Calculated particle density as a function of the final dry sample density reported for the oedometer test samples.

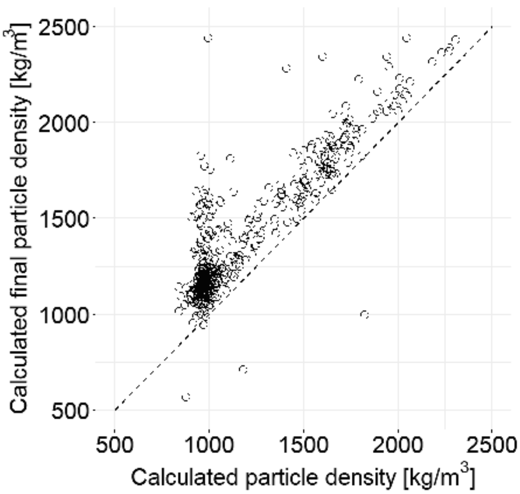

Figure B2: Calculated initial particle density against calculated final particle density.

B.3 Clustering methods

K-Means Clustering

K-Means is a widely used partition-based clustering algorithm that groups data points into a predefined number of clusters, K, based on the shortest distance between the data point in question and the nearest cluster mean. The algorithm begins by randomly initializing K centroids and iteratively refines them by assigning each data point to the nearest centroid. The centroids are then updated by computing the mean of all data points in each cluster, also called the mean of the Voronoi sets. This process continues until the centroids no longer change significantly.

This method is applied by the 'kmeans' function in Rstudio and can be found in the stats package (R Core Team, 2024). It requires several input variables, of which the following have been used: a numeric data matrix 'x', a provided number of clusters or set of initial cluster centres called 'centers', the maximum number of iterations 'iter.max', and the amount of random initializations for the centres of clusters 'nstart', which is used when 'centers' is a number instead of a position matrix. The used data matrix is specified in the methods, as well as the number of clusters. The maximum amount of iterations was left to the default setting of 10, while the amount of initializations was set to 25. By default the algorithm of Hartigan and Wong is used (Hartigan and Wong, 1979), though other algorithms can be chosen.

One of the main advantages of using K-Means to cluster data points is the relative simplicity and straightforward way it works compared to other methods, which also leads to computational efficiency, especially for large datasets. However, the requirement to specify 'centers' in advance and its sensitivity to the initial placement of centroids can be seen as downsides of the method. Because of the sensitivity to initial placement, a significant number of random starts is chosen to account for this potential problem. Additionally, K-Means assumes that clusters are spherical and of similar size, which may not apply to all datasets. The combination of these two limitations may result in unreliable clustering of the data in comparison to other methods (Fig. B3).

Gaussian Mixture Model (GMM)

Gaussian Mixture Modelling (GMM) is a probabilistic clustering method that assumes data points are generated from a mixture of Gaussian distributions. Unlike K-Means, which assigns each data point to a single cluster, GMM provides so-called soft assignments, meaning each data point has a probability of belonging to multiple clusters. Furthermore, GMM is more flexible than K-Means as it can model elliptical clusters with different sizes and orientations. GMM uses the Expectation-Maximization (EM) algorithm to iteratively to reach convergence of the parameters of the Gaussian components, maximizing the likelihood of the observed data (Dempster et al., 1977; Moon, 1996). The convergence limit also implies that there is no maximum number of iterations used as user-defined number.

In Rstudio the 'mclust' function, found in the package with the same name, is used to compute the GMM clusters (Scrucca et al., 2023). The following input variables have been used for this research, though more input variables can be inserted: a numeric vector, matrix or data frame of observations called 'data', an integer or integer vector specifying the amount of desired output clusters 'G', and 'initialization' defining the starting positions of the cluster centres. The output classifications of K-Means for a given number of clusters serves as the starting positions for the GMM method. The combination of the two methods can lead to improved clustering compared to output of the individual use of the methods (Fig. B3).

DBSCAN (Density-Based Spatial Clustering of Applications with Noise)

DBSCAN is a density-based clustering algorithm that groups data points based on their density in a given region (Ester et al., 1996). Unlike K-Means and GMM, DBSCAN does not require a desired number of clusters beforehand. Instead, it relies on two parameters: ε (the maximum distance between data points in a cluster) and minPts (the minimum number of data points required to form a dense region). Data points are classified as core data points when within a radius ε the specified minimum number of data points is located. Border data points are located within radius ε of a core data point, but do not have enough data points within their own radius. Noise is defined as the data points outside of the radius ε of any core data point. Next, clusters are created of a network of core and border data points with inter-distance of radius ε or smaller. Core data points of clusters are therefore separated by at least radius ε.

The 'dbscan' function in Rstudio is part of the 'dbscan' package (Hahsler et al., 2019). It uses three main input variables: data matrix 'x', radius ε called 'eps', and the minimum amount of data points required 'minPts'. The last two are user-defined. For 'minPts' it is suggested to start with a value of the number of dimensions in the dataset plus one (d + 1). Next, 'eps' can be found by using the function 'kNNdistplot' from the same package, which shows the distance to the closest neighbour. The elbow point indicating a sharp increase in distance is usually seen as the boundary with noise data points and the distance is taken for 'eps'.

The key advantage of DBSCAN is its ability to detect clusters of arbitrary shapes and filter out noise in comparison to for example K-Means (Fig. B4). However, DBSCAN struggles with varying density clusters and can be sensitive to the choice of ε and the minimum amount of data points.

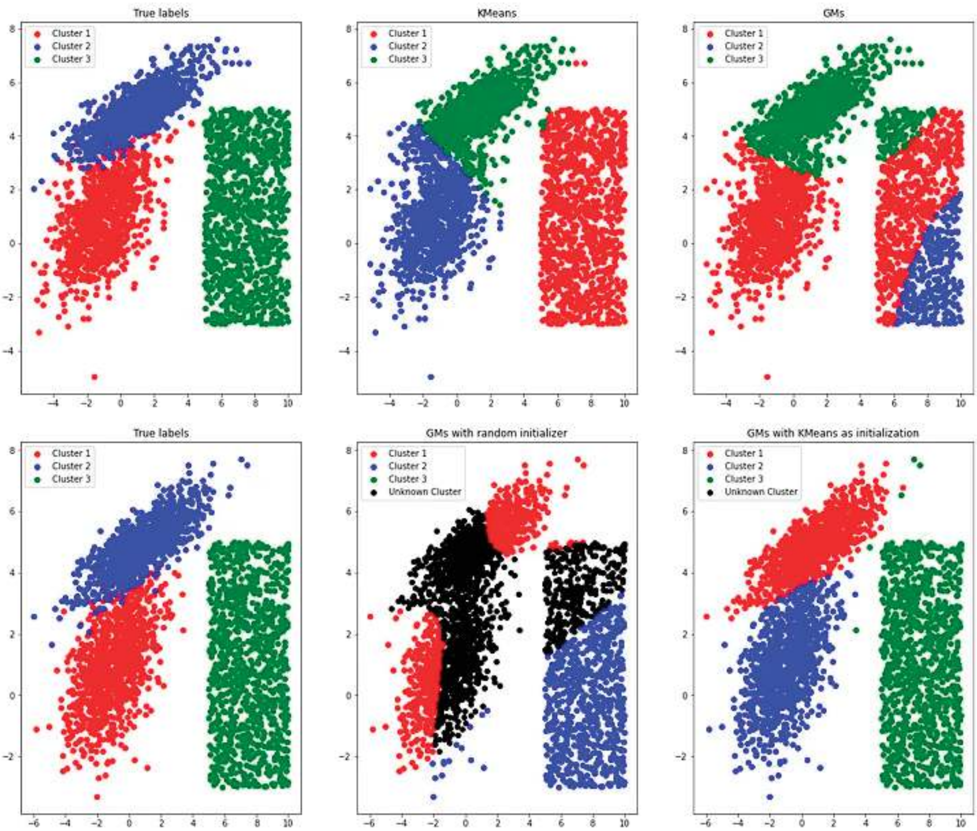

Figure B3: Differences between K-means and Gaussian Mixture Modelling clustering methods and a combination of the two when applied to a random dataset (Kubara, 2020). R-code showing the workflow and origin of the data is provided in Kubara (2020).

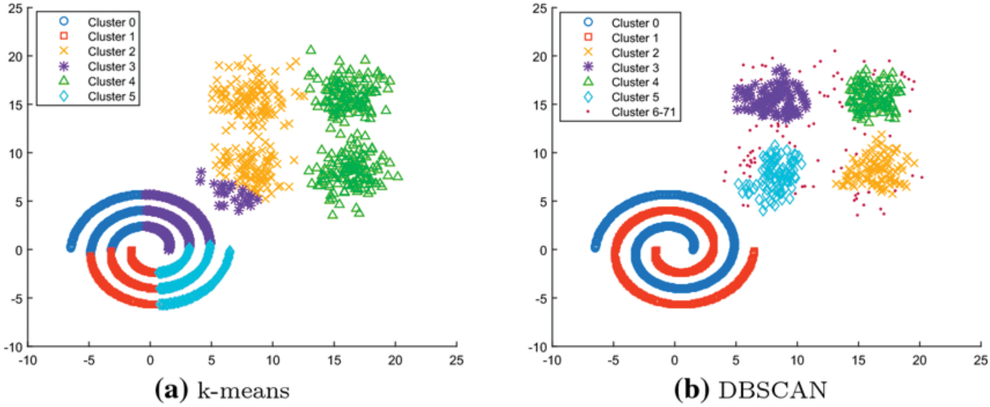

Figure B4: Example of the difference between K-Means and DBSCAN clustering results for the Spiralsquare data set (Liang et al., 2021). Note that the smaller red dots are considered outliers.

B.4 Cluster evaluation techniques

Silhouette score

The Silhouette Score is a metric used to evaluate the quality of clustering or the optimal number of clusters by measuring how similar each data point is to its own cluster compared to other clusters. For a given data point, the silhouette score s is defined as:

$$s = \frac{b - a}{max(a,b)} \tag{B.2}$$

where a is the average distance to all data points within its cluster and b is the average distance from all data points in the closest neighboring cluster. The overall Silhouette Score for a clustering solution is obtained by averaging the individual $s$values of all data points; this mean value is used to compare the quality of different cluster configurations. The silhouette score ranges from -1 to 1, where values close to 1 indicate well-separated clusters, values near 0 suggest overlapping clusters, and negative values indicate misclassified data points. The Silhouette Score may not work well for clusters of varying densities and shapes.

Using the format function 'silhouette' from the 'cluster' package in Rstudio it is possible to calculate the Silhouette Score (Rousseeuw, 1987; Maechler et al., 2023). This function requires two input variables: a vector in which the cluster codes are stored called 'x', and a distance matrix 'dist' following from the command 'dist' found in the 'stats' package applied to the used dataset (R Core Team, 2024). The cluster output of the GMM was taken as input for the 'x' and 'dist' followed from the method described above.

The Silhouette Score for our dataset was calculated for GMM results implementing two to ten clusters. The progression of the score can be seen in Fig. B5. It shows that the best separation of cluster is achieved when three clusters are used. Furthermore, using four clusters would be better than using more clusters or using 2 clusters.

Bayesian Information Criterion (BIC) Score

The Bayesian Information Criterion (BIC) is a model selection criterion used to compare different clustering outputs of K-Means and GMM. It balances model complexity and goodness of fit, penalizing excessive parameters to avoid overfitting. The BIC score is computed as:

$$BIC = k \log n - 2 \log L \tag{B.3}$$

where k is the number of parameters in the model, n is the number of data points, and L is the likelihood of the data given the model (Wit et al., 2012). A lower BIC score indicates a better model, making it useful for selecting the optimal number of clusters. While effective, BIC assumes that data follow an underlying probabilistic distribution, which may not always be the case. Additionally, BIC tends to favor simpler models, sometimes underestimating the true number of clusters (Wit et al., 2012).

The BIC score is automatically calculated by the 'mclust' function described in the GMM paragraph. It can be accessed as one of the output list elements. Fig. B6 shows the BIC Score (a) and the BIC Slope (b) per number of clusters. The BIC score decreases over the entirety of the evaluated number of clusters, apart from the situation with 10 clusters. This means that using nine clusters would be the best option. However, as the aim is to keep the clustering simple, it is also possible to look at the BIC slope (Fig. B6.b) to examine the effect of adding an additional cluster. This method shows that increasing the number of clusters from two to three adds the most value. Further increasing the number of clusters is beneficial up to five clusters, after which the added value of each additional cluster is <100.

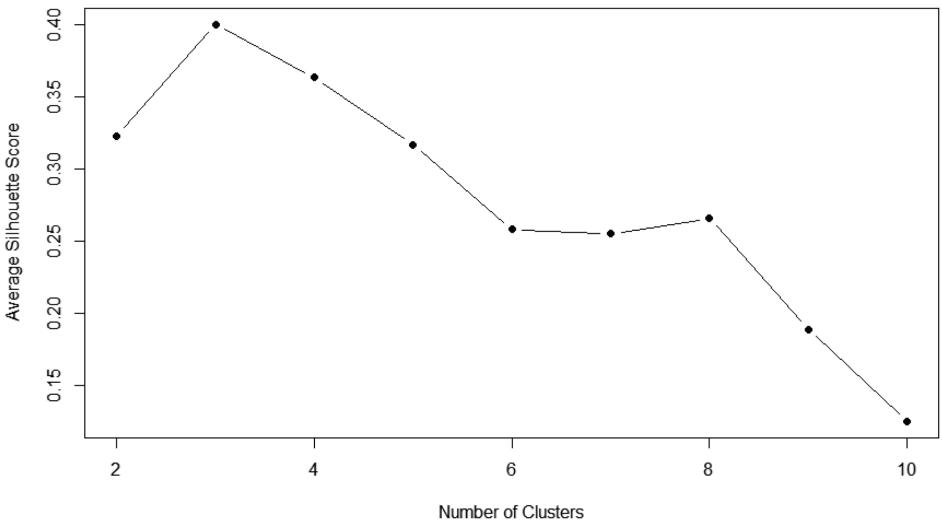

Figure B5: Average Silhouette Score for Gaussian Mixture Model cluster per number of clusters.

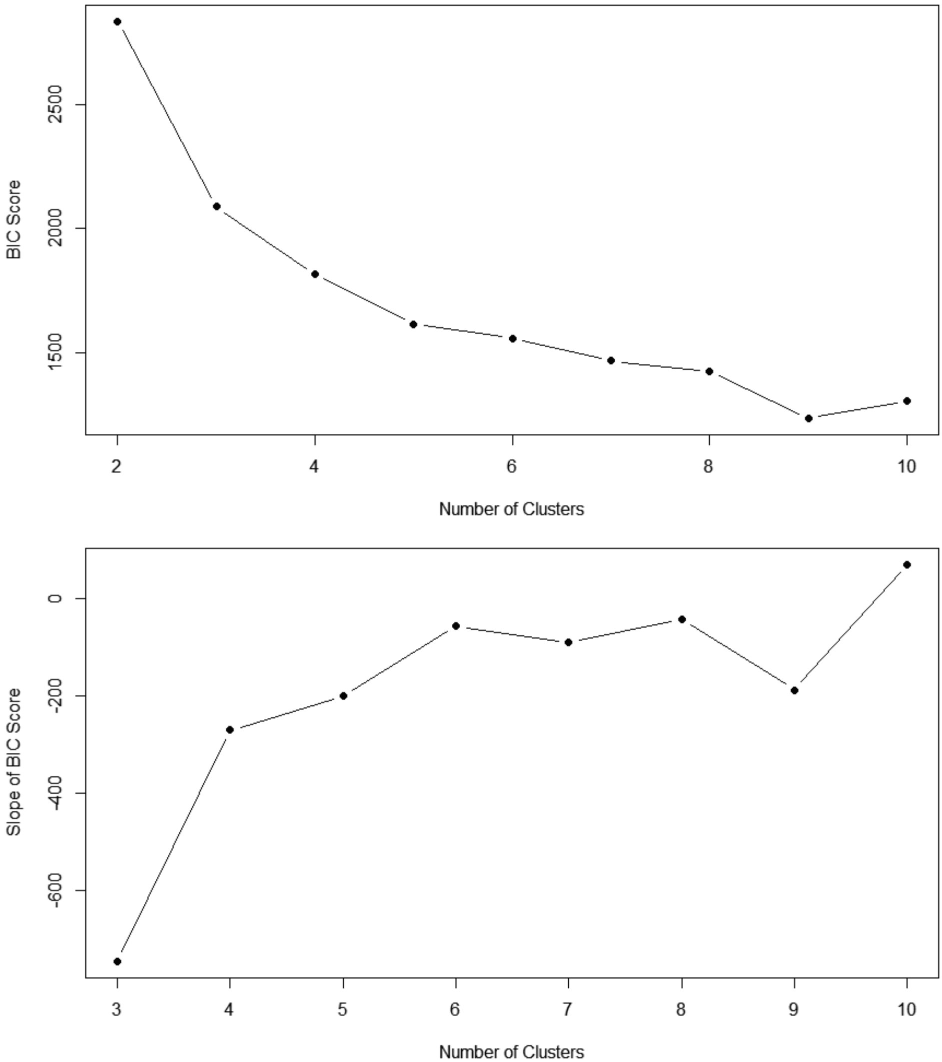

Figure B6: (a) BIC Score per number of clusters and (b) BIC Score Slope per number of clusters

Jensen-Shannon Divergence

Jensen-Shannon Divergence (JSD) is a measure of similarity between probability distributions and is used to assess clustering quality by comparing the distributions of different clusters. It is based on Kullback-Leibler (KL) divergence but is symmetric and always finite, making it more stable. The JSD between two distributions P and Q is given by:

$$JSD\ (P\ ||\ Q)\ =\ \frac{1}{2}\ D_{KL}\ (P\ ||\ M)\ +\ \frac{1}{2}\ D_{KL}\ (Q\ ||\ M) \tag{B.4}$$

where $M = \frac{1}{2}(P+Q)$ and D_{KL} is the KL divergence (Endres and Schindelin, 2003). Given that $P(x)$ and $Q(x)$ span the same domain, the KL divergence from Q to P is defined as (Kullback and Leibler, 1951):

$$D_{KL}(P \,||\, Q) = \sum_x P(x) \log \frac{P(x)}{Q(x)} \tag{B.5}$$

A lower JSD value indicates that the clusters are more distinct. JSD is useful in applications where data is represented as probability distributions, which is why it has been chosen to assess the quality of the GMM results. The JS Divergence scores per number of clusters can be seen in Fig. B7. Scores are relatively low up to seven clusters, indicating distinct clusters. A relatively small increase in the JSD score can be seen from four to five clusters, which shows a small preference for four clusters or less.

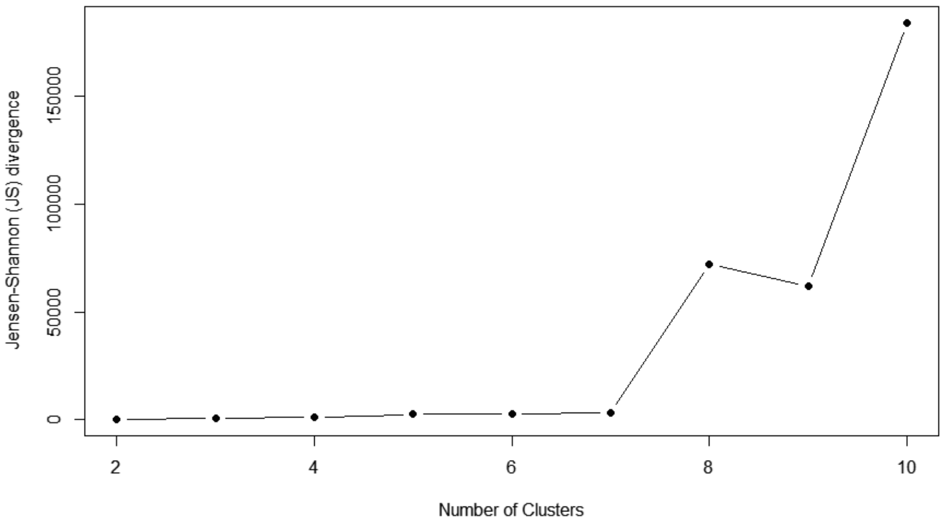

Figure B7: Average Jensen-Shannon Divergence Score, calculated using the Kullback-Leibler Divergence, for the entire dataset per number of clusters.

B.5 Cluster robustness

Insight in the robustness of individual clusters can be achieved when reviewing the clustering results with three and five clusters. When three clusters are used, the Clay and Peat clusters are largely retained, while the Clayey peat and Decomposed peat clusters are merged, indicating that these clusters have most similar material characteristics algorithmically. When five clusters are used, all clusters are retained in their current extent, except for the Clayey peat cluster, which is separated at approximately 1100 kg/m^3 for the wet bulk density and 240% for the water content. This review of clusters points out that Clayey peat cluster is most variable, but its overall material characteristics are more similar to peat than clay. The fact that data points belonging to Clayey peat shift with a varying number of clusters is reasonable, given that these data points are at the tipping point between end-members clay and peat. The fact that Clayey peat merges with Decomposed peat when three clusters are used, highlights that its material characteristics mostly resemble end-member peat and thus that organic matter is controlling characteristics even at relatively low contents.

B.6 Virgin and viscous compression ratios per lithology

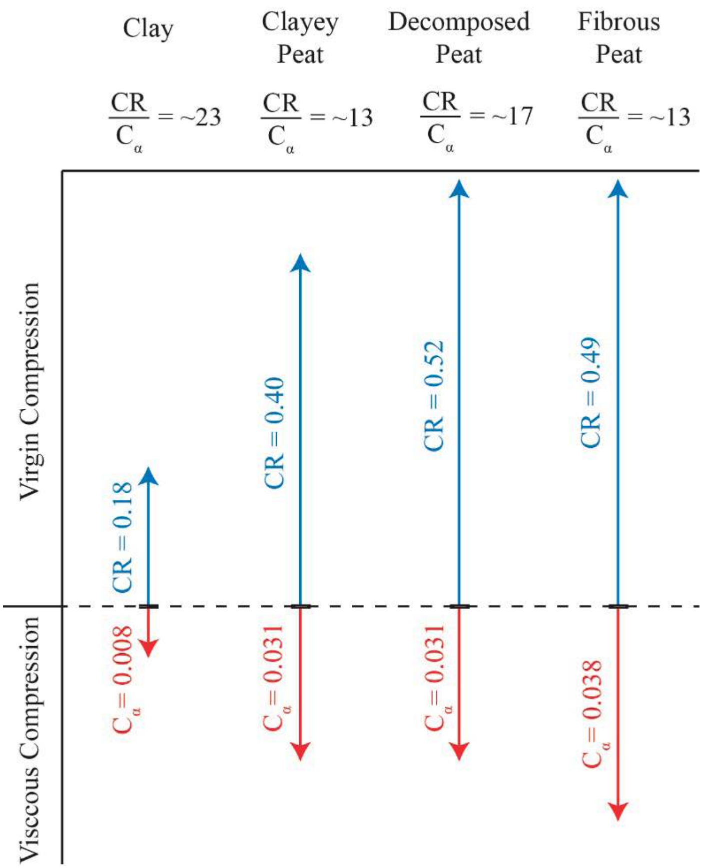

Figure B8: Ratios between mean virgin compression parameter CR and viscous compression parameter C_α values per lithological class. The blue arrow indicates virgin compression following a log-unit increase in pressure, while the red arrow indicates viscous compression after a log-unit of time. The total distance covered by the blue and red arrows is schematic representation of the total compaction. The arrows are not to scale.

Supplement C:

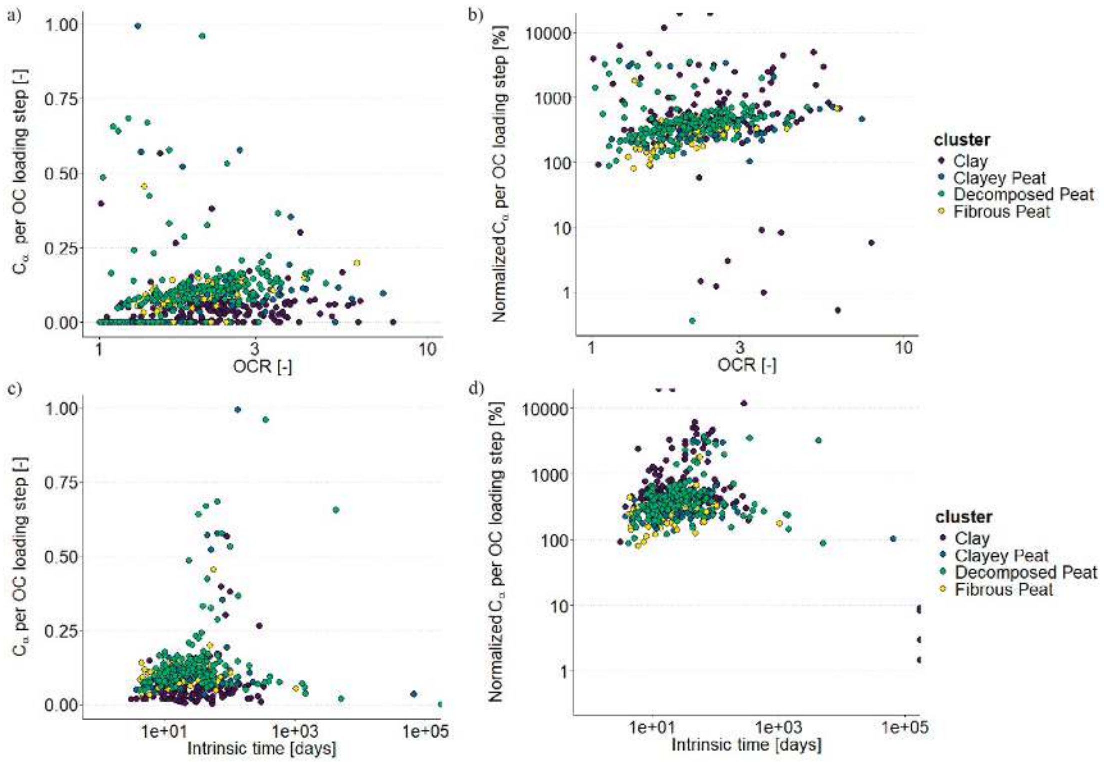

Figure C1: C_α values for samples under overconsolidated (OC) conditions (OCR >1) derived per loading step using the linear regression method per oedometer loading step and clustered by lithological class: (a) plotted against the OCR, (b) plotted normalized as percentage of the reference C_α value of the same oedometer test against the OCR, (c) plotted against the calculated intrinsic time, (d) plotted normalized as percentage of the reference C_α value of the same oedometer test against the calculated intrinsic time.

References

Aben, R. C. H., van de Craats, D., Boonman, J., Peeters, S. H., Vriend, B., Boonman, C. C. F., van der Velde, Y., Erkens, G., & van den Berg, M. (2024). Using automated transparent chambers to quantify CO_2 emissions and potential emission reduction by water infiltration systems in drained coastal peatlands in the Netherlands. https://doi.org/10.5194/egusphere-2024-403

Aho, M. (1986). The ion exchange and adsorption properties of Sphagnum peat under acid conditions (No. 24.).

Al-Khafaji, A. W. N., & Andersland, O. B. (1981). Compressibility and strength of decomposing fibre–clay soils. Geotechnique, 31(4), 497-508.

Allen, J. R. L. (2000). Holocene coastal lowlands in NW Europe: autocompaction and the uncertain ground. Geological Society, London, Special Publications, 175(1), 239-252.

Amaryan, L.S. (1993). Soft soils properties and testing methods. Rotterdam: Balkema, 180p.

Arets, E. J. M. M., van Baren, S. A., Hendriks, C. M. J., Kramer, H., Lesschen, J. P., & Schelhaas, M. J. (2023). Greenhouse gas reporting of the LULUCF sector in the Netherlands: Methodological background.

Asay, D. B., & Kim, S. H. (2005). Evolution of the adsorbed water layer structure on silicon oxide at room temperature. The Journal of Physical Chemistry B, 109(35), 16760-16763.

ASTM D4186/D4186-06 (2006) Standard test method for onedimensional consolidation properties of saturated cohesive soils using controlled-strain loading, ASTM International, West Conshohocken, PA, USA

Atanassova, I., & Doerr, S. (2010). Organic compounds of different extractability in total solvent extracts from soils of contrasting water repellency. European Journal of Soil Science, 61(2), 298–313. https://doi.org/10.1111/j.1365-2389.2009.01224.x

Augustesen, A., Liingaard, M., & Lade, P. V. (2004). Evaluation of time-dependent behavior of soils. International Journal of Geomechanics, 4(3), 137-156.

Baillie, C., & Jayasinghe, R. (Eds.). (2004). Green composites: polymer composites and the environment. Elsevier.

Bakr, M. (2015). Influence of groundwater management on land subsidence in deltas: A case study of Jakarta (Indonesia). Water Resources Management, 29(5), 1541-1555.

Barberon, M., & Geldner, N. (2014). Radial Transport of Nutrients: The Plant Root as a Polarized Epithelium. Plant physiology. 166. 10.1104/pp.114.246124.

Bear, J. (1972). Dynamics of Fluids in Porous Media. Soil Science, 120(2), 162–163. https://doi.org/10.1097/00010694-197508000-00022

Beaudet, L. V., & Charpentier, S. (1998). Mechanical behaviour of silty clay loam/peat mixtures: cyclic compression-release tests and effects of initial water content. Agronomie, 18(4), 261-274.

Beckwith, C. W., & Baird, A. J. (2001). Effect of biogenic gas bubbles on water flow through poorly decomposed blanket peat. *Water Resources Research*, *37*(3), 551-558.

Bell, M. C., Ritson, J. P., Verhoef, A., Brazier, R. E., Templeton, M. R., Graham, N. J. D., Freeman, C., & Clark, J. M. (2018). Sensitivity of peatland litter decomposition to changes in temperature and rainfall. Geoderma, 331, 29–37.

Bellabarba, A., Giagnoni, L., Adessi, A., Marra, E., Laschi, A., Neri, F., & Mastrolonardo, G. (2024). Short-term machinery impact on microbial activity and diversity in a compacted forest soil. Applied Soil Ecology, 203. https://doi.org/10.1016/j.apsoil.2024.105646

Benito Rueda, E., Rodríguez-Alleres, M., & Varela Teijeiro, E. (2016). Environmental factors governing soil water repellency dynamics in a Pinus pinaster plantation in NW Spain. Land Degradation & Development, 27(3), 719-728.

Berendsen, H. J., & Stouthamer, E. (2000). Late Weichselian and Holocene palaeogeography of the Rhine–Meuse delta, the Netherlands. Palaeogeography, Palaeoclimatology, Palaeoecology, 161(3-4), 311-335.

Berendsen, H.J.A., Stouthamer, E. (2001). Palaeogeographic development of the Rhine-Meuse delta, The Netherlands. Assen, Van Gorcum, 270 p.

Bergaya, F., Lagaly, G., & Vayer, M. (2006). Cation and anion exchange. Developments in clay science, 1, 979-1001.

Berry, P. L., & Poskitt, T. J. (1972). The consolidation of peat. Géotechnique, 22(1), 27–52. https://doi.org/10.1680/geot.1972.22.1.27

Berry, P.L. (1983). Application of consolidation theory for peat to design of a reclamation scheme by preloading. Quarterly Journal of Engineering Geology, 16(9): 103–112.

Beven, K., & Germann, P. (1982). Macropores and water flow in soils. Water resources research, 18(5), 1311-1325.

Beylich, A., Oberholzer, H. R., Schrader, S., Höper, H., & Wilke, B. M. (2010). Evaluation of soil compaction effects on soil biota and soil biological processes in soils. Soil and Tillage Research, 109(2), 133–143. https://doi.org/10.1016/j.still.2010.05.010

Biot, M. A. (1941). General theory of three-dimensional consolidation. Journal of Applied Physics, 12(2), 155–164. https://doi.org/10.1063/1.1712886

Bjerrum, L. (1967). Engineering geology of Norwegian normally-consolidated marine clays as related to settlements of buildings. Geotechnique, 17(2), 83-118.

Boelter, D. H. (1968, August). Important physical properties of peat materials.

Boonman, J. (2024). Vaporizing temperate peatlands [Doctoral dissertation, Vrije Universiteit Amsterdam]. https://doi.org/10.5463/thesis.811

Bosch, J. H. A. (2005). Archeologische Standaard Boorbeschrijvingsmethode. Op basis van de Standaard Boor Beschrijvingsmethode versie, 5.

Brigatti, M. F., Galan, E., & Theng, B. K. G. (2013). Structures and mineralogy of clay minerals. Developments in clay science, 1, 19-86.

Brouns, K., Keuskamp, J. A., Potkamp, G., Verhoeven, J. T. A., & Hefting, M. M. (2016). Peat origin and land use effects on microbial activity, respiration dynamics and exo-enzyme activities in drained peat soils in the Netherlands. Soil Biology and Biochemistry, 95, 144–155. https://doi.org/10.1016/j.soilbio.2015.11.018

Brouns, K., Verhoeven, J. T., & Hefting, M. M. (2014). Short period of oxygenation releases latch on peat decomposition. Science of the Total Environment, 481, 61-68.

Bruand, A., Cousin, I., Nicoullaud, B., Duval, O., & Bégon, J. C. (1996). Backscattered electron scanning images of soil porosity for analyzing soil compaction around roots. Soil Science Society of America Journal, 60(3), 895–901. https://doi.org/10.2136/sssaj1996.03615995006000030031x

Buisman, A.S.K. (1940). Grondmechanica. Delft, The Netherlands: Waltman.

Bunt, A. C. (1988). Microelements. Media and Mixes for Container-Grown Plants: A manual on the preparation and use of growing media for pot plants, 151-173.

Carlesso, L., Beadle, A., Cook, S. M., Evans, J., Hartwell, G., Ritz, K., Sparkes, D., Wu, L., & Murray, P. J. (2019). Soil compaction effects on litter decomposition in an arable field: Implications for management of crop residues and headlands. Applied Soil Ecology, 134, 31–37. https://doi.org/10.1016/j.apsoil.2018.10.004

Celik, F., & Canakci, H. (2014). An investigation of the effect of sand content on geotechnical properties of fibrous peat. Arabian Journal for Science and Engineering, 39, 6943-6948.

Chai, J. C., Jia, R., & Hino, T. (2012). Anisotropic consolidation behavior of Ariake clay from three different CRS tests. ASTM International.

Chamindu, D. T. K. K., Clough, T. J., Thomas, S. M., Balaine, N., & Elberling, B. (2019). Density effects on soil-water characteristics, soil-gas diffusivity, and emissions of N_2O and N_2 from a

References

re-packed pasture soil. Soil Science Society of America Journal, 83(1), 118–125. https://doi.org/10.2136/sssaj2018.01.0048

Cohen, K. M., Gouw, M. J., & Holten, J. P. (2005). Fluvio-deltaic floodbasin deposits recording differential subsidence within a coastal prism (central Rhine–Meuse delta, The Netherlands). *Fluvial sedimentology VII*, 295-320.

Conroy, P., Lumban-Gaol, Y., Van Diepen, S., Van Leijen, F., & Hanssen, R. F. (2024, July). First Wide-Area Dutch Peatland Subsidence Estimates Based on InSAR. In *IGARSS 2024-2024 IEEE International Geoscience and Remote Sensing Symposium* (pp. 10732-10735). IEEE.

Cornelis, W. M., Corluy, J., Medina, H., Díaz, J., Hartmann, R., van Meirvenne, M., & Ruiz, M. E. (2006). Measuring and modelling the soil shrinkage characteristic curve. Geoderma, 137(1–2), 179–191. https://doi.org/10.1016/j.geoderma.2006.08.022

Danielson, R., & Sutherland, P. (1986). Porosity. In A. Klute (Ed.), Water retention: laboratory methods (pp. 443–463). SSSA Book Series.

Davies-Vollum, K. S., & Smith, N. D. (2008). Factors affecting the accumulation of organic-rich deposits in a modern avulsive floodplain: examples from the Cumberland Marshes, Saskatchewan, Canada. Journal of Sedimentary Research, 78(10), 683-692.

de Bakker, H., & Schelling, J. (1966). Systeem van bodemclassificatie voor Nederland. De hogere niveaus. Grondboor & Hamer, 20(5), 229-229.Deltares. (2018). D-settlement embankment design and soil settlement prediction: User manual. Deltares.

de Blas, E., Rodríguez-Alleres, M., & Almendros, G. (2010). Speciation of lipid and humic fractions in soils under pine and eucalyptus forest in northwest Spain and its effect on water repellency. Geoderma, 155(3-4), 242-248.

de Bruijn, H.T .J., Visschedijk, M. A. T., van den Ham, G. A. (2014) Dijk op Veen II: eindrapport heterogeniteit, Deltares rapportnummer 1208254-019- GEO-0001.

de Gryze, S., Jassogne, L., Six, J., Bossuyt, H., Wevers, M., & Merckx, R. (2006). Pore structure changes during decomposition of fresh residue: X-ray tomography analyses. Geoderma, 134(1–2), 82–96. https://doi.org/10.1016/j.geoderma.2005.09.002

Degago, S. A., Grimstad, G., Jostad, H. P., Nordal, S., & Olsson, M. (2011). Use and misuse of the isotache concept with respect to creep hypotheses A and B. Géotechnique, 61(10), 897-908.

Delicato, D. (1996). Physical-chemical properties and sorption characteristics of peat (Doctoral dissertation, Dublin City University).

Deltares (2014). D-Settlement: Embankment design and soil settlement prediction. User Manual Version 14.1.34525. Delft, The Netherlands: Deltares.

Deltares (2024). Evaluation linear isotach model; laboratory study and literature review. https://publications.deltares.nl/11206019_010_0005.pdf

Delville, A. (1993). Structure and properties of confined liquids: a molecular model of the clay-water interface. The Journal of Physical Chemistry, 97(38), 9703-9712.

Dempster, A.P., Laird, N.M., Rubin, D.B. (1977). "Maximum Likelihood from Incomplete Data via the EM Algorithm". Journal of the Royal Statistical Society, Series B. 39 (1): 1–38. CiteSeerX 10.1.1.163.7580. doi:10.1111/j.2517-6161.1977.tb01600.x. JSTOR 2984875.

Den Haan, E. J. (1994). Stress-independent parameters for primary and secondary compression. In International conference on soil mechanics and foundation engineering (pp. 65-70).

Den Haan, E. J. (1994). Vertical compression of soils [Doctoral dissertation, Technical University of Delft].

Den Haan, E. J. (1996), A compression model for non-brittle soft clays and peat, Géotechn. 1996 46:1, 1-16, doi: 10.1680/geot.1996.46.1.1

Den Haan, E. J. (2003). Het a, b, c-isotachenmodel: Hoeksteen van een nieuwe aanpak van zettingsberekeningen. Geotechniek, oktober, 28-35.

Den Haan, E. J., & Edil, T. B. (1994). Secondary and tertiary compression of peat. In International Workshop on Advances in Understanding and Modelling the mechanical behaviour of Peat (pp. 49-60).

Den Haan, E. J., & Kruse, G. A. M. (2007). Characterisation and engineering properties of Dutch peats. Characterisation and engineering properties of natural soils, 3, 2101-2133.

Den Haan, E. J., & Feddema, A. (2013). Deformation and strength of embankments on soft Dutch soil. Proceedings of the Institution of Civil Engineers-Geotechnical Engineering, 166(3), 239-252.

Deurer, M., Müller, K., Kim, I., Huh, K. Y., Young, I., Jun, G. I., & Clothier, B. E. (2012). Can minor compaction increase soil carbon sequestration? A case study in a soil under a wheel-track in an orchard. Geoderma, 183–184, 74–79. https://doi.org/10.1016/j.geoderma.2012.02.013

Dhowian, A. W., & Edil, T. B. (1980). Consolidation behavior of peats. Geotechnical Testing Journal, 3(3), 105–114. https://doi.org/10.1520/GTJ10881J

Dick, R. P., Myrold, D. D., & Kerle, E. A. (1988). Microbial biomass and soil enzyme activities in compacted and rehabilitated skid trail soils. Soil Science Society of America Journal, 52, 512–516.

Dinar, A., Esteban, E., Calvo, E., Herrera, G., Teatini, P., Tomás, R., Li, Y., Ezquerro, P., & Albiac, J. (2021). We lose ground: Global assessment of land subsidence impact extent. Science of the Total Environment, 786, 147415. https://doi.org/10.1016/j.scitotenv.2021.147415

Doerr, S. H., Shakesby, R. A., & Walsh, R. (2000). Soil water repellency: its causes, characteristics and hydro-geomorphological significance. Earth-Science Reviews, 51(1-4), 33-65.

Dolinar, B., & Macuh, B. (2016). Determining the thickness of adsorbed water layers on the external surfaces of clay minerals based on the engineering properties of soils. Applied Clay Science, 123, 279-284.

Drexler, J. Z., de Fontaine, C. S., & Deverel, S. J. (2009). The legacy of wetland drainage on the remaining peat in the Sacramento—San Joaquin Delta, California, USA. Wetlands, 29(1), 372-386.

Du, Y., Guo, S., Wang, R., Song, X., & Ju, X. (2023). Soil pore structure mediates the effects of soil oxygen on the dynamics of greenhouse gases during wetting–drying phases. Science of the Total Environment, 895, 165192. https://doi.org/10.1016/j.scitotenv.2023.165192

Dudoignon, P., Causseque, S., Bernard, M., Hallaire, V., & Pons, Y. (2007). Vertical porosity profile of a clay-rich marsh soil. Catena, 70(3), 480-492.

Dunn, C., Jones, T. G., Girard, A., & Freeman, C. (2014). Methodologies for extracellular enzyme assays from wetland soils. Wetlands, 34(1), 9–17. https://doi.org/10.1007/s13157-013-0475-0

Edil, T. B., & Den Haan, E. J. (1994). Settlement of peats and organic soils. In Vertical and Horizontal Deformations of Foundations and Embankments (pp. 1543-1572). ASCE.

Edil, T. B., & Dhowian, A. W. (1979). Analysis of long-term compression of peats. Geotechnical Engineering, 10(2), 159-178.

Edil, T. B., & Wang, X. (2000). Shear strength and K o of peats and organic soils. In Geotechnics of high water content materials. ASTM International.

Endres, D.M.; Schindelin J.E. (2003). "A new metric for probability distributions" (PDF). IEEE Trans. Inf. Theory. 49 (7): 1858–1860. doi:10.1109/TIT.2003.813506. hdl:10023/1591. S2CID 14437777

Erkens, G., de Vries S., Zwanenburg C., van der Kolk B.J., de Bruijn H.T.J. (2013) Dijken op Veen II, veenbeschrijvingsprotocol, Deltares rapportnr. 1208254-013-GEO-002.

Erkens, G. (2009). Sediment dynamics in the Rhine catchment: quantification of fluvial response to climate change and human impact.

Erkens, G., Bucx, T., Dam, R., de Lange, G., & Lambert, J. (2015). Sinking coastal cities. Proceedings of the International Association of Hydrological Sciences, 372(372), 189-198.

Erkens, G., & Stouthamer, E. (2020). The 6M approach to land subsidence. *Proceedings of the International Association of Hydrological Sciences*, *382*, 733-740.

Erkens, G., van Asselen, S., Hommes-Slag, S., Melman, R., Kooi, H., van Essen, H., van den Berg, M., Aben, R., Fritz, C., Boonman, C., Velthuis, M., Heuts, T., Hessel, R., van de Craats, D., Massop, H., Gerritsen, P., van, J., Velthof, G., van den Akker, J., … Smolders, F. (2021). Nationaal Onderzoeksprogramma Broeikasgassen Veenweiden (NOBV) – Data-analyse 2020–2021.

Erkens, G., van der Meulen, M. J., & Middelkoop, H. (2016). Double trouble: Subsidence and CO_2 respiration due to 1,000 years of Dutch coastal peatlands cultivation. Hydrogeology Journal, 24(3), 551–568. https://doi.org/10.1007/s10040-016-1380-4

Ester, M., Kriegel, H., Sander, J., Xiaowei, X. (1996). A Density-Based Algorithm for Discovering Clusters in Large Spatial Databases with Noise. Institute for Computer Science, University of Munich. Proceedings of 2nd International Conference on Knowledge Discovery and Data Mining (KDD-96), 226-231. https://dl.acm.org/doi/10.5555/3001460.3001507

EZK, BZK, LNV, & IenW. (2019). Climate Agreement. Ministerie van Economische Zaken en Klimaat. https://www.klimaatakkoord.nl/binaries/klimaatakkoord/documenten/publicaties/2019/06/28/national-climate-agreement-thenetherlands/20190628+National+Climate+Agreement+The+Netherlands.pdf

Farrell, E. R. (2012) Chapter 32: Organics/peat soils. Manual of Geotechnical Engineering. Proceedings of the Institution of Civil Engineers. Pp. 463–479.

Feng, R., Peng, B., Wu, L., Cai, X., & Shen, Y. (2021). Three-stage consolidation characteristics of highly organic peaty soil. Engineering Geology, 294, 106349. https://doi.org/10.1016/j.enggeo.2021.106349

Filimonova, S. V., Knicker, H., & Kögel-Knabner, I. (2006). Soil micro-and mesopores studied by N2 adsorption and 129Xe NMR of adsorbed xenon. Geoderma, 130(3-4), 218-228.

Fokker, P. A., & Orlic, B. (2006). Semi-analytic modelling of subsidence. Mathematical Geology, 38(5), 565-589.

Fokker, P. A., Gunnink, J. L., Koster, K., & de Lange, G. (2019). Disentangling and parameterizing shallow sources of subsidence: application to a reclaimed coastal area, Flevoland, the Netherlands. Journal of Geophysical Research: Earth Surface, 124(5), 1099-1117.

Fokker, P. A., van Leijen, F. J., Orlic, B., van der Marel, H., & Hanssen, R. F. (2018). Subsidence in the Dutch Wadden Sea. Geologie en Mijnbouw / Netherlands Journal of Geosciences, 97(3), 129–181. https://doi.org/10.1017/njg.2018.9

Fox, P. J., & Edil, T. B. (1996). Effects of stress and temperature on secondary compression of peat. Canadian Geotechnical Journal, 33(3), 405-415.

Fox-Kemper, B., H.T. Hewitt, C. Xiao, G. Aðalgeirsdóttir, S.S. Drijfhout, T.L. Edwards, N.R. Golledge, M. Hemer, R.E. Kopp, G. Krinner, A. Mix, D. Notz, S. Nowicki, I.S. Nurhati, L. Ruiz, J.-B. Sallée, A.B.A. Slangen, and Y. Yu, 2021: Ocean, Cryosphere and Sea Level Change. In Climate Change 2021: The Physical Science Basis. Contribution of Working Group I to the Sixth Assessment Report of the Intergovernmental Panel on Climate Change [Masson-Delmotte, V., P. Zhai, A. Pirani, S.L. Connors, C. Péan, S. Berger, N. Caud, Y. Chen, L. Goldfarb, M.I. Gomis, M. Huang, K. Leitzell, E. Lonnoy, J.B.R. Matthews, T.K. Maycock, T. Waterfield, O. Yelekçi, R. Yu, and B. Zhou (eds.)]. Cambridge University Press, Cambridge, United Kingdom and New York, NY, USA, pp. 1211–1362, doi: 10.1017/9781009157896.011.

Frene, J. P., Pandey, B. K., & Castrillo, G. (2024). Under pressure: Elucidating soil compaction and its effect on soil functions. Plant and Soil. https://doi.org/10.1007/s11104-024-06573-2

Fukue, M., Minato, T., Horibe, H., & Taya, N. (1999). The micro-structures of clay given by resistivity measurements. Engineering geology, 54(1-2), 43-53.

Galloway, D. L., Erkens, G., Kuniansky, E. L., & Rowland, J. C. (2016). Preface: Land subsidence processes. Hydrogeology Journal, 24(3), 547–550. https://doi.org/10.1007/s10040-016-1386-y

Galloway, D. L., Jones, D. R., & Ingebritsen, S. E. (Eds.). (1999). Land subsidence in the United States (Vol. 1182). Geological Survey (USGS).

Gangwar, P., Singh, R., Trivedi, M., & Tiwari, R. K. (2020). Sodic soil: Management and reclamation strategies. Environmental Concerns and Sustainable Development: Volume 2: Biodiversity, Soil and Waste Management, 175-190.

Gebert, J., Zander, F. (2024). Aerobic and anaerobic mineralisation of sediment organic matter in the tidal River Elbe. J Soils Sediments 24, 2874–2886, https://doi.org/10.1007/s11368-024-03799-6

Geertsma, J. (1973). Land subsidence above compacting oil and gas reservoirs. Journal of petroleum technology, 25(06), 734-744.

Gharedaghloo, B., Price, J. S., Rezanezhad, F., & Quinton, W. L. (2018). Evaluating the hydraulic and transport properties of peat soil using pore network modeling and X-ray micro computed tomography. Journal of Hydrology, 561, 494–508.

Goetz, J. D., & Price, J. S. (2015). Role of morphological structure and layering of Sphagnum and Tomenthypnum mosses on moss productivity and evaporation rates. Canadian Journal of Soil Science, 95(2), 109–124. https://doi.org/10.4141/cjss-2014-092

Gonçalvès, J., Rousseau-Gueutin, P., de Marsily, G., Cosenza, P., & Violette, S. (2010). What is the significance of pore pressure in a saturated shale layer?. Water Resources Research, 46(4).

Gong, L., Nie, L., Xu, Y., Ji, X., & Liu, B. (2022). Characterization of micro-scale pore structure and permeability simulation of peat soil based on 2D/3D X-ray computed tomography images. Eurasian Soil Science, 55(6), 790–801. https://doi.org/10.1134/S1064229322060060

Gorham, E. (1957). The development of peat lands. The Quarterly Review of Biology, 32(2), 145-166.

Gouw, M. J. P., & Erkens, G. (2007). Architecture of the Holocene Rhine-Meuse delta (the Netherlands)-a result of changing external controls. Netherlands Journal of Geosciences, 86(1), 23-54.

Griggs, D. (1939). Creep of rocks. The Journal of Geology, 47(3), 225-251.

Gunaratne, M., Stinnette, P., Mullins, A. G., Kuo, C. L., & Echelberger, W. F. (1998). Compressibility relations for peat and organic soil. Journal of Testing and Evaluation, 26(1), 9 pages. https://doi.org/10.1520/JTE11963J

Güven, N. (1992). Molecular aspects of clay-water interactions.

Hahsler, M., Piekenbrock, M., Doran, D. (2019). "dbscan: Fast Density-Based Clustering with R." _Journal of Statistical Software_, *91*(1), 1-30. doi:10.18637/jss.v091.i01 <https://doi.org/10.18637/jss.v091.i01>.

Halbertsma, J. M., & Veerman, G. J. (1994). A new calculation procedure and simple set-up for the evaporation method to determine soil hydraulic functions.

Hanson, J. L., Edil, T. B., & Fox, P. J. (2001). Stress-temperature effects on peat compression. In Soft Ground Technology (pp. 331-345).

Harpenslager, S. F., van Dijk, G., Boonman, J., Weideveld, S. T. J., van de Riet, B. P., Hefting, M. M., & Smolders, A. J. P. (2024). Rewetting drained peatlands through subsoil infiltration stabilises redox-dependent soil carbon and nutrient dynamics. Geoderma, 442, 116787. https://doi.org/10.1016/j.geoderma.2024.116787

Hartigan, J.A. and Wong, M. A. (1979). Algorithm AS 136: A K-means clustering algorithm. Applied Statistics, 28, 100–108. doi:10.2307/2346830.

Hayashi, H., & Hatakeyama, O. (2021). Measuring the Hydraulic Conductivity of Peats and Organic Clays with Various Characteristics. Geotechnical and Geological Engineering, 39(1), 517–531. https://doi.org/10.1007/s10706-020-01510-3

Haygreen, J. G., & Bowyer, J. L. (1982). Forest products and wood science: an introduction (pp. 495-pp).

Helmy, A. K. (1998). The limited swelling of montmorillonite. Journal of colloid and interface science, 207(1), 128-129.

Henry, W. (1803). Experiments on the quantity of gases absorbed by water at different temperatures, and under different pressures. https://doi.org/10.1098/rstl.1803.0004

Hight, D. W., & Leroueil, S. (2003). Characterisation of soils for engineering purposes. *Characterisation and engineering properties of natural soils*, *1*, 255-360.

Hobbs, N. B. (1986). Mire morphology and the properties and behaviour of some British and foreign peats. Quarterly Journal of Engineering Geology, 19(1): 7–80.

Hobbs, N. B. (1987). A note on the classification of peat. Geotechnique, 37, 405–407.

Hoekstra, P., & Doyle, W. T. (1971). Dielectric relaxation of surface adsorbed water. Journal of Colloid and Interface Science, 36(4), 513-521.

Holden, J. (2009). Flow through macropores of different size classes in blanket peat. Journal of Hydrology, 364(3–4), 342–348. https://doi.org/10.1016/j.jhydrol.2008.11.010

Horgan, G. W., & Ball, B. C. (2005). Modelling the effect of water distribution and hysteresis on air-filled pore space. European Journal of Soil Science, 56(5), 647–654. https://doi.org/10.1111/j.1365-2389.2005.00714.x

Huat, B. B. K., Kazemian, S., Prasad, A., & Barghchi, M. (1988). State of the art review of peat: General perspective. International Journal of the Physical Sciences, 6(8). https://doi.org/10.5897/IJPS11.192

Huat, B. B. K. , Asadi, A., & Kazemian, S. (2009). Experimental investigation on geomechanical properties of tropical organic soils and peat. American Journal of Engineering and Applied Sciences, 2(1), 184-188.

Huat, B. B., Kazemian, S., Prasad, A., & Barghchi, M. (2011). State of an art review of peat: General perspective. *International Journal of the Physical Sciences*, *6*(8), 1988-1996.

ISO 17892-5 (2017) Geotechnical investigation and testing-Laboratory testing of soil-Part 5: Incremental loading oedometer test. European Committee for Standardization

Ivakhnova, G. Y., & Nevzorov, A. L. (2020, October). The acceleration of the peat secondary consolidation due to the sorption of bound water with disperse clay. In IOP Conference Series: Materials Science and Engineering (Vol. 945, No. 1, p. 012051). IOP Publishing.

Jayakody, K. P. K., Shimaoka, T., Komiya, T., & Ehler, P. (2014). Laboratory determination of water retention characteristics and pore size distribution in simulated MSW landfill under settlement. International Journal of Environmental Research, 8(3), 619–628. https://doi.org/10.22059/ijer.2014.696

Jayarathne, J. R. R. N., Chamindu Deepagoda, T. K. K., Clough, T. J., Thomas, S., Elberling, B., & Smits, K. M. (2021). Effect of aggregate size distribution on soil moisture, soil-gas diffusivity, and N_2O emissions from a pasture soil. Geoderma, 383, 114737. https://doi.org/10.1016/j.geoderma.2020.114737

Jiménez-Morillo, N. T., Spangenberg, J. E., Miller, A. Z., Jordán, A., Zavala, L. M., González-Vila, F. J., & González-Pérez, J. A. (2017). Wildfire effects on lipid composition and hydrophobicity of bulk soil and soil size fractions under Quercus suber cover (SW-Spain). Environmental research, 159, 394-405.

Johnston, C. T. (2018). Clay mineral–water interactions. Developments in clay science, 9, 89-124.

Jones, C. E., An, K., Blom, R. G., Kent, J. D., Ivins, E. R., & Bekaert, D. (2016). Anthropogenic and geologic influences on subsidence in the vicinity of New Orleans, Louisiana. Journal of Geophysical Research: Solid Earth, 121(5), 3867-3887.

Kay, B. D., & Goit, J. B. (1977). Thermodynamic characterization of water adsorbed on peat. Canadian Journal of Soil Science, 57(4), 497–501. https://doi.org/10.4141/cjss77-055

Keller, J. K., Weisenhorn, P. B., & Megonigal, J. P. (2009). Humic acids as electron acceptors in wetland decomposition. Soil Biology and Biochemistry, 41(7), 1518-1522.

Kellner, E., Waddington, J. M., & Price, J. S. (2004). Pressure variation in peat as a result of gas bubble dynamics. Hydrological Processes, 18(13): 2599–2605.

Kellner, E., Waddington, J. M., & Price, J. S. (2005). Dynamics of biogenic gas bubbles in peat: potential effects on water storage and peat deformation. Water Resources Research, 41(8), W08417, doi:10.1029/2004WR003732.

Keogh, M. E., Törnqvist, T. E., Kolker, A. S., Erkens, G., & Bridgeman, J. G. (2021). Organic matter accretion, shallow subsidence, and river delta sustainability. Journal of Geophysical Research: Earth Surface, 126(12), e2021JF006231.

Kiuru, P., Palviainen, M., Grönholm, T., Raivonen, M., Kohl, L., Gauci, V., Urzainki, I., & Laurén, A. (2022a). Peat macropore networks—New insights into episodic and hotspot methane emission. Biogeosciences, 19(7), 1959–1977. https://doi.org/10.5194/bg-19-1959-2022

Kiuru, P., Palviainen, M., Marchionne, A., Grönholm, T., Raivonen, M., Kohl, L., & Laurén, A. (2022b). Pore network modeling as a new tool for determining gas diffusivity in peat. Biogeosciences, 19(21), 5041–5058. https://doi.org/10.5194/bg-19-5041-2022

Kleimeier, C., Rezanezhad, F., van Cappellen, P., & Lennartz, B. (2017). Influence of pore structure on solute transport in degraded and undegraded fen peat soils. Mires and Peat, 19. https://doi.org/10.19189/MaP.2017.OMB.282

Klingenfuß, C., Roßkopf, N., Walter, J., Heller, C., & Zeitz, J. (2014). Soil organic matter to soil organic carbon ratios of peatland soil substrates. Geoderma, 235–236, 410–417. https://doi.org/10.1016/j.geoderma.2014.07.010

Kooi, H., & Erkens, G. (2020). Creep consolidation in land subsidence modelling; integrating geotechnical and hydrological approaches in a new MODFLOW package (SUB-CR). Proceedings of the International Association of Hydrological Sciences, 382, 499-503.

Kooi, H., Bakr, M., de Lange, G., Den Haan, E., & Erkens, G. (2018). User guide to SUB-CR: A MODFLOW package for land subsidence and aquifer system compaction that includes creep (Deltares internal report 11202275-008).

Kooi, H., Melman, R. R. (2024): Gebruik van InSAR voor parametrisatie van het isotachenmodel in bodemdalingsberekeningen : Onderdeel van Regio Deal Bodemdaling Groen Hart, project 42. Accessed on 10-12-2025 at: https://www.deltares.nl/expertise/publicaties/gebruik-van-insar-voor-parametrisatie-van-het-isotachenmodel-in-bodemdalingsberekeningen-onderdeel-van-regio-deal-bodemdaling-groen-hart-project-42

Koster, K. (2017). 3D characterization of Holocene peat in the Netherlands: Implications for coastal-deltaic subsidence.

Koster, K., Cohen, K. M., Stafleu, J., & Stouthamer, E. (2018a). Using 14C-dated peat beds for reconstructing subsidence by compression in the Holland coastal plain of the Netherlands. Journal of Coastal Research, 34(5), 1035-1045.

Koster, K., Stafleu, J., & Stouthamer, E. (2018b). Differential subsidence in the urbanised coastal-deltaic plain of the Netherlands. Netherlands Journal of Geosciences, 97(4), 215-227.

Koster, K., Stafleu, J., Cohen, K. M., Stouthamer, E., Busschers, F. S., & Middelkoop, H. (2018c). Three-dimensional distribution of organic matter in coastal-deltaic peat: Implications for subsidence and carbon dioxide emissions by human-induced peat oxidation. Anthropocene, 22, 1–9. https://doi.org/10.1016/j.ancene.2018.03.001

Kravchenko, A. N., & Guber, A. K. (2017). Soil pores and their contributions to soil carbon processes. Geoderma, 287, 31–39. https://doi.org/10.1016/j.geoderma.2016.06.027

Kravchenko, A. N., Guber, A., Gunina, A., Dippold, M., & Kuzyakov, Y. (2021). Pore-scale view of microbial turnover: Combining ^{14}C imaging, μCT and zymography after adding soluble carbon to soil pores of specific sizes. European Journal of Soil Science, 72(2), 593–607. https://doi.org/10.1111/ejss.13001

Kubara, K. (2020). Gaussian Mixture Models vs K-Means. Which One to Choose? Comparing the Performance of Two Popular Clustering Algorithms. Written 08-10-2020, available at https://medium.com/data-science/gaussian-mixture-models-vs-k-means-which-one-to-choose-62f2736025f0

Kullback, S. ,Leibler, R.A. (1951).”On information and sufficiency”. Annals of Mathematical Statistics.22(1):79–86. doi:10.1214/aoms/1177729694. JSTOR 2236703. MR 0039968

Kuncoro, P. H., Koga, K., Satta, N., & Muto, Y. (2014). A study on the effect of compaction on transport properties of soil gas and water I: Relative gas diffusivity, air permeability, and saturated hydraulic conductivity. Soil and Tillage Research, 143, 172–179. https://doi.org/10.1016/j.still.2014.02.006

Kurihara, N., Isoda, T., Ohta, H., & Sekiguchi, H. (1994). Settlement performance of the central Hokkaido expressway built on peat. In Advances in understanding and modelling the mechanical behaviour of peat: Proceedings of the internation workshop, 16-18 June, 1993, Delft, Netherlands.

Lagaly, G., & Dékány, I. (2013). Colloid clay science. In Developments in clay science (Vol. 5, pp. 243-345). Elsevier.

Laiho, R. (2006). Decomposition in peatlands: Reconciling seemingly contrasting results on the impacts of lowered water levels. Soil Biology and Biochemistry, 38(8), 2011–2024. https://doi.org/10.1016/j.soilbio.2006.02.017

Landva, A. O. (2007, November). Characterization of Escuminac peat and construction on peatland. In Proc. Of the 2nd Int. Workshop on Characterisation and Engineering Properties of Natural Soils, Singapore.

Landva, A. O., and La Rochelle, P. (1983). Compressibility and shear characteristics of Radforth peats. Testing of Peats and Organic Soils, ASTM STP 820, P.M. Jarrett, Ed., American Society of Testing and Materials, pp. 157–191.

Landva, A. O., and Pheeney, P. E. (1980). Peat fabric and structure. Canadian Geotechnical Journal, 17(3): 416–435.

Langmuir, I. (1938). Repulsive forces between charged surfaces in water, and the cause of the Jones-Ray effect. Science, 88(2288), 430-432.

Lanson, B., Beaufort, D., Berger, G., Bauer, A., Cassagnabere, A., & Meunier, A. (2002). Authigenic kaolin and illitic minerals during burial diagenesis of sandstones: a review. Clay minerals, 37(1), 1-22.

Le, T. M., Fatahi, B., & Khabbaz, H. (2012). Viscous behaviour of soft clay and inducing factors. Geotechnical and Geological Engineering, 30(5), 1069–1083. https://doi.org/10.1007/s10706-012-9535-0

Leifeld, J., Müller, M., & Fuhrer, J. (2011). Peatland subsidence and carbon loss from drained temperate fens. Soil Use and Management, 27(2), 170–176. https://doi.org/10.1111/j.1475-2743.2011.00327.x

Levesque, M., & Dinel, H. (1977). Fiber content, particle-size distribution and some related properties of four peat materials in eastern Canada. Canadian Journal of Soil Science, 57(2), 187-195.

Lexmond, B. R., van Dam, B., Hockin, C. V., Erkens, G., Griffioen, J., & Stouthamer, E. (2024). Measuring shrinkage of expansive soils using a novel automated high-frequency setup. *Soil Science Society of America Journal*, *88*(6), 2343-2352.

Li, Y., Yao, J., & Yang, Y. (2014). The effect of the absorbed fluid layer on flow in a capillary tube. Petroleum science and technology, 32(2), 194-201.

Li, Z., Kravchenko, A.N., Cupples, A., A.H., Gubey, Y., Kuzyakov, G.P., Robertson & E., Blagodatskaya (2024). Composition and metabolism of microbial communities in soil pores. Nat Commun 15, 3578. https://doi.org/10.1038/s41467-024-47755-x

Liang, J., Cui, J., Wang, J., Wei, W. (2021). Graph-based semi-supervised learning via improving the quality of the graph dynamically. Machine Learning. 110. 1-44. 10.1007/s10994-021-05975-y.

Lourenco, M., Fitchett, J. M., & Woodborne, S. (2023). Peat definitions: A critical review. Progress in Physical Geography: Earth and Environment, 47(4), 506-520.

Low, P. F. (1960). Influence of adsorbed water on exchangeable ion movement. Clays and Clay Minerals, 9, 219-228.

Luo, S., Zhou, B., Likos, W. J., & Lu, N. (2024). Determining capillary pore-size distribution of soil from soil–water retention curve. Journal of Geotechnical and Geoenvironmental Engineering, 150(2), Article 04023138. https://doi.org/10.1061/JGGEFK.GTENG-11647

Ma, C. H. I., & Eggleton, R. A. (1999). Cation exchange capacity of kaolinite. Clays and Clay minerals, 47, 174-180.

Maechler, M., Rousseeuw, P., Struyf, A., Hubert, M., Hornik, K.(2023). cluster: Cluster Analysis Basics and Extensions. R package version 2.1.6.

Martin, R. T. (1962). Adsorbed water on clay: A review. Clays and clay minerals, 28-70.

Massey, A. C., Paul, M. A., Gehrels, W. R., & Charman, D. J. (2006). Autocompaction in Holocene coastal back-barrier sediments from south Devon, southwest England, UK. Marine Geology, 226(3-4), 225-241.

Massop, H.T.L., Hessel, R., van den Akker, J.J.H., van Asselen, S., Erkens, G., Gerritsen, P.A. & Gerritsen, F.H.G.A., 2024. Monitoring long-term peat subsidence with subsidence platens in Zegveld, The Netherlands. Geoderma 450: 117039. DOI: 10.1016/j.geoderma.2024.117039.

Matsuo S., Kamon M. (1977) Macroscopic study on deformation and strength on clays. In: Proceedings of the 9th international conference on soil mechanics and foundation engineering, Tokyo, Japan, pp 201–204

Matthiesen, H. (2004). State of Preservation and Possible Settling of Cultural Layers Below Bredsgarden and Bugaden Tenements, Bryggen, Bergen. Department of Conservation, National Museum of Denmark, Report No. 10832–0004–3.

McCarter, C. P. R., & Price, J. S. (2014). Ecohydrology of Sphagnum moss hummocks: mechanisms of capitula water supply and simulated effects of evaporation. Ecohydrology, 7(1), 33–44. https://doi.org/10.1002/eco.1313

McCarter, C. P. R., Rezanezhad, F., Quinton, W. L., Gharedaghloo, B., Lennartz, B., Price, J., Connon, R., & van Cappellen, P. (2020). Pore-scale controls on hydrological and geochemical processes in peat: Implications on interacting processes. In Earth-Science Reviews (Vol. 207). Elsevier B.V. https://doi.org/10.1016/j.earscirev.2020.103227

McGivern, B.B., Tfaily, M.M., Borton, M.A., Kosina, S.M., Daly, R.A., Nicora, C.D., Purvine, S.O., Wong, A. R., Lipton, M. S., Hoyt, D. W. and Northen, T. R., (2021). Decrypting bacterial polyphenol metabolism in an anoxic wetland soil. Nature communications, 12(1), p.2466.

Mendes, R. M., & Marinho, F. A. M. (2020). Soil water retention curves for residual soils using traditional methods and MIP. Geotechnical and Geological Engineering, 38, 5167-5177.

Mesri, G. (1973). Coefficient of secondary compression. Journal of the soil mechanics and foundations division, 99(1), 123-137.

Mesri, G., & Ajlouni, M. (2007). Engineering Properties of Fibrous Peats. Journal of Geotechnical and Geoenvironmental Engineering, 133(7), 850–866. https://doi.org/10.1061/(asce)1090-0241(2007)133:7(850)

Mesri, G., & Funk, J. R. (2015). Settlement of the Kansai international airport islands. Journal of Geotechnical and Geoenvironmental Engineering, 141(2), 04014102.

Mesri, G., & Godlewski, P. M. (1977). Time-and stress-compressibility interrelationship. Journal of the geotechnical engineering division, 103(5), 417-430.

Mesri, G., Lo, D. O. K., & Feng, T. W. (1994). Settlement of embankments on soft clays. In Proceedings of the Conference on Vertical and Horizontal Deformations of Foundations and Embankments. Part 2 (of 2) (pp. 8-56). Publ by ASCE.

Mesri, G., Stark, T. D., Ajlouni, M. A., & Chen, C. S. (1997). Secondary compression of peat with or without surcharging. Journal of Geotechnical and Geoenvironmental Engineering, 123(5), 411-421.

Michel, J. C., Bellon-Fontaine, M. N., & Rivière, L. M. (1999). Characterisation of the Wettability of organic substrates (peat and composted bark) by adsorption measurements. Acta Horticulturae, 481, 129–136. https://doi.org/10.17660/ActaHortic.1999.481.11

Minderhoud, P. S. J. (2019). *The sinking mega-delta: Present and future subsidence of the Vietnamese Mekong delta* (Doctoral dissertation, Utrecht University).

Minderhoud, P. S. J., Erkens, G., Pham, V. H., Vuong, B. T., & Stouthamer, E. (2015). Assessing the potential of the multi-aquifer subsurface of the Mekong Delta (Vietnam) for land subsidence due to groundwater extraction. *Proceedings of the International Association of Hydrological Sciences*, *372*(372), 73-76.

Minderhoud, P. S., Erkens, G., Pham, V. H., Bui, V. T., Erban, L., Kooi, H., & Stouthamer, E. (2017). Impacts of 25 years of groundwater extraction on subsidence in the Mekong delta, Vietnam. Environmental research letters, 12(6), 064006.

Minderhoud, P. S. J., Shirzaei, M., & Teatini, P. (2025). From InSAR-derived subsidence to relative sea-level rise—A call for rigor. *Earth's Future*, *13*(1), e2024EF005539.

Miranda-Trevino, J. C., & Coles, C. A. (2003). Kaolinite properties, structure and influence of metal retention on pH. Applied Clay Science, 23(1-4), 133-139.

Mitchell J. K. (1993), Fundamentals of soil behaviour, 2nd edition, John Wiley & Sons, Inc, New York, 437 pp.

Mitchell, J. K., & Soga, K. (2005). Fundamentals of soil behavior (Vol. 3, p. 558). New York: John Wiley & Sons.

Mitchell, J. K., Campanella, R. G., & Singh, A. (1968) Soil creep as a rate process, Journal of the Soil Mechanics and Foundations Division, ASCE, Vol. 94, No. SM 1, pp. 231–253.

Mohseni, N., & Bol, R. (2021). Variation in the rate of land subsidence induced by groundwater extraction and its effect on the response pattern of soil microbial communities. Earth Surface Processes and Landforms, 46(10), 1898–1908. https://doi.org/10.1002/esp.5133

Moon, T.K. (1996). "The expectation-maximization algorithm," in IEEE Signal Processing Magazine, vol. 13, no. 6, pp. 47-60, doi: 10.1109/79.543975.

Morais, F. I., Page, A. L., & Lund, L. J. (1976). The effect of pH, salt concentration, and nature of electrolytes on the charge characteristics of Brazilian tropical soils. Soil Science Society of America Journal, 40(4), 521-527.

Moret, D., & Arrúe, J. L. (2007). Dynamics of soil hydraulic properties during fallow as affected by tillage. Soil and tillage research, 96(1-2), 103-113.

Mtambanengwe, F., Mapfumo, P., & Kirchmann, H. (1956). Decomposition of Organic Matter in Soil as Influenced by Texture and Pore Size Distribution.

Naganuma, K., Okazaki, M., Yonebayashi, K., Kyuma, K., Vijarnsorn, P., & Bakar, Z. A. (1993). Surface charge and adsorption characteristics of copper and zinc on tropical peat soils. Soil Science and Plant Nutrition, 39(3), 455-462.

NASA, 2023. Sea level change. Observations from space. Understanding sea level. Global Mean Sea Level | Key Indicators – NASA Sea Level Change Portal

Navarro, V., & Alonso, E. E. (2001). Secondary compression of clays as a local dehydration process. Géotechnique, 51(10), 859-869.

Nayak, S. K., Baliyarsingh, B., Mannazzu, I., Singh, A., & Mishra, B. B. (2022). Advances in agricultural and industrial microbiology: Volume 1: Microbial diversity and application in agroindustry. Springer Singapore. https://doi.org/10.1007/978-981-16-8918-5

Nederlands Centrum voor Geodesie en Geo-Informatica (NCG) (2025). Bodemdalingskaart 2.0. https://bodemdalingskaart.portal.skygeo.com/portal/bodemdalingskaart/u2/viewers/basic/

Nederlands Normalisatie Instituut (NNI) (1989) Geotechniek : Classificatie van onverharde grondmonsters, NEN 5104. - NNI, Delft, 23 15 pp.

Nederlands Normalisatie Instituut (NNI) (2006). Geotechnics - TGB 1990 - Basic requirements and loads. Publisher NEN, NEN 6740

Nederlands Normalisatie Instituut (NNI) (2016), NEN-EN 1997-1: Eurocode 7, national annex The Netherlands; Geotechnical design of structures - Part 1: General rules.

Nicholls, R. J., Lincke, D., Hinkel, J., Brown, S., Vafeidis, A. T., Meyssignac, B., Hanson, S. E., Merkens, J. L. and Fang, J. (2021). A global analysis of subsidence, relative sea-level change and coastal flood exposure. Nature Climate Change, 11(4), pp.338-342.

Nieto, F., Mellini, M., & Abad, I. (2010). The role of H3O+ in the crystal structure of illite. Clays and Clay Minerals, 58(2), 238-246.

Nieuwenhuis, H. S., & Schokking, F. (1997). Land subsidence in drained peat areas of the Province of Friesland, The Netherlands. Quarterly Journal of Engineering Geology and Hydrogeology, 30(1), 37-48.

Nishimoto, S., & Hayashi, H. (2008). A case study of the long-term settlement and life cycle cost of a road on peaty ground. In Advances in Transportation Geotechnics (pp. 411-414). CRC Press.

NNI (2019a). NEN-EN-ISO 14688-1, Geotechnisch onderzoek en beproeving – Identificatie en classificatie van grond – Deel 1: Identificatie en beschrijving, Nederlands Normalisatie Instituut, NNI, Delft.

NNI (2019b). NEN-EN-ISO 14688-2, Geotechnisch onderzoek en beproeving – Identificatie en classificatie van grond – Deel 2: Grondslagen voor een classificatie, Nederlands Normalisatie Instituut, NNI, Delft.

O'Kelly, B. C. (2017). Measurement, interpretation and recommended use of laboratory strength properties of fibrous peat. *Geotechnical Research*, *4*(3), 136-171.

O'Kelly, B. C., & Pichan, S. P. (2013). Effects of decomposition on the compressibility of fibrous peat—A review. Geomechanics and Geoengineering, 8(4), 286-296.

O'Kelly, B. C., & Zhang, L. (2013). Consolidated-drained triaxial compression testing of peat. ASTM International.

Oleszczuk, R., Łachacz, A., & Kalisz, B. (2022). Measurements versus estimates of soil subsidence and mineralization rates at peatland over 50 years (1966–2016). Sustainability, 14(24), 16459. https://doi.org/10.3390/su142416459

Osipov, V. I., Karpenko, F. S., & Rumyantseva, N. A. (2015). Active porosity and its effect on the physical mechanical properties of clay. Water Resources, 42, 951-957.

Page, S., Baird, A., Cumming, A., High, K. E., Kaduk, J., & Evans, C. (2020). An assessment of the societal impacts of water level management on lowland peatlands in England and Wales: Report to Defra for Project SP1218: Managing agricultural systems on lowland peat for decreased greenhouse gas emissions whilst maintaining agricultural productivity.

Paul, M. A., & Barras, B. F. (1998). A geotechnical correction for post-depositional sediment compression: examples from the Forth valley, Scotland. Journal of Quaternary Science: Published for the Quaternary Research Association, 13(2), 171-176.

Peng, B., Feng, R., Wu, L., Wang, P., & Shen, Y. (2024). Changes of water in different states during peat soil compression. Bulletin of Engineering Geology and the Environment, 83(1), 10.

Philip, J. R. (1969). Hydrostatics and hydrodynamics in swelling soils. Water Resources Research, 5(5), 1070–1077. https://doi.org/10.1029/WR005i005p01070

Pichan, S., & O'Kelly, B. C. (2013). Effect of decomposition on the compressibility of fibrous peat. Proceedings of the GeoCongress, 4329–4338. https://doi.org/10.1061/9780784412121.445

Pierik, H. J., Stouthamer, E., Schuring, T., & Cohen, K. M. (2018). Human-caused avulsion in the Rhine-Meuse delta before historic embankment (The Netherlands). Geology, 46(11), 935-938.

Pizzuto, J. E., & Schwendt, A. E. (1997). Mathematical modeling of autocompaction of a Holocene transgressive valley-fill deposit, Wolfe Glade, Delaware. Geology, 25(1), 57-60.

Poelman, J.N.B. (1975). Dichtheid van de vaste delen van rivierkleigronden. Boor en Spade XIX: 32-38. Stichting voor Bodemkartering, Wageningen.

Price, J. S., Cagampan, J., & Kellner, E. (2005). Assessment of peat compressibility: is there an easy way?. Hydrological Processes: An International Journal, 19(17), 3469-3475.

Prosperi, A., Longo, M., Korswagen, P. A., Korff, M., & Rots, J. G. (2023). Sensitivity modelling with objective damage assessment of unreinforced masonry façades undergoing different subsidence settlement patterns. Engineering Structures, 286, 116113. https://doi.org/10.1016/j.engstruct.2023.116113

Prost, R., Koutit, T., Benchara, A., & Huard, E. (1998). State and location of water adsorbed on clay minerals: Consequences of the hydration and swelling-shrinkage phenomena. Clays and clay minerals, 46(2), 117-131.

Puzrin, A. M., Alonso, E. E., Pinyol, N., Puzrin, A. M., Alonso, E. E., & Pinyol, N. M. (2010). Unexpected excessive settlements: Kansai international airport, Japan. Geomechanics of failures, 23-43.

Quigley, M. Y., Negassa, W. C., Guber, A. K., Rivers, M. L., & Kravchenko, A. N. (2018). Influence of pore characteristics on the fate and distribution of newly added carbon. Frontiers in Environmental Science, 6(JUN). https://doi.org/10.3389/fenvs.2018.00051

Quinton, W. L., Elliot, T., Price, J. S., Rezanezhad, F., & Heck, R. (2009). Measuring physical and hydraulic properties of peat from X-ray tomography. Geoderma, 153(1-2), 269-277.

R Core Team (2024). R: A language and environment for statistical computing. R Foundation for Statistical Computing, Vienna, Austria. URL: https://www.R-project.org/

R Core Team (2025). R: A language and environment for statistical computing. R Foundation for Statistical Computing. https://www.R-project.org/

Ranjan, G., & Rao, A. S. R. (2011). Basic and applied soil mechanics. New Age International.

Redding, T. E., & Devito, K. J. (2006). Particle densities of wetland soils in northern Alberta, Canada. Canadian Journal of Soil Science, 86(1), 57–60. https://doi.org/10.4141/S05-061

Reinert, E. T. (2014). Dynamic shake testing of a model levee on peaty organic soil in the Sacramento-San Joaquin Delta. University of California, Los Angeles.

Renard, F., & Ortoleva, P. (1997). Water films at grain-grain contacts: Debye-Hückel, osmotic model of stress, salinity, and mineralogy dependence. Geochimica et Cosmochimica Acta, 61(10), 1963-1970.

Revil, A., Grauls, D., & Brévart, O. (2002). Mechanical compaction of sand/clay mixtures. Journal of Geophysical Research: Solid Earth, 107(B11), ECV-11.

Rezanezhad, F., Price, J. S., & Craig, J. R. (2012). The effects of dual porosity on transport and retardation in peat: A laboratory experiment. Canadian Journal of Soil Science, 92(5), 723-732.

Rezanezhad, F., Price, J. S., Quinton, W. L., Lennartz, B., Milojevic, T., & van Cappellen, P. (2016). Structure of peat soils and implications for water storage, flow and solute transport: A review update for geochemists. Chemical Geology, 429, 75–84. https://doi.org/10.1016/j.chemgeo.2016.03.010

Rezanezhad, F., Quinton, W. L., Price, J. S., Elliot, T. R., Elrick, D., & Shook, K. R. (2010). Influence of pore size and geometry on peat unsaturated hydraulic conductivity computed from 3D computed tomography image analysis. Hydrological Processes, 24(21), 2983–2994. https://doi.org/10.1002/hyp.7709

Ricardo, S., Ribeiro da Silva, I., Félix de Barros, N., & de Sá Mendonça, E. (2011). Effect of compaction on microbial activity and carbon and nitrogen transformations in two oxisols with different mineralogy. Revista Brasileira de Ciência do Solo, 35(4), 1141–1149.

Rojstaczer, S. A., Hamon, R. E., Deverel, S. J., & Massey, C. A. (1991). Evaluation of selected data to assess the causes of subsidence in the Sacramento-San Joaquin Delta, California (No. 91-193). US Geological Survey; For sale by the Books and Open-File Reports Section [distributor],.

Romanov, V. V. (1968). Hydrophysics of Bogs. Israel Programme for Scientific Translations, Jerusalem

Rousseeuw, P.J. (1987). Silhouettes: A graphical aid to the interpretation and validation of cluster analysis. J. Comput. Appl. Math., 20, 53–65.

Rowe, R. K., & Li, A. L. (2002). Behaviour of reinforced embankments on soft rate-sensitive soils. Geotechnique, 52(1), 29-40.

Rowell, R. M. (2005). Handbook of wood chemistry and wood composites. CRC press.

Ruamps, L. S., Nunan, N., & Chenu, C. (2011). Microbial biogeography at the soil pore scale. Soil Biology and Biochemistry, 43(2), 280–286. https://doi.org/10.1016/j.soilbio.2010.10.010

Ruamps, L. S., Nunan, N., Pouteau, V., Leloup, J., Raynaud, X., Roy, V., & Chenu, C. (2013). Regulation of soil organic C mineralisation at the pore scale. FEMS Microbiology Ecology, 86(1), 26–35. https://doi.org/10.1111/1574-6941.12078

Ruser, R., Flessa, H., Russow, R., Schmidt, G., Buegger, F., & Munch, J. C. (2006). Emission of N_2O, N_2 and CO_2 from soil fertilized with nitrate: Effect of compaction, soil moisture and rewetting. Soil Biology and Biochemistry, 38(2), 263–274. https://doi.org/10.1016/j.soilbio.2005.05.005

Ryan, M. G., & Law, B. E. (2005). Interpreting, measuring, and modeling soil respiration. Biogeochemistry, 73(1), 3–27. https://doi.org/10.1007/s10533-004-5167-7

Samuel, M. K., & Evers, S. (2024). Translocation of tropical peat surface to deeper soil horizons under compaction controls carbon emissions in the absence of groundwater. Frontiers in Soil Science, 4, 1259907. https://doi.org/10.3389/fsoil.2024.1259907

Sarkar, G., & Sadrekarimi, A. (2020). Compressibility and monotonic shearing behaviour of Toronto peat. Engineering Geology, 278, 105822.

Schäffer, B., Boivin, P., & Schulin, R. (2010). Compressibility of repacked soil as affected by wetting and drying between uniaxial compression tests. Soil Science Society of America Journal, 74(5), 1483–1492. https://doi.org/10.2136/sssaj2009.0381

Schjønning, P., McBride, R. A., Keller, T., & Obour, P. B. (2017). Predicting soil particle density from clay and soil organic matter contents. Geoderma, 286, 83–87. https://doi.org/10.1016/j.geoderma.2016.10.020

Schlüter, S., Leuther, F., Albrecht, L., Hoeschen, C., Kilian, R., Surey, R., ... & Vogel, H. J. (2022). Microscale carbon distribution around pores and particulate organic matter varies with soil moisture regime. *Nature communications*, *13*(1), 2098.

Schoeneberger, P. J., Wysocki, D. A., & Benham, E. C. (Eds.). (2012). Field book for describing and sampling soils. Government Printing Office.

Schoonheydt, R. A., & Johnston, C. T. (2013). Surface and interface chemistry of clay minerals. Developments in clay science, 1, 87-113.

Schothorst, C. J. (1977). Subsidence of low moor peat soils in the western Netherlands. Geoderma, 17(4), 265-291.

Schulz, C., Meier-Uhlherr, R., Luthardt, V., & Joosten, H. (2019). A toolkit for field identification and ecohydrological interpretation of peatland deposits in Germany. Mires and Peat, 24(32), 1-20.

Scott, N. A., Cole, C. V., Elliott, E. T., & Huffman, S. A. (1996). Soil Textural Control on Decomposition and Soil Organic Matter Dynamics. Soil Sci. Soc. Am.J., 60, 1102–1109.

Scrucca L., Fraley C., Murphy T.B., Raftery A.E. (2023). Model-Based Clustering, Classification, and Density Estimation Using mclust in R. Chapman & Hall/CRC, ISBN: 978-1032234953, https://mclust-org.github.io/book/

Sehlstedt-Persson, M. (2008). Impact of drying and heat treatment on physical properties and durability of solid wood (Doctoral dissertation, Luleå tekniska universitet).

Seidel, R., Dettmann, U., & Tiemeyer, B. (2023). Reviewing and analyzing shrinkage of peat and other organic soils in relation to selected soil properties. Vadose Zone Journal, 22(5). https://doi.org/10.1002/vzj2.20264

Shi, X., Xue, Y., Wu, J., Ye, S., Zhang, Y., Wei, Z., & Yu, J. (2008). Characterization of regional land subsidence in Yangtze Delta, China: the example of Su-Xi-Chang area and the city of Shanghai. *Hydrogeology Journal*, *16*(3), 593-607.

Siczek, A., & Frac, M. (2012). Soil microbial activity as influenced by compaction and straw mulching. International Agrophysics, 26(1), 65–69. https://doi.org/10.2478/v10247-012-0010-1

Singh, D. P. (1975, September). A study of creep of rocks. In International journal of rock mechanics and mining sciences & geomechanics abstracts (Vol. 12, No. 9, pp. 271-276). Pergamon.

Singh, P. N., & Wallender, W. W. (2008). Effects of adsorbed water layer in predicting saturated hydraulic conductivity for clays with Kozeny–Carman equation. Journal of Geotechnical and Geoenvironmental Engineering, 134(6), 829-836.

Singh, P. N., & Wallender, W. W. (2011). Effects of soil water salinity on field soil hydraulic functions. Journal of irrigation and drainage engineering, 137(5), 295-303.

Skempton, A. W., & Petley, D. J. (1970). Ignition loss and other properties of peats and clays from Avonmouth, King's Lynn and Cranberry Moss. Geotechnique, 20(4), 343-356.

Sneed, M., Brandt, J. T., & Solt, M. (2013). Land subsidence along the Delta-Mendota Canal in the northern part of the San Joaquin Valley, California, 2003-10 (No. 2013-5142). US Geological Survey.

Sparks, D. L. (Ed.). (1998). Soil physical chemistry. CRC press.

Stevens, C. V. (2010). Industrial applications of natural fibres: structure, properties and technical applications. John Wiley & Sons.

Stokke, D. D., Wu, Q., & Han, G. (2013). Introduction to wood and natural fiber composites. John Wiley & Sons.

Stouthamer, E., Cohen, K. M., & Gouw, M. J. (2011). Avulsion and its implications for fluvial-deltaic architecture: insights from the Holocene Rhine–Meuse delta.

Stouthamer, E., Cohen, K. M., & Hoek, W. Z. (2023). *De vorming van het land: geologie en geomorfologie*. Perspectief uitgevers.

Stouthamer, E., Erkens, G., Cohen, K., Hegger, D., Driessen, P., Weikard, H. P., Hefting, M., Hanssen, R., Fokker, P., van den Akker, J., Groothuijse, F., & van Rijswick, M. (2020). Dutch national scientific research program on land subsidence: Living on soft soils—Subsidence and society. Proceedings of the International Association of Hydrological Sciences, 382, 815–819. https://doi.org/10.5194/piahs-382-815-2020

Strehse, R., Bohne, H., Amha, Y., & Leinweber, P. (2018). The influence of salt on dissolved organic matter from peat soils. Organic geochemistry, 125, 270-276.

Strong, D. T., de Wever, H., Merckx, R., & Recous, S. (2004). Spatial location of carbon decomposition in the soil pore system. European Journal of Soil Science, 55(4), 739–750. https://doi.org/10.1111/j.1365-2389.2004.00639.x

Sweygers, N., Depuydt, D. E., Eyley, S., Thielemans, W., Mosleh, Y., Ivens, J., ... & van Vuure, A. W. (2022). Prediction of the equilibrium moisture content based on the chemical composition and crystallinity of natural fibres. Industrial Crops and Products, 186, 115187.

Szajdak, L., & Szatylowicz, J. (2010). Impact of drainage on hydrophobicity of fen peat-moorsh soils. https://www.researchgate.net/publication/301790219

Taccari, M. L., & Zwanenburg, C. (2019). Large scale triaxial compression tests on three peat samples from Eemdijk, The Netherlands. *Proceedings of the XVII ECSMGE-2019, Reykjavik, Iceland*, 1-6.

Tanaka, H., Hayashi, H., & Yamazoe, N. (2019). Reconsideration of the settlement behavior of peat from view point of hydraulic conductivity. Soils and Foundations, 59(2), 316–325. https://doi.org/10.1016/j.sandf.2018.11.002

Tanaka, H., Udaka, K., & Nosaka, T. (2006). Strain rate dependency of cohesive soils in consolidation settlement. Soils and foundations, 46(3), 315-322.

Tang, L., Chen, H., & Song, J. (2016). Process of pore pressure diffusion in saturated clay soil and impact of adsorbed water. Geosciences Journal, 20, 649-665.

Tavenas, F., Leblond, P., Jean, P., & Leroueil, S. (1983). The hydraulic conductivity of natural soft clays. Part I: Methods of laboratory measurement. Canadian Geotechnical Journal, 20(4), 629-644.

TAW (Technische Adviescommissie voor de Waterkeringen) (1996). Technisch rapport geotechnische classificatie van veen. Report Ministry of Transport and Water Management, Delft, The Netherlands, 102 pp.

Taylor, D. W., & Merchant, W. (1940). A theory of clay consolidation accounting for secondary compression. Journal of Mathematics and physics, 19(1-4), 167-185.

Teatini, P., Ferronato, M., Gambolati, G., Bertoni, W., & Gonella, M. (2005). A century of land subsidence in Ravenna, Italy. Environmental Geology, 47(6), 831-846.

Tempany, H. A. (1917). The shrinkage of soils. *The Journal of Agricultural Science*, *8*(3), 312-330.

Terzaghi, K. (1923). Die berechnung der durchlassigkeitsziffer des tones aus dem verlauf der hydrodynamischen spannungserscheinungen. Sitzungberichte Akademie der Wissenschaften, 132, 125-138.

Terzaghi, K. (1925). Erdbaumechanik auf bodenphysikalischer grundlage. Vienna: Franz Deuticke.

Terzaghi, K. (1941). Undisturbed clay samples and undisturbed clays. Journal of the Boston Society of Civil Engineers, 28(3), 45–65.

Thoang, T. T., & Giao, P. H. (2015). Subsurface characterization and prediction of land subsidence for HCM City, Vietnam. Engineering Geology, 199, 107-124.

Thybring, E. E., & Fredriksson, M. (2021). Wood modification as a tool to understand moisture in wood. Forests, 12(3), 372.

Timmerman, A., Haasnoot, M., Middelkoop, H., Bouma, T., & McEvoy, S. (2021). Ecological consequences of sea level rise and flood protection strategies in shallow coastal systems: A quick-scan barcoding approach. Ocean and Coastal Management, 210, 105674. https://doi.org/10.1016/j.ocecoaman.2021.105674

TNO–GDN (2024) NL3D. TNO – Geological Survey of the Netherlands, https://www.dinoloket.nl/en/subsurface-models/map; visited *2025-12-12*.

Tokunaga, T. K. (2009). Hydraulic properties of adsorbed water films in unsaturated porous media. Water resources research, 45(6).

Tolunay, D., Kowalchuk, G. A., Erkens, G., & Hefting, M. M. (2024). Aerobic and anaerobic decomposition rates in drained peatlands: Impact of botanical composition. Science of the Total Environment, 930, 172639. https://doi.org/10.1016/j.scitotenv.2024.172639

Toosi, E. R., Kravchenko, A. N., Guber, A. K., & Rivers, M. L. (2017a). Pore characteristics regulate priming and fate of carbon from plant residue. Soil Biology and Biochemistry, 113, 219–230. https://doi.org/10.1016/j.soilbio.2017.06.014

Toosi, E. R., Kravchenko, A. N., Mao, J., Quigley, M. Y., & Rivers, M. L. (2017b). Effects of management and pore characteristics on organic matter composition of macroaggregates: Evidence from characterization of organic matter and imaging. European Journal of Soil Science, 68(2), 200–211. https://doi.org/10.1111/ejss.12411

Törnqvist, T. E., Wallace, D. J., Storms, J. E., Wallinga, J., van Dam, R. L., Blaauw, M., ... & Snijders, E. M. (2008). Mississippi Delta subsidence primarily caused by compaction of Holocene strata. Nature Geoscience, 1(3), 173-176.

United Nations Framework Convention on Climate Change (UNFCCC). (2015). The Paris Agreement. https://unfccc.int/sites/default/files/resource/parisagreement_publication.pdf

Uyanık, O. (2019). Estimation of the porosity of clay soils using seismic P-and S-wave velocities. Journal of Applied Geophysics, 170, 103832.

Valat, B., Jouany, C., & Riviere, L. M. (1991). Characterization of the wetting properties of air-dried peats and composts. Soil Science, 152(2), 100–107.

van Asselen, S. (2010). Peat compaction in deltas: implications for Holocene delta evolution.

van Asselen, S. (2011). The contribution of peat compaction to total basin subsidence: Implications for the provision of accommodation space in organic-rich deltas. Basin Research, 23(2), 239–255. https://doi.org/10.1111/j.1365-2117.2010.00482.x

van Asselen, S., & Roosendaal, C. (2009). A new method for determining the bulk density of uncompacted peat from field settings. Journal of Sedimentary Research, 79(12), 918–922. https://doi.org/10.2110/jsr.2009.091

van Asselen, S., Erkens, G., Keogh, M. E., & Stuurman, R. (2024). Shallow-subsidence vulnerability in the city of New Orleans, southern USA. Hydrogeology Journal, 32(3), 867-889.

van Asselen, S., Erkens, G., Stouthamer, E., Woolderink, H. A. G., Geeraert, R. E. E., & Hefting, M. M. (2018). The relative contribution of peat compaction and oxidation to subsidence in built-up areas in the Rhine-Meuse delta, The Netherlands. Science of the Total Environment, 636, 177–191. https://doi.org/10.1016/j.scitotenv.2018.04.141

van Asselen, S., Erkens, G., & de Graaf, F. (2020). Monitoring shallow subsidence in cultivated peatlands. *Proceedings of the International Association of Hydrological Sciences*, *382*, 189-194.

van Asselen, S., Stouthamer, E., & van Asch, T. W. (2009). Effects of peat compaction on delta evolution: a review on processes, responses, measuring and modeling. Earth-Science Reviews, 92(1-2), 35-51.

van de Ven, G. P. (1993). Leefbaar laagland [Liveable lowlands]. Uitgeverij Matrijs, Utrecht, The Netherlands.

van den Akker, J. J. H., Beuving, J., Hendriks, R. F. A., & Wolleswinkel, R. J. (2007). Maaivelddaling, afbraak en CO2 emissie van Nederlandse veenweidegebieden. Leidraad Bodembescherming, afl, 83, 83.

van den Born, G. J., Kragt, F., Henkens, D., Rijken, B., van Bemmel, B., & van der Sluis, S. (2016). Dalende bodems, stijgende kosten. Planbureau voor de leefomgeving, the Hague, the Netherlands, 94.

van der Net, L., Coenen, P. W. H. G., van Mil, S. E. H., Rienstra, J. D., Zijlema, P. J., Baas, K., ... & van Zanten, M. C. (2025). National Inventory Document 2025: greenhouse gas emissions in the Netherlands 1990-2023.

van Elderen, P., Erkens, G., Zwanenburg, C., Middelkoop, H., & Stouthamer, E. (2025). Viscous compression of clay and peat. Earth-Science Reviews, 104993.

van Genuchten, M. Th. (1980). A Closed-form Equation for Predicting the Hydraulic Conductivity of Unsaturated Soils. Soil Science Society of America Journal, 44(5), 892–898. https://doi.org/10.2136/sssaj1980.03615995004400050002x

van Leer, M. D., Zaadnoordijk, W. J., Zech, A., Buma, J., Harting, R., Bierkens, M. F., & Griffioen, J. (2023). Dominant factors determining the hydraulic conductivity of sedimentary aquitards: A random forest approach. Journal of Hydrology, 627, 130468.

van Raij, B., & Peech, M. (1972). Electrochemical properties of some Oxisols and Alfisols of the tropics. Soil Science Society of America Journal, 36(4), 587-593.

Vargaftik, N. B., Volkov, B. N., & Voljak, L. D. (1983). International Tables of the Surface Tension of Water. Journal of Physical and Chemical Reference Data, 12(3), 817–820. https://doi.org/10.1063/1.555688

Venables, W.N., Ripley, B.D. (2002). Modern Applied Statistics with S, Springer-Verlag.

Vergote, T. A., Leung, C. F., & Chian, S. C. (2022). Modelling creep and swelling after unloading under constant load and relaxation with Bayesian updating. *Géotechnique*, *72*(6), 496-509.

Vermeersen, B. L. A., Slangen, A. B. A., Gerkema, T., Baart, F., Cohen, K. M., Dangendorf, S., Duran-Matute, M., Frederikse, T., Grinsted, A., Hijma, M. P., Jevrejeva, S., Kiden, P., Kleinherenbrink, M., Meijles, E. W., Palmer, M. D., Rietbroek, R., Riva, R. E. M., Schulz, E., Slobbe, D. C., … van der Wegen, M. (2018). Sea-level change in the Dutch Wadden Sea. Geologie en Mijnbouw / Netherlands Journal of Geosciences, 97(3), 79–127. https://doi.org/10.1017/njg.2018.7

Vernes, R. W., Bosch, A. J., Harting, R., de Heer, E., & Griffioen, J. (2010). Towards a physical and chemical characterization of the shallow subsurface of the Netherlands. In First International Conference on Frontiers in Shallow Subsurface Technology (pp. cp-150). European Association of Geoscientists & Engineers.

Visschedijk, M. (2010). Isotachen berekeningen op een sigarendoosje. Geotechniek, 14(3), 30.

Volarovich, M. P., & Churaev, N. V. (1966). Effect of surface forces on transfer of moisture in porous bodies. Research in surface forces, (2), 212-219.

Vos, P., van der Meulen, M., Weerts, H., & Bazelmans, J. (2020). Atlas of the Holocene Netherlands: Landscape and habitation since the last Ice Age.

Vos, P. C., & van Heeringen, R. M. (1997). Holocene geology and occupation history of the Province of Zeeland. *Mededelingen. Nederlands Instituut voor Toegepaste Geowetenschappen*.

Voyiadjis, G. Z., Zhou, Y., & Abdalla, A. (2024). Creep-induced subsidence along coastal Louisiana with GPS measurements and finite element modeling. Geoenergy Science and Engineering, 238, 212840.

Walpen, N., Getzinger, G. J., Schroth, M. H., & Sander, M. (2018a). Electron-donating phenolic and electron-accepting quinone moieties in peat dissolved organic matter: quantities and redox transformations in the context of peat biogeochemistry. Environmental science & technology, 52(9), 5236-5245.

Walpen, N., Lau, M. P., Fiskal, A., Getzinger, G. J., Meyer, S. A., Nelson, T. F., Lever, M. A., Schroth, M. H. & Sander, M. (2018b). Oxidation of reduced peat particulate organic matter by dissolved oxygen: quantification of apparent rate constants in the field. Environmental science & technology, 52(19), 11151-11160.

Wang, J. X., Feng, B., Hu, L. S., Tang, Y. Q., Yan, X. X., Wang, H. M., & Liu, J. B. (2013). Application of geo-environmental capacity of ground buildings in urban planning. Environmental earth sciences, 69, 93-102.

Wang, J., Zhang, Q., Song, Z., & Zhang, Y. (2020). Creep properties and damage constitutive model of salt rock under uniaxial compression. International Journal of Damage Mechanics, 29(6), 902-922.

Wang, N., & Zhang, T. (2024). Soil pore structure and its research methods: A review. Soil and Water Research, 19(1), 1–24. https://doi.org/10.17221/64/2023-SWR

Waniek, J. J., Schulz-Bull, D. E., Kuss, J., & Blanz, T. (2005). Long time series of deep water particle flux in three biogeochemical provinces of the northeast Atlantic. Journal of Marine Systems, 56(3–4), 391–415. https://doi.org/10.1016/j.jmarsys.2005.03.001

Wanner, H., Albinsson, Y., Karnland, O., Wieland, E., Wersin, P., Charlet, L., (1994). The acid/base chemistry of montmorillonite. Radiochim. Acta 66 (67), 157–162.

Wardwell, R. E., Charlie, W. A., & Doxtader, K. A. (1983). Test method for determining the potential for decomposition in organic soils. In Testing of peats and organic soils. ASTM International.

Weber, T. K. D., Iden, S. C., & Durner, W. (2017). A pore-size classification for peat bogs derived from unsaturated hydraulic properties. Hydrology and Earth System Sciences, 21(12), 6185-6200.

Wensink, E. J. W., Hoffmann, A. C., Apol, M. E. F., & Berendsen, H. J. C. (2000). Properties of adsorbed water layers and the effect of adsorbed layers on interparticle forces by liquid bridging. Langmuir, 16(19), 7392-7400.

Wind, G. P. (1968). Capillary Conductivity Data Estimated by a Simple Method. In P. E. Rijtema & H. Wassink (Eds.), Water in the unsaturated zone (pp. 181–191). UNESCO.

Wit, E., van den Heuvel, E., Romeyn, J. (2012). "'All models are wrong...': an introduction to model uncertainty" (PDF). StatisticaNeerlandica. 66 (3): 217–236. doi:10.1111/j.1467-9574.2012.00530.x., S2CID7793470

Wong, L. S., Hashim, R., & Ali, F. H. (2009). A review on hydraulic conductivity and compressibility of peat. Journal of Applied Sciences, 9(18), 3207-3218. https://doi.org/10.2112/JCOASTRES-D-17-00093.1 https://doi.org/10.3923/jas.2009.3207.3218

Wu, J., Shi, X., Xue, Y., Zhang, Y., Wei, Z., & Yu, J. (2008). The development and control of the land subsidence in the Yangtze Delta, China. Environmental Geology, 55, 1725-1735.

Wu, Y., Zhang, N., Slater, G., Waddington, J. M., & de Lannoy, C. F. (2020). Hydrophobicity of peat soils: Characterization of organic compound changes associated with heat-induced water repellency. Science of the Total Environment, 714, 136444.

Xotta, R., Zoccarato, C., Minderhoud, P. S. J., & Teatini, P. (2022). Modeling the role of compaction in the three-dimensional evolution of depositional environments. Journal of Geophysical Research: Earth Surface, 127(9), e2022JF006590.

Xu, X., Shi, Z., Li, D., Rey, A., Ruan, H., Craine, J. M., Liang, J., Zhou, J., & Luo, Y. (2016). Soil properties control decomposition of soil organic carbon: Results from data-assimilation analysis. Geoderma, 262, 235–242. https://doi.org/10.1016/j.geoderma.2015.08.038

Yamazoe, N., Nishimura, S., Tanaka, H., Ogino, T., & Kochi, T. (2025). Long-term settlement behavior of peat after unloading and applicability of isotach law. Soils and Foundations, 65(1), 101560.

Yan, Z., Liu, C., Todd-Brown, K. E., Liu, Y., Bond-Lamberty, B., & Bailey, V. L. (2016). Pore-scale investigation on the response of heterotrophic respiration to moisture conditions in heterogeneous soils. Biogeochemistry, 131(1–2), 121–134. https://doi.org/10.1007/s10533-016-0270-0

Ye, S., Xue, Y., Wu, J., Yan, X., & Yu, J. (2016). Progression and mitigation of land subsidence in China. Hydrogeology Journal, 24(3), 685-693.

Yin, J. H. (2002). Calculation of settlements of foundation soils considering creep.

Yuan, Y., & Whittle, A. J. (2018). A novel elasto-viscoplastic formulation for compression behaviour of clays. *Géotechnique*, *68*(12), 1044-1055.

Yuan, Y., & Whittle, A. J. (2021). Formulation of a new elastoviscoplastic model for time-dependent behavior of clay. *International Journal for Numerical and Analytical Methods in Geomechanics*, *45*(6), 843-864.

Yuill, B., Lavoie, D., & Reed, D.J. (2009). Understanding subsidence processes in coastal Louisiana. Journal of Coastal Research, (10054), 23-36.

Zaffar, M., & Lu, S.-G. (2015). Pore size distribution of clayey soils and its correlation with soil organic matter. Pedosphere, 25(2), 240–249. https://doi.org/10.1016/S1002-0160(15)60009-1

Zagwijn, W. H. (1986). *Nederland in het Holoceen* (p. 46). Haarlem: Rijks geologische dienst.

Zain, N. H. B. (2019) Effect of Oxidation on the Compression Behaviour of Organic Soils. Delft University of Technology Institutional Repository. https://doi.org/10.4233/uuid:aa7fe90a-7bf5-4c91-aa3e-c6a594a7d59d

Zhao, D., Gao, Q. F., Hattab, M., Hicher, P. Y., & Yin, Z. Y. (2020). Microstructural evolution of remolded clay related to creep. Transportation Geotechnics, 24, 100367.

Zoccarato, C., Minderhoud, P. S., Zorzan, P., Tosi, L., Bergamasco, A., Girardi, V., ... & Teatini, P. (2022). In-situ loading experiments reveal how the subsurface affects coastal marsh survival. Communications Earth & Environment, 3(1), 264.

Zwanenburg, C. (2017). The development of a large diameter sampler. In Proceedings of the 19 th International Conference on Soil Mechanics and Geotechnical Engineering, https://doi.org/10.1016/j.scitotenv.2019.136444 Seoul.

Zwanenburg, C., Den Haan, E. J., Kruse, G. A. M., & Koelewijn, A. R. (2012). Failure of a trial embankment on peat in Booneschans, the Netherlands. *Géotechnique*, *62*(6), 479-490.

Zwanenburg, C., & Jardine, R. J. (2015). Laboratory, in situ and full-scale load tests to assess flood embankment stability on peat. Géotechnique, 65(4), 309-326.

Acknowledgements

The stereotype of a PhD is that they are on a small island workwise. Often by themselves working on their project can make feel lonely. Now I think that everyone who knows me will confirm that I am incapable of that as I typically do not hesitate to get into a conversation anywhere. It got me a lot of friends and connections over the years and therefore I cannot say that I was lonely throughout the PhD. And I think that most PhD's do not need to be as long as you can find some colleagues to get together with. Just know that if you feel down: it's okay, everyone goes through that a couple of times. Try to take a small step back, breathe, do something fun with friends or colleagues. Everything will be okay and have people to support you. I did this exact same thing, got a lot of help, support and comfort during the PhD, and want to take this opportunity to thank quite a significant amount of people for that.

Esther, we know each other for 10 years already in which you have seen me change from a young bachelor student to the researcher I am now. We had countless discussions on modelling, geotechnical theory, fieldwork, presentation and many other things. During those you always pushed me to be as concrete as possible, a mantra I will always remember. We also shared great field trips to both congresses and institute visits, particularly the China visit was special, but also the years of supervision of the students in Italy. Your door was always open and although I sometimes muddle along longer than necessary, I could bring up problems I was facing. Thank you for everything and we are bound to meet in the future within the still (too) small subsidence research community.

Gilles, the man with a plan, the prince of peat. You always had an eye for the practical side of it all. With a quick meeting, you were able to advance an idea, sharpen a storyline and propose a new link. Those contributions have enabled me to improve and extent the idea of decomposition as facilitator for continuing compaction. But you did not only contribute on the content. I also enjoyed your many interesting and sometimes almost unbelievable stories during drinks and dinners. And every visit to a peatland in the Netherlands I could learn something new from what you were telling us. Thank you too for making it possible for me to work at Deltares, which turned out to be a good learning experience.

Hans, I really value the input you provided on my chapters. The topic was not linked to your background that strongly, but you put in the effort to learn. Partially you did by yourself, but also during our meetings where it was clear you wanted to understand by the enthusiastic and thorough questions you kept asking. I hope that you also enjoyed learning about this part of your beloved delta as I certainly did. And your delta-oriented view also helped me to refrain from drowning in the details of the small scale of the soil I was studying. As a result, the knowledge can be put into a wider perspective.

My Soil Sisters, I am so happy to be part of this group. It started within the office with **Bente** and **Kim**, making jokes, pulling faces and making work fun, which meant I wanted to be at the department as much as possible. Thank you so much for being my paranymphs and aiding me during the defence day. It is not a given that you honour my idea of being each other's paranymphs proposed 1 month into the PhD. But we are 5 sisters: **Chayenne** and **Irene** also made sure that no day would go by without coffee/tea breaks (multiple if possible), endless interesting stories (many about babies and marriage) and walks through the botanical gardens. I cannot imagine the PhD without you, as you shared the best moments of the PhD, but also definitely pulled me through when things didn't work out like I wanted. From the clay of fieldwork days in Italy to the mud of the survival run, I could always rely on you.

Duygu, never would I have thought to find such a great new friend at work. Being both organizing people, we quickly clicked. Drinks, talks, walks, dinners which cannot happen without a nice bottle of prosecco, for us it did not stop at the end of the working day. But you also taught me so much about the biological/ecological side of peat which I knew little about. Without it, I would not have been able to write my thesis, also of course with collaboration chapter, but also land my Postdoc afterwards. I look forward to many more years of friendship.

Cor, jij hebt een enorme bijdrage gehad aan mijn begrip van de mechanische kant van compactie en viskeuze compressie, en hoe dit weerspiegeld wordt in de diagrammen van bijvoorbeeld Den Haan. Je nam rustig de tijd om in enkele meetings mij onderdelen uit te leggen en gaf waardevolle feedback bij de artikelen die ik heb geschreven. Met mijn Utrecht achtergrond miste ik die specifieke kennis die je typisch aan de TU Delft leert, maar wel essentieel is gebleken voor deze PhD. Het is mogelijk de persoonlijke ontwikkeling waar ik het meeste aan ga hebben.

I also want to say a big thanks to my colleagues from the **Department of Physical Geography**. It is crazy to realise I spent 10 years here since I started as a student-assistant in the third year of my bachelor. It feels a bit like family almost and I have had great contact over coffee, meetings or outings with almost all of you! Special mentions are due: **Ruth**, thank you for being the kind, helpful and joyful you. I cherish the chats since starting at the department at the same time and that bit of extra interest in how we were doing. **Elisabeth**, you gave a great chance to develop my teaching skills further and believed in me doing a good job. **Wim**, during work in the field and laboratory we had some very nice talks and discussions, and I felt the support when we were exploring our collaboration.

To my **Deltares colleagues**, I might not have been at the office as often, but I whenever I was there, I felt very welcome. Be it at the coffee corner, lunch at the Daltonlaan or in the lab in Delft, I always could chat and discuss. But the best times were the drinks or activities with

the unit or the subsidence working group. You are very close and that helps so much when trying to fit in despite not working on actual Deltares projects.

Like I said at the start of the chapter, I truly believe that friends outside of academia provide the necessary relaxation and reality checks during your PhD. I always could rely on my university friends from the **VSTB**, whether it was cycling, drinks, dinners, pubquizes or holidays, you knew how to get my head out of work mode and remove some tension. **Royce**, you were the steady dinner night factor in my week, especially during the beginning. You showed continuing interest in the work events (and those outside of work) and were always able to put the ups and downs I was experiencing into perspective. And I have many more friends who listened to me rambling about work or were there to spend time with me and do fun activities together. Thank you all, I could not do it without you.

Ik had het ook zeker niet kunnen doen zonder mijn ouders. **Pap & Mam**, jullie steunden me ongeacht wat er gebeurde of hoe ik me voelde, net zoals jullie al mijn hele leven hebben gedaan. Thuis kon ik altijd even echt tot rust komen, want niks hoefde, alles mocht. En hoewel dat in Utrecht ook kan, heeft thuis een speciale werking op me, of dat nu in Breda was of sinds kort in Baarland. Jullie wilden altijd weten wat de nieuwste ontwikkelingen waren en deden altijd jullie best om regelmatig te bellen als ik niet naar het zuiden afzakte of jullie in de regio Utrecht te vinden waren, om te supporteren, op te beuren of nieuws van het familiefront mee te delen. Dit boek is ook zeker een beetje van jullie.

Tomas, ik denk niet dat er iemand is met wie ik uitvoeriger en dieper heb gesproken over mijn PhD. Met jouw sterke intrinsieke interesse in de wetenschap in de brede zin (waarvan ik hoop dat je die nog een keer kan etaleren in jouw eigen PhD) was het altijd supermakkelijk om te praten over mijn onderwerp, de methodes die ik gebruikte of de presentaties die ik moest geven. Maar ook kon je meepraten over de sociale kant van het verhaal, ook vanuit jouw eigen ervaringen, terwijl we een van de online spellen speelden om een brug te slaan tussen Nederland en Engeland. Je bent een topbroer en ik hoop dat je ook in de toekomst altijd zo geïnteresseerd blijft in mijn doen en laten, zoals ik dat ben in het jouwe.

Dan last, but not least: lieve **Myrthe**. Ik plaag wel eens door te zeggen dat jou ontmoeten het beste resultaat van mijn PhD is, waarna jij een beetje over je nek gaat van de klefheid. Maar zonder grappen of grollen, ben ik wel echt zo blij met jou en alle steun die je me hebt gegeven. Met onze andere persoonlijkheden kijken we verschillend naar hoe je problemen moet aanpakken, maar dat levert juist ook nieuwe inzichten op en duwt me af en toe het drempeltje over als ik het niet zelf kan. Je staat altijd aan mijn kant, zorgt met veel liefde ervoor dat het leven om veel meer draait dan alleen de PhD en probeert mij werk te ontnemen als het allemaal even te veel dreigt te worden. Dank je voor alle steun, liefde en geduld, en weet dat ik je ook dubbel en dwars steun in jouw PhD tocht.

About the author

Being born in Breda on the sandy subsurface in the south of the Netherlands, I did not get into contact with land subsidence much in my childhood and likely did not know what it was. What did have my interest, was the world and every aspect of it. My childhood dream job was world traveller/explorer, and I was very sad when I learned that was not a real job. I memorized all the capitals of Europe and most of the world at an early age and geography was my favourite subject at primary and high school. During those classes, the natural side of our earth and its systems fascinated me which, together with my continued desire to travel and see other countries, made me choose to study *Earth Sciences* at Utrecht University.

Sometimes you do not know what the future holds. I started my bachelor programme with the idea of becoming a vulcanologist. A presentation by Philip Minderhoud about subsidence in the Mekong Delta in Vietnam at the end of my first year changed all that. Before I knew I fully got caught up in subsurface subsidence research. I started assisting with the lowland genesis fieldwork in Italy for the second-year students and graduated from my bachelor in 2017 under guidance of Philip on the analysis of subsurface heterogeneity of Ho Chi Minh City in the light of high-resolution subsidence modelling.

Continuing at Utrecht University with the master *Earth, Surface and Water*, I focussed on the morphodynamics of delta, coastal and tidal systems, and how the processes in these systems shape the subsurface as well. Add a bit of hydrology to the mix and it was a logical step to a master thesis on delta-scale subsidence modelling of the Yangtze River Delta in China, trying to highlight the effect of groundwater extractions in different cities. I graduated cum laude from the master in December 2020.

In January 2021, my PhD journey at the *Department of Physical Geography of Utrecht University* took off during which I studied the slow deformation of peat and organic clay leading to long-term subsidence. A topic operating at a much smaller scale than the scales I was looking at before. It was not the easiest time to start with COVID-19, but slowly but surely the project developed. During the first year I also started working one day a week at *Deltares Research Institute* to extend the collaboration for my project. The PhD enabled me to learn so much about the, before this, unknown geotechnical side of the subsurface I was studying for all these years. But, also, I was able to deepen my teaching experience, which is another part of academia that I love, host events at the department, and present my work at various congresses. Although doing a PhD can be difficult at times, I definitely did not regret my decision to start (and now finish) it.

And therefore, it may not come as a surprise that I have stayed in academia by starting as a postdoctoral researcher at the *Department of Earth Sciences of Vrije Universiteit Amsterdam*. While keeping it familiar by staying in the peatlands, I nonetheless shift my perspective slightly: the coming years I will study the greenhouse gas emissions from those peatlands and in particular how oxygen intrusion and availability in the soil helps us better predict and mitigate the amount of greenhouse gas emissions.

List of publications

Journal articles as first author

Published:
van Elderen, P., Erkens, G., Zwanenburg, C., Middelkoop, H., & Stouthamer, E. (2025). Viscous compression of clay and peat. *Earth-Science Reviews*, *260*, 104993.

Under review/Submitted:
Tolunay, D., **van Elderen, P.**, Hefting, M.M., Kowalchuk, G.A., Stouthamer, E., Erkens, G. (2026). The Effect of Compaction on Short-Term Decomposition Rates in Peat Samples with Different Degradation Status. (Shared first author paper) *Submitted to Terrestrial, Atmospheric and Oceanic Sciences, special issue; Ground Deformation in a Changing World: Land Subsidence, Climate, and Resilience.*

van Elderen, P., Erkens, G., Zwanenburg, C., van Essen, H., Stouthamer (2025). The Effect of Compaction on Short-Term Decomposition Rates in Peat Samples with Different Degradation Status. *Under review at Netherlands Journal of Geosciences, special issue; Land Subsidence.*

Conference proceedings:

van Elderen, P., Erkens, G., Zwanenburg, C., Kooi, H., & Stouthamer, E. (2024). The relationship between organic content and compressibility of peat and clay soils. *European Geosciences Union General Assembly 2024 (EGU24)*, 8379.

Utrecht University
Faculty of Geosciences
Department of Physical Geography

ISSN 2211-4335